BACK-MIXING STUDIES IN THE PRESENCE OF AN UNSTABLE DENSITY GRADIENT IN A RECIPROCATING PLATE EXTRACTION COLUMN

BY

KANNAN ARAVAMUDAN, M. TECH.

A Thesis

Submitted to the School of Graduate Studies

in Partial Fulfilment of the Requirements

for the Degree

Doctor of Philosophy

McMaster University

BACK-MIXING STUDIES IN A RECIPROCATING PLATE COLUMN

Dedicated to my parents and my sister

If I have seen farther it is by standing on the shoulders of giants

Sir Isaac Newton

Doctor of Philosophy (1995) McMaster University

(Chemical Engineering) Hamilton, Ontario

Title: Back-mixing Studies in the Presence of an Unstable Density Gradient in a Reciprocating Plate Extraction Column

Author: Kannan Aravamudan, B. Tech. (A. C. College of Technology)

M. Tech. (Indian Institute of Technology)

Supervisor: Professor M. H. I. Baird

Number of Pages : xx, 335

ABSTRACT

The efficient design of extraction columns calls for the accounting of flow non idealities, collectively termed axial mixing, in the phases involved. Axial mixing occurs mainly through back-mixing caused by circulation, wake transport with dispersed drops and induced turbulence due to mechanical agitation. Non uniform velocity profiles and forward mixing due to drops of different sizes are the other factors. A new factor identified to significantly enhance back-mixing, is the increase in the density of the continuous phase with column height termed as the unstable density gradient. In this thesis, attention was focussed on this factor using a 5 cm reciprocating plate extraction column (RPC).

A new approach based on the Kolmogoroff isotropic turbulence theory was developed to model the continuous phase back-mixing under two phase flow conditions. The contribution due to mechanical agitation, dispersed phase flow and the unstable density gradient were accounted in the model in terms of their respective energy dissipation rates and mixing lengths. The parameters were estimated by fitting the model to the experimental data obtained through the steady state tracer injection technique under non mass transfer conditions. The results showed that the unstable density gradient played an important role in enhancing the back-mixing even though its energy dissipation rate was very small relative to the other two contributing factors. This was due to the large mixing length associated with the unstable density gradient effect. At high mechanical agitations, the contributions of the dispersed phase and the density gradient declined.

A preliminary study was also performed to investigate the unstable density gradient effect

under mass transfer condition. Water was used as the solvent to extract *i*-propanol from Isopar M drops in the extractor. As increasing amount of alcohol was extracted, the density of water decreased leading to an unstable density gradient. To ensure the reliability of the estimation of the back-mixing coefficient (E_c), a non transferring tracer dye was also injected steadily into the continuous phase. E_c values were determined simultaneously from the concentration profiles of the tracer and the solute, thereby providing two independent estimates for each experiment. The results were comparable under most operating conditions thereby validating the tracer technique. The dispersed phase hold-up, drop size and the mass transfer coefficient were also estimated and compared critically with the models available in literature.

The hydrodynamics in the column were significantly altered by the interfacial effects associated with the transfer of solute from the dispersed phase to the continuous phase. In particular coalescence was promoted leading to large drops. Under these conditions the Kolmogoroff model could not isolate the influence of the density gradient from other contributing factors. However the experimental results clearly showed an enhancement in the back-mixing relative to the non mass transfer case.

Based on these observations it is concluded that care must be taken to avoid the unstable density gradient created either inadvertently during tracer measurements involving ionic compounds or during mass transfer.

ACKNOWLEDGEMENTS

It was a wonderful and enriching experience to conduct research under the supervision of Prof. M. H. I. Baird. I express my great respect and appreciation for his able guidance and support throughout the course of the Ph.D. program. I will cherish this phase of my academic career throughout my life.

I express my gratitude to Prof. G. F. Round and Prof. J. Vlachopoulos for their interest and excellent advice during the committee meetings. I thank Prof. R. H. Pelton for providing permission to use his image analysis equipment and Prof. D. R. Woods for useful discussions regarding interfacial phenomena. I also thank Dr. I. A. Feuerstein and Dr. J. M. Dickson for their critical evaluation and useful suggestions during my comprehensive examination. The excellent introduction to GAMS and its availability provided by Dr. A. N. Hrymak is gratefully acknowledged. Prof. T. E. Marlin was helpful in gaining access to the Advanced Process Control VAX computers for parameter estimation.

All the members in my supervisor's research group were extremely helpful, co-operative and friendly. Dr. N. V. Rama Rao proved to be very knowledgable. The help provided by Dr. Wuhai He and Mr. Phil Moruzi on several occasions too numerous to mention is gratefully acknowledged. Their way of handling esoteric software and unrelenting hardware was truly instructive.

I could always count on Ivan Miletic and Mike Kempe for their assistance in resolving problems showing up during HYSIM and MATLAB calculations. Eduardo Vivaldo-Lima was

very informative about application software which saved considerable time.

Mrs. Justyna Derkash, Mr. Paul Gatt and Mr. Gord Slater were always available despite their busy schedule to sort out difficulties encountered with measuring instruments and construct accessory parts to my equipment. Their competence and efficiency will be remembered. Mrs. Barbara Owen helped often to sort out the temperamental photocopy machine. Mrs. Sara Gallo - O'Toole was most informative and helpful regarding administrative matters.

TABLE OF CONTENTS

LIST OF FIGURES

LIST OF TABLES

CHAPTER 1

THE CONCEPT OF LIQUID-LIQUID EXTRACTION AND AXIAL MIXING

This chapter is divided into three parts. In the first part solvent extraction is briefly introduced. This is followed by the classification of extractors and description of those with oscillatory forms of agitation. In the second part the concept of axial mixing and its modelling are described. In the final part, the scope of this thesis is outlined.

1.1 Introduction to liquid-liquid extraction

Liquid-liquid extraction is a separation process in which one or more solutes present in a liquid are removed to an appreciable extent by bring it in contact with another immiscible liquid termed the solvent. The extraction equipment contains provisions for effective inter-phase mixing and phase separation after contact. The terminology used in solvent extraction (henceforth simply

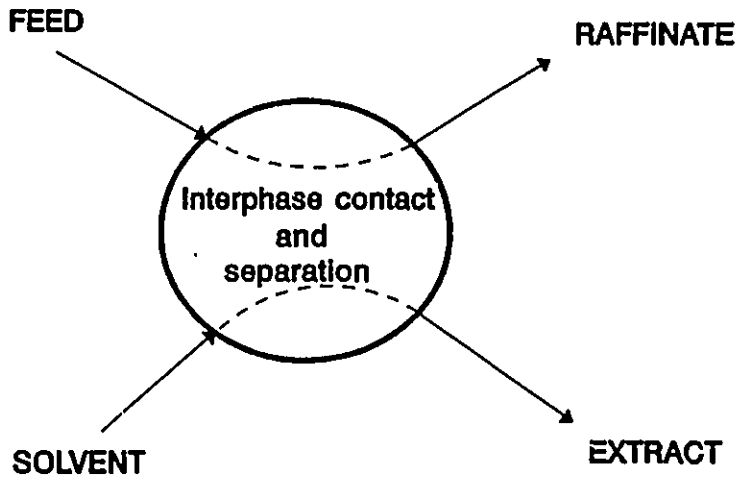

Fig. 1.1 Terminology used in solvent extraction

termed extraction) is illustrated in figure 1.1.

1.2 Requirements of a good solvent (Treybal, 1981)

To make the extraction process feasible the solvent should satisfy the following criteria:

1. The solvent must have high selectivity for the solute. Selectivity is defined as follows :

   $$\frac{\text{the ratio of the solute to solute free feed in the solvent}}{\text{the ratio of the solute to solute free feed in the feed rich solution at equilibrium}}$$

2. The solute should have a high preference for the solvent phase than for the feed phase.
3. The downstream process recovery for the solvent must be free of complications.
4. A large difference between the densities of the mutually saturated phases is essential so that a) phase inversion due to solute transfer is prevented b) the settling and separation of the two liquid phases after contact is rapid.
5. A moderate interfacial tension is required as a compromise between the energy required to disperse one of the phases and the ease of coalescence of the emulsions after contact.
6. The solvent should be stable and non corrosive towards the material of construction used. This criterion may be satisfied by having flexibility in adjusting the conditions of pH and temperature.
7. The solvent must have low vapour pressure and freezing point to facilitate handling and storage.
8. The solvent should be non toxic and easily available.

1.3 Relevance of Extraction in Industry

Extraction is similar to distillation but the solvent replaces heat in accomplishing the separation. Based on economic considerations distillation is a more popular tool for separation

than extraction and the decision to use solvent extraction is often made only after distillation has been found to be inconvenient. However extraction enjoys the following advantages over distillation (King, 1993) :

1. Separation of a compound or a class of compounds can be made solely on the basis of differences in chemical structure i.e. solvent extraction is chemically specific.
2. The consideration of volatility of the solute to be separated does not arise.
3. The energy requirement for the extraction process is low if the solvent has a high preference for the solute. The energy considerations for the primary extraction process plus the solvent regeneration process (by distillation) can sometimes work out more favourably than the primary distillation process alone. Extraction is more energy efficient if the primary distillation process has a considerably lower relative volatility than the solvent regeneration step.
4. Solutes in very dilute concentrations can be separated from the solution even when they are non-volatile or have a lower volatility than the liquid in which they are dissolved. If solvent requirements are low, small flows are encountered in the primary and regeneration steps making equipment and energy costs lower.
5. Extraction is mandatory if the compounds to be separated are heat sensitive.

Extraction also suffers its share of disadvantages and they are listed below:

1. There is a need for regenerating the solvent to make the process feasible and environmentally acceptable.
2. Mutual solubility of solvent and feed can cause contamination and need for further purification.
3. Solvents can be environmentally hazardous. Further problems are also encountered in the

disposal of the raffinate, for example, aqueous streams contaminated with the solvent.

1.4 Extraction Equipment in general

In gas-liquid contact the density difference between the two phases is very high and buoyant energy is sufficient to disperse one phase in the other. However for liquid-liquid contact the density difference is relatively small and mechanical agitation is often required to bring about a good dispersion. Pratt and Stevens (1992) have developed a comprehensive extractor selection chart based on design requirements like total throughput, number of theoretical stages, floor area available, physical properties of the phases etc. One common characteristic of all extractors is that the internals must be preferentially wet by the continuous phase in order to prevent dispersed phase coalescence on the surface. With reference to the current thesis, only the extractors with oscillatory form of agitation are described. A detailed description of other solvent extraction equipment can be found in standard text books, for eg. those due to Godfrey and Slater (1994), Thornton (1992) and Lo et al. (1983).

1.5 Classification of extractors

Extractors can be broadly classified into differential and stage-wise types. In the differential contactors the phases are in continuous contact and the concentration profile of the phases inside vary smoothly. In stage-wise contactors the phases are in intermittent contact and the concentration profile is stepwise. A typical classification is given in figure 1.2.

1.6 Extractors with oscillatory forms of agitation

Van Dijck (1935) proposed in his patent that an oscillatory form of agitation could be used as an alternative to the rotary form. The oscillation could be induced by either reciprocating the perforated plates supported on a vertical shaft or by pulsing the liquids through a stationary

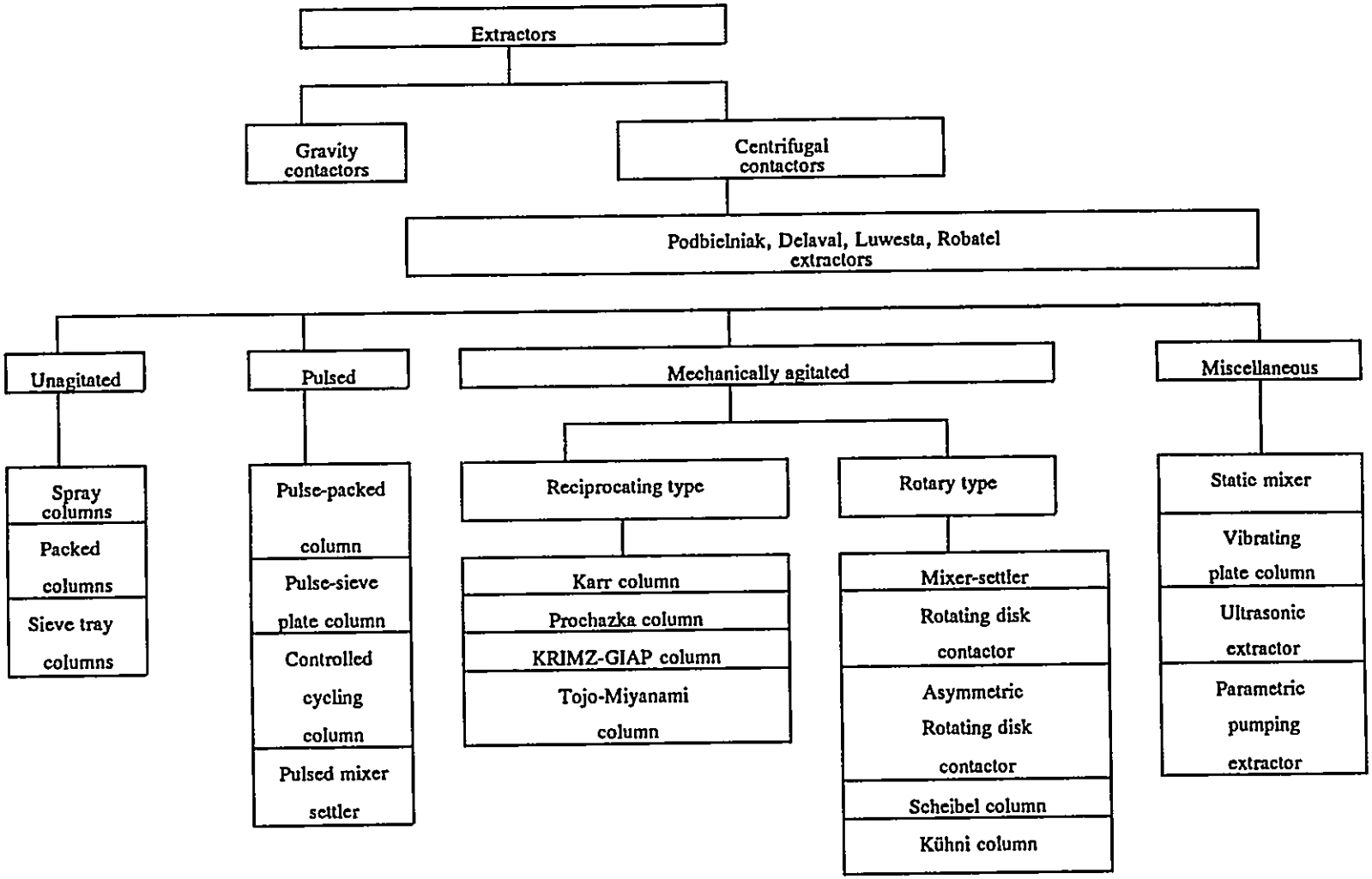

Figure 1.2 Classification of solvent extraction equipment (Lo and Baird, 1994)

perforated plate stack. The former method led to the development of reciprocating plate extraction columns (RPCs) while the latter resulted in the pulsed plate columns which are described below.

1.6.1 Pulsed plate extraction columns

In pulsed columns (figure 1.3) the light liquid is dispersed by forcing it through the holes during the upward pulse and the continuous phase is forced downward during the downward stroke. Pulsing is cyclic, usually sinusoidal. Thus the fluid phases are pumped as they flow counter-currently. Agitation is accomplished without the need for moving internals. The design of the pulsing unit which can be either pneumatic or mechanical is critical. For these columns, energy requirements are high and throughput is limited. The chief application of the pulsed column is in the nuclear industry where the pulsing mechanism can be located in a safe place and frequent maintenance of the column is not required. The columns are also used in processing organic intermediates and stripping of antibiotics from solvents.

1.6.2 Reciprocating plate extraction column (Baird et al. 1994)

The part of the patent by Van Dijck involving reciprocating the perforated plates for inter-dispersing the phases lay almost dormant for about 25 years until Karr (1959) published data on a 76 mm diameter column. Since then there has been a great interest shown in this column resulting in modifications of the plate geometry, extensive pilot plant studies for scale-up and widespread industrial applications.

The RPC consists of a vertical cylindrical shell housing a central shaft on which a number of horizontal perforated plates are supported (figure 1.4). The shaft is reciprocated in a sinusoidal fashion while trapezoidal forms are also possible. Usually the frequencies and stroke (defined as twice the amplitude) of oscillation are in the range 0.5-5 Hz and 0.5-4 cm

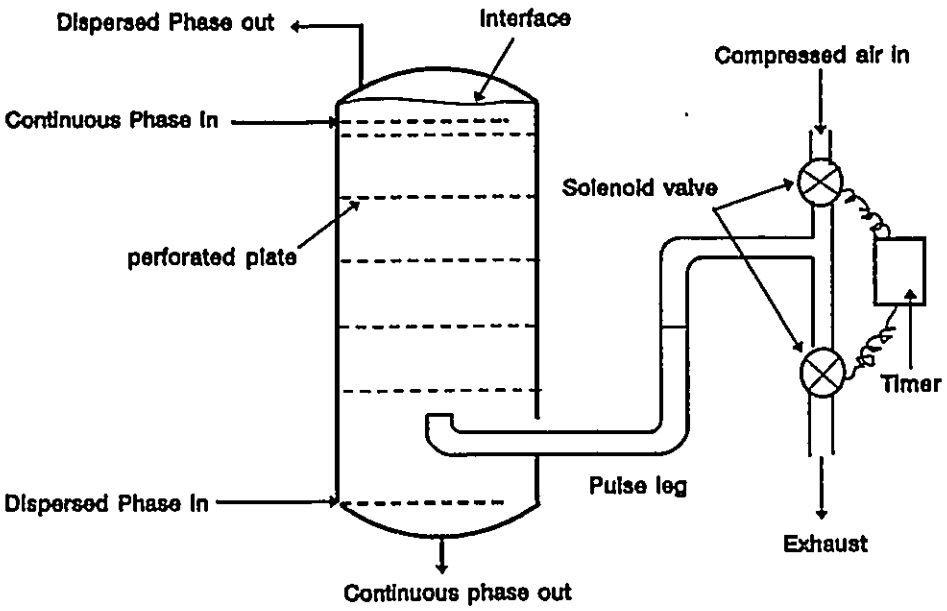

Figure 1.3 Pulsed plate extraction columns (Cusack and Fremeaux, 1991)

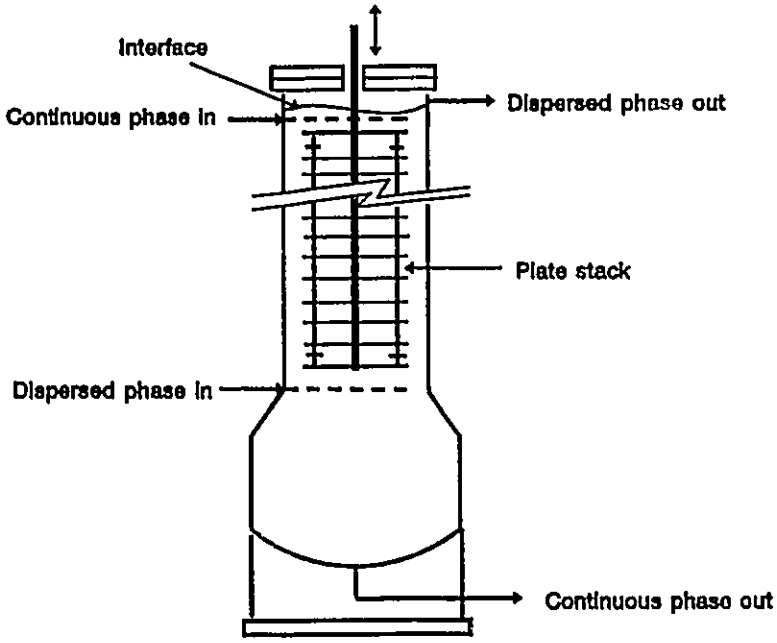

Figure 1.4 Karr reciprocating plate extraction column (Cusack and Fremeaux, 1991)

respectively. There are several versions of the RPC depending mainly on the plate geometry like design, hole size, fractional open area and presence of downcomers. Prominent among the RPCs are those due to Karr and Prochazka.

1.6.2.1 Karr column The distinguishing feature of the Karr columns is the open structure of the plates. When diameters exceed 15 cm, a doughnut baffle is added for every 5 Karr plates in the plate stack. The main advantages of Karr columns are high throughput, high extraction efficiency and ability to handle emulsifiable material and material containing suspended solids (Lo and Prochazka, 1983). The constructional and operating characteristics of the Karr columns are explained in more detail in chapters 2 and 3 of this thesis.

1.6.2.2 Prochazka columns In Prochazka RPCs the plates resemble sieve trays with the presence of downcomers. The downcomers are located at opposite ends in small columns to create a cross flow pattern. In larger diameter columns the downcomers are so arranged creating cross-flow of phases along several parallel sections. Vertical skirts are present at the circumference of the plate extending against the flow of the dispersed phase. Similar lining may also be present in the downcomers. In another version of this extractor the adjacent plates are reciprocated with 180° phase lag such that they move opposite to one another. This is made possible by using two drive mechanisms to which alternate plates are connected. The advantages of Prochazka RPCs are high maximum throughput, ability to handle liquid systems with wide range in physical properties, low energy consumption and mechanical stress on the column and simple scale-up. The main features of these two RPCs are compared in table 1.1 and illustrated in figure 1.5 (a, b).

1.6.2.3 Tojo-Miyanami column In the multistage vibrating disk contactor, originally developed by Tojo et al. (1974, 1975) the plates are central disks and they alternate with static doughnut shaped baffles attached to the column wall (figure 1.6). The disks can rotate and vibrate

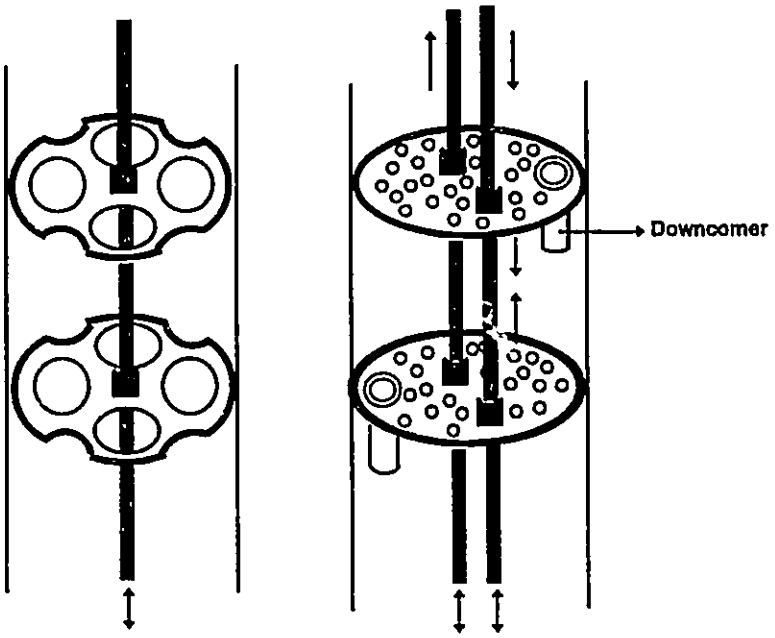

Figure 1.5 Typical Reciprocating plate extraction columns a) KRPC b) PRPC (Baird et al., 1994)

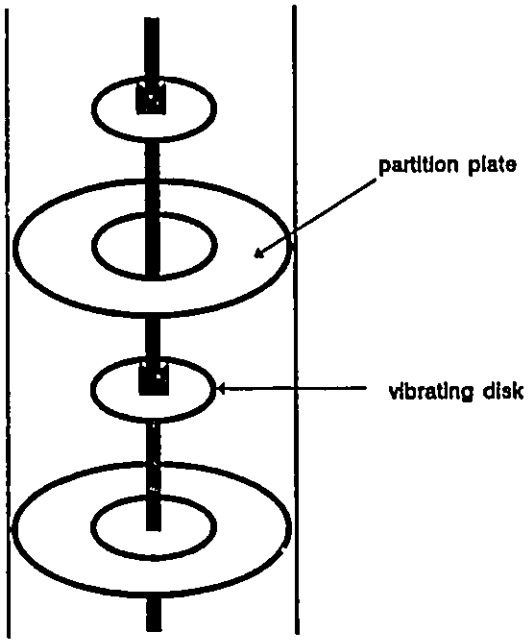

Figure 1.6 Tojo-Miyanami column (Baird et al., 1994)

Table 1.1 Comparison of Karr and Prochazka RPCs

Classification	Karr RPC	Prochazka RPC
Plate hole diameter	10-16 mm	2-5 mm
Fractional free area of the plate	55-60 %	4-20 %
downcomer	absent	may be present
operation regime	only emulsion[1]	Mixer settler and emulsion
Plate oscillation	Uniform	Uniform or alternate plates move with 180° phase lag

simultaneously. The area available for flow is determined by the ratio of disk to column diameter. When these columns are used for gas-liquid contact the disks are not perforated.

1.6.2.4 RPC with reciprocating wire mesh An extractor with reciprocating wire mesh packing was developed by Wellek et al. (1969). The void volume of the packing is 95% and the diameter of the mesh wire is around 0.27 mm.

1.6.2.5 GIAP and KRIMZ columns In the GIAP and KRIMZ extraction columns developed in former USSR and used also in eastern Europe the plates are modified to promote radial mixing and enhance uniformity of flow (Gorodetski et al. 1988; Olevskii et al. 1986). The plates have inclined vanes which direct the flow path of the liquid. The plates are illustrated in figure 1.7.

1.6.2.6 Miscellaneous Reciprocating plate columns

Some studies have also been conducted on RPCs in which the plates are reciprocated at very high frequencies (Issac and De Witte 1958; Landau et al. 1964; Novotny et al. 1970; Rama

[1] The terms "emulsion" and "mixer settler" regimes are explained in chapter 2

Rao et al. 1991). The stroke length is around 2 mm and frequencies of oscillation exceed 10 Hz and can go up to as high as 100 Hz.

1.6.3 Applications of RPCs

Karr type RPCs are widely used in the pharmaceutical, petrochemical, chemical, hydrometallurgical and waste-water treatment plants. The Prochazka, GIAP and KRIMZ columns have been used industrially in Russia and Eastern Europe. Further information about these RPCs have been reviewed by Baird et al. (1994).

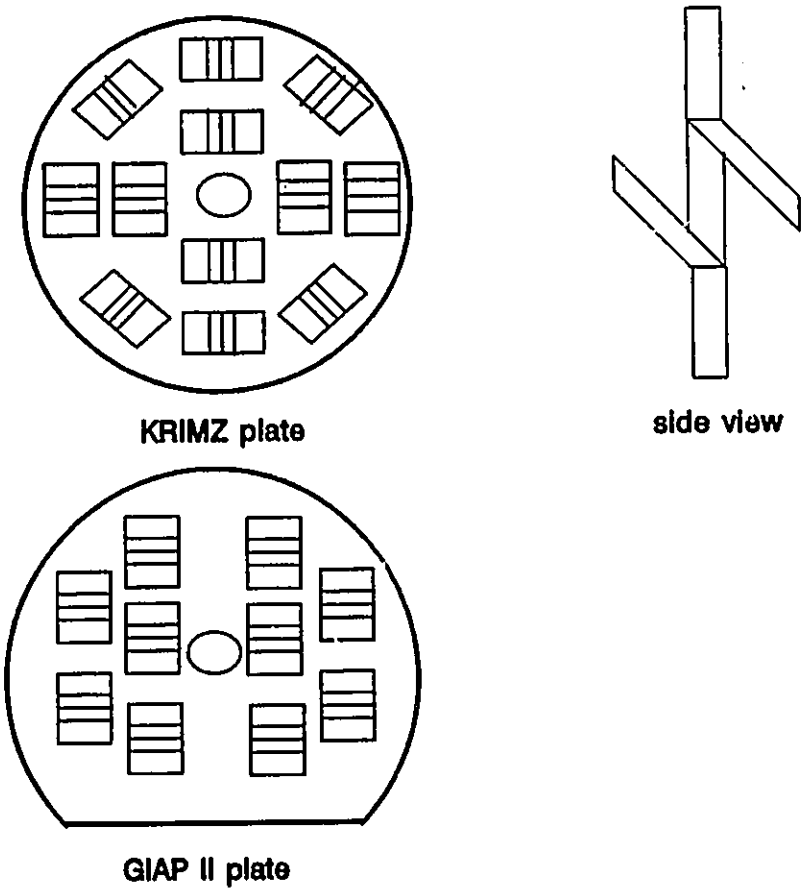

Figure 1.7 Plates of GIAP and KRIMZ RPCs (Baird et al. 1994)

1.7 Introduction to axial mixing

One of the assumptions made in elementary counter-current extractor design is the plug flow of both the phases. Plug flow refers to a condition wherein each fluid element of a particular phase has the same residence time and the velocity profile is flat. However due to a combination of factors these ideal conditions are rarely attained in practice and therefore the concentration driving force for interphase mass transfer is lower than expected. The flow non idealities were termed as **back-mixing, axial mixing** and **forward mixing.** As shown below these terms are not equivalent. For an extractor design to meet the required performance specifications, allowance should be made for axial mixing effects. Since the study of axial mixing is the aim of this research, a detailed discussion of its theory is presented in the following sections.

1.7.1 The 'discovery' of Axial Mixing

The earliest observations of flow non ideality were made in spray columns. Morello and Poffenberger (1950) observed bulk mixing in the continuous phase. Geankoplis and Hixon (1950) during the study of extraction of ferric chloride in an aqueous solution using isopropyl ether as solvent observed an unexpected discontinuity at the continuous phase inlet. Their discovery was made possible by their pioneering effort in sampling the internal concentration profile of the continuous phase. The aqueous phase concentration sampled *inside* the column at the phase inlet was significantly lower than the feed concentration. They termed this phenomenon as an inlet effect. They postulated that the discontinuity could be due to turbulence induced by the coalescing drops at the interface. Newman (1952) however was critical of this theory and proposed that the extractor concentration profile was intermediate between true counter-current (i.e. plug) flow and perfectly mixed flow. Gier and Hougen (1953) sampled both the dispersed

and continuous phase concentrations in their study on extraction of adipic acid from water using diethyl ether as solvent. Discontinuities in concentration were observed at both the phase inlets. The jumps in concentration at the phase inlet were not reflected by a corresponding change in the concentration of the second phase leaving the contactor, but the magnitudes of the jumps were significantly larger than the sampling and analytical errors. It was proposed that the continuous phase dilute in the solute moved co-currently upwards along with the dispersed phase to mix with the more concentrated continuous phase feed at the inlet, leading to an abrupt change in concentration as in figure 1.8a. This effect was more serious in a spray column than in a packed column. The continuous phase was thought to recirculate back to the inlet thereby destroying the true counter-current nature of the separation. If carried to the extreme, then perfect mixing will prevail and the incoming liquid will immediately drop to the exit phase concentration. Then the extractor will have the performance of a single theoretical stage. The effect of axial mixing on extraction performance is illustrated in figures 1.8a,b.

Cavers and Ewanchyna (1957) studied the operation of a spray extraction column using the system water (continuous)-acetic acid (solute)- MIBK (dispersed). When solute transfer was from the continuous phase to the dispersed phase, coalescence at the interface was accompanied by considerable agitation. Hence the inlet concentration jump was proposed to be due to circulation and coalescence. There was also a small discontinuity in concentration at the dispersed phase outlet. When the transfer was in the reverse direction coalescence was smooth and no jump in concentration was observed at the dispersed phase inlet. The inlet effect was then attributed to circulation effects alone.

Research on other types of equipment, for example, tubular reactors indicated similar non-ideal flow patterns. Depending on the occurrence of non ideal flow in the downstream or

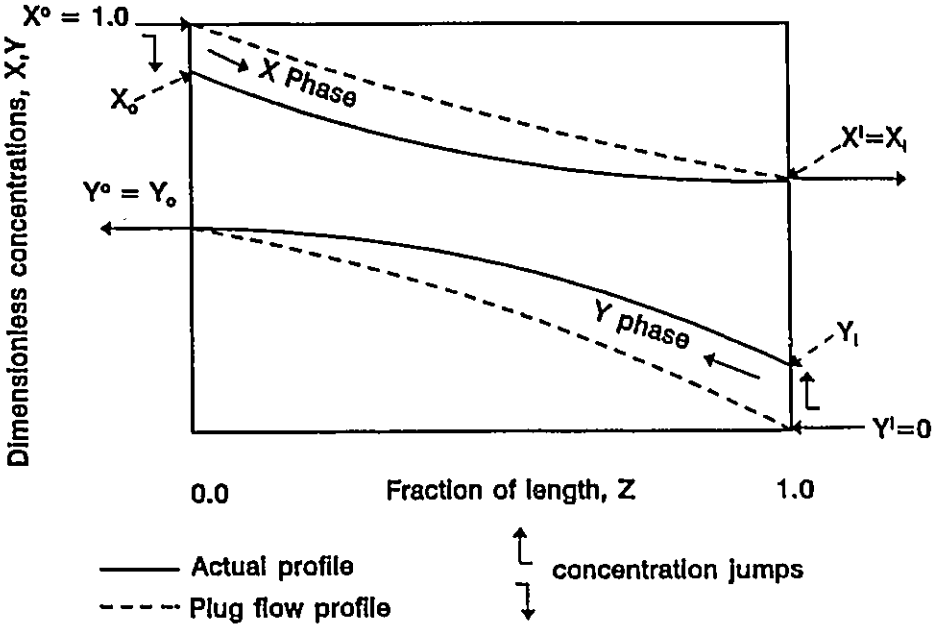

Figure 1.8 a Effect of axial mixing on concentration driving force (Pratt and Baird, 1983)

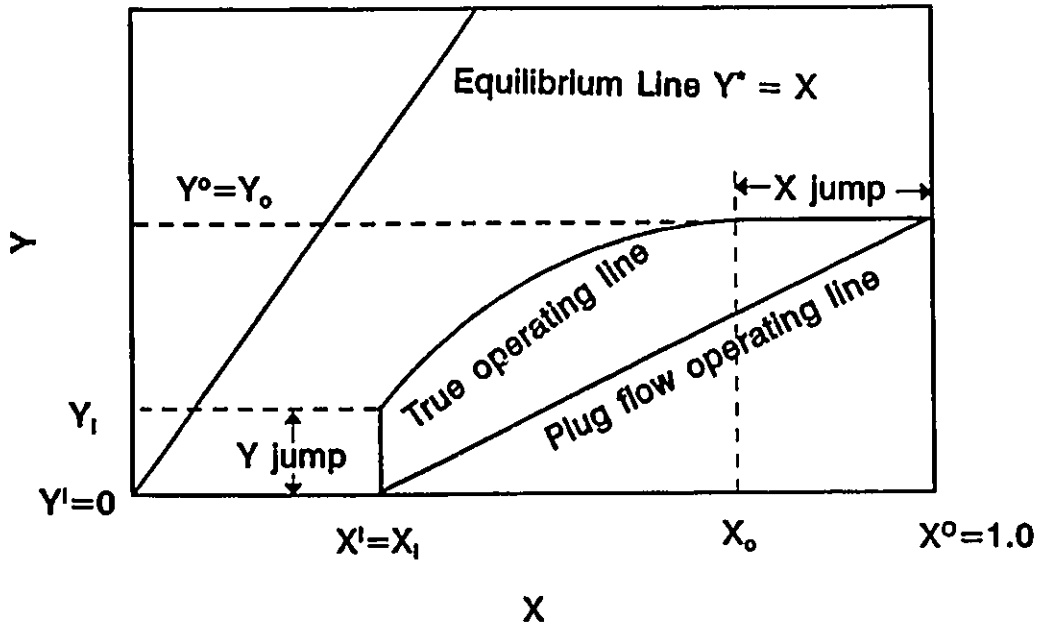

Figure 1.8b Effect of axial mixing on operating line of extractor force

upstream sides, reactors have been classified into closed-closed, open-closed and open-open types. For the closed-closed case, Danckwerts (1953) developed boundary conditions which are also applicable to extractors. The boundary conditions are discussed in section 1.8.1.3

1.7.2 Causes of axial mixing

The factors as summarized by Pratt and Baird (1983) and Pratt and Stevens (1992) are listed below:

1. Circulation induced by droplet motion

Anderson and Pratt (1978) developed a theory in which it was proposed that a drop moving at its terminal velocity transfers momentum to adjacent elements of the continuous phase resulting in its acceleration. The continuous phase is constantly translated by the drops leaving trails which accumulate to form the circulatory flow. This process can also be viewed as the dissipation of the potential energy of the drops into the continuous phase leading to its circulation.

2. Entrainment of continuous phase as wakes in drops

Geankoplis (1952) discussed the possibility of the drops carrying with them an "atmosphere" of the continuous phase. Cavers and Ewanchyna (1957) observed the drops to carry an "envelopes" of the continuous phase up the column which were discharged as the drops coalesced at the interface. The entrained continuous phase was later termed wakes. Among the contributors to the wake theory were Letan and Kehat (1968) who studied the mechanism of heat transfer in a spray column. Only the continuous phase was sampled and a sharp jump in temperature was observed at the inlet. The same authors (Kehat and Letan, 1971) also developed a model for extraction in spray columns using the wake theory . Different zones were identified in the column and they were classified as wake formation zone, wake shedding zone, mixing zone and the coalescence zone. The wakes after growing to a maximum volume start shedding

cyclically and mixing with the bulk liquid. The wake region is replenished by the continuous phase.

The drops reach the mixing zone where they contact the fresh continuous liquid and the returning wakes from coalescing zone. At the boundary between the mixing zone and the coalescing zone the jump in concentration occurs due to the mixing of the continuous phase of different concentrations resulting in the instantaneous reduction in the concentration driving force.

3. Induced turbulence due to agitation

Circulatory flow can also be promoted by agitation. Significant turbulence is created and eddy diffusion of the continuous phase occurs along the radial and longitudinal directions. Molecular diffusion effects are several magnitudes lower in comparison.

4. Non-uniform velocity profiles

These develop in the contactor due to frictional effects of the contactor internals. A distribution in residence times of liquid elements results. This effect is relatively small for two phase flow.

5. Channelling

Poor design of the contactor geometry and internals or packing can cause channelling and maldistribution of the phases. Laminar flow is a special case of channelling wherein the channels are infinitely thin (Mecklenburgh and Hartland, 1975). Channelling can sometimes occur in a properly designed contactor at very low dispersed phase flow rates.

6. Forward mixing

The droplets formed by agitation of the column contents are not of uniform size. Hence a spectrum of drop velocities exist leading to a condition termed as forward mixing. The smaller drops have longer residence times and come closer to equilibrium with the continuous phase than

the larger droplets. Hence there is no unique operating curve (Rod, 1966).

7. Unstable density gradient in the continuous phase

When a density difference created along the length of the column in the continuous phase proves to be unstable, local circulation currents are set up leading to the enhancement of the axial mixing effects. This is discussed in more detail later in this chapter when the scope of this thesis is defined.

Factors 1, 2, 3 and 7 lead to back-mixing in the extractor. Mecklenburgh and Hartland (1975) describe the various circumstances in which different flow patterns are possible. The liquid pathways instead of being unidirectional can also bend back among in the reverse direction leading to back-flow. When agitation and baffles are used to improve contacting of the phases radial mixing and to some extent backflow are promoted. If backflow dominates over radial mixing then complete mixing occurs. If both factors are comparable then back-mixing results. When radial mixing is completely dominant, plug flow conditions are obtained. Back-mixing differs from channelling since in the latter the flow occurs only in the forward direction.

1.8 Axial Mixing Models

There are two main approaches to model extractor performance affected by axial mixing. They are

1. The dispersion model (applicable for differential extractors)
2. The backflow model (applicable for stage-wise extractors)

Extractors which cannot be strictly identified as stage-wise or differential have been modelled by both the approaches. However as discussed later, it can shown that there is a unique relationship between the two models.

1.8.1 Dispersion Model

In this model axial mixing in either the dispersed or the continuous phase is represented in terms of a turbulent diffusion coefficient superimposed on the bulk flow of the phases.

1.8.1.1 Model Assumptions (Sleicher, 1959)

The assumptions made in this model are as follows:

1. The average velocity and concentration are radially uniform.
2. The volumetric mass transfer coefficient is constant or taken as the average over the entire column.
3. The concentration profiles inside the column are continuous except at the inlets.
4. The solvent and raffinate phases are immiscible or have a constant solubility irrespective of solute concentration.
5. The volumetric flow rates of the feed and solvent are constant throughout the extractor.
6. The equilibrium curve is linear or can be effectively represented by a linear relationship over the range of concentrations involved.

1.8.1.2 Derivation of the model equations

As shown in figure 1.9 material balance is made across a differential section of the extractor. For simplicity, the two phases represented by X and Y are assumed to flow through separate vertical channels and mass transfer occurs through the interface separating the channels. The concentration change in the solute is due to three effects:

1. The mass transfer flux assuming that the transfer occurs from the X phase to the Y phase: $k_{ox}a(c_x-c_x^*)$.
2. The convective flux caused by the bulk flow of the phases : u_jc_j (j= X,Y).
3. Axial mixing flux is represented by a diffusion-like expression: E_jdc_j/dz. It is assumed

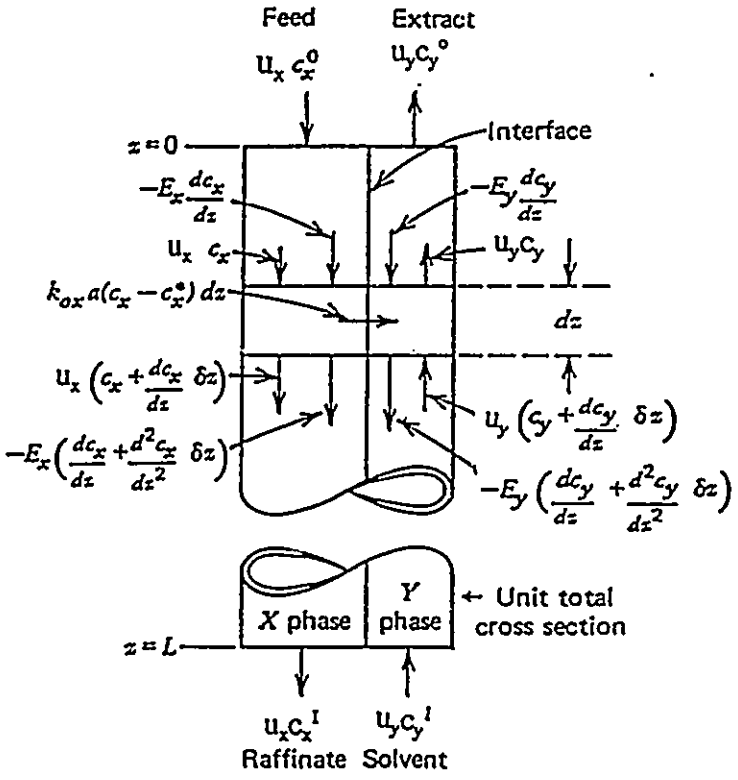

Figure 1.9 Dispersion model: material balance over differential section (Pratt and Baird, 1983)

that these three fluxes are additive even though the parameters characterizing the fluxes can influence each other. The material balance equations can be summarized as follows:

$$E_x \frac{d^2c_x}{dz^2} - u_x\frac{dc_x}{dz} - k_{ox}a\ (\ c_x - c_x^*\ ) = 0 \qquad (1.1)$$

$$E_y \frac{d^2c_y}{dz^2} + u_y \frac{dc_y}{dz} + k_{ox}a\ (\ c_x - c_x^*\ ) = 0 \qquad (1.2)$$

When axial mixing effects are removed by setting E_j's to zero, the equations reduce to plug flow conditions. If the equilibrium line can be expressed as

$$c_x^* = m_e c_y + q^* \qquad (1.3)$$

The equations can be made dimensionless by using the co-ordinate transformation as illustrated in figure 1.10. The dimensionless concentrations are expressed as follows:

$$X = \frac{c_x - (\ m_e c_y + q^*)}{c_x^0 - (\ m_e c_y^I + q^*)} \qquad (1.4)$$

$$Y = \frac{m_e\ (\ c_y - c_y^I\ )}{c_x^o - (\ m_e c_y^I + q^*\ )} \qquad (1.5)$$

After some manipulation the equations can be expressed in a dimensionless form as follows:

$$\frac{d^2X}{dZ^2} - Pe_x B\frac{dX}{dZ} - N_{ox}Pe_x B\ (\ X - Y\ ) = 0 \qquad (1.6)$$

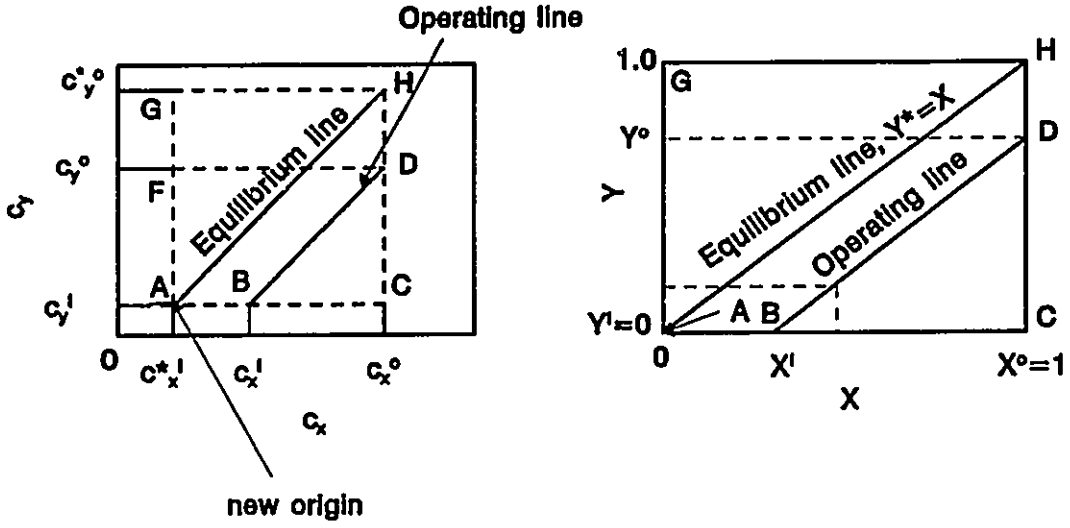

Figure 1.10 Transformation into dimensionless co-ordinates (Pratt, 1983)

$$\frac{d^2Y}{dz^2} + Pe_yB\,\frac{dY}{dZ} + \Lambda N_{ox} Pe_yB(X - Y) = 0 \qquad (1.7)$$

The dimensionless groups are described as follows:

$Z = z/L$, fractional distance within the contactor

$Pe_jB = u_jL/E_j$, Peclet number of the j^{th} phase

$B = L/d_c$, dimensionless distance based on characteristic dimension d_c

$N_{ox} = k_{ox}a\ L/u_x$, true number of transfer units

$\Lambda = m_e\ u_x/u_y$, Extraction factor

1.8.1.3 Boundary Conditions (Miyauchi and Vermeulen 1963; Sleicher 1959; Wehner and Wilhelm 1956)

Since there are 2 second order ordinary differential equations, 4 boundary conditions are

required. They are listed below:

1. Y Phase, Z = 1.0 Making a material balance at Z=1.0 leads to the following expression:

$$u_y c_y^{\,I} - E_y \frac{dc_y}{dz} = u_y c_{yI} \tag{1.8}$$

Using equations 1.4, 1.5 and the dimensionless group (Peclet number) equation 1.8 can be re expressed as follows:

$$[\frac{dY}{dZ}]_I = - Pe_y B\ Y_I \tag{1.9}$$

2. Y Phase, Z = 0.0

$$u_y\ c_{yo} = u_y\ c_y^{\,o} - E_y(\frac{dc_y}{dz})_o \tag{1.10}$$

This equation can be rearranged to give:

$$u_y\ (c_{y_o} - c_y^{\,o}) = -E_y\ (\frac{dc_y}{dz})_o \tag{1.11}$$

The term on the R.H.S. is positive because the concentration gradient is negative. But the term on the L.H.S. is negative when c_{yo} is considered to be lower than $c_y^{\,o}$. Thus equation 1.11 can only be satisfied when both R.H.S. and L.H.S. are equal to zero. This can be expressed in the dimensionless form as follows:

$$[\frac{dY}{dZ}]_o = 0 \tag{1.12}$$

The boundary conditions for the X phase can be obtained by following a similar approach.

3.X phase Z=0.0

$$-[\frac{dX}{dz}]_o = Pe_x B\ (\ 1\ -\ X_o\ ) \tag{1.13}$$

4. Y phase Z=0.0

$$[\frac{dX}{dZ}]_I = 0 \tag{1.14}$$

1.8.1.4 Solution of the Model Equations

Case A: Pe_x, Pe_y finite

The solution to the set of differential equations 1.6 and 1.7 can be expressed as follows:

$$X = \sum_{i=1}^{4} A_i\, e^{\omega_i Z}\ ;\quad Y = \sum_{i=1}^{4} A_i a_i e^{\omega_i Z} \tag{1.15}$$

where

$$a_i = \frac{\Lambda\ (\ 1\ -\ \dfrac{\omega_i}{P_x B}\ )}{(\ 1\ +\ \dfrac{\omega_i}{P_y B}\ )} \tag{1.16}$$

The complementary function (which in this case is same as the general solution) can be obtained by solving the characteristic equation given in equation (1.17).

$$\omega[\omega^3 - B(Pe_x - Pe_y)\omega^2 - (N_{ox}B\{Pe_x + \Lambda Pe_y\} + Pe_x Pe_y B^2)\omega - N_{ox} Pe_x Pe_y B^2(1-\Lambda) = 0 \tag{1.17}$$

The unknown constants A_i's can be found by using the boundary conditions derived in the previous section. The solutions to the general case are given below:

$$A_1 = \frac{D_{A_1}}{D_{A_1} - D_A} \tag{1.18}$$

where

$$D_A = \begin{vmatrix} 1-\frac{\omega_2}{Pe_x B} & 1-\frac{\omega_3}{Pe_x B} & 1-\frac{\omega_4}{Pe_x B} \\ a_2\omega_2 & a_3\omega_3 & a_4\omega_4 \\ \omega_2 e^{\omega_2} & \omega_3 e^{\omega_3} & \omega_4 e^{\omega_4} \end{vmatrix} \tag{1.19}$$

$$D_{A_1} = \begin{vmatrix} a_2\omega_2 & a_3\omega_3 & a_4\omega_4 \\ \omega_2 e^{\omega_2} & \omega_3 e^{\omega_3} & \omega_4 e^{\omega_4} \\ a_2 e^{\omega_2} f(\omega_2) & a_3 e^{\omega_3} f(\omega_3) & a_4 e^{\omega_4} f(\omega_4) \end{vmatrix} \tag{1.20}$$

where

$$f(\omega_i) = \left(1 + \frac{\omega_i}{Pe_y B}\right) \tag{1.21}$$

$$D_{A_2} = \omega_3\omega_4 \left(a_4 e^{\omega_3} - a_3 e^{\omega_4}\right) \tag{1.22}$$

$$D_{A_3} = \omega_2\omega_4 \left(a_2 e^{\omega_4} - a_4 e^{\omega_2}\right) \tag{1.23}$$

$$D_{A_4} = \omega_2\omega_3 (a_3 e^{\omega_2} - a_2 e^{\omega_3}) \tag{1.24}$$

Note on the solution

When the boundary conditions were substituted in the general solution, a system of four linear equations with A_is as unknowns were obtained. One method of obtaining analytical solution is to use Kramers rule in Determinant theory (Miyauchi and Vermeulen 1963a). Sleicher (1959) used the numerical method to solve the above set of differential equations. It must be noted that the above solution is only valid when the extraction factor (Λ) is not equal to unity. This condition was satisfied for all the mass transfer runs in this thesis. The solutions for cases when the extraction factor is unity are given by Pratt and Baird (1983) and Pratt and Stevens (1992). The solutions for the limiting cases ($P_xB \to \infty$, P_yB finite) and (P_xB and $P_yB \to \infty$) are given below for the dispersion model since they are used in this thesis.

Simplified approximate solutions based on the special properties of the roots of the characteristic equations have been proposed by Pratt (1975, 1976) for both the dispersion and back-flow models.

Case B: $P_x \to \infty$ P_y finite

$$X = A_1 + A_3 e^{\omega_3 Z} + A_4 e^{\omega_4 Z} \tag{1.25}$$

$$Y = A_1 + A_3 a_3 e^{\omega_3 Z} + A_4 a_4 e^{\omega_4 Z} \tag{1.26}$$

where

$$\omega_3, \omega_4 = -\frac{(N_{ox} + Pe_y B)}{2} \pm \sqrt{\left[\frac{(N_{ox} - Pe_y B)^2}{4} - N_{ox} Pe_y B\,(1-\Lambda)\right]} \tag{1.27}$$

with the positive sign for ω_4 and

$$A_1 = \frac{D_{A_1}}{D_{A_1} + D_A} \tag{1.28}$$

where

$$D_{A_1} = \Lambda \left[a_3 \omega_3 e^{\omega_4} - a_4 \omega_4 e^{\omega_3} \right] \tag{1.29}$$

$$D_{A_3} = a_4 \omega_4 \tag{1.30}$$

$$D_{A_4} = -a_3 \omega_3 \tag{1.31}$$

$$D_A = (a_4 \omega_4 - a_3 \omega_3) \tag{1.32}$$

Case C: Pe_x, $Pe_y \to \infty$ (ideal plug flow conditions)

$$X = \frac{\exp [\omega_4 (1-Z)] - \Lambda}{\exp(\omega_4) - \Lambda} \tag{1.33}$$

$$Y = \frac{\Lambda \exp [\omega_4 (1 - Z)] - \Lambda}{\exp (\omega_4) - \Lambda} \tag{1.34}$$

where

$$\omega_4 = N_{ox}(1 - \Lambda) \tag{1.35}$$

1.8.2 Back-Flow Model

In this model a series of mixers (with or without settlers) are connected in series. The model assumptions are listed below.

1. Each stage is well mixed and back-mixing is represented as an entrained flow of the phases

($\alpha_j F_j$) in the direction opposite to the bulk flow (F_j), j=x,y.

2. The extent of back-mixing is the same for all stages. Back-mixing is expressed as α_j which is the ratio of the back-mixed to net forward inter-stage flow.
3. All the mass transfer occurs in the mixer.
4. The product of the stage volumetric coefficient ($k_{ox}a$) and the stage volume is constant for each stage.

The assumptions regarding the equilibrium line, volumetric flow rates of the phases and the mutual miscibility of the phases are the same as in the dispersion model (section 1.8.1.1).

Due to the stage-wise nature of the process, the equations are in finite difference form. The solutions to these equations have been summarized by Pratt and Baird (1983) and Pratt and Stevens (1992). In this thesis, since the solution to the axial mixing model in the differential form (section 1.8.1) were used and for reasons of space the solutions to the back-flow model are not given.

1.9 Relationship between the models

Even though the two models described above are for entirely different classes of extractors it can be shown that when there is a large number of stages there is an unique relationship between them. When the differential equations for the dispersion models are expressed in a finite difference form and the coefficients are compared with the equations for back-flow model it can be shown that for the limiting case of large N (Miyauchi and Vermeulen, 1963b) :

$$\alpha_j = \frac{N}{Pe_j B} - \frac{1}{2} \qquad (1.36)$$

Thus either model can be used for extractors with a large number of stages.

1.10 Effect of Axial Mixing on Number of Transfer Units

Qualitatively it can be inferred that due to the reduction in the concentration driving force for mass transfer, the operating line shifts closer to the equilibrium curve and the actual number of transfer units (for a differential contactor) will be greater than that required under plug flow conditions. This implies a longer tower for a given overall performance or for the same length a deterioration in the separation performance. This can be shown mathematically (Pratt and Baird 1983; Pratt and Stevens 1992).

Integrating equation (1.1) between the limits c_{xo} and c_{xJ}' , the interior terminal concentrations in the extractor, gives the number of "true" number of transfer units N_{ox}.

$$N_{ox} = \frac{k_{ox}aL}{u_x} = \int_{c_{xJ}'}^{c_{x,o}} \frac{d[\, c_x - (\frac{E_x}{u_x})(\frac{dc_x}{dz})]}{(c_x - c_x^*)_{BM}} \qquad (1.37)$$

Here $c_{x,J}'$ refers to the exit concentration under axial mixing conditions and the subscript BM denotes the concentration driving force under back-mixed conditions. The plug flow number of transfer units N_{oxp} is given by equation (1.38).

$$N_{oxp} = \frac{k_{oxp}a\ L}{u_x} = \int_{c_{xJ}}^{c_{x,o}} \frac{dc_x}{(c_x - c_x^*)_p} \qquad (1.38)$$

When comparing the number of transfer units given by the equations 1.37 and 1.38 it can be seen that the amount of solute transferred in the former case is reduced by an amount $(E_x/u_x)(dc_x/dz)$. Also the concentration driving force is reduced (figure 1.8a). Since dc_x/dz is negative, the result of these two effects is to increase the value of N_{ox} relative to N_{oxp}. Therefore if the terminal concentrations for both the cases are to be the same, the extractor with axial

mixing will require more number of transfer units. If N_{ox} is the same as N_{oxp} then $c_{xl}' > c_{xl}$ i.e., lesser amount of solute is extracted. Either way the extractor performance is relatively poor with axial mixing.

1.10.1 Relation Between Plug flow and True Number of Transfer Units

Geankoplis et al. (1950,1951) and Gier and Hougen (1953) attempted to use the driving force $(c_x-c_x^*)$ based on the experimentally measured concentration profile in equation (1.38). This NTU termed as measured number of transfer units (N_{oxm}) gives values between N_{ox} and N_{oxp}. A simple empirical equation often used in extractor design to account for axial mixing is given in equation 1.39.

$$\frac{1}{N_{oxp}} = \frac{1}{N_{ox}} + \frac{1}{N_{oxD}} \qquad (1.39)$$

An empirical method to correlate N_{oxD} in terms of the column Peclet numbers was given by Miyauchi and Vermeulen (1963a). A more rigorous method using equation (1.39) was suggested by Pratt (1975).

1.11 Measurement of Axial Mixing in the continuous phase

Tracers are commonly used to detect and estimate axial mixing. The spread of the tracer can indicate the type of flow occurring inside the column. Detection of the tracer upstream of the injection point indicates the presence of backflow. If the tracer injection and sampling are independent of location along the cross section of the column, back-mixing is present. If the tracer can be detected downstream but not upstream then only channelling is present (Mecklenburgh and Hartland, 1975).

The requirements of the tracer measurement technique are listed below:

1. The tracer should be non transferring, i.e. only soluble in the phase for which the mixing coefficients are required.
2. The physical properties like viscosity, density and interfacial tension must not be altered on addition of the tracer. Any change in these properties can alter the flow patterns and drop sizes inside the contactor so that the predictions will be of little practical significance. Tracers used for one system may not be applicable for another. For example, ionic tracers like sodium chloride can be used in the aqueous phase with non polar solvents like kerosene and toluene but not with polar solvents like methyl isobutyl ketone and butyl acetate (Pratt and Stevens 1992).
3. For the purpose of detection physical properties like electrical conductivity, refractive index or light absorbance may be altered. Radio-active tracers have also been employed, especially for the dispersed phase .
4. The tracer should not get absorbed on the column internals thereby altering the wetting characteristics.
5. The column should be of sufficient length so that the continuous phase is evenly distributed and a steady state drop size distribution has been established.
6. The tracer should be uniformly mixed at the injection point.
7. It is preferable for the tracers to be easily detectable even at very low concentrations. This will facilitate the introduction of the tracer at very small flow rates thereby limiting tracer consumption, avoiding significant change in superficial velocity and accurate measurement.

There are essentially 3 methods for estimating axial mixing coefficients. They are (i) steady state tracer method (ii) Unsteady state tracer method (iii) Measurements from actual mass transfer concentration profile. These methods are described briefly in the following

sections.

1.11.1 Steady State Tracer Injection Method

Tracer is injected in a continuous manner at a pre-determined location in the column into the phase whose back-mixing coefficient is required (figure 1.11a). Back-mixing leads to the establishment of the tracer profile upstream of the liquid flow. The tracer concentration profile is obtained by sampling at a number of locations so that the properties of the steady state profile especially the slope, can be estimated with confidence. The material balance equation (1.1) in the absence of mass transfer reduces to the expression given by equation (1.40).

$$E_j \frac{d^2 c_j}{dz^2} - u_j \frac{dc_j}{dz} = 0 \qquad (1.40)$$

Here the subscript j refers to the phase in which the measurement is being carried out. Equation (1.40) can be further simplified upon integration into

$$E_j \frac{dc_j}{dz} - u_j c_j = constant \qquad (1.41)$$

If c_j° is the tracer feed concentration then equation (1.41) can be solved to give:

$$c_j = c_j^\circ \exp\left(\frac{U_j z}{E_c}\right) \qquad (1.42)$$

The sign convention is that z increases along the direction of flow. Equation (1.42) is valid for differential contactors. For stage-wise contactors equation (1.43) can be derived.

The steady state method is a measure of back-mixing only. It cannot be used to determine the axial mixing in the contactor.

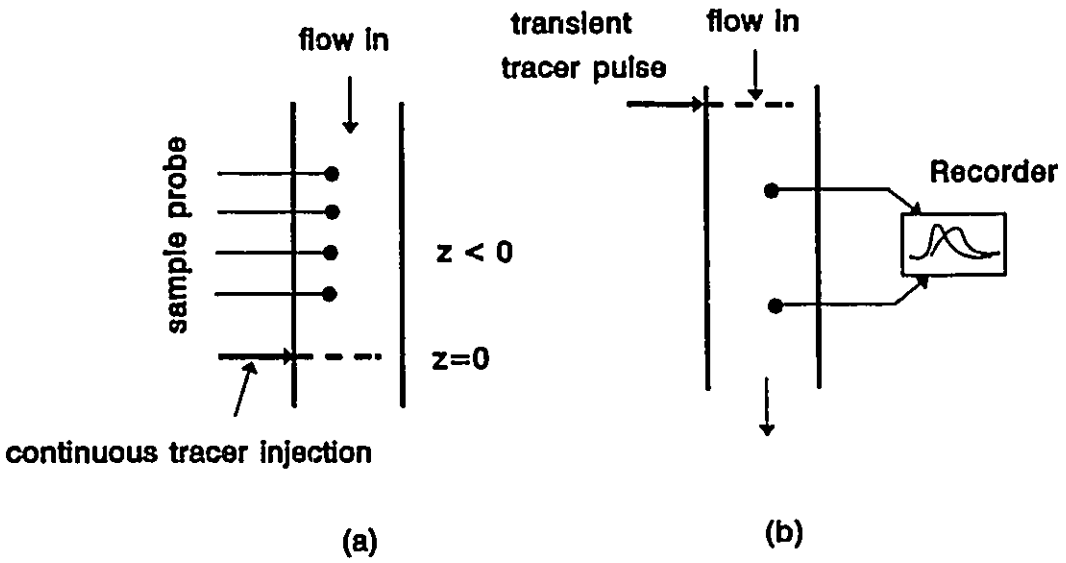

Figure 1.11 Measurement techniques (a) steady state (back-mixing) (b) unsteady state (axial mixing) [Pratt and Stevens, 1992]

$$c_{j,n} = c_j^o \left(\frac{\alpha_j}{1+\alpha_j}\right)^{N'} \tag{1.43}$$

1.11.2 Unsteady State Method

In the most common version of this method a sharp pulse of tracer is injected into the flow and the response is recorded downstream by a probe continuously over a period of time. (figure 1.11b). A Dirac impulse, which gives the mathematically simplest solution is aimed at, although a step or sinusoidal impulse is also possible. To avoid end effects the column should stretch to infinity on both ends relative to the test section (doubly open conditions). The

transport equation to be solved is:

$$E_j \frac{\partial^2 c_j}{\partial z^2} - u_j \frac{\partial c_j}{\partial z} = h_j \frac{\partial c_j}{\partial t} \qquad (1.44)$$

where h_j is the hold-up of the j^{th} phase. The solution to the Dirac impulse test under two phase flow conditions (Levenspiel and Smith 1957) adapted for two phase flow is given by equation (1.45) after omitting the subscript j.

$$C(\theta) = \sqrt{[\frac{Pe_c h}{4\theta}]} \exp\left[- \frac{Pe_c h(1 - \frac{\theta}{h})^2}{4\theta} \right] \qquad (1.45)$$

In this equation

$C(\theta) = cSL/m_t$, the ratio of the concentration of tracer to the mean concentration in the test section

m_t is the mass of tracer injected at time t=0.

$\theta = tu/(Lh)$, is the dimensionless time since injection.

$Pe_c = uL/E$, the column Peclet number.

Levenspiel and Smith (1957) used the mean (first moment) and the variance (second moment) of the response curve to estimate the column Peclet number in the following manner:

$$\frac{1}{Pe_c} = \frac{E}{uL} = \frac{\sqrt{(8\sigma^2+1)}-1}{8} \qquad (1.46)$$

Where

$$\mu = \frac{\int_0^\infty C(t)t\ dt}{\int_0^\infty C(t)\ dt} \approx \frac{\sum C(t)t}{\sum C(t)} \tag{1.47}$$

$$\sigma^2 = \frac{\int_0^\infty C(t)t^2\ dt}{\int_0^\infty C(t)\ dt} - \mu^2 \approx \frac{\sum C(t)t^2}{\sum C(t)} - \mu^2 \tag{1.48}$$

In using this method it is imperative to record the response accurately since the parameter prediction (of Pe_c) is sensitive to the tail portion of the curve.

A simpler method was suggested by Vergnes (1976). In this method, the maximum concentration in the response curve (c_{max}) and the time at which it occurred (t_{max}) were used. Assuming an open system and an ideal Dirac impulse the Pe_c could be obtained from the following equation[2]:

$$4\pi R^{*2} = [\sqrt{(1+Pe_c^2}-1]\ \exp\ [\ Pe_c - \sqrt{(1+Pe_c^2)}\ ] \tag{1.49}$$

and

$$R^* = \frac{c_{max}t_{max}}{\int_0^\infty c(t)\ dt} \tag{1.50}$$

It can be seen that the above two methods require the assumption of an ideal impulse which is practically not feasible. Moreover the distribution of the initial impulse signal over the cross section of the column is difficult. Aris (1959) and Bischoff (1960) proposed a method

---

[2] When Pe_c exceeds 10, then Equation (1.49) can be approximated with an error of < 1% according to $Pe \approx 4\ \pi\ R^{*2} + 1.5$

which could overcome these limitations. According to this method, an imperfect signal could be used provided it was monitored at *two* downstream locations. The column Peclet number was estimated using the equations given below:

$$\frac{1}{Pe_c} = \frac{E}{uL'} = \frac{\sigma_2^2 - \sigma_1^2}{2\tau_r^2} \qquad (1.51)$$

In equation (1.51), τ_r is the residence time and L´ is the distance between the two measuring points. τ_r is given by equation (1.52).

$$\tau_r = \mu_2 - \mu_1 \qquad (1.52)$$

where τ_1, τ_2 and σ_1^2, σ_2^2 are the first and the second moments respectively of the response curve at the two measurement points. The first and second moments were defined earlier by equations (1.47) and (1.48) respectively.

The above methods are applicable to differential contactors. For stage-wise contactors the unsteady state material balance is written in the finite difference form as follows:

$$(1 + \alpha_j) c_{j,n-1} - (1 + 2 \alpha_j) c_{j,n} + \alpha_{j,n+1} = \frac{Vh_j}{F_j}\frac{dc_j}{dt} \qquad (1.53)$$

where the subscript j refers as before to the phase in question and F_j refers to the volumetric flow rate. Since the tracer is non transferring the mass transfer term is omitted. The solution due to Sawinsky and Hunek (1981) is given below:

$$C_m(\theta) = 2N\, a^{n-p}\, \alpha \sum_{i=1}^{N} D_i \exp(-z_i\theta) \qquad (1.54)$$

Here N refers to total number of stages in the extractor with the tracer injected in stage p and

response measured in stage n. The terminology for the other variables in this solution is given below.

$C_m(\theta)$ = dimensionless concentration on stage m at time θ

θ = dimensionless time, $tF/(V_t h_j)$

$a = [(1+\alpha)/\alpha]A^{1/2}$

$D_i = (-1)^{i+1}E_i F_i/(1+z_i)$

$E_i = a \sin (N+1-n)\Psi_i - \sin(N-n)\Psi_i$

$F_i = a \sin p\Psi_i - \sin(p-1)\Psi_i$

$z_i = N[1+2\alpha (1- a \cos\Psi_i)]$

and Ψ_i is the i^{th} root of the following equation

$$(a-1)\left(\tan\left(\frac{i\pi}{2} - \frac{N\Psi_i}{2} \right) \right) = (a + 1) \tan\left(\frac{\Psi_i}{2}\right) \qquad (1.55)$$

However this solution was limited to lower values of α when the response curve oscillated strongly at small values of θ. The method developed by Dongaonkar (1989) was applicable under these conditions.

A variation of the unsteady state tracer injection is the technique developed by Kim and Baird (1976a). In this method the tracer undergoes an instantaneous chemical reaction with the phase whose axial mixing parameters are to be determined. An indicator which changes colour during the course of this reaction is used to determine E_j. However the system used in the study may demand special material of construction to avoid corrosion problems. A typical example is the reaction of sodium hydroxide (tracer) with hydrochloric acid (continuous phase) using phenolphthalein as indicator in the estimation of E_c.

1.11.3 Estimation of Axial mixing parameters from profiles obtained during mass transfer

The dispersion model and the backflow model described in sections 1.8 can be used to estimate the axial mixing parameters based on the data obtained from actual mass transfer runs. The samples of both the phase are withdrawn from different positions along the column. The sampling technique is critical because contamination of one phase with the other can drastically affect the accuracy of the results. The experimental data points ($X_{expt.}$ and $Y_{expt.}$) are compared with the dispersion or backflow model predictions ($X_{pred.}$ and $Y_{pred.}$). A parameter estimation procedure involving the minimization of a suitably chosen objective function is often used. A typical objective function is represented by equation (1.56)

$$Z = \sum_{i=1}^{N_s} [\ \gamma_i\ (X_{expt.}-X_{pred.})^2 + \ \delta_i\ (Y_{expt.}-Y_{pred.})^2] \qquad (1.56)$$

Here N_s refers to the number of samples obtained from the column and γ_i and δ_i are suitably chosen weights to enhance the accuracy of the estimation process. An advantage of this technique is that the true number of transfer units can also be estimated.

1.11.4 Comparison of the Measurement Techniques

The relative merits of the different tracer measurement techniques are summarized in table 1.2.

1.12 Measurement of axial mixing in the Dispersed Phase

All the techniques described above have limitations when applied to the dispersed phase. It is difficult to inject the tracers uniformly into the dispersed phase. Estimating the dispersed phase axial mixing coefficient directly under mass transfer conditions is complicated by the difficulty in obtaining uncontaminated samples of the dispersed phase. Further the concept of

Table 1.2 Comparison of tracer techniques

Method	Advantages	Disadvantages
Steady state tracer	Easy to model	High tracer consumption
		Detects only back-mixing
Unsteady state tracer	Minimal tracer use	Mathematically more complicated to model
	Estimates axial mixing	
Chemical reaction technique	No sampling is required	The system is corrosive to the column
Mass transfer concentration profile measurements	Axial mixing effects on mass transfer can be directly determined	Special samplers must be used

axial mixing is not strictly applicable to the dispersed phase. As mentioned earlier forward mixing of the drops is more important than back-mixing. Levenspiel and Fitzgerald (1983) warned against the misuse of the axial mixing model for the dispersed phase. The Gaussian response curve obtained by this model can also be obtained by the more realistic forward mixing model. The statistical information obtained from the residence time distribution of the two models had different functional relationships with the column parameters. For example the standard deviation from the axial mixing model's RTD was proportional to square-root of the column length whereas the forward mixing model predicted a linear relationship.

1.13 Relevance of Axial Mixing Concept in Industry

Since the early 1960s, a voluminous amount of research has been done on axial mixing in academic institutions. A survey was conducted (Aravamudan, 1993) to study advances in practical application of research on axial mixing in industries. This survey classified axial mixing studies into i) Research undertaken by industries alone based on information available in open literature ii) collaborative research involving industries and academic institutions iii) Research

undertaken by universities to specifically suit industrial needs. Some of the results of the survey are presented below.

In industries there is a definite trend to incorporate the axial mixing effects as an increment to the plug flow height of transfer unit. This increment is usually expressed as a function of the continuous phase and dispersed phase Peclet numbers. A summary based on the information contained in the Handbook of Solvent Extraction (Lo et al. 1983) is given in table 1.3. Industries are often concerned with the scaling up of data available from small diameter (pilot scale) columns to columns used in industry. In most extractors, axial mixing increases with column diameter. Unfortunately, data available from academic institutions are mainly from small diameter columns. Elsässer and Bühlman (Kühni AG, Switzerland) adopted a scaling up procedure by conducting tests on a pilot plant and industrial Kühni extractors. The effect of scale was determined on the back-mixing parameters. The pilot plant column (15 cm in diameter) operated on a side stream from an industrial column (80 cm in diameter). Methylene chloride was used as the solvent to extract DMF from an aqueous effluent. The dispersion coefficients were obtained in both columns by steady and dynamic tracer injection tests. The columns were operated and the concentration profiles were determined. The backflow model was used to obtain the concentration profiles and scaled back-mixing parameters were used in the industrial column. However, the volumetric mass transfer coefficient ($k_{ox}a$) obtained in the pilot plant column was used in the industrial column. The data obtained in the industrial column was in good agreement with the backflow model predictions.

Some typical industry-university collaborative work on axial mixing studies is given in table 1.3. In recent times there is an increasing trend for academicians to make the research on axial mixing meaningful to the industry. Ricker et al. (1981) developed a calculation procedure

for simulating multi-solute counter-current extraction process with complex equilibrium relationships. Arun Kumar and Hartland (1989) used previously published data to develop a single general correlation for predicting continuous phase axial mixing in pulsed columns. Data was obtained from steady state and transient tracer injection experiments. In all, 28 systems were considered and 992 data points were processed. The significance in this correlation lies in the inclusion of the physical properties along with the column and operating variables. The authors recommend the correlation to be used for design purposes under mass transfer conditions. This correlation considers that the column diameter to have an insignificant effect on axial mixing. Similar correlations were proposed by the same authors (1992) to predict axial mixing coefficients in the continuous and dispersed phases under mass transfer conditions for both Rotating disk and Asymmetric rotating disk extraction columns. These were based on 1055 data points.

Pratt and Stevens (1992) describe a scaling up procedure for extraction columns in which axial mixing effects are included. The effect of column diameter on the axial mixing parameters are determined. The performance of the pilot scale column is determined in terms of the extract composition at the outlet. Using Pratt's (1975, 1976) simplified solutions to the diffusion and backflow model and the pilot column height and performance the true height of transfer units (H_{ox}) are determined for the differential contactors and the number of transfer units (N_{ox}) for stage-wise contactors respectively. These parameters and the desired column performance are then used in the simplified solutions to calculate the full scale column length or number of stages. For stage-wise contact the agitation rate for the industrial column is adjusted in such a way that mean drop sizes and velocity are similar to those of the pilot column. Some adjustment may be required for N_{ox}.

Table 1.3 Summary of correction methods for axial mixing in commercial extraction equipment (Lo et al., 1983)

Column	Author and affiliation	Axial Mixing correction	Additional Details
RPC	T.C. Lo[3] J. Prochazka[4]	$(f_2/f_1)=(D_2/D_1)^{-0.14}$	Optimum Agitation rate decreases with increase in column diameter due to axial mixing.
RDC	W.C.G.Kosters[5]	$HTU_{industrial}=HTU_{pilot\ scale}+HDU;$ $HDU=f(Pe_c,Pe_d)$	Both Peclet numbers are functions of column diameter.
ARDC	T. Mišek[6] J. Marek[7]	$HTU_{corrected}=HTU_1+f(E_c, E_d)$	HTU_1 incorporates the forward mixing effects also.
Kühni columns	A. Mogli and U. Bühlmann[8]	$HTU_{overall}=HTU_{plug}+HDU$	Procedure was refined subsequently (Elsässer and Bühlmann 1986)
PPC	A.J.F. Simons[9]	$HTU_{overall}=HTU_{od,plug}+HDU_{od}$ $HDU=f(Pe_c, Pe_d)$	Axial Mixing is independent of column diameter

[3] Hoffman La Roche, Inc. U.S.A.

[4] Institute of Process Fundamentals, Prague

[5]Shell Internationale Petroleum Maatschaoppij B.V. The Netherlands

[6]Research Institute of Chemical Equipment, Czechoslovakia

[7]Luwa AG, Switzerland

[8] Kühni Ltd. Switzerland

[9] DSM / Central Laboratory Geleen, The Netherlands

Table 1.4 Collaboration between industry and university on axial mixing research

Column	Author	Affiliation	Nature of the work
Kühni	1.Breyesse 2.Bühlmann 3. Godfreys (1984)	1. Rhode Poulenc., France 2. Kühni Ltd., Switzerland 3. University of Bradford, U.K.	Single phase stationary tracer tests on industrial and pilot scale columns.
PPC	1.Simons, Van Sluys 2. Goebel, Fortuin (1986)	1. DSM Research BV 2. University of Amsterdam	Tracer studies on lab and industrial scale
Pulsed Column	1. Hussain, 2. Slater 3. Marrocchelli (1986)	1. University of Bradford, U.K. 2. ENEA, Italy	Stationary tracer tests on columns of different diameters
RPC	1. Karr, Ramanujam 2. Lo 3. Baird (1987)	1. Chem Pro, U.S.A. 2. Hoffman La Rosche Inc., U.S.A. 3. McMaster University, Canada	Axial mixing studies on columns of different diameters determine scale up formulae.
RDC	1. Janosi 2. Hunek (1988)	1. Chinoin Drug and Chemical Unit Operations, Budapest 2. Department of Chemical Unit Operations, Budapest	Axial mixing studies using pulse injection method
RPC	1. Holmes 2. Karr 3. Baird (1990)	1. Otto York Company, U.S.A. 2. McMaster University, Canada	Effect of density gradient in the continuous phase on axial mixing values.

1.14 Scope of the present thesis

1.14.1 Introduction

The aim of this thesis is to investigate the axial mixing characteristics of a 2 inch reciprocating plate extraction column in the presence of an unstable density gradient in the continuous phase. The density gradient in the continuous phase may be induced either when measuring E_c by the tracer techniques or during actual mass transfer conditions. Depending on the variation of density with axial distance, the gradient can be stable or unstable. Defining the origin at the continuous phase inlet at the top of the column and the positive direction as upwards, the density gradient is **stable** if the continuous phase density increases with decreasing distance (-z). When the density decreases with decreasing z i.e. when a denser continuous phase is above the lighter one, the density gradient is **unstable** since it disturbs the equilibrium resulting in natural convection currents. Baird et al. (1992) identified the possible situations in which the unstable density gradient can arise in extraction columns. In this table, the density coefficient k, is defined as $d\rho_c/dc$.

Table 1.5 Conditions for unstable density gradient in extraction columns, c - continuous, d- dispersed (from Baird et al. 1992)

#	Flow direction of continuous phase	Mass transfer direction	Effect of increasing solute concentration on density
1	upward	c→d	reduces (k< 0)
2		d→c	increases (k>0)
3	downward	c→d	increases (k>0)
4		d→c	reduces (k<0)

1.14.2 Evidence of unstable density gradient influencing mixing in the continuous phase

In this section, some instances in the literature where the unstable density gradient effects were present in the continuous phase are described. As shown below , the works on pilot scale extraction equipment under mass transfer and non mass transfer conditions in the presence of unstable density gradient in the continuous phase indicate increasing inefficiency as shown by increase in H.T.U. values or more directly axial mixing coefficients.

1. Taylor (1954) One of the earliest works in which the unstable density gradient effects were studied was due to Taylor (1954). In this work Taylor briefly discussed the effect of gravity on the diffusion and mass transport. A solution of higher density was placed over that of a pure solvent in a tube. Both horizontal and vertical arrangements were considered. In the former case the dispersion current due to buoyancy were found negligible when compared to that of the convection. When the tube was vertical the heavier solution descended into the lighter one forming the downward current. The displaced solvent moving upward formed the counter current. The solute in the downward current diffused into the rising current of solvent and thereby reduced the density difference which drove the current. Gradually equilibrium was attained and the vertical current ceased at a critical axial density gradient. The critical density gradient was defined as

$$\frac{dc}{dz} = 67.94\frac{D_{AB}\mu_c}{g\rho_c kr^4} \qquad (1.57)$$

where D_{AB} is the coefficient of molecular diffusion and r is the radius of the tube. After this gradient is attained, the vertical transport is only due to molecular diffusion. Taylor (1954) suggested the use of this method to determine D_{AB}. Lowell and Anderson (1982) extended this

method to two solutes in vertical capillary tubes with radii around 1 mm. It was found that at critical concentration gradient conditions, both the solutes (sodium dichromate and mannose) had penetrated to the same extent down the tube. Quinn et al. (1986) confirmed the applicability of Taylor's hydrodynamic instability criterion in determining the diffusion coefficient for solutes ranging from simple molecules to colloidal particles. It must be noted that this work was done in narrow tubes of diameters approximately 1 mm in diameter.

2. Sege and Woodfield (1954) Rosen and Krylov (1967) observed that channelling phenomenon can be encountered in plate extraction columns when the density of the phase moving downwards is sharply reduced on account of extraction. This was explained to be due to the axial circulations which develop in the heavy continuous phase. As an example, they cited the example of the extraction of uranyl nitrate as studied by Sege and Woodfield (1954). In this study the performance characteristics of a 3 inch diameter pulsed column were determined. Tributyl phosphate (TBP) with carbon tetrachloride was used as the organic (O) phase while the aqueous phase (A) was uranyl nitrate $UO_2(NO_3)_2$ dissolved in nitric acid. Both extraction and stripping operations were studied. The density gradient in the continuous phase can be either stable or unstable depending on the direction of mass transfer and the density of the solute involved. Some typical cases examined in this study are given in table 1.6. It can also be noted that either phase can be dispersed without affecting the nature of the density gradient in the continuous phase. The study indicated that when the mean diametric clearance between the plates and the wall of a 3 inch diameter column was increased from 0.015 inches to 0.125 inches, the H.T.U. for system 1 was not adversely affected. However in system 2 considerable channelling along the wall for plates with higher clearance resulted in an approximately 50% increase in HTU. The authors also compared the HTU s of a 3 inch diameter column with those of an 8 inch diameter column.

Systems with an unstable density gradient consistently exhibited a higher HTU in the larger diameter column. The increase in HTU s were for some cases as high as 90 % (system 3). These increases were attributed to increased channelling. However when systems with stable density gradient were used, column diameter did not usually have a significant effect on the HTU It must be noted that Sege and Woodfield (1956) did not identify the density gradient effect with the increase in HTU values.

3. Bensalem (1985) studied the mass transfer characteristics of a 7.6 cm diameter Karr column using the system water(c↓)-acetone-toluene(d↑). Since the density of acetone is lower than that of water, mass transfer in the d→c direction resulted in an unstable density gradient. The gradient was stable for the reverse mass transfer process. Axial mixing estimation from the concentration profiles indicated that E_c under d→c conditions were much higher than the c→d direction. The E_c values in the latter case were close to those obtained in the absence of mass transfer. Bensalem (1985) attributed the increase in E_c values for the d→c mass transfer case to the circulation effects induced in the continuous phase by the presence of large drops. Again, the density gradient effect was not identified by Bensalem (1985) as a possible contributor to increasing axial mixing.

4. Cusack and Karr (1991) were the first to specifically identify the density gradient effect as one of the key areas of investigation in pilot plant studies. According to these authors, unstable density gradients in the continuous phase resulted in significant circulation in the continuous phase which manifested in form of increased axial mixing. The density gradient effect was found to be more serious in columns of large diameters. The authors cited practical experience with this phenomenon and recommended that pilot scale studies should be performed in the column with the largest feasible diameter and prudent safety factor should be included in the scale-up. It was

Table 1.6 Nature of density gradient in the continuous phase; typical examples in counter-current metal extraction process

(from Sege and Woodfield, 1954)

System	Diluent	Direction of U transfer	Aqueous influent[10]	Organic influent[1]	A/O[11]	($d\rho/dz$)
1	CCl_4	A→O	0.8 $UO_2(NO_3)_2$; 2.4 HNO_3; sp.gr., 1.35	sp.gr., 1.4	0.5	stable
2	CCl_4	O→A	0.03 HNO_3; sp.gr.,1.0	0.4 $UO_2(NO_3)_2$; 0.2 HNO_3; sp.gr., 1.5	1.75	unstable
3	Hydro-carbon	A→O	0.18 $UO_2(NO_3)_2$; 3.3 Na salts; 2.6 HNO_3; sp.gr., 1.3	sp.gr., 0.81	0.6	unstable
4	Hydro-carbon	O→A	0.01 HNO_3; sp.gr.,1.0	0.11 $UO_2(NO_3)_2$; 0.1 HNO_3; sp.gr., 0.85	0.8	stable

[10] Solute concentrations in moles per litre.

[11] A/O - Aqueous to Organic flow rates

also noted that apart from practical experience there was virtually no published literature on this phenomenon.

The authors recommended that the unstable density gradients can be avoided by

1. Refluxing the continuous phase.
2. Switching the dispersed and continuous phase.
3. Using a single mixer settler stage before the phase enters the extraction column proper. This procedure is useful especially when most of the density gradient occurs in the initial sections of the column.

5. Dongaonkar et al. (1991) studied the mass transfer and axial dispersion in a 72.45 mm diameter Kühni extraction column for the system MIBK(d↑)-acetic acid-Water(c↓). In most cases, acetic acid transferred in the c→d direction. The axial mixing coefficient was measured by the continuous and transient tracer techniques. When the comparison was made under non mass transfer conditions, the two methods gave comparable results. Under mass transfer conditions, the axial mixing coefficient was estimated from the solute concentration profiles using the backflow model.

In some of the mass transfer runs a pulse of non transferring tracer was simultaneously injected into the continuous phase and the unsteady state response was monitored. Thus two independent estimates of α_c were obtained. The experimental results revealed the following:

1. α_c values from mass transfer profiles were always significantly smaller than those obtained from the tracer profiles.
2. When the transient tracer results obtained from mass transfer runs were compared with those obtained from non mass transfer conditions it was found that the former conditions mostly resulted in higher values of α_c (table 1.7)

The authors attributed the smaller mass transfer profile predictions of α_c to non uniform conditions prevailing in the lower section and the settling zone at the top of the column. When zero weight was given to these upper and lower sections of the column in the parameter estimation procedure, α_c values increased but were still lower than the transient tracer results

Table 1.7 Effect of solute transfer on axial mixing coefficient (Dongaonkar et al. 1991)

#	$Q_c(cm^3/s)$	$Q_d(cm^3/s)$	Rotor speed (rpm)	α_c		
				mass transfer profiles	transient tracer	
					Mass transfer	
					present	absent
1	4.78	9.26	120	0.48	1.35	1.15
2	3.76	6.16	110	1.39	2.20	1.37
3	3.76	6.16	130	1.09	2.10	1.63
4	3.76	8.20	120	1.01	1.35	1.45
5	4.78	10.34	120	0.53	1.77	1.20
6	4.78	8.20	120	0.55	1.90	0.90
7	4.78	9.26	120	0.32	1.87	1.15
8	3.76	9.26	120	0.98	2.35	1.37
9	6.34	9.26	120	0.56	1.55	0.97

obtained in the presence of mass transfer. The enhancement in α_c due to mass transfer was explained to be due to the contribution of entrained wakes behind droplets. However the authors admitted that the increase in α_c due to mass transfer required further investigation.

Since acetic acid is heavier than water, its extraction into MIBK leads to a decrease in the density

of the continuous phase down the column resulting in unstable density gradient conditions. This possibility was not discussed by Dongaonkar et al. (1991).

6. Holmes et al. (1991) observed that RPCs used in industry suffered from excessive back-mixing when the extraction conditions led to a significant unstable density gradient in the continuous phase. To quantify their observations, they conducted single phase steady state axial mixing measurements in a 7.62 cm diameter KRPC. Typically a 44% by weight calcium chloride solution was introduced at the top of the column while pure water was introduced from the bottom. The unstable density gradient was induced by the flux of $CaCl_2$ due to back-mixing. Solution samples were analyzed by the refractive index method and the concentration profiles thus generated were used in determining the back-mixing coefficient. The results indicated that the E_c values were considerably greater than those obtained with uniform density (neutrally buoyant) liquids. While the E_c values in this study were in the order of 5-50 cm^2/s in the density difference range 0.001 to 0.1 g/cm^3, Kim and Baird (1976) and Hafez et al. (1979) obtained values around 1-3 cm^2/s for 5.08 and 15 cm diameter columns respectively in the absence of densitty gradient. When extrapolating the results to very small density values Holmes et al. (1991) observed that the E_c values tended to cluster around the same range viz. 1-3 cm^2/s. Further the E_c values were not constant axially along the column. Holmes et al. (1991) characterized the density effect in terms of the buoyant energy dissipation rate per unit mass (ϵ_b) similar to that of mechanical energy dissipation (ϵ_m). ϵ_b was defined as follows:

$$\epsilon_b = \frac{g u_c \Delta \rho}{\rho_c} \qquad (1.58)$$

When the E_c values in the absence of mechanical agitation were correlated with ϵ_b the following

expression was obtained:

$$E_{co} = 9.32\epsilon_b^{0.347} \tag{1.59}$$

When the effects of mechanical agitation were included the back-mixing coefficients could be correlated as

$$E_c = 9.52\epsilon_b^{0.535}\epsilon_t^{-0.186} \tag{1.60}$$

where ϵ_t was taken as the sum of ϵ_b and ϵ_m. The authors noted that when $\epsilon_m \rightarrow 0$, the exponent on ϵ_b in equation (1.60) was 0.349 which compared favourably with that of 0.347 obtained in equation (1.59). Applying the Kolmogoroff's isotropic turbulence theory (to be explained in detail in section 2.4.1) to the case with no agitation the authors further noted that the theory predicted

$$E_{co} = l^{\frac{4}{3}}\epsilon_b^{\frac{1}{3}} \tag{1.61}$$

which was in close agreement with the equation (1.59) where E_{co} was related to $\epsilon_b^{0.347}$. Using dimensional analysis, Holmes et al. (1991) related the axial mixing coefficient to the density gradient and gravitational constant as follows:

$$E_c = l^2\left(\frac{g}{\rho_c}\frac{d\rho}{dz}\right)^{\frac{1}{2}} \tag{1.62}$$

7. Baird and Rama Rao (1991) extended this study to very small density gradients induced by feeding hot water (75 °C) at the bottom of the column as the main continuous phase and adding cold water which entered at the top. Due to back-mixing the cold water mixed with the hot water and a temperature profile was established in the axial direction. Due to the non linear variation

of the density with temperature the buoyant energy dissipation term in equation (1.58) was modified as:

$$\epsilon_b = u_c g(T-T_2)\frac{1}{\rho_c}\frac{d\rho}{dT} \tag{1.63}$$

where T_2 was the temperature of the hot water entering the column. A few experiments were also conducted using NaCl as the tracer. Since the equation (1.59) unrealistically indicated that the mixing length in the presence of mechanical agitation but no buoyancy ($\epsilon_b \rightarrow 0$) would become zero, the authors modified the overall mixing length l as follows:

$$l = l_m + (l_b - l_m)(\frac{\epsilon_b}{\epsilon_t})^n \tag{1.64}$$

where l_m is the mixing length determined by mechanical energy dissipation. Hence using the Kolmogoroff concept the back-mixing coefficient was modelled as

$$E_c = [l_m+(l_b-l_m)(\frac{\epsilon_b}{\epsilon_t})^n]^{\frac{4}{3}}(\epsilon_m + \epsilon_b)^{\frac{1}{3}} \tag{1.65}$$

This equation indicated that when $\epsilon_b \rightarrow 0$, E_c is still given by

$$E_c = l_m^{\frac{4}{3}}\epsilon_m^{\frac{1}{3}} \tag{1.66}$$

Regression analysis on the experimental data indicated that l_m, l_b and n were respectively 0.301 cm, 4.02 cm and 0.34. When this equation was used to determine the effect of the buoyant energy dissipation on E_c relative to values obtained only in the presence of mechanical agitation, these authors found that E_c was significantly enhanced as soon as ϵ_b exceeded zero.

E_c values doubled when the buoyant energy dissipation was only a very small fraction (0.0002) of the mechanical energy dissipation.

8. Baird et al. (1992) studied the effect of the unstable density gradient in a single phase system under transient state conditions. A pulse of dense tracer (sodium chloride solution) was injected at the top the column into a tube containing a stationary mass of pure water. Similar axial mixing measurements under transient state conditions reported in literature had been presumably carried out by using a tracer whose density was identical to that of the bulk continuous phase. The unsteady state equation for the dispersive flux N_z can be expressed as follows:

$$\frac{\partial N_z}{\partial z} = \frac{\partial c}{\partial t} \tag{1.67}$$

The flux in turn can be written as

$$N_z = -E_c \frac{\partial c}{\partial z} \tag{1.68}$$

Hence, using equation (1.62) and equation (1.68) in equation (1.67), the following expression is obtained

$$\frac{\partial c}{\partial t} = \alpha \frac{\partial}{\partial z}\left(\frac{\partial c}{\partial z}\right)^{\frac{3}{2}} \tag{1.69}$$

where α is defined as

$$\alpha = l^2\left(\frac{gk}{\rho_c}\right)^{\frac{1}{2}} \; ; \; k = \frac{d\rho}{dc} \tag{1.70}$$

The boundary conditions applicable to this situation are given below:

$$z < 0,\ t = 0,\ c = 0 \tag{1.71}$$

$$z = 0,\ t = 0,\ c = \frac{m_t}{A_{cs}}\delta_o(z) \tag{1.72}$$

$$z = 0,\ t > 0,\ \frac{\partial c}{\partial z} = 0 \tag{1.73}$$

$$z = -\infty,\ t \geq 0,\ c = 0 \tag{1.74}$$

Further the amount of tracer (m_t) injected over a cross sectional area A should be a constant at all time t which leads to the following equation:

$$\frac{m_t}{A_{cs}} = \int_{-\infty}^{0} c\ dz \tag{1.75}$$

The analytical solution to the partial differential equation subject to the above boundary conditions was developed using the Lie group technique. The solution given in equation was verified by solving the p.d.e. numerically using the finite difference technique.

$$c(z,t) = 0.6646\left(\frac{m_t}{A_{cs}}\right)^{\frac{5}{6}}(\alpha t)^{-\frac{1}{3}}\left[1-\left(-0.2662z\left(\frac{m_t}{A_{cs}}\right)^{-\frac{1}{6}}(\alpha t)^{-\frac{1}{3}}\right)^{\frac{5}{3}}\right]_+^3 \tag{1.76}$$

The subscript + indicates that the concentration profile is applicable only for values of z ranging from 0 to $-z_o$ when the term c(z,t) is positive. At values of $z \rightarrow z_o$, c(z,t) tends to zero. The limiting value of z_o is given by

$$z_o = -3.756\left(\frac{m_t}{A_{cs}}\right)^{\frac{1}{6}}(\alpha t)^{\frac{1}{3}} \qquad (1.77)$$

This represents the limit of salt penetration at a given time. Experiments were conducted in tubes of different diameters and the mixing lengths obtained using the above model are given in table 1.8. In the 2.63 cm diameter tube, experiments were also conducted in the presence of a stationary plate stack and using a viscous glucose solution. Flow visualization studies indicated that with decreasing tube diameter and increasing viscosity, the flow acquired an increasingly laminar character. In the viscous glucose solution large fluctuating striations termed fingers were observed. Under these conditions the mixing length corresponded to the stable length of these "fingers" which could exceed the column diameter (table 1.8). Further discussion on these aspects in relation to this work is given in chapter 4.

9. Baird and Legree(1994) investigated the natural convection of heated air in insulated vertical tubes of various diameters and open at the top. The unstable gradient was applied by heating the air at the bottom, thereby decreasing its density relative to the top. The resulting heat transfer due to natural convection was modelled in terms of the steady state one dimensional mixing length concept. Temperature profiles along the axis of the tubes were obtained and the heat flux (q) was related in terms of the eddy thermal diffusivity (E_c) as follows:

$$q = -\rho_c E_c C_p \frac{dT}{dz} \qquad (1.78)$$

Following Holmes et al. (1991), the eddy diffusivity was related to the temperature gradient as

$$E_c = l^2\left(-\left(\frac{g}{T}\right)\frac{dT}{dz}\right)^{\frac{1}{2}} \qquad (1.79)$$

Using ideal gas theory for ρ_c (= P/{RT}) and the expression for E_c, the following expression for Q was obtained.

$$Q = l^2 C_p \frac{Pg^{\frac{1}{2}}}{R}\left(-\frac{1}{T}\frac{dT}{dz}\right)^{\frac{3}{2}} \qquad (1.80)$$

The mixing lengths were obtained from the slope of the semi-logarithmic plot of experimental temperature vs. axial distance by re-expressing equation as follows:

$$-\frac{d(\ln T)}{dz} = \left(\frac{QR}{l^2 C_p Pg^{\frac{1}{2}}}\right)^{\frac{2}{3}} \qquad (1.81)$$

The results indicated that the axial mixing coefficients characterizing the eddy diffusivity were 3 orders of magnitude greater than the thermal diffusivity represented by $k/\rho C_p$ thereby confirming the turbulent nature of the process. The *l*/D ratios obtained in this study are given in table 1.8.

1.14.3 Summary and discussion on the density gradient effects identified in the literature

The previous studies on unstable density gradients due to Taylor (1954), Lowell and Anderson (1982), Quinn et al. (1986) have focussed on capillary tubes whose diameters were only a few millimetres in diameter. Laminar flow conditions prevailed in these experiments. The quantitative treatment on the unstable density gradient effect on axial mixing under turbulent flow conditions is relatively new even though Rosen and Krylov (1967), who cited Sege and Woodfield's (1954) work and Karr and associates (1990,1991) noted its influence. The reason why quantitative treatment of the unstable density gradient effect had not been attempted earlier could be due to its rather small magnitude and the difficulty of distinguishing its effects from

those of other contributing factors to axial mixing.

The knowledge on the unstable density gradient effect prior to the work related to this thesis can be summarized as follows:

1. Quantitative axial mixing studies involving the unstable density gradient have been conducted under single phase conditions by Holmes et al. (1991), Baird and Rama Rao (1991), Baird et al. (1992) and Baird and Legree (1994). In all these studies the mixing length concept has been used to correlate the axial mixing coefficient and the density gradient group. The value of the mixing length under no agitation (l_s) as compared to that of the column diameter under study is given in table 1.8.
2. Baird et al. (1992) noted that as the column diameter became smaller the ratio of the estimated mixing lengths to column diameter were no longer similar.
3. When mechanical agitation is applied it was found that the overall mixing length decreased. Holmes et al. (1991) explained this observation to the reduction in the eddy size leading to lower axial mixing.
4. The above studies have focussed on the single phase flow conditions only.

   induced is given in parenthesis.

In order to make the study more relevant to industrial situation, axial mixing data are required under two phase flow conditions especially in the presence of mass transfer. Hence in this study two phase axial mixing data were collected initially under non mass transfer conditions. In the next stage axial mixing data in the presence of mass transfer-induced unstable density gradient conditions were obtained.

Table 1.8 Summary of mixing lengths obtained by previous workers

#	Researchers	System	Column	D (cm)	l_b (cm)	l_b/D (-)
1	Holmes et al. (1991)	Water ($CaCl_2$ soln.)	KRPC	7.62	5.3	0.70
2	Baird and Rama Rao (1991)	Cold Water (Hot water) Water (NaCl soln.)	KRPC	5.08	4.02	0.79
3	Baird et al. (1992)	Water (NaCl soln.)	E.T.[12]	2.63	2.5	0.95
			Tube + baffle	2.63	2.5, 2.2[13]	0.95 0.84
			E.T.	1.91/ 1.48	2.4/ 2.1	1.26/ 1.42
		Glucose solution (NaCl soln.)	E.T.	2.63	7.5	2.85
			Tube + baffle	2.63	6.0, 7.5	2.28 2.85
4	Baird and Legree (1994)	Cold air (Hot air)	E.T.	21.3 24.5 27.7	32.6 35.0 36.0	1.53 1.43 1.30

Note: System refers to the continuous phase only. The method by which the density gradient was

1.15 Summary and Conclusions

The reciprocating plate column is a versatile and commonly used type of extractioon equipment in the industry. The Karr RPC, which is studied on the pilot scale form in the present work, is used in U.S.A. while the Prochazka RPC and KRIMZ, GIAP columns are used in East Europe and Russia. Agitation, in the oscillatory form, is used in RPCs to increase interfacial area and efficiency of mass transfer. However, the flow pattern deviates significantly from ideal

[12] E.T. - Empty cylindrical tube

[13] l= 2.5 cm for plate spacing, H = 5.15 cm and 2.2 cm for H = 2.65 cm

plug flow conditions leading to reduction in the concentration driving force for mass transfer. These effects, originally attributed to circulation effects in bubble columns, were also later identified with mechanical agitation and channelling. Wehner and Wilhelm (1956), Sleicher (1959, 1960) quantified these effects while Miyauchi and Vermeulen (1963a) obtained analytical expressions for the concentration profiles after solving the model equations. Since axial dispersion leads to a considerable loss in efficiency of an extractor, it is critical to have reliable estimate of its value. For this purpose, steady state or transient tracer tests are performed and quantitative expressions are available to estimate the axial dispersion parameters from the tracer profile. A relatively less common approach involves the direct estimation of axial mixing from concentration profiles due to mass transfer. Until this technique was perfected, the results from non mass transfer experiments were applied to mass transfer conditions as well. Regardless of the technique used it is important that the hydrodynamic situation in the column should be correctly interpreted if the correlations and scale-up design are to be accurate. This study focuses on a new factor responsible for back-mixing, viz. the presence of an unstable density gradient in the continuous phase.

CHAPTER 2

LITERATURE REVIEW ON HYDRODYNAMIC AND MASS TRANSFER ASPECTS OF RPCS

2.1 Introduction

The first part of this chapter is a review of the literature on reciprocating plate extraction columns (RPC). The literature on RPCs may be classified into two categories:

(i) Performance studies on pilot scale and industrial columns mainly involving the estimation of mass transfer parameters like height equivalent to a theoretical stage (HETS) and volumetric efficiency.

(ii) Fundamental studies in academic institutions which include measurement of drop size, hold-up and axial mixing.

A brief summary on the first category where limited information is available in the open literature is given. The review for the second category includes results on hold-up, drop size, mass transfer and axial mixing in both gas-liquid and liquid-liquid systems. Research on pressure drop is omitted from this review for reasons of space and for not being relevant to the present thesis. The work on power consumption is briefly described in chapter 4 for modelling purposes. Since a considerable amount of literature on RPCs has accumulated over the years this review had to be organized in the following manner:

1. The aspects of RPCs other than axial mixing are summarized with a general discussion and table of correlations/model equations. Correlations having theoretical basis or developed using several systems and hence covering a range of physical properties are tabulated.

Purely empirical correlations developed for only one system and hence having very limited applicability are not reproduced. However these references are cited in a separate table for completion. Finally, in table 2.13 the experimental details like column used and ranges of experimental variables are given for all the works mentioned.

2. Hydrodynamic and mass transfer studies on KRIMZ and GIAP columns, which has been discussed in detail by Konstanyan et al. (1973, 1977, 1979 and 1980) are not included in this review. A brief summary on these type of columns including the industrial design methodology is provided by Baird et al. (1992, 1994).
3. A detailed review on axial mixing is given in section 2.4.

2.2 Industrial performance studies

Prochazka et al. (1971) outlined the features and advantages of a vibrating plate extractor and gave some performance results for both pilot and production scale units. The process used in this illustration involved the extraction of caprolactam from its aqueous reaction mixture by tri-chloroethylene solvent and its re extraction from the organic solvent by pure water. The results are reproduced in table 2.1. The 50 cm diameter column is used in the industry with a capacity of 18000 tonnes per annum of caprolactam.

Karr made an extensive study of mass transfer performance in pilot and industrial scale reciprocating plate columns. The two systems used in this study were

1. MIBK - acetic acid - water (Easy system)
2. O-Xylene - acetic acid - water (Difficult system)

Typical results for system 2 are illustrated in figure 2.1.

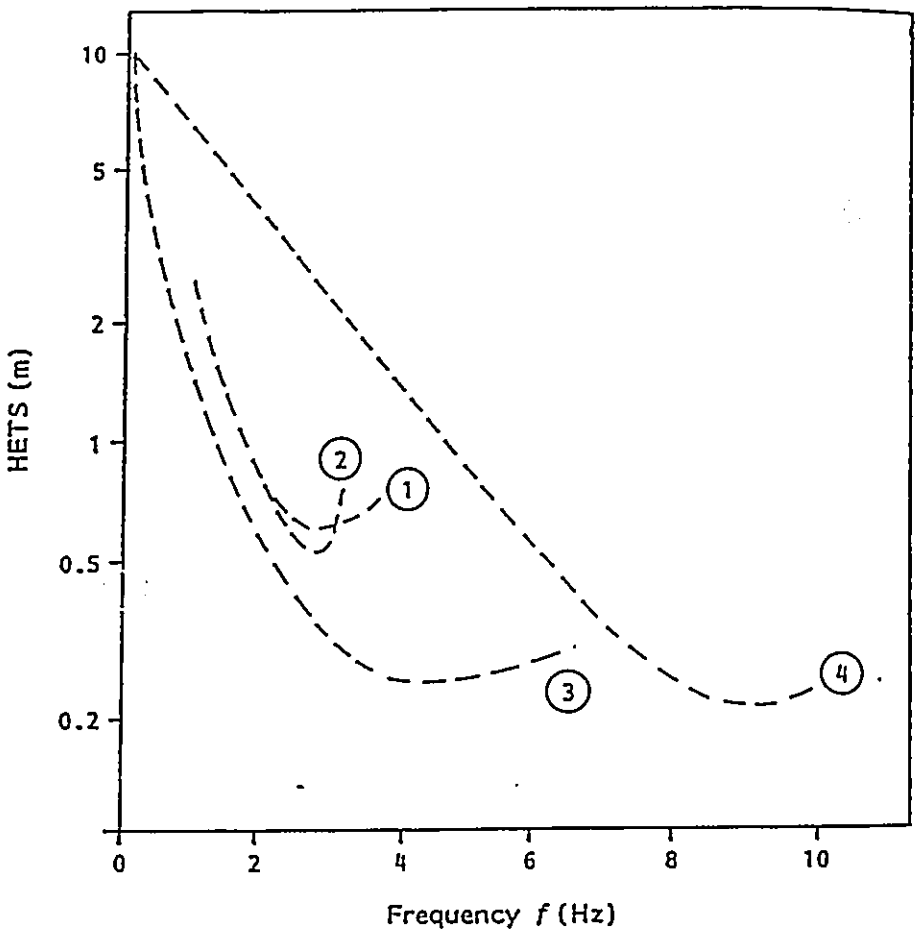

Figure 2.1. Effect of reciprocating speed on HETS, *o*-xylene–acetic acid–water system (redrawn from Karr and Lo, 1979). Water dispersed, $H = 25$ mm, $(V_c + V_d) = 4.8$ mm/s

Curve	D_C (mm)	A_p (mm)	Mass transfer direction
1	914	12.7	$c \rightarrow d$
2	914	12.7	$d \rightarrow c$
3	76	12.7	$c \rightarrow d$
4	76	6.3	$c \rightarrow d$

Table 2.1 Pilot and industrial scale RPC performance data for Caprolactam extraction (Prochazka et al., 1971)

Column/operating variables	Direction of solute transfer					
	aqueous (d) → organic(c)			organic(d) → aqueous(c)		
diameter (cm)	14.0	29.3	50.00	5.00	14.0	50.00
Effective height of column (m)	3.6	5.5	6.0	3.0	3.6	8.0
Throughput (m^3/m^2h)	73	73	60	92	90	80
HETS (m)	0.46	0.48	0.70	0.44	0.52	1.10
Volumetric efficiency, η^* (h^{-1})	159	152	85	210	173	71

The classification into easy and difficult systems was based on the extent of agitation required for good dispersion and high mass transfer performance. It is to be noted that interfacial tension for system 2 is higher than system 1. Experiments were conducted in 1, 3, 12 and 36 inch columns using the above systems. The following characteristics were observed in common:

1. The HETS decreased with agitation until the flooding limit was reached, beyond which it started to increase (fig. 2.1)
2. The minimum attainable HETS increased with increase in column diameter and throughput.

The results obtained were summarized by Lo and Prochazka (1983) and a representative sample is reproduced in table 2.2.

On the basis of these data, scale-up ratios were suggested by Karr and Lo (1971, 1976 and 1979) and they have been successfully implemented on commercial level. The scale-up procedure

suggested by the authors consisted of the following steps:

1. Mass transfer data were obtained in 1, 2 and 3 inch columns for specified throughput.
2. The optimum conditions using the criterion of maximum volumetric efficiency and plate spacing were determined. (Volumetric efficiency was defined as the ratio of throughput to HETS.) According to Karr and Lo (1971) the plate spacing is dictated by the variation in interfacial tension along the column. Since increasing solute concentration reduced interfacial tension and hence drop size the authors recommended a larger plate spacing in the rich zone of the column to reduce the power input by mechanical agitation. The following equation was proposed for optimum plate spacing:

$$H \propto \frac{1}{\Delta\rho_{cd}^{\frac{5}{3}}\gamma^{\frac{3}{2}}} \tag{2.1}$$

3. The minimum $HETS_2$ corresponding to optimum design column performance can be scaled from pilot plant data using equation 2.2 given below.

$$\frac{(HETS)_2}{(HETS)_1} = \left(\frac{D_c}{D_1}\right)^{0.38} \tag{2.2}$$

The exponent 0.38 was higher than the average value (=0.25) obtained for the easy system. However the exponent value of 0.38 was based on the difficult system, and was recommended for a conservative design. However if the system used in the design column varied significantly from the difficult system the exponent may be slightly varied depending on the required agitation.

Table 2.2 a: Pilot and Industrial scale performance data for KRPC system (i) Lo and Prochazka (1983)

D (cm)	A (cm)	H (cm)	f (Hz)	extractant	dispersed phase	$(HETS)_{min}$ (cm)	Throughput (m/h)	η^* (hr^{-1})
2.54	2.54	2.54	6	MIBK	Water	7.87	23.31	296
2.54		2.54	2.53	Water	MIBK	20.57	41.97	204
7.62		2.54	5.5	MIBK	Water	12.45	24.45	196
7.62		2.54	3.83	Water	Water	17.01	47.59	280
7.62		5.08	4.0	Water	Water	19.69	69.55	353
30.48	2.54	2.54	7.17	Water	MIBK	14.73	22.29	151
			4.07	MIBK	MIBK	11.18	24.41	218
			4.17	MIBK	Water	18.29	24.53	134
			3.75	Water	Water	17.78	22.61	127
			4.58	Water	MIBK	24.13	48.04	199

Table 2.2 b: Pilot and Industrial scale performance data for KRPC system (ii) Lo and Prochazka (1983)

D (cm)	A (m)	H (cm)	f (Hz)	Extractant	dispersed phase	$(HETS)_{min}$ (cm)	throughput (m/h)	η^* (h^{-1})
7.62	5.08	2.54	4.45	Water	Water	23.11	17.28	75
7.62	2.54	2.54	8.95			20.83	17.28	83
91.44	5.08	5.08	5.67			23.11	32.76	142
91.44	5.08	2.54	2.8			59.18	17.32	29
91.44	5.08	2.54	2.8	o-Xylene	Water	50.80	18.00	36

4. The amplitude, plate spacing and throughput are maintained the same as the pilot column. The required agitation speed was calculated from

$$\left(\frac{f_2}{f_1}\right) = \left(\frac{D_1}{D_2}\right)^{0.14} \qquad (2.3)$$

5. For large diameter columns baffle plates were recommended.

The deterioration in efficiency with increasing column diameter as indicated by increase in minimum HETS was attributed mainly due to axial mixing. The correlations developed by Karr and Lo though being simple and commercially practical are still empirical. Karr et al. (1987) used the two phase axial mixing data from 2.54 cm and 15 cm columns and single phase axial mixing data from a 50.8 cm diameter column in order to verify the empirical scaling relations. It was assumed, due to the lack of 2 phase experimental data for the largest column, that the scale effect on E_c under two phase flow conditions was similar to that observed for single phase flow conditions. When a constant value of E_d (=10 cm^2/s) was assumed, the authors found that the exponent was 0.36 which was close to that given in equation (2.2).

2.3 Basic hydrodynamic and mass transfer phenomena in RPCs

In this section the basic hydrodynamic variables necessary for the design of a reciprocating plate column are described. Axial mixing is described in greater detail in a separate section.

For efficient design of any extraction column it is important to understand the properties of the system to be used in the process. The physical properties mainly interfacial tension, density (difference), and to a limited extent viscosity play a vital role in determining the hydrodynamic variables in the column. Power dissipation along with the physical properties determine the drop size and hence the hold-up. Columns can handle only a certain throughput

after which it is no longer possible to maintain the counter-current flow. The variation of hold-up value at flooding with respect to the flow rates determines the operating limit and the minimum column diameter required for the operation. The conservative diameter value is chosen after fixing the performance at a certain percentage of the flooding. The safe flow velocities are then determined. Using the drop size and hold-up, interfacial area and estimates of the overall mass transfer coefficient can be obtained. The HTU is determined from the overall mass transfer coefficient and the flow velocity. The specified degree of extraction and HTU determine the height of the column under ideal plug flow conditions. The plug flow value is refined by taking axial mixing into consideration. Axial mixing influences the entire design procedure in a complex way since it is a function of column diameter and alters the value of the mass transfer coefficient and HTU from the plug flow values. The design flow sheet, based on Lo and Prochazka (1983) is illustrated in figure 2.2.

2.3.1 Drop Sizes

Drop size plays an important role in determining the extraction efficiency and the operating limit of the contactor. While agitation increases the interfacial area, it also increases the residence time of the droplets and ultimately flooding may result. Drop sizes and their distribution are usually measured by a photographic technique followed by a suitable counting procedure. An average estimate of the drop sizes in the column is given by the Sauter mean diameter expressed as follows:

$$d_{32} = \frac{\Sigma_{j=1}^{n} d_j^3}{\Sigma_{j=1}^{n} d_j^2} \qquad (2.4)$$

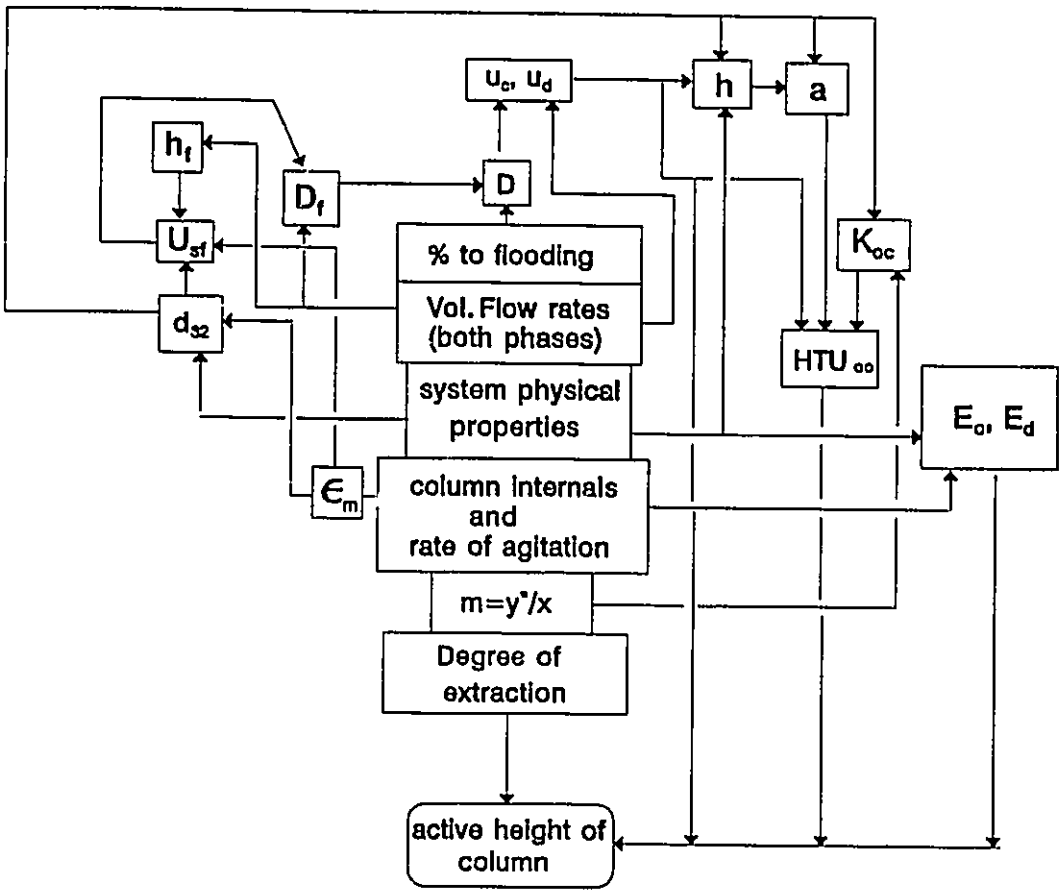

Figure 2.2 Interaction of basic hydrodynamic variables in extractor design (Lo and Prochazka, 1983)

Hinze (1955) was one of the earliest investigators to quantitatively predict the drop diameter in dilute drop dispersions where coalescence effects were negligible compared to drop breakage. The drop in the liquid medium is subject to surface stress (τ) leading to deformation of the drop and interfacial stress (γ/d) which tends to counteract this deformation. A generalized Weber group ($N_{We}=\tau d/\gamma$) representing the ratio of these stresses was defined. Due to the external stress acting on the drop, internal flows were created which led to a viscous stress of magnitude (μ_d/d) $(\tau/\rho_d)^{0.5}$. These stresses, expressed by dimensionless combinations of the three, determined the deformation and break-up of the drop. One such combination resulted in the viscosity group ($N_{vi}=\mu_d/(\rho_d\gamma d)^{0.5}$) which was determined only by the physical properties. Since the Weber group and viscosity group contain all the three stresses, they are sufficient to describe the drop deformation and break-up. Experimentally it was shown that when the Weber number equalled or just exceeded a critical value the drop breakage occurred in a simple fashion and the Weber group was related to the viscous group as

$$(N_{We})_{crit.} = C[1+f(N_{vi})] \tag{2.5}$$

where C is an empirical constant. Under turbulent flow conditions the viscous group term becomes negligible and the Weber number was described by

$$N_{We_{crit.}} = \frac{\rho_c \overline{v^2} d_{max}}{\gamma} = C \tag{2.6}$$

In this equation it can be noted that the dynamic pressure forces in turbulent flow assumed to cause the drop breakage are represented in the following manner:

$$\tau = \rho_c \overline{v^2} \tag{2.7}$$

These forces were created because of the velocity variations over a distance equal to the maximum drop diameter (d_{max}). v^2 is the square of the velocity differences over a distance equal to d_{max} averaged across the entire flow field. If isotropic turbulence can be assumed, then the turbulence pattern characterised by v^2 can be related to the energy dissipation rate per unit mass ϵ in a simple manner. Kolmogoroff (1941) proposed the following relationship:

$$\overline{v^2} = K(\epsilon d_{max})^{\frac{2}{3}} \tag{2.8}$$

Substituting this relationship in equation (2.6) and solving for d_{max} yields the following equation:

$$d_{max} = C_1 \frac{(\frac{\gamma}{\rho_c})^{0.6}}{\epsilon^{0.4}} \tag{2.9}$$

Since ϵ is related to the energy dissipation rate per unit volume (ψ) by

$$\epsilon = \frac{\psi}{\rho_c} \tag{2.10}$$

equation (2.9) is often represented as

$$d_{max} = C_1 \frac{\gamma^{0.6}}{\rho_c^{0.2} \psi^{0.4}} \tag{2.11}$$

The average drop diameter in the dispersion is of more practical importance than the maximum drop diameter. Boyadzhiev and Spassov (1982) noted that based on experimental studies of drop formation in agitated vessels the ratio d_{32}/d_{max} is in the range of 0.38-0.67. The expression for

d_{32} used by these authors is given in table 2.3.

The above equation finds frequent application in Karr RPC literature under moderate to high agitation conditions. When the agitation is non existent or very small the above equation is not valid. The drops sizes are then determined by the distributor design and the balance of forces between buoyancy and the interfacial tension. The approximate equation for drop size under these conditions is given by:

$$d_{32} = C_2\left(\frac{\gamma}{g\Delta\rho_{cd}}\right)^{\frac{1}{2}} \tag{2.12}$$

For RPCs with very small holes and fractional free area the drop diameter in the mixer-settler regime is also determined by the balance between interfacial tension and buoyancy forces at the plate perforation (Baird et al., 1994). It can be expressed as:

$$d_{32} = C_3\left(\frac{6d_o\gamma}{g\Delta\rho_{cd}}\right)^{\frac{1}{3}} \tag{2.13}$$

Jiricny and Prochazka (1980) studied the drop size distribution along the column length for the system 1,2 dichloroethane (d↓)-water(c↑)[1]. They found in general that the fractional volume distribution of the drops indicated a bimodal distribution at the top of the column which gradually changed to a uni-modal one towards the continuous phase inlet. The bimodal distribution was explained to the production of fines by the distributor, unsymmetrical breakage of large drops and entrainment of the small drops by the continuous phase. With increasing distance away from the distributor, repeated breakage and coalescence and entrainment of the

[1] The arrows indicate the direction of flow of the phases

smallest drops resulted in a uni-modal distribution. At very high agitation intensities where the breakage effects were dominant the authors found that there was an increasing tendency towards uni-modal distribution.

Sovova (1983) developed a stage-wise poly-dispersion model for the Karr column in which the drop size distribution and the hold-up were described as functions of drop transport, breakage and coalescence. A binary system, water (c↓)-di-chloroethane (d↑) under non mass transfer conditions was used to illustrate the use of the model.

Jares and Prochazka (1987) studied the breakup rate and size distributions of droplets in a Karr column using the binary systems of water-1,2 dichloroethane, water-toluene and water-n-butanol. Kolmogoroff's isotropic turbulence was assumed and drop breakage was attributed to turbulent eddies in the continuous phase. The mother drop was observed to be split into Ω daughter droplets very close to the downstream side of the plate. The conditional probability of a drop breaking into daughter droplets decreased with increase in Ω. The authors explained this due to the shift in the turbulent energy distribution towards higher energy containing eddies. The drop size distribution was approximated by a beta distribution.

Sovova (1990) has reviewed the correlations developed for d_{32} in both pulsed and reciprocating plate columns. The author made the following critical observations:

1. The effect of the distributor is ignored implying that the drops had passed through a sufficient number of plates. Further variation in drop size distribution along the column is not a factor in these correlations.
2. The coalescence of drops are not taken into account. The interfacial tension effect on drop size depending on mass transfer direction was also not considered. Thus the correlations can at best be used for slowly coalescing systems. Notable among the correlations considered

were those developed by Baird and Lane (1973), Nemecek and Prochazka (1974) and Boyadzhiev and Spassov (1982).

3. The correlations developed did not cover the whole range of agitation rates i.e. from no agitation to high agitation. At low agitation rates drops were broken by a) collision with the plates b) shear forces due to large drops moving through plate holes c) force due to gravity. At high agitation rates the drops were broken by the turbulent eddies.

Sovova (1990) gave the following correlation applicable over the entire range of agitation rates.

$$d_{32} = \frac{1}{\sqrt{\left[\frac{1}{\left(\frac{0.81\gamma}{\Delta\rho_{cd}\, g}\right)} + \frac{1}{d_o^2} + \frac{1}{d_{32}'^2}\right]}} \qquad (2.14)$$

The drop diameter due to turbulent eddies d_{32}' is determined by the energy dissipation rate with the pre-constant of 0.37 (equation 2.11). ϵ was related to agitation rate as follows:

$$\epsilon = 18.3\, I^3 \frac{(1-S_p^2)}{S_p^2\, z^*} \qquad (2.15)$$

S_p is the effective free area of the plate equipped with downcomer, I is the intensity of agitation and z^* is the height of the region of dissipation. S_p and I are defined as follows:

$$S_p = \frac{S_d}{(1-S_c)} \qquad (2.16)$$

$$I = k\, a^{0.9} f^{1.1} \; ; \; k = 1(ms)^{0.1} \qquad (2.17)$$

where S_d is defined as the fractional free area in the hole region of the plate and S_c is the fractional free area in the downcomer region (applicable for Prochazka RPCs).

(Different exponents are used on amplitude and frequency to indicate that the intensity increases at a slightly faster rate with frequency than with amplitude for harmonic vibration of the plates).

The height of agitated zone z^* was given by

$$z^* = \min(0.17\ S_q^{-0.33}\ I^{0.5}\ ;\ H) \tag{2.18}$$

Here S_q is the sum of S_d and S_c.

The more general correlations for d_{32} are given in table 2.3 and the remaining references are listed in table 2.4. The numbers in parenthesis in tables 2.3 and 2.4 refer to the location of the references in the list of experimental conditions (table 2.13).

Table 2.3 Correlations for d_{32} in Reciprocating plate columns

1(1)[2]Baird and Lane (1973)

kerosene (c↓)-water (d↑)
kerosene+mineral oil (c↓)-water(d↑)
kerosene(c↓)-aqueous NaCl solution(d↑)
MIBK(c↓)-water(d↑)

for high agitation levels

$$d_{32} = 0.357\frac{\gamma^{0.6}}{\psi^{0.4}\rho^{0.2}}$$

for low agitation levels

$$d_{32} = 0.357\frac{\gamma^{0.6}}{\rho_c^{0.2}(\psi_1+\psi_2)^{0.4}}$$

where

$$\psi_1 = \frac{2\pi^2}{3}\frac{(1-S^2)}{C_o^2 S^2 h}\rho_c (Af)^3 \quad ; \quad C_o = 0.7$$

and

$$\psi_2 = g\Delta\rho_{cd}\left(u_d + \frac{h}{1-h}u_c\right)$$

2(6) Miyanami et al. (1975)

MIBK/toluene/n-hexane/kerosene (d↑) - water (c↓)

(ii) drop size (cm)

when Af is zero or small;

$$d_{32} = 0.5\sqrt{\frac{\gamma}{\Delta\rho_{cd}}}$$

---

[2] The numbers in parenthesis refer to the locations of these references in the list of experimental conditions (table 2.13)

Table 2.3 continued ...

At higher Af,

$$d_{32} = \sqrt{\frac{2.45\ \gamma}{\Delta\rho_{cd}\ g}}\ \left(We \le 0.032\ (Bo^*)^{0.83} \right)$$

$$d_{32} = 0.18 We^{-\frac{3}{5}} d_d \quad (We > 0.032(Bo^*)^{0.83})$$

where the modified Bond number is defined as follows:

$$Bo^* = \left(\frac{\Delta\rho_{cd}\ d_d^2\ g}{\gamma}\right)$$

3(10) Boyadzhiev and Spassov (1982) kerosene+carbon tetra chloride(d↑)-water(c↓)

$$d_{32} = k_2 \frac{\left(\frac{\gamma}{\rho_c}\right)^{\frac{3}{5}} S^{\frac{4}{5}} d_o^{\frac{2}{5}}}{(Af)^{\frac{6}{5}}} \quad when\ \frac{\rho_c (Af)^3}{2S^2} > 0.48 \qquad [kg/s^3]$$

$$k_2 = 0.57 \pm 0.11 \quad [-]$$

4(11) Rama Rao et al. (1983)

kerosene(d↑)-water(c↓)

11(iii)
when Af=0.0, $K_1 = 0.025\ (cm/s^2)^{0.5}$

$$d_{32} = K_1 \left(\frac{\gamma}{\Delta\rho_{cd}}\right)^{0.5}$$

when Af > 0 the following is valid

Table 2.3 continued ...

$$d_{32} = 0.45(0.5Af)^{-1.2} = 0.287\frac{\gamma^{0.6}}{\rho_c^{0.2}\psi^{0.4}}$$

5 (20) Prabhakar et al. (1988) kerosene (d↑)-benzoic acid-water(c↓); both d→c and c→d
kerosene (d↑)-butyric acid-water(c↓); both d→c and c→d

$$d_{32} = K(\frac{\gamma^{0.6}}{\rho_c^{0.2}\psi^{0.4}})h^{0.2}S^{-0.2}$$

solute	Mass transfer direction	K_1
Benzoic acid	d→c	0.10
	c→d	0.13
n-butyric acid	d→c	0.17
	c→d	0.13

6 (18 ii)Rama Rao and Baird (1988) air (d↑)-water(c↓)

$$d_{32} = 0.357\frac{\sigma^{*0.6}}{\rho_m^{0.2}\psi_m^{0.4}}$$

7 (21) Sundaresan and Varma (1990) air (d↑) - water(c↓)

Mixer settler region, Af ≤ 2.5 cm/s

$$d_{32} = 0.65(0.5Af)^{-0.33}u_d^{0.06}u_c^{-0.206}d_o^{-0.1}S^{0.21}$$

Emulsion regime, Af > 2.5 cm/s

$$d_{32} = 0.42(0.5Af)^{-0.17}u_d^{0.3}u_c^{-0.38}d_o^{-0.1}S^{0.16}$$

[c.g.s. units]

Table 2.4 List of remaining references on drop size measurements in RPCs

number	source	system
1(2)	Nemecek and Prochazka (1974)	Trichloroethylene (d↓)-water(c↑)
2(3)	Tojo et al. (1974b)	Air(d↑)-CO_2-Water (c↑); d→c
3(4)	Tojo et al. (1975)	MIBK (d↑)-acetic acid-water(c↓); d→c
4(14 ii, iv and v)	Bensalem (1985)	Toluene(d↑)-acetic acid-water(c↓); no mass transfer, d→c, c→d
5(23)	Chen and Liu (1991)	Air(d↑)-water(c↓)

It must be noted that these correlations are applicable when coalescence is not a major factor. Coalescence effects become important when :

1. The drop populations increase and a very dense dispersion is formed (i.e. very high agitations leading conditions close to flooding).
2. Mass transfer induced interfacial phenomena occur (Groothuis and Zuiderweg, 1960). For instance when an interfacial tension lowering solute transfers from the dispersed to continuous phase, enhanced drop coalescence will result. Since the solute transfer into the film separating the two drops produces a greater decrease in the interfacial tension than the transfer into the bulk liquid, there is a variation in the interfacial tension along the drop. This creates interfacial tension gradients causing the film to drain off rapidly (figure 2.3) and drop coalescence is promoted. When the same solute transfers from continuous to dispersed phase, then the gradients promote the flow of the bulk liquid into the film thereby hindering drop coalescence.

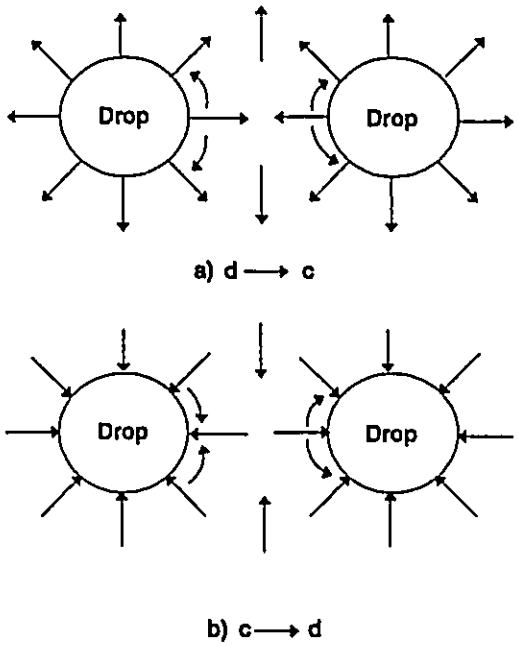

Figure 2.3 Effect of solute transfer direction on coalescence of drops (Laddha and Degaleesan, 1983)

2.3.2 Hold-up

Hold-up is defined as the ratio of the volume of the dispersed phase to the total operating volume of the contactor. It can be classified into *operational* hold-up and *static* hold-up. Operational hold-up refers to freely moving drops which are mainly responsible for the mass transfer, while static hold-up refers to the dispersed phase trapped at the contactor internals and contributes very little to the mass transfer. (Laddha and Degaleesan, 1983). Hold-up is an important design variable and is closely related to the drop size and interfacial area according to the relation:

$$a = \frac{6h}{d_{32}} \tag{2.19}$$

2.3.2.1 Hold-up in Reciprocating Plate Columns

The hold-up behaviour with respect to the operating variables such as flow rates and agitation in RPCs is determined by the operation regime. In the **mixer settler** regime observed in contactors having plates with small fractional free area ($S < 0.4$) and small perforation diameters a light dispersed phase tends to accumulate under the plate as a discrete layer. When the plate moves up the continuous phase is displaced down through the perforations. During the downward motion the dispersed phase is forced through the perforations as globules which rise and then coalesce to form a discrete layer below the next plate (Rama Rao et al., 1983). The operation in this regime is facilitated by a high interfacial tension and low interphase density difference of the system. The hold-up in the mixer settler regime is determined primarily by the depth of the dispersed phase formed under each plate. Prabhakar et al. (1988) observed that the plate perforation diameter played an important role in determining the hold-up in this regime.

In the **emulsion** regime, the dispersed phase is uniformly distributed in the continuous phase as drops and does not collect at the plates. Karr columns operate only in the emulsion regime. Typical hold-up versus agitation plots for the main types of RPCs is illustrated in figure 2.4 (Baird et al., 1994). The hold-up plot for Tojo-Miyanami columns is similar to that of the Karr column. The fractional free area of the plate plays an important role in determining the hold-up in this regime (Prabhakar et al., 1988).

The common practice in hydrodynamic studies has until recently been to assume an uniform hold-up in the column. However this is not always the case as shown in a study by Jiricny and Prochazka (1980). The authors measured the variation of hold-up along the column using a series of differential pressure transducers. The system used was 1-2 dichloroethane (d↓)-water(c↑) with a stagnant region of the continuous phase at the bottom of the column. It was

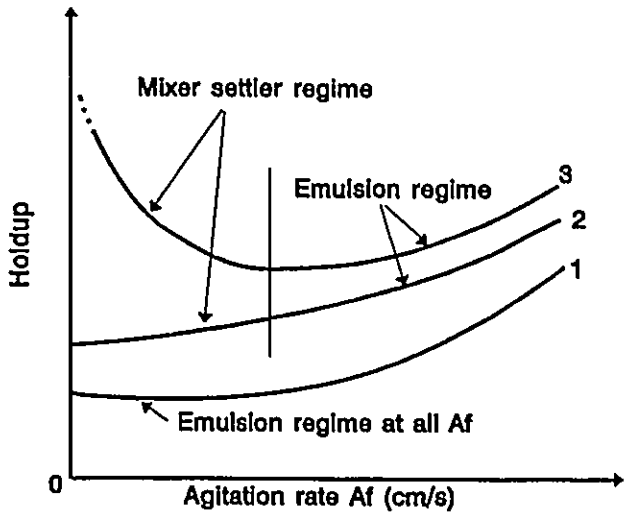

1.Karr RPC 2. Prochazka RPC

3.RPC with no downcomers and low fractional free area

Figure 2.4 Hold-up characteristics of different types of RPC (Baird et al., 1994)

observed that the hold-up profile had two maxima along the length of the column at high flow rates of either the dispersed or continuous phase. At moderate values only one maximum was observed. When both the flow rates or the agitation intensity (Af) were high, a monotonically decreasing hold-up profile with two inflection points was obtained. The observations were attributed to the formation of fine droplets and their transportation towards the continuous phase exit and accumulation, leading to local increases in hold-up especially at high throughput and agitation rates. The accumulation was further aided by the presence of a large settling section for the continuous phase at the top of the column which prevented carry over of the dispersed phase. It must be noted in this study that the distributor design, the enlarged continuous phase settling zone and the stagnant zone beneath the continuous phase inlet had significant effects on the hold-up profiles.

2.3.2.2 Equations for Hold-up in Karr column

Hold-up under counter-current flow conditions is related to the phase flow rates according to the following classical relationship the concept of which was proposed by Lapidus and Elgin (1957):

$$\frac{u_c}{1-h}+\frac{u_d}{h} = U_s \tag{2.20}$$

The slip velocity U_s can be expressed by the following equation:

$$U_s = \bar{u}_o(1-h) \tag{2.21}$$

where $\bar{u}_o$ is the characteristic velocity. The characteristic velocity is correlated in terms of the system properties, average drop size *and* hold-up.

Baird and Lane (1973) attempted to develop a model for hold-up in RPCs by extending the analogy of pressure drop in fluidized beds using Ergun's (1952) equation to liquid-liquid dispersions. Expressing the void fraction in the column h' in terms of dispersed phase hold-up (h) by:

$$h' = (1-h) \tag{2.22}$$

and assuming that the drops were of uniform size with sphericity factor unity, Ergun's equation can be rewritten as

$$(\frac{\Delta P}{z})\frac{d_{32}(1-h)^3}{\rho_c v_s^2 h} = \frac{150h}{Re} + 1.75 \tag{2.23}$$

where v_s, the superficial velocity of the continuous phase relative to the drops is given by

$$v_s = U_s(1-h) = (\frac{1-h}{h})u_d + u_c \qquad (2.24)$$

The drop Reynolds number in equation (2.23) was based on v_s. The pressure drop term can be related to the net weight of the dispersed phase by the equation:

$$\frac{\Delta P}{z} = h\ \Delta\rho_{cd}\ g \qquad (2.25)$$

Substituting this equation (2.25) into equation (2.23), Baird and Lane (1973) obtained the following equation:

$$\frac{d_{32}(1-h)^3 g \Delta\rho_{cd}}{\rho_c v_s^2} = \frac{150h}{Re} + 1.75 \qquad (2.26)$$

Baird et al. (1971) approximated the R.H.S. of equation (2.26), at intermediate drop Reynolds number, as a multiple of $Re^{-0.5}$. This assumption was based on the observations by Gayler et al. (1953) regarding the similar relationship of the drag coefficient of single particles, with Reynolds number at intermediate values. Hence,

$$\frac{d(1-h)^3 g \Delta\rho_{cd}}{\rho_c v_S^2} = K^*(\frac{h}{Re})^{0.5} \qquad (2.27)$$

The value of the empirical parameter K is determined by the degree of circulation of the drop.

$$K^* = 15 \text{ (circulating drops)} \qquad (2.28\ a)$$

$$K^* = 30 \text{ (rigid drops)} \qquad (2.28\ b)$$

From equations (2.24) and (2.27) velocity (U_s) can be expressed as follows.

$$U_s = \frac{(1-h)d_{32}}{K^{*\frac{2}{3}}h^{\frac{1}{3}}}\left[\frac{g^2\Delta\rho_{cd}^2}{\rho_c\mu_c}\right]^{\frac{1}{3}} \tag{2.29}$$

Slater (1985) developed a modified slip velocity equation which is given below:

$$U_s = \bar{u}_o(1-h)^m + bh^n \tag{2.30}$$

The above equation was used by Slater and co-workers previously for RDC (1984) and Kühni (1985) extraction column data. According to Slater (1985), the characteristic velocity was found comparable to the terminal velocity of the particle and can be estimated by assuming either rigid or mobile conditions. The second part of the above equation is important only at conditions of high coalescence rates leading to hold-up greater than 50 %. When extending the application of this equation to KRPCs using the hold-up at flooding data of Baird and Shen (1984), the exponent m in equation (2.30) was related empirically to d_{32} as

$$m = 24\ d_{32} \tag{2.31}$$

where d_{32} is in cm.

Kumar and Hartland (1988) reviewed the published results on hold-up measurements in Karr columns and developed a general correlation for its prediction.

$$h = [k_1 + k_2(Af)^3]u_d^{0.81}(u_c+u_d)^{0.32}\Delta\rho_{cd}^{-0.98} \tag{2.32}$$

They found that the effect of interfacial tension was insignificant. The constants k_1 and k_2 for different operating conditions are tabulated in table 2.5[3].

Since hole size and continuous phase density did not vary over a wide range in the data

---

[3] note: S.I. units are used throughout in this correlation; Hence the constants are very high.

considered they were not accounted for in this correlation.

Table 2.5 Constants used in generalized hold-up correlation

operating condition	k_1	k_2
no mass transfer	3.87×10^3	3.71×10^7
mass transfer (d→c)	2.14×10^3	1.65×10^7
mass transfer (c→d)	3.25×10^3	7.54×10^7
plates wetted by dispersed phase	7.91×10^3	3.23×10^6

The important correlations developed for predicting hold-up in RPCs are given in table 2.6 while the empirical correlations of limited applicability are referred to in table 2.7. The experimental conditions pertaining to all these works on hold-up are given in table 2.13.

Table 2.6 Correlations used for predicting hold-up (h) in RPCs

1(1) Baird and Lane (1973)

kerosene (c↓)-water (d↑)
kerosene+mineral oil (c↓)-water(d↑)
kerosene(c↓)-aqueous NaCl solution(d↑)
MIBK(c↓)-water(d↑)

hold-up

$$\frac{d(1-h)^3 g(\rho_c-\rho_d)}{\rho_c v_s^2} = \frac{150h}{Re} + 1.75$$

(c.g.s. units)

2(6) Miyanami et al. (1975)

MIBK/toluene/n-hexane/kerosene (d↑) - water (c↓)

When $Af < Af_c$

$$h_o = 0.21 u_d$$

where Af_c= 2.4 cm/s (for triangular and sinusoidal vibrational wave forms)
= 0.9 cm/s (for trapezoidal wave form)

When $h_o \leq 0.09$, $h \leq 0.50$, $N_h \leq 5.0$ and for all Af

$$\ln(\frac{h}{h_o}) = 2.17[1-\exp(-0.8N_h)]$$

where

$$N_h = \frac{\rho_m}{\Delta\rho_{cd}} We^{\frac{3}{5}} Fr$$

with

Table 2.6 continued..

$$We = \frac{\rho_m}{\gamma}(n\ a'f)^2 d_d\ ;\ Fr = \frac{4n(a'f)^2}{g d_d}$$

where n is a factor charracterizing the vibrating wave form

3 (11) Rama Rao et al. (1983)

a) air(d↑)-water(c↓)
b) air(d↑)-kerosene (c↓)
c) kerosene(d↑)-water(c↓)
d) MIBK (d↑)-water(c↓)

(11 i) **Gas-Liquid (systems a and b)**

$$h_{MS} = 0.049 We^{0.37} Re^{-0.05} \left(\frac{D}{d_o}\right)^{0.53} N^{0.4} \left[\frac{\sigma_c^*}{\sigma_w^* - \sigma_d^*}\right]^{0.23}$$

$$h_{EM} = 0.017 We^{0.37} Fr^{0.16} Re^{0.147} \left(\frac{D}{d_o}\right)^{0.36} N^{0.66} \left[\frac{\sigma_c^*}{(\sigma_w^* - \sigma_d^*)}\right]^{-0.88}$$

(11 ii) **Liquid-Liquid (system c and d)**

$$h_{MS} = 0.335 We^{0.37} Re^{-0.145} \left(\frac{D}{d_o}\right)^{0.43} N^{0.4} \left[\frac{\sigma_c^*}{\sigma_w^* - \sigma_d^*}\right]^{-0.4}$$

$$h_{EM} = 3\times10^{-3} We^{0.37} Fr^{0.16} Re^{0.66} \left(\frac{D}{d_o}\right)^{0.85} N^{0.4} \left[\frac{\sigma_c^*}{(\sigma_w^* - \sigma_d^*)}\right]^{-0.15}$$

where modified Reynolds number (Re) is defined as $(Af)d_o\Delta\rho/(S\mu_c)$

and the subscripts MS and EM refer to the mixer settler and emulsion regimes respectively.

The following correlation was also proposed:

$$\frac{u_d}{h} + \frac{(u_c + Af)}{(1-h)} - \frac{W_1\ h}{(1-h)} = W_2$$

Table 2.6 continued...

system	W_1	W_2
gas-liquid (a and b)	55	19
Liquid-liquid (c and d)	42	3

4 (18) Rama Rao and Baird (1988a) system: air (d↑)- water (c↓)

18(i)

$$\frac{u_d}{h} + \frac{(u_c+Af)}{1-h} - 55\frac{h}{1-h} = 19$$

5 (20) Prabhakar et al. (1988)

a) kerosene (d↑)-water(c↓)
b) kerosene (d↑)-benzoic acid-water(c↓); both d→c and c→d
c) kerosene (d↑)-butyric acid-water(c↓); both d→c and c→d

A. Hold-up for systems a, b and c

Mixer-Settler region

$$h = A(Fr)^{0.3}\left(\frac{u_d}{u_c+Af}\right)^{0.15}$$

Emulsion regime

When Af < 2.5 cm/s

$$h = B\ Fr_m\ Ga^{0.35}\ S^{-0.5}$$

Af ≥ 2.5 cm/s

$$h = C\ Fr_m\ Ga^{0.35}\ S^{-1}$$

where

Table 2.6 continued...

Constant	No Mass Transfer	With Mass Transfer		
		Benzoic acid	n-butyric acid	
		d→c	d→c	c→d
A	1.950	1.900	-	-
B	0.183	0.110	0.16	0.19
C	0.093	0.072	-	-

and

$$Fr = \frac{u_d^2}{gd_o}; \quad Fr_m = \frac{u_d^{0.75}(u_c+Af)^{1.25}}{gd_o}; \quad Ga = \frac{d_o^3 g \rho_d^2}{\mu_d^2}$$

(ii) Hold-up for systems b and c were also compared with the following correlation

$$\frac{u_d}{h} + \frac{u_c+Af}{1-h} = \frac{h}{1-h} S^{0.85} + 0.03$$

6 (21) Sundaresan and Varma (1990) a) air (d↑) - water(c ↑ & ↓)
b) carbon dioxide (d↑) - water(c ↑ & ↓)

(i) Hold-up (system b)

Co-current flow

$$h = 10 Fr^{0.38} We^{0.3} Ga^{-0.04} S^{-0.19}$$

Counter-current flow
for mixer settler regime, Af ≤ 2.5 cm/s

$$h = 0.85\ Fr^{0.42} \left(\frac{u_d}{u_c+Af}\right)^{0.13} Ga^{0.04}\ S^{0.03}$$

For emulsion regime, Af > 2.5 cm/s

Table 2.6 continued...

$$h = 8.68Fr^{0.38}We^{0.3}Ga^{-0.04}S^{-0.19}$$

7 (22) Chen and Liu (1991)

a) kerosene(d↑)-benzoic acid-water (c↓)
b)MIBK(d↑)-acetic acid-water(↓)

$$U_s = \frac{u_d}{[(1-\delta)h]} + \frac{u_c}{[(1-\delta)(1-h)]} = \bar{u}_o(1-h)$$

(where δ = column voidage)

(for system a alone the following equation is valid)

$$\bar{u}_o = 5.26[\frac{(0.5Af)^3}{(H\beta)}]^{-\frac{1}{3}}H^{0.27}$$

(for systems a and b the following equation is valid)

$$\bar{u}_o = 5.26[\frac{(0.5Af)^3}{(H\beta)}]^{-\frac{1}{3}}H^{0.27}(\frac{\gamma}{\gamma_{K-W}})^{\frac{1}{6}}$$

where

$$\beta = \frac{\alpha^2}{[(1-\alpha)(1-\alpha^2)]}$$

and α = plate voidage

8 (23) Gomma et al. (1991)

air(d↑)-water(c↓)

$$\frac{u_d}{h}+\frac{u_c+0.5Af}{1-h} = 0.38\frac{h}{1-h} + 0.112$$

Table 2.7 Remaining references on hold-up investigations in RPCs

Number	Source	System
1(2)	Nemecek and Prochazka (1974)	Trichloroethylene(d↓)-water(c↑)
2(3)	Tojo et al. (1974 b)	air(d↑)- CO_2- water(c↑); d→c
3(4)	Tojo et al. (1975)	MIBK (d↑)-acetic acid-water(c↓); d→c
4(7)	Miyanami et al. (1978)	water/ glycerol (c↑)-air (d↑)
5(9)	Taylor et al. (1982)	kerosene (d↑)-water(c↓)
6(14 i,iii and v)	Bensalem (1985)	toluene(d↑)-acetone-water(c↓) No mass transfer, d→c and d→c

2.3.3 Flooding in Reciprocating plate columns

Flooding is the limiting condition in extraction columns beyond which the counter-current nature of the operation cannot be sustained. Due to the inherent instability of the phenomenon it is difficult to precisely estimate the onset of flooding. Thornton (1956) proposed the following mathematical criterion for determining the onset of flooding.

$$\frac{du_c}{dh} = 0 \; ; \frac{du_d}{dh} = 0 \qquad (2.33)$$

Using the slip velocity concept (equation 2.20 and 2.21) and the above equation, Thornton (1956) derived an analytic expression for hold-up at flooding which is listed in table 2.8.

For systems with strong coalescence tendencies flooding manifests itself as phase inversion whereas in systems with weak coalescence properties flooding occurs due to excessive agitation resulting in massive entrainment of the dispersed phase drops by the continuous phase (Baird et al., 1994). The flooding due to entrainment can also be observed at comparatively low hold-ups when the dispersed phase velocity is small.

For columns using plates with low fractional free areas flooding can occur even at zero or insufficient agitation. This happens due to the build up of the dispersed phase at the plates. The thickness of the dispersed layer increases with time and ultimately prevents the flow of the continuous phase (Rama Rao et al., 1983). At flooding in the emulsion regime the same authors observed non uniform drop/bubble distribution. The drops of the dispersed phase formed a very dense band increasing the resistance to flow of the continuous phase through the interstices. Nemecek and Prochazka (1974) observed that at flooding the drop distribution became non homogeneous. The large coalesced drops had axial motion which was similar to that of the mixer settler regime and the small drops retained the erratic motion of the emulsion regime.

In Karr columns Hafez et al. (1979) identified the onset of flooding as heavy entrainment of the dispersed phase or disappearance of the interface. Under non mass transfer or c→d mass transfer conditions, flooding can be identified by the growth of an emulsion layer of the dispersed phase usually from the middle of the column (Baird et al. 1971; Baird and Shen, 1984). The direction of mass transfer and the plate material can also influence flooding. When the transfer occurs in the d→c condition Baird and Shen (1984) observed a dense region of smaller drops at the top of the column and bigger drops near the distributor under stable operating conditions. At flooding the band of smaller drops grows from the top and fills the entire column and the dispersed phase is prevented from freely moving upwards. When the dispersed phase wet the plates, Baird and Shen (1984) observed the hold-up to increase very slowly with agitation and the flooding limit was increased. At the operating limit the dispersed phase was entrained heavily in the continuous phase.

At flooding, the counter-current throughput capable of being sustained by the column decreases significantly. The limiting throughput at flooding $(u_c+u_d)_f$ for the main RPCs is

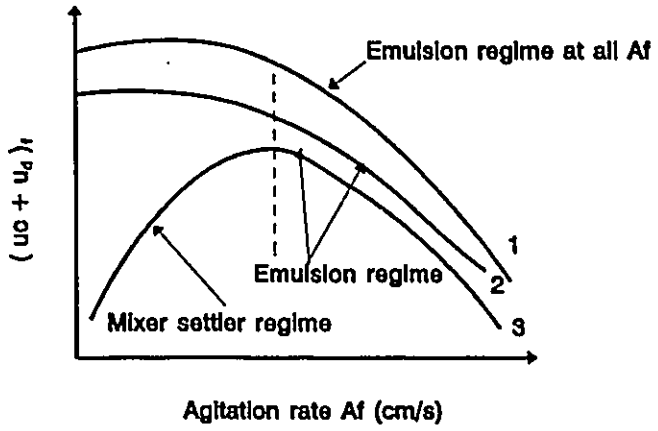

1. Karr RPC 2. Prochazka RPC

3. RPC with no downcomers and low fractional free area

Figure 2.5 Throughput capacities of typical RPC types (Baird et al., 1994)

illustrated in figure 2.5. Baird et al. (1971) initiated the studies on flooding in a 5.08 cm KRPC. Assuming a flooding hold-up value of 0.4 the authors found that the superficial velocity of the continuous phase relative to the dispersed phase (v_s) was constant. Based on the results from 4 systems viz. (i) kerosene (ii) kerosene + mineral oil (iii) kerosene + CCl_4 (iv) kerosene+CCl_4 + mineral oil (c↑) - water(d↓) the following general equation was proposed when AF > 3 cm/s :

$$v_s = U_s(1-h) = 2.24\times10^{-2}\left(\frac{\gamma^3}{\psi^2\rho_m}\right)^{0.2}\left(\frac{g^2(\Delta\rho_{cd})^2}{\rho_c\mu_c}\right)^{\frac{1}{3}} \qquad (2.34)$$

Slater (1985) and Kumar and Hartland (1988) also developed general equations for hold-up and velocities at flooding. Table 2.8 gives the results of flooding studies by Hafez et al. (1979) and Baird and Shen (1984).

Table 2.8 Flooding studies in KRPC.

1 (8) Hafez et al. (1979) kerosene(d↑)-water(c↓)

$$v_{sf} = [\frac{(1-h_f)^3}{K^* h_f^{0.5}}]^{\frac{2}{3}} d_{32} [\frac{g^2 \Delta \rho_{cd}^2}{\rho_c \mu_c}]^{\frac{1}{3}}$$

for AF > 3 cm/s

where

$$h_f = \frac{\sqrt{(L_f^2 + 8L_f)} - 3L}{4(1-L_f)} \; ; \; L_f = \frac{u_d}{u_c}$$

based on Thornton (1956) relation

(c.g.s. units)

2 (13) Baird and Shen (1984)

a) water b) salt water c) water+carbon tetrachloride (c↓) - kerosene(d↑) water(c↓)- d)Isopar M e) methyl acetate(d↑)

$$h_f = \frac{\sqrt{(9L_f^2+54L_f+1)} - 7L_f - 1}{10(1-L_f)}$$

2.3.4. Mass Transfer Coefficient

The overall volumetric mass transfer coefficient is defined as the product of the overall mass transfer coefficient and the interfacial area. While the latter is obtained from hold-up and drop size it is necessary to use a variety of models to get estimates of the former. Sometimes depending on the nature of the solute and its relative affinity towards the solvent it is possible to isolate the resistance to one phase only and relate the overall coefficient to the individual coefficient using the two resistance concept.

If the resistance was in the dispersed phase the mass transfer coefficient is determined by

$$\frac{1}{K_y a} = \frac{1}{k_y a} + \frac{m}{k_x a} \qquad (2.35)$$

the mobility of the drop. Under conditions of high agitation and/or contamination, the drop mobility is greatly reduced due to suppression of internal circulation and rigid drop conditions can be assumed. The commonly used models under rigid and circulating drop conditions are given in table 2.9.

Table 2.9 Typical drop side mass transfer coefficient models

drop characteristics	source	equation for k_d (cm/s)
rigid drop	Newman (1931)	$(2\pi^2/3)(D_{AB}/d_{32})$
oscillating drop	Handlos and Baron (1957)	3.75×10^{-3} $U_*/(1+\mu_d/\mu_c)$
circulating drop	Kronig and Brink (1950)	$17.63\ D_{AB}/d_{32}$

The estimates of the continuous phase mass transfer coefficients under various hydrodynamic situations can be obtained from the models given in table 2.10.

Table 2.10 Correlations for continuous phase mass transfer coefficients

Source	$k_c d_{32}/D_c$
Linton and Sutherland (1960)	$0.582\ Re_c^{0.5} Sc_c^{0.33}$
Garner and Tayeban (1960)	$50+8.5\times10^{-3}\ Re_c Sc_c^{0.7}$

Some important correlations for mass transfer experiments conducted in RPCs are given in table

2.11. It must be noted that the coefficients are not corrected for axial mixing mainly because under the experimental conditions it was found to be of negligible importance.

Table 2.12 completes the references for mass transfer coefficient estimation in RPCs.

As noted before, the numbers in parethesis in these tables refer to the location of these references in the table of experimental conditions (table 2.13).

Table 2.11 Correlations for mass transfer coefficient (plug flow basis)

1(5) Tojo et al. (1975) MIBK (d↑)-acetic acid -water(c↓); d→c

Overall mass transfer coefficient (s^{-1})

$$K_c a = 4.65\times10^{-3} + 5.08\times10^{-5}\phi^{0.49}$$

where

$$\phi = \frac{S_d \rho_c (n\ 0.5Af)^3}{2}$$

when

n	Type of waveform
4	Triangular
4.72	Sinusoidal
8.9-12.3	Trapezoidal
∞	Rectangular (not physically realizable)

(c.g.s. units)

2 (16) Veljkovic and Skala (1988a)

system:

(i) distilled water, (ii) sucrose soln. (iii) sodium sulphite soln, (iv) sucrose+sodium sulphite soln, (c↑)-oxygen-air(d↑); d→c

Volumetric Mass Transfer Coefficient [s^{-1}]

$$k_L a = 0.467(P_{Lg})_{max}^{0.25} u_g^{0.6}$$

where

$$(Po_{Lg})_{max} = 3.16\times10^{-4} N \rho_c (1-h)(\pi Af)^3 h^{-2.02} d_o^{0.01} \ ;\ S.I.\ units$$

3 (17) Veljkovic and Skala (1988 b)

Table 2.11 continued..

system:

distilled water/sodium sulphite soln./sucrose+sodium sulphite soln. (c↑)-oxygen-Air(d↑); d→c

Liquid phase mass transfer coefficient [m/s]

if $(Po_{Lg})_{max} > Po_{cr}$

$$k_L = 2.62\times10^{-4}(P_{Lg})_{max}^{-0.05}$$

if $(Po_{Lg})_{max} < Po_{cr}$

$$k_L = 2.94\times10^{-4}(Po_{Lg})_{max}^{0.25}$$

where

$$(Po_{Lg})_{max} = 3.16\times10^{-4}N\rho_c(1-h)(\pi Af)^3h^{-2.01}d_o^{0.01}$$

and

$$Po_{cr} = 4.2(1-h)u_g^{0.25}$$

Table 2.12 Other references for mass transfer coefficient estimation in RPCs

(plug flow basis)

number	source	system
1(3)	Tojo et al. (1974 b)	air(d↑)-CO_2- water (c↑); d→c
2(4)	Tojo et al. (1975)	MIBK (d↑)-acetic acid-water(c↓); d→c
3(12)	Noh and Baird (1984)	Kerosene (d↑)-acetic acid-water+NaOh; d→c
4(15)	Yang et al. (1986 b)	nitrogen (d↑)- oxygen - water (c↑); d→c
5(19)	Rama Rao and Baird (1988b)	air(d↑)-oxygen-water(c↓); d→c
6(22)	Chen and Liu (1991)	kerosene(d↑)-benzoic acid-water(c↓); d→c

Table 2.13 Experimental conditions

#	RPC	u_c (cm/s)	u_d (cm/s)	A (cm)	F(hz)	D (cm)	S (-)	H (cm)	d_o (mm)	N -
1	KRPC	0.4-0.7	0.25-0.7	0.14-4.15	0.0-2.30	5.08	0.55	2.86	12.7	65
2	PRPC	0.3-0.5	< 0.45	0.3-0.9	0.4-10	5.0	0.044-0.192	5-15	0.25-0.35	2-5
3	MVDC	0.16-0.79	1.15-6.20	0-2.4	0-7	5.0	-	3.5	d_d[4]=30-36 d_h[5]=12,20	7,9
4	MVDC	0.21-0.96	0.12-1.00	0-1.54	0-10			3.8	d_d=40 d_h=2	8
5	MVDC	0.21-0.96	0.12-1.00	0-1.54	0-10			3.8		8
6	MVDC	0,0.1	0.12-0.42	0.5-1.8	2-4			3.8		8

[4] d_d - diameter of vibrating disk

[5] d_h - Partition plate hole diameter

Table 2.13 (continued ...)

#	RPC	u_c (cm/s)	u_d (cm/s)	A (cm)	F (hz)	D (cm)	S (-)	H (cm)	d_o (mm)	N (-)
7	MVDC	0-0.33	0.37-1.12	2-6	0-4.3	17.2	-	12	d_h=36 d_d=100-135	4
8	KRPC[6]	u_{df}/u_{cf}=0.4-2.0 $u_{df}+u_{cf}$=2.0		0.636-2.54	0-8	14.96	0.581 -0.6	5.2	14.7	various
9	KRPC	0-3.5	1.35-2.7	2.54	0-5		0.581	5.08		42
10	RPCND[7]	0.29	0.15	1-3.5	2-3	5	0.198	5.0	2	21
11(i)	RPCND	1.24-3.72	0.04-5.10	1.4-6.35	0.75-4.0	9.3	0.09-0.29	5.6-28[8]	3-8	2-10
11(ii)		0.01-0.33	0.02-0.33	1.4-6.2	0.75-3.5	15.3	0.125-0.29	5-18[8]		5-18

[6] A wide variety of plate configurations were used (Hafez et al. 1979)

[7] RPCND - RPC with no downcomer and low fractional free area

[8] estimated

Table 2.13 (continued ...)

#	RPC	u_c (cm/s)	u_d (cm/s)	A (cm)	F (hz)	D (cm)	S (-)	H (cm)	d_o (mm)	N (-)
11 iii	RPCND	0.0725-0.3326	0.0815-0.3317	1.4-6.2	0.0-2.4	15.3	-	5.0	5	18
12	KRPC	4.1-10.2	1.0-7.0	4.5	0-5.0	5.08	0.61	2.54/5.08	13.7	29/58
13	KRPC	0.15-0.96	0.15-0.57	4.5	0.67-4.62	5.08	0.57	2.7	13.5	55
14(i)	KRPC	0.51-1.03	0.17-0.69	0.5-1.6	0.0-5.83	7.6	0.58	29.10	16	54[9]
14(ii)		0.17-1.17	0.17-1.17	Af = 1.83-6.42						
14(iii)		0.12-1.43	0.54-1.5	Af=0.83-6.42						
14(iv)		0.33-0.85	0.54-1.43	Af=0.92-5.5						
14(v)		.344-0.69	0.55-0.69	Af=1-5.4						
14(vi)		0.344-0.687	0.62-1.02	Af=0.83-6.42						

[9] with 6 doughnut plates to minimize axial mixing

Table 2.13 (continued ...)

#	RPC	u_c (cm/s)	u_d (cm/s)	A (cm)	F (hz)	D (cm)	S (-)	H (cm)	d_o (mm)	N (-)
15	KRPC	0.931-4.34	0.724-4.98	3.6 ≤ Af≤ 15.0		5.08	0.53	2.54	NG[10]	84
16	RPCND	0.055-0.5	0.2-1.2	0 < Af < 20		2.54	0.41 & 0.51	2.54-5.08	6/7 (mean)	33/65
17	RPCND	0.44-1.23	0.275-3.02	0.2-4.0	1-6	2.54	0.51	2.54 & 5.08	7 (mean)	33/65
18(ii)	KRPC	0.0-3.95	0.1-0.99	4.5	0-6	5.08	0.57	2.7	14	54
18(iii)		0.0-3.95	0.247-0.99	4.5	0-3			2.7-7.75		19-54
19(i)	KRPC	0.0	0.23-0.99	0 ≤ Af ≤ 14		5.08	0.57	2.7	14	54
19(ii)		1.97-3.95	0.49-0.99	3.0-4.5	0-3.4					
20	RPCND	0.017-0.91	0.03-0.63	1.4-6.2	0.66-3	15.3	0.092-0.0517	5-10	3-12	8-17
21	RPCND	0.409-3.681	0.6-4.6	1.4-5.0	0.75-3.0	9.3	0.09-0.306	5.6	3-6.5	10

[10] NG - not given

Table 2.13 (continued ...)

#	RPC	u_c (cm/s)	u_d (cm/s)	A (cm)	f (Hz)	D (cm)	S (-)	H (cm)	d_o (mm)	N (-)
22	RSPC[11]	0.15-0.50	0.082-0.54	0-3.76	0-5	5.08	0.61-0.78	5-15	0.58-0.84[12]	0-22
23	LRPC	0.5-2.8	0-5.65	0.32-0.64	5-30	10.0	0.38 (overall)[13]	10-30	1.6	NG

[11] RSPC - Reciprocating Screen Plate Column

[12] wire thickness

[13] open area of perforations based on plate area = 0.23, downcomer open area based on overall cross section area of column = 0.20 and overall open area = 0.38

2.4 Axial Mixing

The causes and effects of axial dispersion were outlined in Chapter 1. In this chapter the review of axial mixing studies in RPCs is presented. Due to the complex nature of the fluid turbulence and drop hydrodynamics it is difficult to model axial mixing on a purely theoretical basis. Hence semi-empirical or fully empirical correlations are used, the latter sometimes strictly applying only to the extractor under investigation and the range of experimental variables involved. In this review, a brief description of the important axial mixing models available in literature is given. This is followed by the summary on the research on axial mixing investigations in RPCs.

2.4.1. Semi-empirical models

(i) Kolmogoroff's isotropic turbulence theory:

The complex nature of turbulent flow can be made tractable for engineering purposes under certain conditions which permit considerable simplification. The discussion in this section is mainly based on the comprehensive review on the application of Kolmogoroff isotropic turbulence theory to bio-reactor design by Kawase and Moo Young (1990). In turbulent flow the eddies can be classified as large, intermediate and small. The large or primary eddies having a scale comparable to that of the main flow stream possess only about 20% of the total kinetic energy and break down into intermediate range eddies. These eddies possess most of the turbulent kinetic energy in the system and are also termed energy-containing eddies. They in turn, break into smaller terminal eddies which dissipate the energy through viscous effects. Thus there is continuous transfer of energy from the generating source (e.g. mechanical agitation, dispersed phase flow etc.) through the eddies to viscous dissipation. The turbulent energy spectrum, illustrated in figure 2.6, is characterized by wavenumbers which are inversely

proportional to the size of the eddies.

Kolmogoroff postulated that when the Reynolds number is sufficiently high there exists a range of high wave numbers corresponding to smaller eddies, at which the turbulence can be considered to be statistically in dynamic equilibrium. Rapid interchange of energy between eddies of different sizes soon leads to an equilibrium distribution of energy among the various eddy sizes. This distribution becomes independent of the detailed initial conditions of turbulence. Two bulk parameters, the specific energy dissipation rate ϵ (with units cm^2/s^3) and kinematic viscosity ν are sufficient to describe this state of turbulence. The range of eddy sizes falling in this category is called the universal equilibrium range. In a volume of liquid whose dimensions are smaller than that of the main flow, the root mean square of the fluctuating components of the velocity are equal and **isotropic turbulence** is said to prevail. The universal equilibrium range can be divided into the viscous dissipation sub-range and inertial sub-range. In the former region viscous effects dominate when $Re_{eddy} \ll 1$. The eddy size at which the eddy Reynolds number equals unity is called the Kolmogoroff micro-scale (η). From dimensional analysis the micro-scale can be calculated as

$$\eta = \nu^{\frac{3}{4}} \epsilon^{-\frac{1}{4}} \tag{2.36}$$

Eddies larger than the micro-scale belong to the inertial sub-range. At equilibrium the energy transferred from the medium scale eddies is equal to the energy required for creating smaller scale eddies. Since these medium scale eddies have a high eddy Reynolds number the turbulence in this region is independent of viscous effects and solely determined by the energy input (ϵ). By dimensional analysis it can be shown that

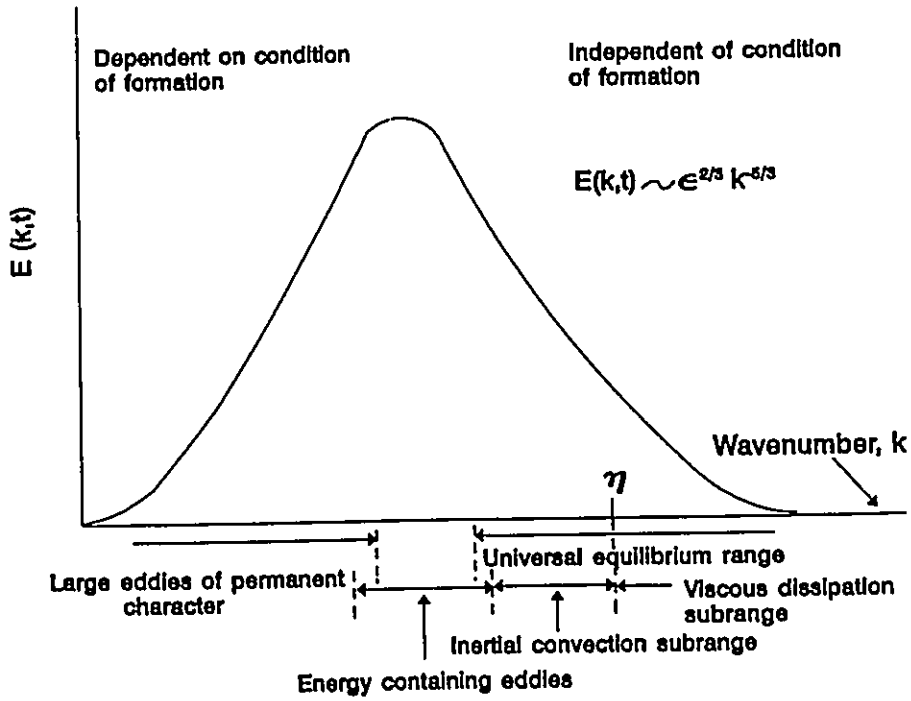

Figure 2.6 Turbulent energy spectrum (van Suijdam and Metz, 1981)

$$u \sim (\epsilon l)^{\frac{1}{3}} \tag{2.37}$$

where u is the root mean square turbulence velocity between two points in the fluid separated by a distance l. l is characteristic of the intermediate eddies such that

$$\eta \leq l \leq L \tag{2.38}$$

where η and L are the scales of the terminal and primary eddies respectively. The use of this approach to determine the maximum stable drop size has already been discussed in section 2.3.1. The application for expressing axial mixing coefficient is described below.

If the axial mixing coefficient under isotropic turbulent conditions can be considered as a product of the turbulent velocity u and the characteristic scale l, then

$$E_c \sim u\, l \tag{2.39}$$

Substituting the expression for u, E_c can be expressed as equation (2.40).

$$E_c = l^{\frac{4}{3}}\, \epsilon_m^{\frac{1}{3}} \tag{2.40}$$

It must be emphasized that the assumption of isotropic conditions is needed to simplify the complicated nature of turbulence for engineering purposes. Because of the simple nature of this model it has enjoyed wide popularity in accounting for the hydrodynamic aspects of bubble columns and stirred tanks. The use of the model approach obviates the need of detailed measurement of the turbulence spectrum and provides a dimensionally consistent correlation for axial mixing (Baird and Rice, 1975). It is interesting to note that the correlations based on other models also have a form very similar to that of the isotropic model (Kawase and Moo Young, 1991). For instance, Zehner (1982) used the cylindrical eddy model to obtain a correlation

$$E_z = 0.368 D^{4/3} (u_d\, g)^{\frac{1}{3}} \tag{2.41}$$

Kawase and Moo Young (1986) used the mixing length concept and energy balance to obtain

$$E_c = 0.343\, D^{\frac{4}{3}} (u_d\, g)^{\frac{1}{3}} \tag{2.42}$$

These two equations can be compared to equation (2.40) and the length term and energy dissipation term can be compared.

Baird and Rice (1975) also compared the axial mixing model with data on bubble columns obtained from various sources using column diameter as the characteristic length. Table 2.14 gives a representative list for the characteristic length (l) used in different contactors.

Table 2.14 Characteristic lengths for different contactors

Column	Main source of energy dissipation	Reference	*l*/D
Bubble column	dispersed phase	Baird and Rice (1975)	0.455
		Kawase and Moo Young (1989)	0.25
Stirred Tank	mechanical stirring	Brajinskii et al. (1986)	0.225
KRPC	buoyancy + mechanical agitation	Holmes et al. (1990)	0.70

(ii) Model based on hydraulic non-uniformities

Rosen and Krylov (1967, 1974) observed that the rule of similarity characterized by dimensionless groups like Reynolds number, Froude number etc does not provide a sufficient criterion for scaling up laboratory scale extractors to industrial scale. This was attributed to the differences in spatial hydrodynamic conditions between the two scales. When the column dimensions increase, the non uniformities in flow are enhanced in the transverse direction. This leads to a non uniform velocity profile across the cross section of the column with the liquid flowing preferentially along certain paths. In the extreme, channelling can occur. This in turn leads to increases in axial mixing and height of transfer unit. The axial mixing coefficient for industrial contactors was expressed as the sum of true longitudinal dispersion coefficient (D_o) and its augmentation (D_{tn}) due to transverse non uniformity. Therefore,

$$E_c = D_o + D_{tn} \tag{2.43}$$

D_o and D_{tn} were defined by the following relationship

$$D_o = H_c\, u_{eff}\, l \; ; \; D_{tn} = \frac{f'\, D^2\, u_{eff}^2}{D_r} \qquad (2.44)$$

Here H_c is a numerical coefficient, l is a characteristic dimension and u_{eff} is the effective velocity of the continuous phase expressed as the sum of u_c and twice the pulsation intensity. Similar expressions were derived for the dispersed phase. It can be seen that when D_r, defined as the average coefficient of radial dispersion, increases the effect of the transverse non uniformity contribution decreases. D_r was considered to be comparable to D_o and defining f′ in equation (2.44) according to

$$f' = f_o \frac{(\Delta u)^2}{u_{eff}^2} \qquad (2.45)$$

where Δ u is the average deviation from a uniform velocity distribution in the column and f_o is a coefficient depending on geometry, equation (2.44) becomes

$$E_c = H_c\, u_{eff}\, l + \frac{f_o\, D^2 (\Delta u)^2}{H_c\, u_{eff}\, l} \qquad (2.46)$$

It can be seen from the above equation that since the transverse non uniformity effect is a function of column diameter, it can be assumed to be negligible for the lab scale extractor. Thus the scaling effect in the continuous phase, defined in terms of the difference between the dispersion coefficients for the industrial and lab scale column, can be expressed as

$$\Delta E = H\, (\, l - l_{lab}\,)\, u_{eff} + \frac{f_o\, D^2\, (\, \Delta u\,)^2}{H\, l\, u_{eff}} \qquad (2.47)$$

It can be seen from the above expression that especially for large diameter columns the

axial dispersion coefficient is high at low flow rates and agitation intensities. With increasing agitation, the radial mixing is promoted and flow becomes more uniform causing the axial dispersion to go through a minimum. With increasing agitation there is an increase in the dimension *l* characterizing turbulent pulsations, which cause the axial mixing coefficient to increase again. This phenomenon has been observed in RDCs, RPCs and pulsed packed columns (Rosen and Krylov 1974; Goebel et al. 1986; Karr et al. 1987; Kumar and Hartland 1992).

(iii) Two zone model

This approach was developed by Prochazka and co-workers (1970, 1974) who observed that the actual stages in pulsed extraction columns are not perfectly mixed. They observed two distinct zones in the extractor (figure 2.7). The first zone corresponds to the region of perfect mixing encompassing the plates with backflow of the liquid through the plates. The diffusion model is inadequate under these conditions. Between the two well mixed zones on adjoining plates there is a zone of imperfect mixing termed the diffusion region, in which the backflow model is inapplicable. Hence a combination of the two models are required to describe the axial mixing process. The effective back-mixing coefficient (q_e) is related to the net backflow coefficient through the plate (q) and the turbulent diffusion region coefficient (E) in the imperfect mixing zone as follows:

$$\frac{1+q_e}{q_e} = \frac{1+q}{q}\alpha;\ \alpha = e^{Pe} \qquad (2.48)$$

where the Peclet number Pe is given by

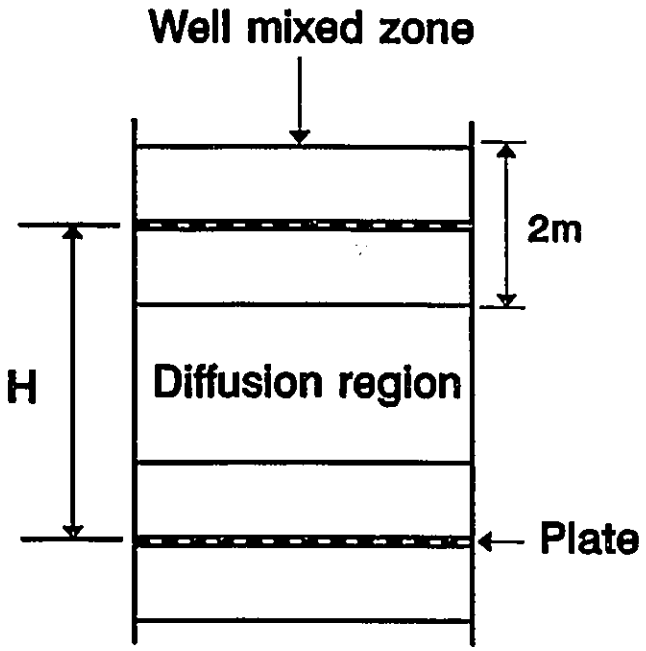

Figure 2.7 Two zone model for RPC (Prochazka and co-workers, 1970, 1974)

$$Pe = \frac{u_c(H-2m)}{E_c} \; ; \; E_c = K \frac{Af\, d_o}{S^{\frac{3}{2}}} \qquad (2.49)$$

Only when $E_c \rightarrow \infty$, $\alpha \rightarrow 1$ and q and q_e are identical. Otherwise the actual back-mixing coefficient for a real stage q_e is less than the back-mixing coefficient for the ideal stage. Hence design based on q will be too conservative. Novotny and Prochazka (1970) used steady state tracer injection technique to estimate the backflow coefficient under single phase flow condition. Using the material balance equations for the tracer concentration and equations for the backflow velocity a correlation was developed for q which is given in table 2.15. The axial dispersion coefficient E was expressed as a product of the fluctuating velocity v′ and a characteristic length *l*. In this paper the authors related v′ to the mean pulsating velocity of the stream leaving the holes of the plate and *l* to the pitch of the plate holes.

Nemecek and Prochazka (1974) extended the approach of Novotny et al. (1970) to two phase flow conditions. The steady state tracer technique was again used to estimate the backflow coefficient. Depending on the intensity of agitation three distinct hydrodynamic regimes were identified which were classified into the mixer settler, dispersion and emulsion types. There is no backflow of the dispersed phase through the plates in the mixer settler and dispersion regime. Equations developed for q_c and q_d are given in table 2.17. The effect of the dispersed phase on the axial dispersion coefficient within the stage was expressed in terms of an increment to the single phase axial mixing value. It must be noted that the height of the well mixed region is a function of the plate spacing, fractional free area and agitation rate. Novotny et al. (1970) fitted a constant value of 4.5 cm for m in their single phase work which was considered by Nemecek and Prochazka (1974) to be a good average estimate.

Stevens and Baird (1990) also adopted the approach of Novotny et al. (1970) to study axial mixing in a Karr RPC. The steady state tracer technique was used to measure the back-mixing coefficient in a 5.08 cm diameter column containing either one or two plates. A mobile probe was used to sample the tracer concentration at different axial positions along the column. From the concentration profiles thus obtained it was possible to determine the heights of the well mixed zone and the poorly mixed zone. The study indicated that the mixing due to an isolated plate was less than two or more plates. When two reciprocating plates were used the height of the well mixed region corresponded to a fraction of the half stroke swept by the plates. The axial mixing coefficient (E_c)in the poorly mixed zone was found to be a constant and was represented by

$$E_c = C_1 v' l \tag{2.50}$$

where v´ defined as the characteristic vortex velocity was expressed as the maximum jet velocity relative to the plate achieved by the liquid through the holes. Thus

$$v' = \frac{u_c + \pi A f}{S} \tag{2.51}$$

and l was equated to the web (minimum distance between hole edges) of the plates since the vortices were assumed to form under the web. The height of the well mixed zone was considered to be a fraction of the agitation stroke. The model developed for the effective axial dispersion coefficient for the column is given in table 2.15. The height of the well mixed zone was not physically realistic when large amplitudes and small plate spacings were used. Hence under these conditions the height of the well mixed zone was limited to accommodate a minimum distance (32% H) for the poorly mixed zone. Stevens and Baird (1990) tested the model against single phase axial mixing data sources in the literature (Kim and Baird 1976a, b; Novotny 1970; Baird and Rama Rao 1988). In spite of differences in column diameter (maximum 7.5 cm) and different tracer measurement techniques the authors found the model to have a reasonable fit for the data.

In this section, the discussion on axial mixing in the continuous phase is classified into investigations in single phase and two phase flow conditions. The latter is subdivided into non mass transfer and mass transfer conditions. The axial mixing in the dispersed phase is considered separately.

2.4.2 Axial Mixing Data in the Continuous Phase

In the continuous phase the non-idealities in flow can be satisfactorily described by the axial dispersion models. The important observations and conclusions made by several investigators are listed in the main text while the correlations and experimental conditions are given in table 2.15 and table 2.16 respectively.

2.4.2.1 Single Phase Studies

(i) Novotny et al. (1970)

The ideas behind the model developed by Novotny et al. (1970) were already discussed in section 2.4.1. The study revealed that

a. The back-mixing coefficient increased rapidly with decreasing pitch of the holes in the plate.
b. The Peclet number increased rapidly with plate spacing for H greater than 5 cm implying reduced mixing within the stage.
c. The back-mixing values increased slowly with increasing viscosity of the liquid. This was not expected since the turbulent eddies responsible for the back-mixing are independent of the viscosity of the liquid.

(ii) Kim and Baird (1976 a)

The axial mixing coefficient in a 5.08 cm diameter Karr RPC was determined by a novel colour change technique. A pulse of strong base (1 N NaOH) was injected into the column where it reacted with the down flowing solution of dilute hydrochloric acid containing phenolphthalein as indicator. Two neutralization zones were formed which ultimately moved towards one another, mingled and disappeared. The location of the zones with respect to time

was used to determine the axial dispersion coefficient using the solution to the unsteady state dispersion equation. The following points were noted:

1. E_c values with stainless steel plates were about 30% more than the Teflon plates which however were more than twice the thickness.
2. Comparing the data on a 15 cm diameter pulsed column (Baird, 1974) with similar plate geometry, the authors concluded that column diameter did not have an effect on E_c.
3. Experiments conducted with highly viscous solutions revealed an insignificant decrease in E_c confirming the essentially turbulent nature of the process.

(iii) Kim and Baird (1976 b)

In the sequel to the above study the authors investigated the effect of plate geometry on the hydrodynamics of the KRPC. E_c was found to increase with increasing hole size and decreasing plate thickness.

(iv) Hafez et al. (1979)

The authors made a comprehensive study of flooding and axial mixing in a 15 cm KRPC. They tried a wide variety of plate types and arrangements such as standard plates at different plate spacings, a set of standard Karr plates alternating with a doughnut plate functioning as baffle, a special fan plate etc. The axial mixing was determined by the colour change method and the conventional salt tracer injection method. The latter method was preferred under conditions of low agitation because circulation current developed in the continuous phase and invalidated the colour indication technique. The findings from this study were

a. E_c varied linearly with Af at sufficiently agitated conditions.
b. At zero agitation E_c values were very high and this was attributed to a radially non uniform continuous phase flow pattern ("fingering").

c. Increasing the agitation improved radial non uniformity and reduced E_c.

d. The presence of baffles caused an increase in the single phase axial mixing coefficient which was attributed to a higher primary scale of turbulence relative to the standard plate.

(v) Karr et al. (1987)

Axial mixing studies were conducted in a 2.54 cm diameter laboratory column and an industrial 50.8 cm diameter column using the transient tracer technique. In the latter column only single phase axial mixing studies were conducted. The conclusions based on single phase studies were

a. High values of E_c were obtained at zero agitation rate and they decreased with increasing agitation, the trend being most pronounced at the highest column diameter.

b. Comparing the results from a 15 cm diameter column without baffles (Hafez et al., 1979) with those obtained from the 2.54 cm column it was observed that under well agitated conditions column diameter did not have any effect on E_c over this range of diameters.

c. The minimum E_c value was around 1 cm^2/s for both the 2.54 cm and 15 cm diameter columns.

d. Under well agitated conditions E_c could be considered to vary linearly with Af.

e. Under single phase flow conditions, the presence of baffles increased axial mixing as was shown by the data from a 15 cm diameter column (Hafez et al. 1979).

f. When the axial mixing data (including those of Hafez et al., 1979) expressed as E_c/Af were plotted against column diameter (2.54-50.8 cm) for well agitated conditions ($Af > 4$ cm/s), an approximate linear relationship was obtained. However the data of Hafez et al. (1979) for RPC without baffles did not fall in this trend (as noted in b.)

g. The axial mixing coefficient was found to vary approximately as the 0.67 power of diameter

based on the diameter range 25.4 mm (unbaffled) - 508 mm (baffled).

(vi) Stevens and Baird (1990)

In this study the data were obtained locally around the Karr plate in order to develop the model. The model was compared with existing literature data. Please refer to section 2.4.1 under axial mixing models for more details. The model equation is given in table 2.15.

Note: In tables 2.15 and 2.16, the sub-divisions in parenthesis, given in roman numerals, correspond to those in the text (section 2.4.2.1).

Table 2.15 Correlations for single phase flow axial mixing coefficient[14]

1. (i) Novotny et al. (1970) water / glycerol

SS[15], Tracer: Potassium chromate (water), fuchsine (glycerol)

$$\frac{1+q}{q}\alpha = \frac{1+q_e}{q_e}$$

where

$$\alpha = \exp\left[\frac{Ku_c(H-2m)S^{\frac{3}{2}}}{a'fd_o}\right]$$

$$q_e = \frac{1}{\left(\frac{q+1}{q}\right)\exp\left[\frac{K(H-2m)S^{\frac{3}{2}}u_c}{d_o(0.5A)f}\right]-1} \quad ; H \geq 2m$$

where

$$q = \frac{\phi}{\pi}-\frac{1}{2}+\frac{Af}{u_c}\cos\phi \; ; \; \phi = \sin^{-1}\left(\frac{u_c}{\pi Af}\right)$$

and

K=6.6 and 2m=4.5 cm

2.(ii) Kim and Baird (1976a) Aqueous HCl solution (5 mmol/L)

USS[16] color change, tracer: 1.0 N NaOH

$$E_c = 1.98(0.5\ A)^{1.74}f^{0.96}H^{-0.69}$$

(Teflon plates)

---

[14] c.g.s. units used unless mentioned otherwise

[15] SS - Steady state injection

[16] USS - Unsteady state colour change

Table 2.15 continued...

$$E_c = 5.56(0.5A)^{1.77} f\, H^{-1.32}$$

(Stainless steel plates)

3.(iii) Kim and Baird (1976b) Aqueous HCl solution (5 mmol/L)

USS color change, tracer: 1.0 NaOH

$$E \propto (A)^{1.8}\, f\, d_o^{1.8} d_t^{-0.3} H^{-1.3}$$

4. (vi) Stevens and Baird (1990) Water

SS, tracer: NaCl

$$E_c = \frac{1}{\frac{\ln(\frac{1+q}{q})}{Hu_c} + \frac{2S(1-\frac{C_2 a'}{H})}{C_1 d_o (u_c + 2\pi a' f)[(\frac{\pi}{2\sqrt{3}S})^{0.5} - 1]}}$$

where

$C_1 = 0.184$ and $C_2 = 1.46$

(S.I. units)

Table 2.16 Experimental conditions for single phase axial mixing studies

#	RPC	u_c (cm/s)	A (cm)	f (hz)	D (cm)	S (-)	H (cm)	d (mm)	N (-[17])
i	PRPC	0.277-1.5	0.2-0.4	6.67-13.33	5.16	0.03-0.146	2.5-15.0	1.5-3.0	8-40
ii	KRPC	0-1.2	1.2-4.5	0.5-6.0	5.08	0.49 (STS)[18] 0.57 (Teflon)	2.7[19]-5.23 (STS) 2.89-13.1 (Teflon)	13.6 (STS) 14.3 (Teflon)	14-60 35-70
iii	KRPC	0	2.2-4.5	0.5-6.0	5.08	0.49 STS	2.70 (STS)	6.35	70
iv	KRPC[20]	0.0-1.2	0.636-2.54	0-8	14.96	0.581	2.60-5.2[19]	14.7 (std. plate)	various
v	KRPC	1.13	$0.0 \leq Af \leq 10.5$		2.54	0.584	2.54	not given	130
		0.56-0.93	$0.0 \leq Af \leq 8.5$		50.8	0.603	5.08 (zone 1)	15.9	20
							2.54 (zone 2)		180
vi	KRPC		2.15-3.7	2.23-3.83	5.08	0.27-0.55	5-7	6.35-13.6	1 or 2

[17] Approximate estimates except for case vi

[18] STS - stainless steel plates

[19] Plate spacing calculated = 2.54 (plate spacer length)+plate thickness (d_t) [cm]

[20] 6 different types of plate and baffle arrangements used with different plate spacings.

2.4.2.2 Continuous Phase Axial Mixing Data under Two Phase Flow Conditions

(i) Souhrada and Prochazka (1966)

The authors compared the different techniques of estimating the back-mixing coefficients in a 7.0 × 3.5 cm rectangular reciprocating plate column for the system water (c↓)-acetone-toluene(d↑) with the solute transfer from the disperse to the continuous phase. The authors obtained very good agreement between the estimates from the mass transfer profile and the steady state and transient tracer injection techniques. However it must be noted that the comparisons were not based on tests conducted *simultaneously* in one experiment. The study indicated that the back-flow coefficient α_c

1. cannot be described by combining the effect of amplitude and frequency into one variable, Af alone.
2. was not affected much by changes in u_c.
3. decreased with increase in u_d. This was attributed to a higher layer of the dispersed phase building up on the plates hindering the backflow of the continuous phase.
4. increased with plate spacing.

(ii) Miyanami et al. (1973)

In this study on axial mixing in a MVDC (described in chapter 1), electrolytically generated bromine was used to induce a step change in the colour intensity of the continuous phase and the response was monitored downstream. The variance from the response curve was used to calculate the number of well mixed stages N_{eq} and the backflow ratio (α_c). The authors observed that in the range of vibrating speeds studied, the vibrating disk divided the gas liquid dispersion into two regions. Hence the vibrating disk was considered to contribute to partitioning the stage as well. The authors considered that since the order of magnitudes of the annular area

between the disk and the column wall was similar to the partition plate hole, a constant value for α_c could be used. The number of well mixed cells (N) used in the backflow model was set at twice the number of stages. The backflow coefficient (α_c) was modelled to be the sum of contributions by disk vibration (α_v) and dispersed gas flow (α_g). The former was estimated under non gas flow conditions when α_c was only due to α_v. It was found that under two phase flow conditions

$$\alpha_v = \alpha_g = \frac{\alpha_c}{2} \tag{2.52}$$

provided α_c exceeded 0.1. The results from the investigation indicated that the back-flow ratio was

a. strongly affected by the hole diameter in the partition plate

b. weakly affected by the disk frequency and continuous phase velocity.

c. influenced at only small values of the dispersed phase flow velocity.

(iii) Nemecek and Prochazka (1974)

The two zone axial dispersion model developed by Novotny et al. (1970) was extended to two phase flow conditions. The details of this approach were given in section 2.4.1. The authors observed three distinct hydrodynamic regimes in the operation of the RPC. In the mixer settler regime and in the dispersion regime, the latter characterized by discrete layers of drops clustering near the plates, there was no back-mixing of the dispersed phase through the holes. The third regime was the emulsion regime where both q_c and q_d were important. The expression explicit in q_c (form B in table 2.17) is not of much use in mixer settler and dispersion regimes because of non uniform hold-up. However the second expression also involving q_d, but independent of hold-up (form A) can be used for these regimes since q_d is zero. The axial

dispersion coefficient within the stage E_{c2} under two phase flow conditions was modelled by an increment ΔE to single phase flow conditions E_{c1} and the equations applicable to the various regimes are given in table 2.23. The other major observations and the explanations of the authors are summarized below.

a. The circulation induced by large drops and entrainment in the wakes of the drops became major contributing factors to E_{c2} in the mixer settler and dispersion regimes.

   Thus at very low agitation intensities the backflow through the stage was small and the longitudinal mixing within the stage was a major factor.

b. With increasing agitation the size of the drops decreased and they were more uniformly distributed in the column. Hence the circulation and entrainment effects became less important.

c. However at very high agitation levels the hold-up increased leading to increased drop coalescence. This resulted in a coarse dispersion similar to the dispersion regime and E_{c2} increased rapidly.

d. When the fractional free area of the plate increased, the increase of E_{c2} at high agitation rates was sluggish and was in fact lower than single phase conditions. This effect was due to the fine drop dispersion hindering the spread of the turbulent disturbances from the plates to the bulk of the stage.

e. The increase in stage height had no effect in the mixer-settler regime while in the dispersion and emulsion regime this resulted in a lower effective back-mixing coefficient q_e.

f. The dispersed phase velocity u_d, which had no effect in the mixer-settler and dispersion regimes, strongly influenced hold-up and hence q_e in the emulsion regime.

(iv) Tojo et al. (1974)

In this study with the MVDC the effect of axial mixing on the absorption of carbon dioxide by water was investigated under co-current flow conditions. The expression for the backflow coefficient was based upon the results of an earlier study for the air-water system (Miyanami et al., 1973) under non-mass transfer conditions (table 2.17). Using this expression in the solution to the backflow model and the experimental inlet and exit concentrations the volumetric mass transfer coefficient was obtained by trial and error.

The mass transfer results indicated that at low liquid velocity and high gas velocity the axial mixing effects became noticeable and the overall mass transfer is not promoted appreciably by disk vibration. At very low liquid velocity, mass transfer perfomance decreased with disk vibration.

(v) Tojo et al. (1976)

The axial mixing in a MVDC was determined by the transient tracer technique for the system MIBK(d↑)-water(c↓). The authors used the model developed by Miyauchi and Vermeulen (1963b) relating the Peclet number(Pe) to the back flow ratio (α).

$$\frac{E_c}{u_c H} = \frac{1}{2\beta - \frac{1}{N}} + \frac{\alpha_v}{\beta} \qquad (2.53)$$

where the number of well mixed cells per stage (β) was set to 2. For sinusoidal disk vibration α_v was derived to be

$$\alpha_v = -\frac{\omega}{\pi} + \{\frac{Af(1-h)}{u_c}\frac{S_h}{S_l}\sin\psi\}\frac{S_d}{S_l} \qquad (2.54)$$

with

$$\omega = \cos^{-1}\left(\frac{u_c}{\pi A f(1-h)}\frac{S_l}{S_h}\right) \qquad (2.55)$$

The final equation obtained after using the above expression for α_v and some simplifications is given in table 2.17.

The authors also studied the effect of superimposing a rotary motion upon the vibratory motion of the disk. In the lower range of rotational speeds (N $\leq$ 300 rpm) axial mixing decreased by as much as 70%. This was attributed to the shearing force induced by the disks opposing the longitudinal mixing.

It must be noted that the axial mixing coefficients obtained in this study were in the order of 3 cm^2/s and hence rather low. Tojo et al. (1975) assumed plug flow conditions in their mass transfer investigations where acetic acid transferred from the MIBK to the aqueous phase.

(vi) Kim and Baird (1976)

Two phase axial mixing data were obtained for air(d↑)-water(c↓) and Kerosene(d↑)-water(c↓) systems. For the gas-liquid system

a. The poor distribution of the bubbles caused vertical circulation currents at zero and low frequencies.
b. At very low frequencies E_c increased with frequency and passed through a maximum around 0.5 Hz.
c. Increased reciprocation improved radial uniformity and reduced E_c such that at high agitations they approached single phase values.

For the liquid-liquid system

a. the dispersed phase flow did not have a statistically significant effect on E_c under agitated conditions even though some trends could be noticed.

b. at zero agitation however circulations induced by the dispersed phase flow, especially at lower values, became important and E_c values were high.

c. E_c increased with plate spacing.

(vii) Kim and Baird (1976b)

The above study was extended for the liquid-liquid system to examine the effect of plate geometry.

a. When E_c was plotted as a function of u_d, the curve for the smaller plate hole diameter passed through a maximum at moderate values of u_d and small agitation rates.

b. With increasing u_d the E_c values decreased and at values greater than 0.4 cm/s they became insensitive to both agitation and u_d.

c. E_c values were much lower at higher plate hole diameters.

However the column cannot be operated under conditions of very high u_d for plates with small holes because the flooding condition restricts the allowable agitation rates. These effects were less serious at larger plate spacing. The plates with smaller holes produced smaller drops and hence larger interfacial area. However this was accompanied by higher hold-up, hence increased flooding tendencies. Further, axial mixing was also increased. These factors led the authors to conclude that plates with small holes are limited to applications where a large number of equivalent theoretical stages is more important than high throughput.

(viii) Miyanami et al. (1978)

In this work, the absorption of CO_2 into water was investigated using the correlation for continuous phase back-mixing ratio from an earlier study by Tojo et al. (1976). The backflow model incorporated twice the number of stages assuming that each stage (between partition plates) comprised of two well mixed regions. Backflow through the stage partition plate was

differentiated from the vibrating disk based on the fractional free flow area (table 2.17). The backflow coefficient corresponding to the partition plate was identical to that obtained by Tojo et al. (1976). The backflow coefficient for the flow through the disk is given in table 2.17.

(ix) Hafez et al. (1979)

The effect of different plate arrangements on axial mixing was extended to two phase flow conditions. The study indicated that

a. In the absence of baffles the E_c values showed a maximum when Af was 1 cm/s. This effect was more important at smaller value of u_d. This increase in E_c for Af < 1.0 cm/s was explained to be caused by massive circulation effects aggravated by the large diameter of the column. At very small dispersed phase flow rates the maximum in E_c was observed at zero agitation.

b. The baffles, especially the fan type plates, and the arrangement of set of standard plates accompanied by doughnut baffles and disk plate were very effective in reducing the axial mixing at zero and low agitations.

c. At high agitation rates there was not much difference between the axial mixing values for the different plate arrangements.

(x) Heyberger et al. (1983)

These authors investigated the possibility of treating the back-flow ratio in both phases and the stage efficiency as variable parameters with respect to stage number. Experiments were conducted in a 8.5 cm diameter Prochazka type RPC using water(c↓)-acetone-toluene(d↑); (d→c). The parameters were expressed as a polynomial function as follows:

$$p_i(k) = \sum_{j=0}^{n} a_{ij} k^j \qquad (2.56)$$

where p_i denotes α_c, α_d or the stage efficiency e ,n is the order of the polynomial and k is the ordinal number of the stage. The coefficients were optimized with respect to the measured concentration profiles of both phases. Polynomials of 4th degree were found sufficient to describe the model parameters. It was observed that when constant parameters were used the deviations between the model predictions and experimental values increased with increasing agitation frequency. The variation in the model parameters from stage to stage was attributed to the inhomogeneity in the dispersed phase distribution. Further the local values of these parameters were found to be sensitive to the shape of the concentration profiles.

(xi) Parthasarathy et al. (1984)

The residence time distribution (RTD) in the continuous phase was measured for air(d↑)-water(c↓) and kerosene(d↑)-water(c↓) systems using the transient tracer injection technique. The experimental RTD data was matched with the axial dispersion model and correlations for the dispersion numbers were obtained for both systems. The RTD data was also used to determine the equivalent number of theoretical stages (j) in the column. It was found that the Gamma function extension of the ideal cascade model (Buffham and Gibilaro 1968) gave a better fit of the experimental RTD data than the dispersion model. Hence the authors concluded that the mixing within the stage was more important than back-mixing between the stages when plates with small hole size and fractional free area were used.

(xii) Bensalem (1985)

In this work axial mixing in a 7.6 cm diameter Karr column was investigated both in the

presence and absence of mass transfer using the system water (c↓)-acetone-toluene (d↑). Mass transfer in both directions was investigated. The correlations giving the influence of the operating variables are given in table 2.17.

(xiii) Yang et al. (1986)

The axial dispersion coefficient in a 5.08 cm diameter Karr column was determined in the continuous phase using the steady state tracer injection technique for the air(d↑)-water(c↑) system. It was found that

a. E_c increased with increasing gas flow rate especially at high values (> 5 cm/s). The pattern of this increase was not significantly different in the presence of plate oscillation.

b. The agitation rate had an effect only when Af exceeded 1.88 cm/s.

c. The liquid flow velocity had little effect on E_c in the range of u_c 0.6-1.86 cm/s.

d. The dispersed phase flow was concluded to be the main variable affecting the back-mixing in the column.

e. The axial mixing values observed in the range of 3-13 cm^2/s were very small when compared with those of conventional bubble columns without internals.

When these E_c values were used in the calculations for the process of nitrogen absorption into water the axial mixing correction required for the mass transfer coefficient k_la was found to be negligible.

(xiv) Karr et al. (1987)

The two phase liquid-liquid flow conditions were investigated in a 2.54 cm diameter column. The following observations were made:

a. The presence of the dispersed phase resulted in the increase in the continuous phase axial mixing coefficient, the effect being prominent at zero agitation rate.

b. With increasing agitation the E_c values passed through a minimum before increasing in a linear fashion.

c. The authors believed that the radial non uniformity effects were further enhanced in this column because the Teflon plate stack was wetted preferentially by the dispersed n-heptane.

(xv) Baird and Rama Rao (1988)

E_c values were determined by the transient tracer injection technique for air(d↑) - water (c↓) system. The observations of the authors are listed below.

a. The continuous phase velocity had a significant effect on the E_c values.

b. The pulsation stroke had an effect on E_c *in addition* to the agitation rate Af.

c. At highest agitation rates, the E_c values at the lowest stroke used were *smaller* than those obtained under single phase flow. This was explained as due to the clustering of the bubbles around the plates providing a barrier for the liquid mixing between the plates.

d. At moderate agitation rates the increase in plate spacing increased the axial dispersion. However at high values of Af the E_c values at the lowest plate spacing increased above those of the higher plate spacings.

e. The E_c values passed through a shallow minimum when plotted against agitation rate. The location of this minimum was dependent on the plate spacings used.

These axial mixing data were used in the mass transfer study which involved the absorption of oxygen from air using deoxygenated water. However it was found that the axial mixing correction for k_la was around 1 % and hence plug flow assumption was justified.

(xvi) Harikrishnan et al. (1994)

In this study the true mass transfer coefficient was determined and correlated to the operating variables. The axial mixing coefficients E_c used in this study were obtained under non

mass transfer conditions by previous workers on the same column. (Srinikethan et al., 1987).

NOTE: The subdivisions in this section correspond to those listed in table 2.17 and in table 2.18.

Table 2.17 Correlations for axial mixing coefficient under two phase flow conditions[21]

1. (ii) Miyanami et al. (1973) air (d↑)-water(c↑)

USS; Tracer: chemical reaction of Br^- with Methyl Orange

$$\alpha_v = [-\frac{1}{2}+2f\beta+\frac{Af(1-h)}{u_c}(\frac{d_h}{d_l})^2](\frac{d_d}{d_l})^2$$

2. (iii) Nemecek and Prochazka (1974) trichloro ethylene (d↑)-water(c↓)

SS; Tracer: potassium chromate

$$\frac{1+q_e}{q_e} = [\frac{1+q}{q}]\alpha$$

where

$$\alpha = e^{\frac{\overline{u_c}(H-2m)}{E_c}}$$

Equations for net backflow coefficients (q_c and q_d) for well mixed zones

[when $s \neq 1$, the following are applicable]

$$q_c = [\frac{(1-s)}{(\pi)}][\phi+\cot\phi-(\frac{\pi}{2})]-[s(1+q_d)] \qquad [A]$$

$$=(\frac{1}{\pi})[\phi+(1-h)(1-s)]\cot\phi-(\frac{\pi}{2})] \qquad [B]$$

[21] c.g.s units used unless mentioned otherwise

table 2.17 continued...

$$q_d = (\frac{1}{\pi})[-\phi+\frac{1-s}{s}h\ \cot\phi-\frac{\pi}{2}]$$

[when s=1, the following are valid]

$$q_c = [\frac{Af}{u_c}]-(1+q_d) = \frac{(1-h)Af}{u_c}-\frac{1}{2}$$

$$q_d = \frac{h\ Af}{u_c}-\frac{1}{2}$$

where

$$\phi = \sin^{-1}\frac{u_c(1-s)}{\pi Af}\ ,\ s = -\frac{u_d}{u_c}$$

Equations for two phase axial mixing coefficient (E_{c2}) within the stage

$$E_{c2} = E_{c1} + \Delta E$$

where E_{c1} = Axial mixing coefficient under single phase flow

ΔE = increment due to the dispersed phase flow

$$E_{c1} = 0.3\frac{H-2m_1}{H-4.5}\frac{Afd_o^2}{S}$$

where, for $2m_1 < 0.65(H+2.35)$

$$2m_1 = 1.05(\frac{Af}{S})^{0.29}$$

table 2.17 continued...

elsewhere the following relation is valid

$$2m_1 = 0.65(H+2.35)$$

Expressions for ΔE

ΔE (Mixer Settler regime: $Af/S^{0.66} < 6.0$)

$$= 55.0(H-2m_2)d_{32}^3$$

ΔE (Dispersion regime: $6.0 \leq$ Af over $S^{0.66} \leq 13.0$)

$$= 55.0(H-2m_2)d_{32}^3-0.3$$

ΔE (Emulsion regime: $13.0 < Af/S^{0.66}$)

$$= 0.40\frac{h}{S^{1.2}}-1.01$$

Expressions for $2m_2$

when $AF/S < 13.0$

$$2m_2 = 1.00$$

when $Af/S \geq 13.0$ and $2m_2 < 0.54(H+3.60)$

$$2m_2 = 0.21\frac{Af}{S}$$

elsewhere

table 2.17 continued ...

$$2m_2 = 0.54(H+3.60)$$

3.(iv) Tojo et al. (1974) CO_2 (d↑)-water (c↑); d→c

USS; Tracer: chemical reaction of Br^- with methyl orange (earlier work due to Miyanami et al., 1973)

At high vibrating speeds

$$\alpha = \frac{2Af(1-h)}{u_c}\left(\frac{d_h}{d_i}\right)^2\left(\frac{d_d}{d_i}\right)^2$$

4.(v) Tojo et al. (1976) water(c↓)-MIBK(d↑)

USS; Tracer: 0.1 mol/L aqueous KCl solution

For sinusoidal disk vibration

$$\frac{1}{Pe_c} = 0.258+0.503\frac{S_d}{S_i}\frac{S_h}{S_i}\frac{0.5Af(1-h)}{u_c}$$

For Sinusoidal vibration and disk rotation

$$\frac{1}{Pe_c} = 0.181+0.35\frac{S_d}{S_i}\frac{S_h}{S_i}\frac{0.5Af(1-h)}{u_c}$$

5.(vi) Kim and Baird (1976) kerosene(d↑)-water(c↓)

$$E_c = 5.62A^{1.41}f^{0.73}H^{-0.88}$$

table 2.17 continued...

6. (viii) Miyanami et al. (1978) CO_2(d↑)-water(c↑)

$$\alpha_c = -\frac{\omega}{\pi}+[Af\frac{(1-h)}{u_c}](1-\frac{d_d^2}{d_l^2})(\frac{d_d}{d_l})^2$$

(for backflow past the vibrating disk)

$$\alpha_c = -\frac{\omega}{\pi}+[Af\frac{(1-h)}{u_c}](\frac{d_h^2}{d_l^2})(\frac{d_d}{d_l})^2$$

(for backflow through the partition hole)

where

$$\omega = \cos^{-1}[\frac{u_c(\frac{d_l}{d_d})^2}{\pi Af(1-h)}]$$

7.(xi) Parthasarathy et al. (1984) a) air(d↑)-water(c↓)

b) kerosene(d↑)-water(c↓)

USS; Tracer: 5 N NaCl solution

Axial Mixing Coefficient

System a)

$$\frac{E_c}{u_c L} = 4.58\times10^{-2}(0.5A)^{0.564}f^{0.622}u_c^{-0.39}d_o^{0.26}S^{-0.653}H^{-0.71}$$

table 2.17 continued...

System b)

$$\frac{E_c}{u_c L} = 4.22\times10^{-2}(0.5A)^{0.457} f^{0.344} u_c^{-0.37} d_o^{0.274} S^{-0.68} H^{-0.687}$$

Equivalent Theoretical number of stages

System a)

$$\frac{j_{actual}}{j_{ideal}} = 0.02 Re_v^{0.6} Re^{-0.4} (L/H)^{0.6}$$

System b)

$$\frac{j_{actual}}{j_{model}} = 0.053\ Re_v^{0.44} Re^{-0.2} \left(\frac{L}{H}\right)^{0.7}$$

where $Re_v = (0.5\ Af) d_o \Delta\rho / (S\mu_c)$ and $Re = d_o u_c \Delta\rho / \mu_c$

8(xii) Bensalem (1985) (i) water(c↓)-toluene(d↑)

USS; Tracer: 1.0 mol/L KCl solution

$$E_c = 16.20(Af + u_c)^{-0.707} u_d^{-0.425} h^{0.523}$$

Mass Transfer Measurements

(ii) water(c↓)-toluene(d↑); d→c

$$E_c = 28.04(Af)^{0.009} (u_c)^{1.95} (u_d)^{-0.82} h^{0.555}$$

table 2.17 continued...

(iii) water(c↓)-toluene(d↑); c→d

$$E_c = 11.05(Af)^{-0.223}(u_c)^{0.22}(u_d)^{0.06}h^{0.473}$$

9.(xiv) Karr et al. (1987) n-heptane (d↑)-water(c↓)

USS; Tracer; neutrally buoyant 9% ammonium chloride solution

$$E_c = 0.3(u_c+Af)+\frac{[f_o(\Delta w)^2]\times 2.54^2}{0.3(u_c+Af)}$$

$$f_o(\Delta u)^2 = 0.12 \text{ cm}^2.\text{s}^{-2} \text{ for } u_d = 0.148 \text{ cm/s}$$

$$= 0.45 \text{ cm}^2.\text{s}^{-2} \text{ for } u_d = 0.281 \text{ cm/s}$$

10.(xvi) Hari Krishnan et al. (1994) kerosene (d↑)-water(c↓)

USS; Tracer: NaCl solution

Mixer Settler region: Af ≤ 1 cm/s

$$\frac{NE_c}{u_c H} = 3.65\left(\frac{0.5Af}{u_c}\right)^{0.3}\left(\frac{\mu_c}{u_c d_o \rho_c}\right)^{0.2}\left(\frac{d_o}{H}\right)^{0.45} S^{-0.22}$$

Emulsion region: Af > 1 cm/s

$$\frac{NE_c}{u_c H} = 3.25\left(\frac{0.5Af}{u_c}\right)^{0.3}\left(\frac{\mu_c}{u_c d_o \rho_c}\right)^{0.2}\left(\frac{d_o}{H}\right)^{0.8} S^{-0.8}$$

Table 2.18 Experimental conditions for two phase axial mixing studies

#	RPC	u_c (cm/s)	u_d (cm/s)	A (cm)	f (Hz)	D (cm)	S (-)	H[22] (cm)	d_o (mm)	N (-)[23]
i	PRPC	0.266	0-0.43	0.25	6.67-13.3	7×3.5				
ii	MVDC	0.16-0.77	0-4.2	0-3.0	0-3.33	5.0	-	3.5	12-40[24]	14
iii	PRPC	0.3-0.5	0.0-0.45	0.3-0.9	0.4-10.0	5.0	0.044-0.192	5-15	2.5-3.5	2-5
iv	MVDC	0.16-1.12	1.15-7.72	0-2.4	0-7	5.0	-	3.5/7	6-40	4-9
v	MVDC	0.16-1.18	0-0.43	0.24-1.5	0-6	5.0	-	3.8	30	8
vi	KRPC	0.27	0.22-0.72	1.2-4.5	0.5-6.0	5.08	0.49 (STS)	2.7-5.23	13.6	35-68
vii	KRPC	0.0	0.0-0.55	2.2-3.1	0.5-1.0	5.08	0.54(STS)	2.70	6.35	68
viii	MVDC	0-0.33	0.37-1.12	2-6	0-4.3	17.2	-	12	36	4
ix	KRPC	0.5	0.22-0.44	0.636-2.54	0-8	14.96	0.581	2.6/5.2	14.7[25]	various
x	PRPC	u_c+u_d=0.55-0.73 cm/s		0.4	2-3.5	8.5	0.10	unknown	3	unknown

[22] Height between two standard Karr plates (or) height of stage

[23] Approx. estimate of number of plates for RPCs and (accurate) number of stages for MVDC.

[24] Hole diameter of partition plate

[25] for standard Karr plate; Baffles and special Fan plates also used.

Table 2.18 continued..

#	RPC	u_c (cm/s)	u_d (cm/s)	A (cm)	f (Hz)	D (cm)	S (-)	H (cm)	d_o (mm)	N (-)
xi	RPCND (GL)[26]	1.24-3.72	0.043-0.092	1.4-8.0	0.6-3.6	9.3	0.09-0.3	2-5.6	3-8	10
xi	RPCND (LL)[27]	0.18-0.33	0.027-0.33	1.4-4.4	0.75-3.0	15.3	0.125-0.3	2-5	0.3-0.8	18
xii	KRPC (NMT)[28]	0.34-1.03	0.17-0.69	0.5-1.60	0.0-5.83	7.6	0.58	2.54	16	64
xii	MT[29] (d→c)	0.33-0.87	0.55-1.45	0.586 ≤ Af ≤ 6.41						
xii	MT (c→d)	0.34-1.55	0.34-0.69	0.586 ≤ Af ≤ 2.75						
xiii	KRPC	0.6-1.88	0.8- 8.7	0 < Af <7.5		5.08	0.53	2.54		84
xiv	KRPC	0.85-1.13	0-0.28	0 ≤ Af ≤ 12.5		2.54	0.584	2.54	not given	130
xv	KRPC	0.49-3.95	0-0.99	4.5	0-3.5	5.08	0.57	2.7	14	54
xvi	RPCND	0.05-0.9	0.03-0.85	1.4-5.0	0.66-2.5	15.3	0.125-0.517	5.0	5-12	18

[26] GL - Gas Liquid system

[27] LL- liquid-liquid system

[28] NMT - Non Mass Transfer

[29] MT - Mass Transfer

2.4.3 Axial mixing data in the dispersed phase

Only a few experimental studies have also been made in the dispersed phase. Since these measurements were also accompanied by similar measurements in the continuous phase the experimental conditions and column details can be obtained from the previous tables (2.17 and 2.18).

(i) Souhrada et al. (1966)

Back-mixing in the dispersed phase was determined by the steady state method using anthracene as tracer in a 7.0 × 3.5 cm rectangular RPC. The results indicated that back-mixing in the dispersed phase was insignificant. Further, the dispersed phase back-mixing values obtained from tracer measurements under non mass transfer conditions were used in the calculations under mass transfer conditions to reduce the number of experiments.

(ii) Nemecek and Prochazka (1974)

The net backflow coefficient through the stage q_d was found to be important only at high agitation rates when the drop rise velocities were small in comparison with the pulsation velocity. The correlations for q_d have already been listed in table 2.17. It can be seen that q_d is linked with q_c in one expression and can be expressed independently as a function of hold-up in the second. The authors recommend the use of the second expression under emulsion conditions where hold-up is more uniform along the column. As already mentioned, back-mixing is non existent in the dispersed phase in the mixer settler and dispersion regimes.

(ii) Hafez et al. (1980)

A model which accounted for drop hydrodynamics, flooding restriction, mass transfer specifications and axial mixing was developed to determine the height of the extraction column. This was tested on a column of known dimensions (15 cm diameter and 205 cm in length) by

conducting mass transfer experiments on a simple system viz. kerosene (d↑)-acetic acid-water(c↓); d→c. The E_c values obtained by Hafez et al. (1979) were used while 3 assumptions were tested for estimating E_d viz. (i) $E_d = E_c$ (ii) $E_d = 0.5\ E_c$ (iii) $E_d = 0$. It was found that simulations for the column length gave the best result when assumption (i) was used. Assumption (iii) which implies plug flow conditions led to a significant overestimation of the column performance at high agitation rates. A similar result was obtained for the system o-xylene(d↑) - acetic acid - water (c↓).

(iii) Heyberger et al. (1983)

When investigating the variation of back-mixing and plate efficiency parameters stage-wise, the authors found that α_d was small and could be treated as a constant. For other parameters, a fourth degree polynomial function of stage number was required.

(iv) Shen et al. (1985)

The true height of transfer unit (H_{ox}) was estimated by using the analytical solution to the dispersion model. The model required estimates of E_c and E_d. E_c values were obtained from the work of Kim and Baird (1976) and E_d was set equal to E_c.

(v) Bensalem (1985)

The E_d values were obtained by the pulse injection of an organic dye into the dispersed phase and the response was monitored downstream at two points. The probes comprised of a photo cell facing a light emitting diode and measured the dye concentration in the coloured drops. The correlations under non mass transfer and mass transfer conditions are given in table 2.19. The experimental conditions for the mass transfer runs are the same as those for E_c. For non mass transfer runs the following range of variables were studied:

(i) u_c=0.69-1.03 cm/s (ii) u_d=0.17-0.69 cm/s (iii) Af=0.83-6.62 cm/s

(vi) Karr et al. (1987)

E_d values were obtained in the 2.54 cm diameter column by the transient tracer technique for the system n-heptane(d↑)-water(c↓). Teflon plates were used to avoid wetting by the aqueous phase (usually wetting by the continuous phase is promoted). The study indicated that the superficial dispersed phase axial mixing coefficient was not significantly affected by the agitation or flow rates. In this study the scaling up of RPC was also studied as mentioned in section 2.2. Setting a constant value of E_d (=10 cm^2/s) led to a scale-up relation which was similar to the one used in the industry. When E_d was set equal to E_c the scale-up relation became very conservative. It must be noted that in the scale-up exercise, it was assumed that under well agitated conditions the scale effect on E_c was same as that for single phase flow.

(vii) Harikrishnan et al. (1994)

The authors used the correlation for E_d developed in a previous non mass transfer study (Srinikethan et al. 1987) for the estimation of the true mass transfer coefficient. The correlation is given in the following table 2.19.

Table 2.19 Axial dispersion in the dispersed phase (c.g.s. units)

#	Author	Equation/Correlation used for E_d or α_d
1	Souhrada et al. (1966)	$\alpha_d \rightarrow 0$
2	Nemecek and Prochazka (1974)	Refer table 2.17 for correlation for q_d
3	Hafez et al. (1980)	$E_d=E_c$; E_c based on Hafez et al. (1979)
4	Heyberger et al. (1983)	α_d is small and constant
5	Shen et al. (1985)	$E_d=E_c$; E_c based on Kim and Baird (1976)
6	Bensalem (1985); NMT [MT]; d→c	$E_d = 2.016\ (Af)^{-0.137}\ u_c^{-0.148} u_d^{0.503} h^{-1.293}$
		$E_d = 22.98\ (Af)^{-0.134} u_c^{-1.289} u_d^{1.38} h^{0.2}$
	[MT]; c→d	$E_d=3.58\ (Af)^{0.41} u_c^{-0.015} u_d^{2.25} h^{-1.44}$
7	Karr et al. (1987)	E_d= 10 cm²/s for scale-up purposes
8	Harikrishnan et al. (1994)	$\frac{NE_c}{u_d H} = 1.513\left(\frac{0.5Af}{u_d}\right)^{0.25}\left(\frac{d_o}{H}\right)^{0.13} S^{-0.22}$ Mixer Settler regime ; Af ≤ 1 cm/s $\frac{NE_d}{u_d H} = 0.238\left(\frac{0.5Af}{u_d}\right)^{0.7}\left(\frac{d_o}{H}\right)^{0.18} S^{-0.46}$ Emulsion regime ; Af > 1 cm/s

2.4.4 Axial Mixing Correction for Volumetric Mass Transfer Coefficient

As described briefly in chapter 1, the volumetric mass transfer coefficient based on the exit and inlet concentrations is representative of the column performance only under plug flow conditions. When there is axial mixing the true operating line shifts towards the equilibrium line thereby reducing the concentration driving force for mass transfer, so that the calculations based on an assumed plug flow operating line will tend to underestimate the true mass transfer coefficient. Equivalently the height of transfer unit under assumed plug flow conditions will be more than the true value. The previous section already indicated the correction applied to the mass transfer coefficient (Yang et al. 1986; Baird and Rama Rao, 1988) for gas liquid contact.

(i) Bensalem (1985)

This author studied various possible methods for determining the true mass transfer coefficient K_x, with units kg/(m^{2}s), from the experimental concentration profiles. The interfacial area in the model equations were determined from equation (2.19). The various possibilities investigated for one typical c→d experiment were (i) use of α_c and α_d estimated from transient tracer method under non mass transfer conditions (ii) assuming $\alpha_d = 0.0$ (iii) assuming $\alpha_d = \alpha_c$ (iv) assuming only α_c and estimating α_d and the true mass transfer coefficient K_x and (v) estimating all parameters viz., α_c, α_d and K_x. For cases (i)-(iv) the variation in the estimated K_x values were in the order of $\pm$ 11% in agreement and the fits of the experimental data with the simulation profiles were very good. Case (v) gave a value of K_x which was quite different from previous estimates, while α_c and α_d were within 14.5% and 11.8% of the transient tracer estimates.

The K_x values for remaining experiments were based on the assumptions used in case (i). The results indicated that

1. K_x decreased with increase in agitation rate. K_x was higher for d→c mass transfer than the

reverse case. This was explained as being due to coalescence effects.

2. The true height of transfer unit (H_{ox}) obtained from K_x values decreased with increasing agitation until flooding occurred. The values were lower than plug flow values.
3. A correlation was proposed for the true mass transfer coefficient in the form Sherwood number (expressed as $Sh=K_x d_{32}/\rho_c D_{AB}$) versus Reynolds number ($Re=d_{32}U_s \rho_c/\mu_c$).

$$Sh = 1.924(Re)^{0.92} \qquad (2.56)$$

The column details are given in table 2.18 (xii) and the ranges of experimental conditions under which this equation is valid are

u_c : 0.30-0.76 cm/s, u_d : 0.50 - 1.28 cm/s

h: 0.06-0.24, d_{32} : 0.20-0.68 cm, Re: 54-574.

(ii) Shen et al. (1985)

The authors investigated the effect of mass transfer direction and plate material on column performance. The system studied was kerosene (d↑)-n butyric acid-water(c↓); d→c and c→d. The plates used were (A) stainless steel and (B) stainless steel with Teflon plates in between. The axial dispersion model was used and E_d was assumed to equal E_c. The E_c values were taken from the work of Kim and Baird (1976). The authors adjusted by trial and error, the true number of units ($N_{ox} = k_{ox}$ a Z/u_c). Here X represents the continuous phase and Z denotes the total length of the column. N_{ox} was adjusted until the computed solution for the continuous and dispersed phase exit concentrations matched with the experimental values. It must be noted that the non linear equilibrium curve was approximated by a chord drawn between the inlet and exit concentrations. Pratt's (1975) simplified method was used in the calculations. The findings of the authors are summarized below.

1. The study indicated that the true height of transfer unit (H_{ox}) was much greater for the d→c than for c→d mass transfer especially at high agitation levels. This was attributed to mass transfer induced coalescence effects leading to larger drop sizes (almost 2 times) for the d→c direction, resulting in reduced hold-up and hence interfacial area. However the coalescence effect was also responsible for a greater permissible operating frequency and drop surface mobility. The latter led to a higher mass transfer coefficient k_{oc} for the d→c case.
2. The k_{ox} values were also found to be insensitive to agitation. The modified plate arrangement (B) had the effect of increasing the permissible throughput (1.5-2 times) before flooding occurred, relative to arrangement (A).
3. However for both directions of mass transfer the H_{ox} values were lower for the plate stack (A) indicating superior mass transfer performance.

(iii) Kannan et al. (1990)

A method was developed to determine the true mass transfer coefficient which was applicable to even those cases characterized by a non linearity in the equilibrium curve. This involved the conversion of the 4 boundary conditions characterizing the 2nd order ordinary differential equations into 4 initial conditions so that the 4th order Runge Kutta method could be used. Two nested iteration cycles were used. In the first iteration at the outer cycle, the true mass transfer coefficient was assumed to be the same as the plug flow value as a starting estimate. Using this value the X phase inlet jump concentration was iterated upon until the exit X concentration value (X_{sim}) equalled the experimental one (X_{expt}). However, the slope of the X concentration profile $(dX/dz)_{z=1.0}$ was not usually zero as stipulated by the boundary condition. Hence another value of k_{ox} was assumed and the entire procedure was repeated until both the requirements viz. $X_{sim} = X_{expt}$ and $(dX/dz)=0.0$ were met at $Z=1.0$. The predicted value of the Y concentration at

convergence at Z=1.0 was determined as the Y inlet jump. The Regula Falsi (modified secant) method greatly improved the speed of the iteration process. This method compared satisfactorily with the method developed by Pratt (1975, 1976).

(iv) Harikrishnan et al. (1994)

The mass transfer performance of a RPC with no downcomers has been studied using the systems water (c↓)-benzoic acid-kerosene (d↑); d→c, and Water (c↓)-n butyric acid - Kerosene(d↑); d→c and c→d. The axial mixing coefficients were based on correlations obtained from RTD studies under non mass transfer conditions (Srinikethan et al. 1987). The true volumetric mass transfer coefficient was determined by the boundary iteration technique due to Kannan et al. (1990). The variation of the volumetric mass transfer coefficient $k_c a$ was similar to that of the interfacial area. Unlike the results from Shen et al. (1985) the $k_c a$ values for d→c mass transfer were higher than those for c→d mass transfer. However in both these studies, the volumetric efficiencies were higher for the d→c mass transfer case. When the mass transfer coefficients were compared with the rigid drop model and the circulating drop model predictions the values were found to be intermediate to the two predictions. The correlations for the true mass transfer coefficient are given below. The range of experimental variables and column details were already given in table 2.18.

$$\frac{k_c}{(k_c)_{Af=0}} = 1+0.035\psi^{0.4}\left(\frac{u_c}{u_d}\right)^{0.1} \qquad (2.58)$$

where

$$(k_c)_{Af=0} = c\, u_d^{0.21} \qquad (2.59)$$

Table 2.20 constants in equation 2.59 (c.g.s. units)

#	solute	mass transfer direction	c
1	benzoic acid	d→c	1.8×10^{-3}
2	n-butyric acid	d→c	3.8×10^{-4}
3		c→d	3.0×10^{-4}

2.5 Discussion and summary

2.5.1 Scale-up of RPCs

In section 2.2 the performance results of industrial scale RPCs were provided. The empirical scale-up rules developed for the Karr columns were described. These rules have been successfully applied to scale-up commercial RPCs up to 1 m in diameter (Lo and Prochazka, 1983). The scale-up exponent of 0.38 may turn out to be too conservative for extraction systems which require lower agitation and column diameter. Hence there is a degree of uncertainty in applying the empirical scale-up rule. Further, axial mixing is not explicitly accounted for. Hence there is a need for scale-up procedures which incorporate reliable axial mixing predictions which take into consideration not only the operating conditions but also the physical properties of the systems used. As can be noted from table 2.18 the maximum column diameter used in two phase axial mixing studies is lower than 20 cm. However industrial columns can be designed up to a meter in diameter. Since axial mixing coefficient increases with column diameter due to more severe radial non uniformity, reliable scale-up rules can be only developed with accurate data obtained in columns of large diameters. This may be accomplished by cooperative research between industries and academic institutions.

2.5.2 Drop size predictions

As can be seen from table 2.3, the model based on Kolmogoroff isotropic turbulence theory is widely used to predict the Sauter mean drop diameter. However the following factors must considered before applying this model.

1. To apply the Kolmogoroff model accurate prediction of the energy dissipation term, especially that due to mechanical agitation, is important. In Karr RPCs, the mechanical energy dissipation predicted by the quasi-steady state model developed by Hafez and Baird (1978) for Karr columns will no longer be applicable at very low amplitudes. Hence Baird and Rama Rao (1995) found that the acoustic model developed by Baird and Stonestreet (1995) applied under these conditions. Similar model corrections may be necessary to other columns as well.
2. Baird and Lane (1973), following Calderbank's recommendation (1960) added the dispersed phase energy dissipation to the mechanical energy dissipation term in order to extend the model to conditions of low agitation. However at zero agitation, the drop size is determined by its formation at the distributor, balance between buoyancy and interfacial tension forces, shearing effect with the stationary plate etc. Hence a unified expression similar to the one proposed by Sovava (1990) equation (2.14) seems more applicable for predicting the drop size even at zero and moderate agitation.
3. The Kolmogoroff model is not accurate when the interfacial behaviour of the system is affected by mass transfer induced coalescence, wetting of the dispersed phase at the plates and presence of surfactant.

In spite of these limitations, the Kolmogoroff model has proved to be very useful to give reasonable estimates of the mean drop diameter under well agitated conditions.

2.5.3 Hold-up predictions

Hold-up is an important variable since its variation with agitation determines the flooding and hence limiting characteristics of the column. Further, considered along with drop size it also determines the interfacial area for mass transfer (equation 2.19). Hence it is important to have reliable estimates of hold-up. The slip velocity equation concept proposed by Lapidus and Elgin (1957) is commonly used to determine hold-up. Relating the slip velocity in terms of the product of a characteristic velocity $\bar{u}_o$ and a hold-up function $(1-h)^n$ is also a common practice.

The accurate predictions of the hold-up in turn depends strongly on the estimation of the characteristic velocity. However, unlike spray columns, in mechanically agitated columns such as RPCs it more difficult to find an expression for the characteristic velocity since the phase flow rates are not the only variables involved; $\bar{u}_o$ will also vary with the mechanical agitation. This problem has been tackled by describing the characteristic velocity in terms of the drop size (Baird and co-workers 1971, 1984; Slater 1985). The proposed correlations (equations 2.29, 2.30) were functions of the physical properties of the system as well. Slater (1985) assumed that the characteristic velocity is comparable with the terminal velocity of the drops, which considering the complicated hydrodynamics of agitated dispersions may be only approximate. However the prediction of rise velocity of drops under hindered flow conditions is by itself a complicated phenomenon which has not been resolved yet. Further, when using the correlations suggested for $\bar{u}_o$ caution should be exercised to see that the physical properties of the new system fall in the range of applicability of the correlation. For instance, the correlation proposed by Baird and co-workers incorporating an empirical parameter K^* (equation 2.28) is applicable for interfacial tension in the range 20-25 mN/m.

The slip velocity correlation based on the recirculating flow model proposed by Ueyama

and Miyauchi (1979) and adapted for RPCs by Varma and co-workers (1983, 1988) for liquid-liquid and gas-liquid systems also deserves attention (table 2.6). The study by Veljkovic and Skala (1989) however indicates that the correlation could not be used as a general prediction for gas-liquid systems. However Gomma et al. (1991) used this approach and estimated the parameters of the model from the experimental data (table 2.6).

2.5.4 Axial mixing models

The Rosen and Krylov model developed for pulsed packed columns does not completely take into account the dispersed phase flow behaviour and the interaction of its effect with mechanical agitation. Hence when this model (equation 2.47) was applied to KRPCs, Karr et al. (1987) found it necessary to fit two different values of $f_o(\Delta u^2)$ at two different dispersed phase flow rates (table 2.17). Further the constants used in the model are also specific to the geometry of the column used.

The two zone model developed by Prochazka and co-workers (1970,1974) is an important advance in the understanding of the mechanism of back-mixing in agitated contactors. Analytical expressions were derived for the mixer settler, dispersion and emulsion regimes. However their estimated parameters of these models like the height of the well mixed zone and the back-mixing coefficient in the diffusion zone are specific to their column only. Stevens and Baird (1990) successfully extended this model to single phase axial mixing data from columns equipped with Karr plates. Even though they recommended extending this study for two phase flow conditions it is somewhat surprising that it has not been undertaken. However it must be noted that Prvcic et al. (1989) could not fit their axial mixing data from pulsed columns using the correlations from Nemecek and Prochazka (1974). Hence they had to modify the two zone model for their data.

The Kolmogoroff model based on isotropic turbulence approach has been found to be a promising approach in predicting axial mixing in bubble columns as indicated in a review by Kawase and Moo Young (1990). The extension of this approach to mechanically agitated columns (under single phase flow conditions) was initiated by Holmes et al. (1991) and Baird and Rama Rao (1991). The extension of this application to two phase mechanically agitated systems is implemented in this study.

Despite significant advances in the modelling of axial mixing there is still a trend to correlate the axial mixing coefficients empirically with the operating conditions (Kim and Baird 1976 a, b; Parthasarsathy and Varma 1984; Bensalem 1985; Harikrishnan et al. 1994). However the columns used were different and the range of operating conditions covered were narrow, so that Kumar and Hartland (1994) concluded that it was not possible to correlate the entire body of data. The variation of axial mixing coefficients with operating conditions and column geometry were listed for different investigators in section 2.4.

2.5.5 Axial mixing under mass transfer conditions

Until now, very little work has been done in estimating axial mixing parameters under mass transfer conditions in RPCs. Only Souhrada and Prochazka (1966), Heyberger et al. (1983) and Bensalem (1985) have estimated E_e values under mass transfer conditions. Other workers (Tojo et al. 1974; Miyanami et al. 1978; Shen et al. 1985; Yang et al. 1986; Karr et al. 1987; Baird and Rama Rao 1988; Kannan et al. 1990 and Harikrishnan et al. 1994) used axial mixing data obtained from tracer tests from previous measurements under non mass transfer conditions. This approach may prove erroneous if known solute transfer induced phenomena significantly alter the hydrodynamic and hence liquid phase mixing characteristics of the column.

2.5.6 Axial mixing in the dispersed phase

In contrast to continuous phase axial mixing studies under both single phase and two phase flow conditions, dispersed phase axial mixing coefficients are comparatively rare. Sometimes certain assumptions have been used by different workers (Hafez et al. 1980; Shen et al. 1985; Karr et al. 1987) as noted in table 2.19. Since the very existence of back-mixing in the dispersed phase has been questioned (for eg., Pratt and Stevens 1992) and the relatively low values obtained for E_d when compared with E_c (Souhrada and Prochazka 1966; Heyberger et al. 1983; Bensalem 1985) it now appears that the complicated forward mixing model is a better representation of the dispersed phase flow non idealities.

CHAPTER 3

Experimental Apparatus, Systems and Procedures

3.1 Apparatus

In this study, experiments were conducted in a 5.08 cm internal diameter Karr column fitted with a stack of stainless steel plates supported on a central shaft. The column itself was built from a series of flanged PYREX glass sections. The flanges were separated by stainless steel collars and adjacent flanges were connected by bolts. The plate stack could be reciprocated at a predetermined frequency and amplitude by a variable speed motor (560 W, 0-400 rpm) with an adjustable Yoke drive. A photograph showing the column is given in figure 3.1. The Karr plate and its spacer are shown in figure 3.2a. The PYREX glass sections used in this work are shown in figure 3.2b. The details of the column internals and glass sections are given in table 3.1.

Table 3.1 Important dimensions of the RPC used in this study

#	Column Variable	Characteristic	Dimension
1	Plate	Outer diameter	4.83 cm
2		Hole diameter (d_h)	13.56 ± 0.01 mm
3		Thickness (d_t)	1.54 ± 0.02 mm
4		Fractional Free Area (S)	0.56
5	Spacer	Outer diameter	9.52 ± 0.02 mm
6		Length	2.55 cm
7	Glass Section	Length	15 / 30 cm
8		Inner diameter (D)	5.08 cm
9		Thickness	7.8 ± 0.1 mm

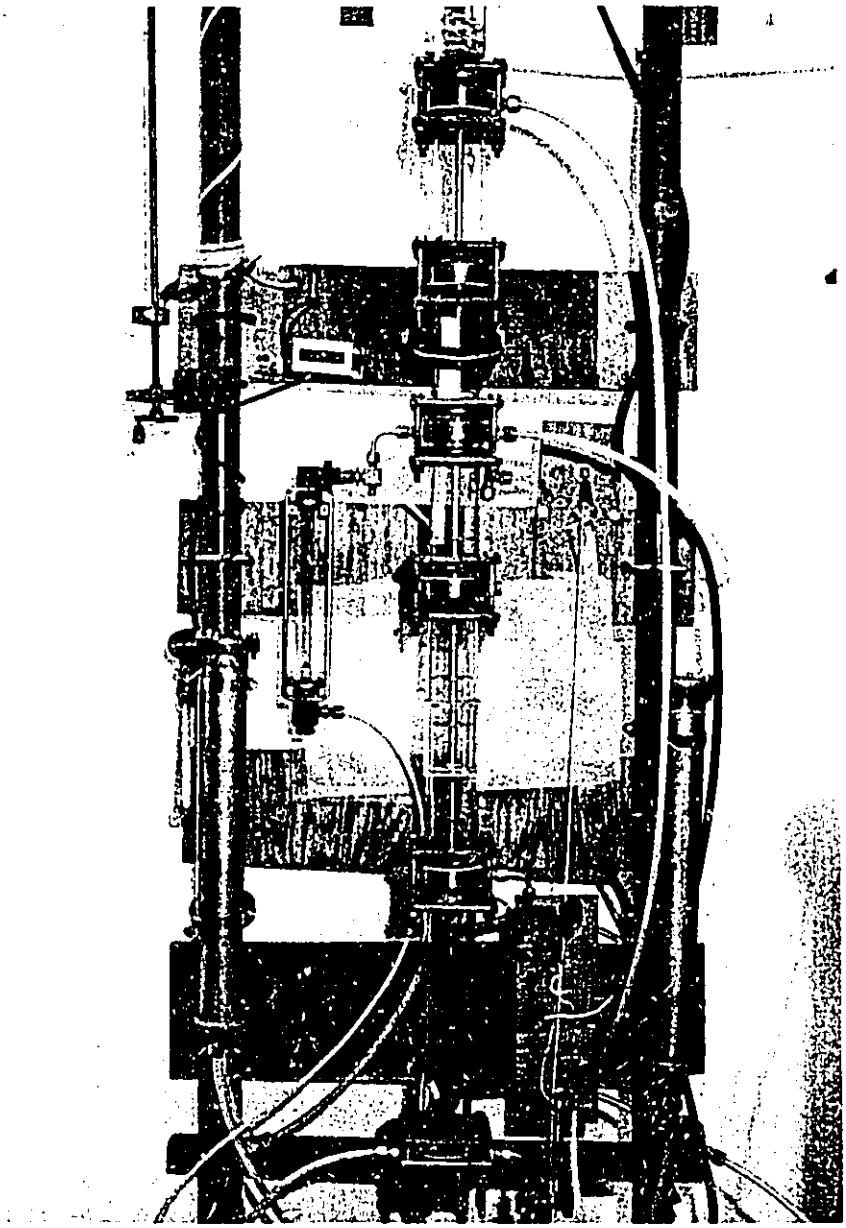

Figure 3.1 Photograph of the reciprocating plate column

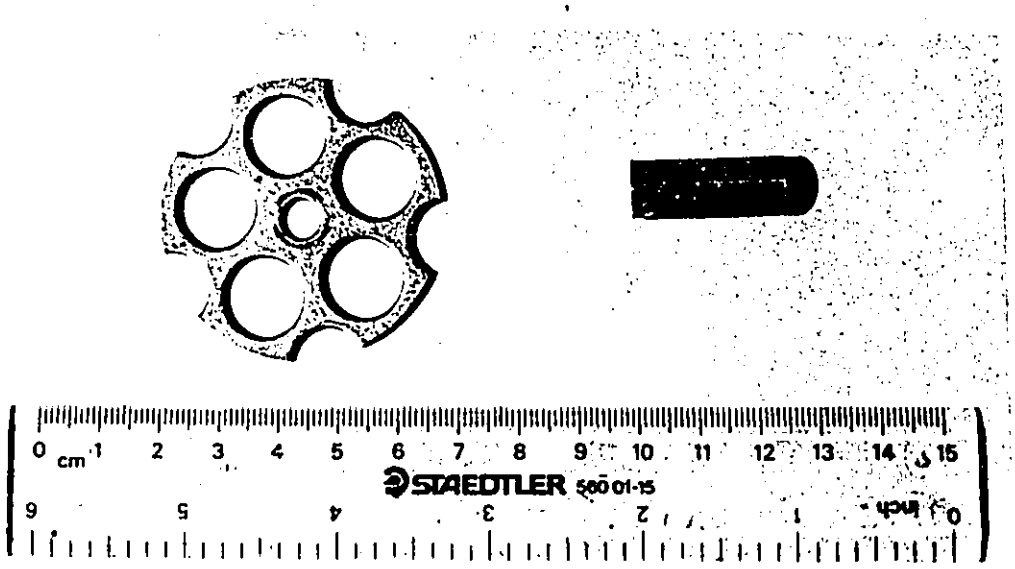

Figure 3.2 a Photograph of a Karr plate and its spacer used in this study

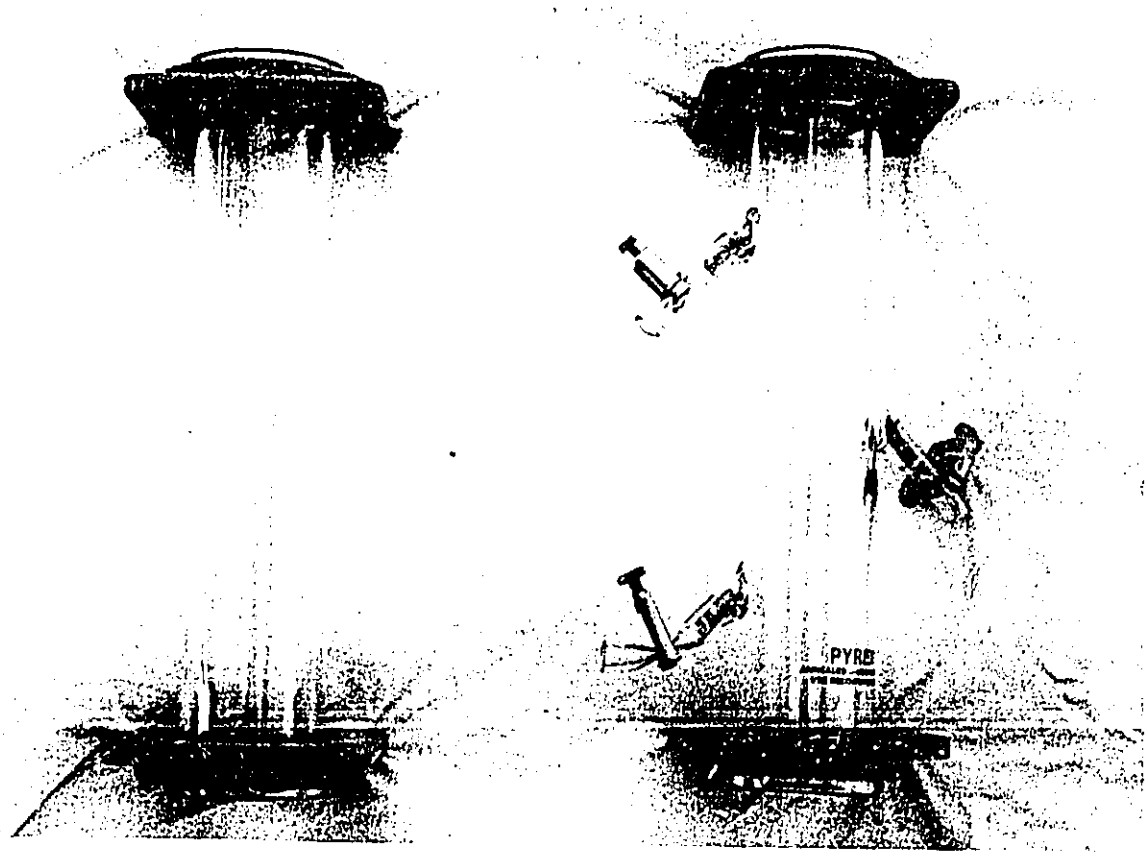

Figure 3.2 b Photograph of PYREX glass sections constituting the reciprocating plate column

3.2 Back-mixing measurements under co-current non mass transfer conditions

In this study back-mixing in the continuous phase was studied both in the presence and absence of an unstable density gradient using steady state tracer injection technique. The following conditions were employed.

a. Single Phase only (water)

b. Two phase studies using the system Isopar M (d↑)-water(c↑).

The studies were conducted both in the presence and absence of mechanical agitation. The physical properties of Isopar M and water are given in table 3.2. The Isopar M has an average molecular weight of 191 and consists of isoparaffinic compounds. For the sake of comparison a few representative runs were carried out under neutrally buoyant conditions in which the density gradient in the continuous phase was zero. The means of attaining the unstable density gradient and the neutrally buoyant conditions are discussed in the following section.

3.2.1 Experimental Procedure

The overall experimental set-up for the co-current non mass transfer work is given in figure 3.3. The dispersed phase was Isopar M, an odourless petrochemical resembling kerosene. The continuous phase was tap water. The column was initially filled with water and agitation whenever applicable was switched on. As shown, the water and Isopar M (for two phase conditions) were pumped co-currently upwards using a Milton-Roy Duplex pump P. Simultaneously, the sodium chloride solution, pumped from tank T3 at a constant rate (17 ml/s) by a centrifugal pump through the rotameter R_c entered the column at the top. The unstable density gradient in the continuous phase is induced by the continuous flow of the denser sodium chloride solution at the top of the column. The NaCl apart from causing the density gradient also served as the tracer for the steady state axial mixing measurements. The concentration of the

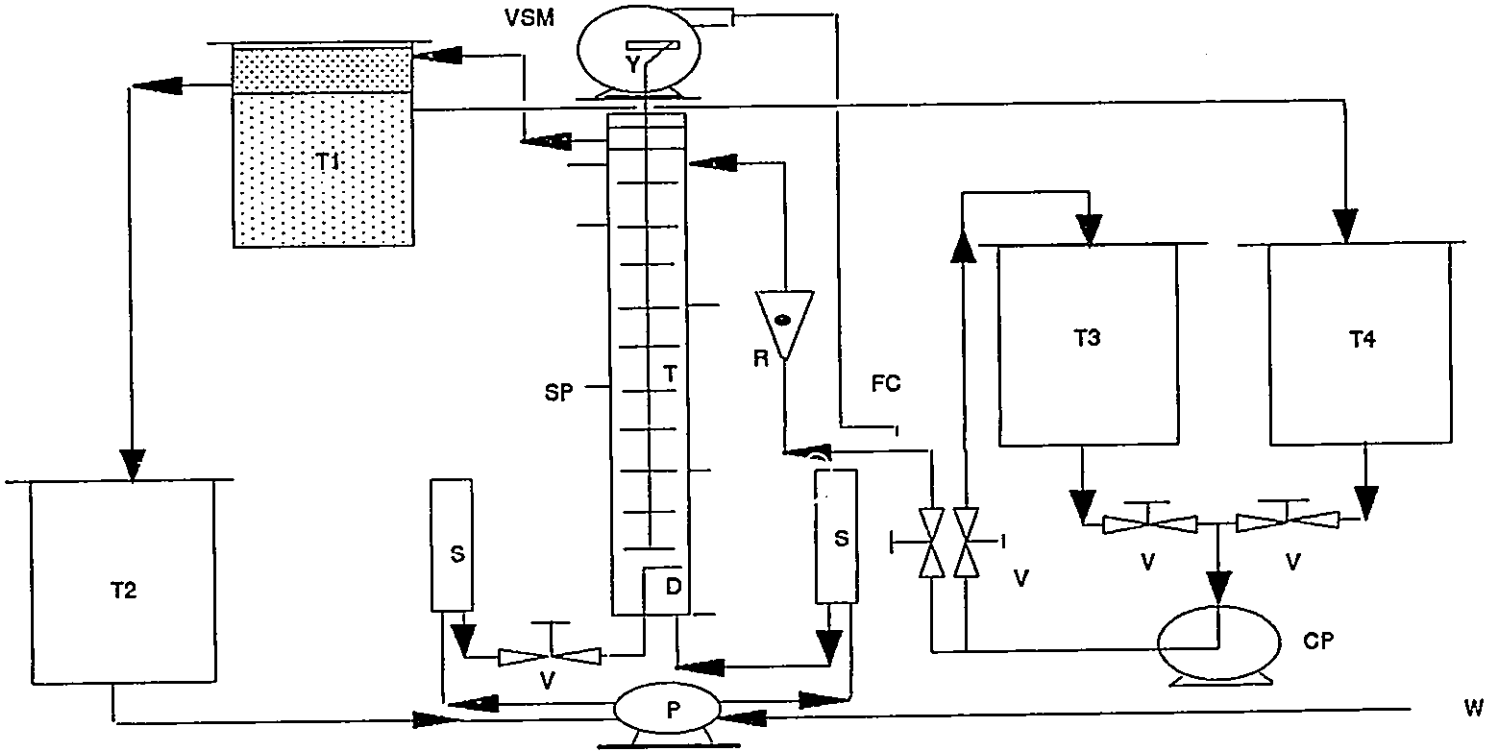

Figure 3.3 Flow diagram for co-current flow experimental set up

CP-Centrifugal Pump, D-distributor, FC- frequency controller, P-pump, S-surge cylinder, SP-sample port, T-plate-stack, T1-two phase tank, T2-Isopar storage tank, T3,T4- NaCl tanks, V-flow control valve, VSM-variable speed motor, W-tap water storage, Y-yoke

feed NaCl solution was typically 7% and its density at the top of the column was around 1.04 g/ml as compared to that of pure water which had a density of 0.9972 g/ml. The two phase mixture overflowed into the two phase receiving tank T1. The organic phase was recycled to tank T2.

Due to back-mixing in the continuous phase there was a dispersive flux of the NaCl solution in the negative z direction, if the origin is defined at the tracer inlet. Hence a tracer profile was established in the column. The tracer profile shape was determined by sampling approximately 15 ml of the tracer at the upstream locations after allowing the column to come to steady state. The basis for this was taken to be the displacement of 3-4 times the effective column volume. The sample ports were located at the tracer entry point and distances 18.2, 37.7, 55.2, 72.7 and 105 cm further upstream (figure 3.4) The sampling was carried out in a staggered fashion at intervals of 3 minutes so that a sufficient time period existed between sampling at adjoining taps to avoid excessive disturbance of the column operation. To economize on the use of NaCl solution, a recycle arrangement was incorporated involving tanks T3 and T4. After the end of the experiment, the diluted NaCl was recycled from tank T4 to tank T3 and the solution was made up to the original concentration.

The same procedure was adopted when the continuous phase was made neutrally buoyant. This was accomplished by adding sufficient methanol to a 3% tracer solution so that its specific gravity was adjusted to be the same as that of water. A lower salt concentration was used to minimize the methanol consumption.

3.2.2 Analysis of the samples

The concentration of the tracer was analyzed using a pre-calibrated conductivity meter, type CDM3 (Radiometer, Copenhagen). For analysis under neutrally buoyant conditions a

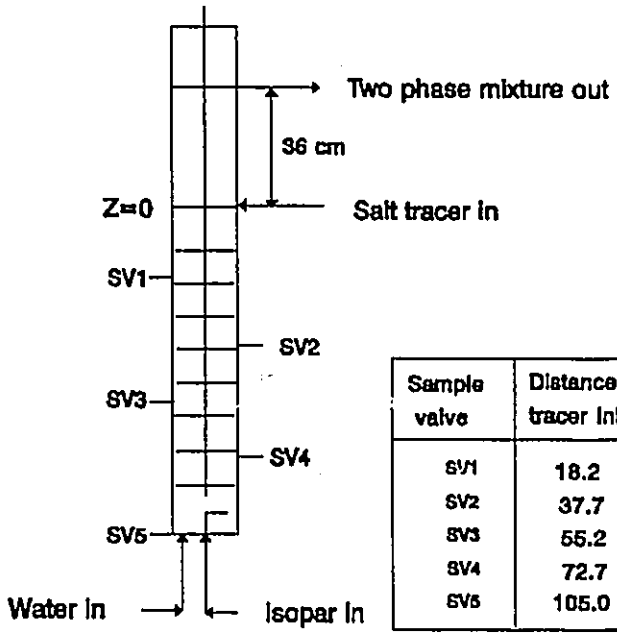

Sample valve	Distance from tracer inlet (cm)
SV1	18.2
SV2	37.7
SV3	55.2
SV4	72.7
SV5	105.0

Figure 3.4 Details on back-mixing scheme and sampling

separate calibration chart was required, since methanol caused a significant change in the conductivity. The calibration charts of conductivity vs NaCl are given in figures 3.5 a and b.

3.3 Back-mixing Measurements under two phase counter-current flow conditions

The co-current non mass transfer work described in the previous section constituted the main part of this thesis. As a preliminary step towards the understanding of the effect of unstable density gradient *induced* by mass transfer, a few experiments on back-mixing in the continuous phase were carried out under counter-current flow situations. The unstable density gradient in the continuous phase was created due to solute transfer. Under non mass transfer situations, i.e. when only pure Isopar M and water are contacted the density of the continuous phase remains neutrally buoyant. Experiments were performed under both mass transfer and non mass transfer conditions so that the results could be compared. The mass transfer system was so chosen that a measurable density gradient was set up in the continuous phase. The transferring solute chosen

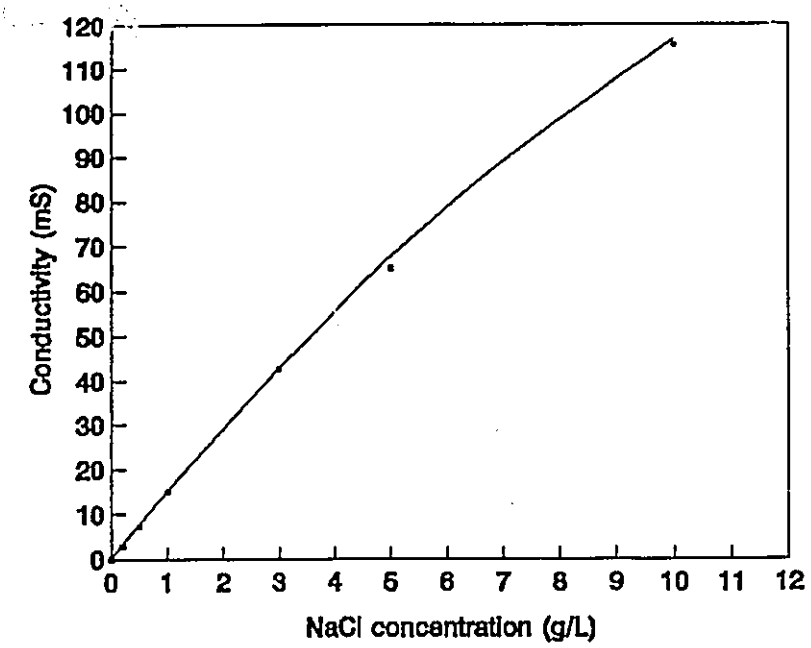

Figure 3.5a Calibration chart of conductivity meter for salt solution

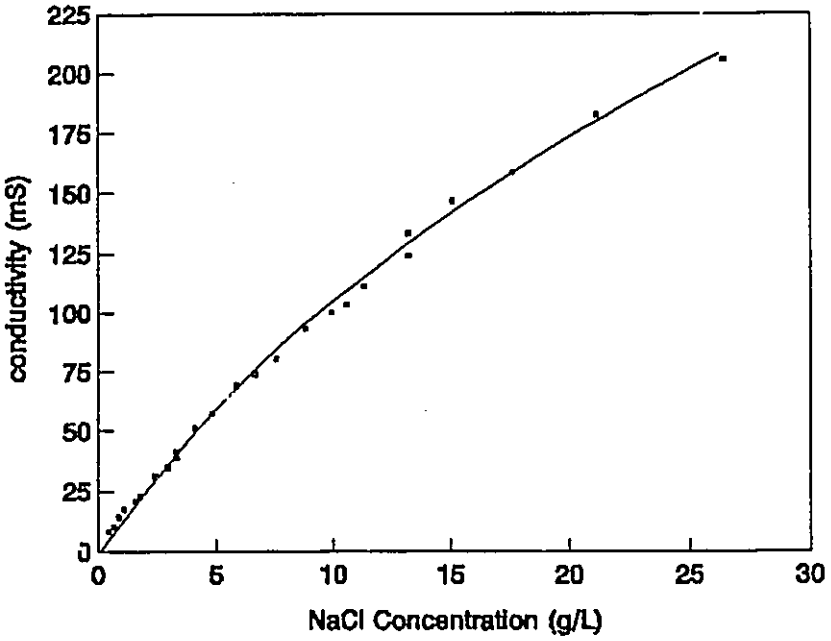

Figure 3.5b Calibration of conductivity meter for salt + methanol solution

in this study and its properties are described below.

3.3.1 Choice of the System

The choice of the system was restricted by environmental acceptability under the available laboratory conditions. Hence standard systems involving MIBK, toluene, benzene and solutes like acetic acid, acetone had to be discarded on the grounds of unpleasant smell, fire and health hazards and waste disposal limitations. Other standard systems involving solutes like benzoic acid and butyric acid had to be omitted on the considerations of very limited solubilities. Hence to induce a measurable density gradient and also satisfy the environmental regulations, it was decided to use a system involving one of the lower molecular weight aliphatic alcohols as the solute. On account of their polar nature these alcohols are soluble in both organic and aqueous phases to a significant extent.

Some preliminary studies involving secondary butyl alcohol were carried out and had to be discarded on accounts of pungent smell and limited solubility. Finally the system Isopar M (d↑)-isopropyl alcohol-water (c↓) with the solute transfer occurring in the d→c direction was chosen for this study.

3.3.2 Properties of the system

3.3.2.1 Physical properties

The physical properties of the system used are given in tables 3.2 and 3.3. The effect of alcohol (in the range of concentrations observed during this study) on the density, viscosity and refractive index of Isopar M and water were also determined and expressed as a third order polynomial function. For instance, the aqueous phase viscosity was represented as shown below. Here the concentration of alcohol (c_{alc}) is in g/L and the coefficients are tabulated in table 3.3.

$$\mu_c = \alpha + \beta\, c_{alc} + \gamma\, c_{alc}^2 \qquad (3.1)$$

The concentration range in which the fit is valid is also tabulated.

Table 3.2 Physical properties of chemicals used in this study

#	Chemical and supplier	density[1] (g/mL)	refractive index[2]	viscosity[3] (cp)
1	Demineralized water	0.9972	1.3329	1.0
2	Isopar M (Esso Petroleum, Canada)	0.7853	1.4380	2.4
3	Isopropyl alcohol (Van Waters and Rogers)	0.7819	1.3760	2.1

The interfacial tension for Isopar M water system was determined by the ring method as 50 mN/m.

Table 3.3 Physical property variations for solutions of alcohol in water and Isopar M

chemical	physical property	concn. range (g/L)	polynomial function coefficients (eq. 3.1)		
			α	$\beta \times 10^4$	$\gamma \times 10^5$
Water	density (g/cc)	0-80	0.9973	-1.8275	0.0166621
	viscosity (cp)	0-80	1.00162	2.78374	3.68579
Isopar M	viscosity (cp)	0-80	2.3928	-74.3816	3.89114
	refractive index	0-90	1.4381	-0.843547	-

[1] determined by PAAR densitometer at 24 ± 0.1°C.

[2] measured by ABBE refractometer at 24 ± 0.2°C.

[3] determined by Cannon Fenske viscometer at 24 ± 1°C.

3.3.2.2 Determination of equilibrium relationship for water/Isopar M /*i*-propanol

1. Ternary diagram

This plot gives the estimate of the region of heterogeneity for the constituents of the ternary system. The ternary diagram was obtained by adopting an experimental procedure suggested by Othmer et al. (1941).

A known binary mixture of *i*-propanol and water/Isopar was taken in an Erlenmeyer flask and Isopar M / water was added drop-wise through a burette. The endpoint characterises the boundary between the homogeneous and heterogeneous system. The ternary diagram is given in figure 3.6. Experiments were conducted from both the Isopar rich ends and water rich ends. For instance, when a water-alcohol mixture was taken (water rich end) Isopar was the liquid added through the burette. The criterion for the endpoint was the appearance of turbidity for the Isopar rich end and the presence of minute droplets of Isopar for the water rich end experiments. The endpoint was difficult to detect for the water rich end experiments using the turbidity criterion, because the addition of alcohol to water itself made the solution turbid. Throughout the entire experiments the temperature was controlled at 24°C using a constant temperature bath. The data obtained on a weight percent basis from these experiments are given in table 3.4.

2. Tie Line Determination

The tie line determination requires the estimation of the solute content of both the organic and aqueous phases at equilibrium. A measured volume of alcohol in Isopar M of known concentration was mixed with an equal volume of pure distilled water in an Erlenmeyer flask. The two phase mixture was stirred using a magnetic stirrer and the temperature was controlled

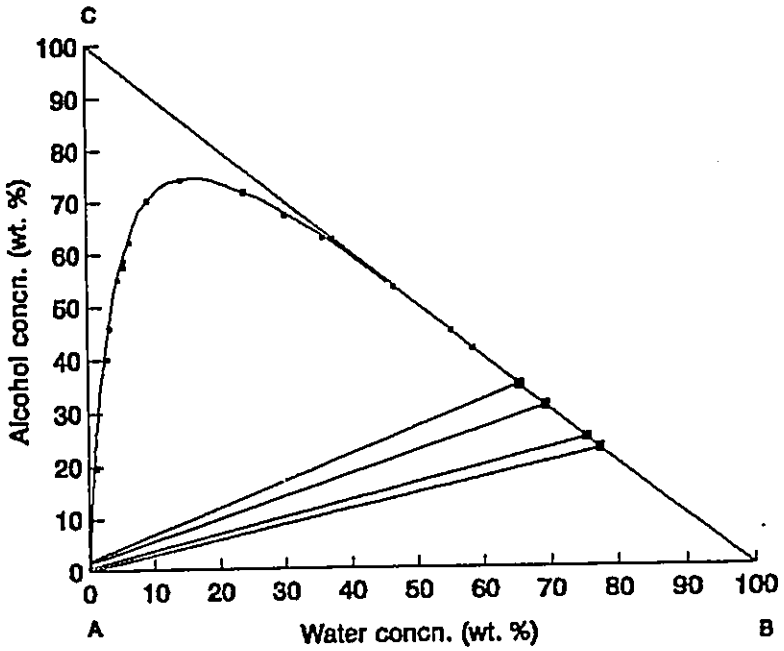

Figure 3.6 Ternary diagram for Isopar M (A)-isopropyl alcohol (C)-Water (B) at 24°C

Table 3.4 Equilibrium data for determining the Ternary diagram (wt. % basis)

	Isopar rich phase			Water rich phase		
#	% alcohol	% Isopar	% water	% alcohol	% Isopar	% water
1	19.7	79.097	1.203	41.465	0.073	58.461
2	40.03	57.163	2.807	44.765	0.106	55.129
3	45.903	50.872	3.226	53.288	0.208	46.504
4	55.110	40.256	4.634	58.689	35.806	5.506
5	57.623	36.936	5.441	62.588	0.178	37.234
6	62.345	31.221	6.434	62.735	1.441	35.824
7	70.288	20.408	9.304	67.222	2.511	30.266
8	74.174	11.541	14.285	71.760	4.295	23.945

at 24°C using a constant temperature bath. After 20 minutes of stirring the mixture was separated by a separating funnel. The aqueous phase was analyzed for alcohol concentration by means of the PAAR densitometer. Since the density difference between alcohol and Isopar M is low the densitometer could not be used for measurements in the organic phase. Preliminary results indicated that the alcohol concentrations in Isopar at equilibrium were so low that the refractive index method was also insufficient. Hence an alternate technique had to be used for the organic phase. Hence it was decided to adopt a wet test procedure involving the use of pyromellitic dianhydride (PMDA) as recommended by Siggia et al. (1979). The procedure involving the PMDA technique is given in Appendix A. The equilibrium concentrations are given in table 3.5.

The partition coefficient P^* is defined as follows:

$$P^* = \frac{c^*_{org.}}{c_{aq.}} \tag{3.2}$$

where $c^*_{org.}$ and $c_{aq.}$ are the concentrations in g/L at equilibrium for the organic and aqueous phases respectively. The data was also converted into mass fraction units x and y.

Table 3.5 Equilibrium data for x-y diagram (figure 3.7)

no.	$c^*_{org.}$ (g/L)	$c_{aq.}$ (g/L)	P^* (-)	$x^*_{org.}$	$x_{aq.}$	$x^*_{org}/x_{aq.}$
1	7.651	217.711	0.03514	0.0097	0.2264	0.0428
2	9.681	236.144	0.04099	0.0123	0.2465	0.0499
3	12.524	290.960	0.04304	0.01595	0.3076	0.0519
4	14.660	323.930	0.04526	0.01867	0.3456	0.0540

Based on this information the tie lines could be constructed in the ternary diagram. It can be seen

from figure 3.5 that Isopar M is insoluble in aqueous solutions even at high concentrations of alcohol. Therefore the densities of the aqueous samples obtained may be considered to be a function of alcohol concentration only. Since in the organic phase the alcohol concentration is low (less than 10%) it can be assumed that the water concentration in the Isopar medium is negligible.

From figure 3.6 and table 3.5 it can be seen that *i*-propanol has a much greater preference for the aqueous phase than for the organic phase. Kertes and King (1987) in their review of the extraction chemistry of low molecular weight aliphatic alcohols listed some typical partition coefficients for monomeric alcohols. From this review, some typical values are given in table 3.6. Hence the observed average P^* value of 0.041 obtained in this study is of similar magnitude to those listed in table 3.6. The equilibrium distribution ratio (based on mass fraction basis) is 0.0493. Figure 3.7 illustrates the equilibrium relationship on a mass fraction basis.

Table 3.6 Typical values of the Partition coefficient (From : Kertes and King, 1987)

#	System	P^*
1	n decane - propanol - water	0.03
2	cyclohexane- isopropanol-water	0.017

3.3.3 Estimation of the back-mixing coefficient

To ensure the reliability of the estimates of the back-mixing coefficient under mass transfer conditions two independent methods were *simultaneously* employed.

In the first method, the alcohol concentration profile in the column was used to estimate $\dot{E}_c$. The dispersion model containing the mass transfer flux term was used as described in section 1.11.3.

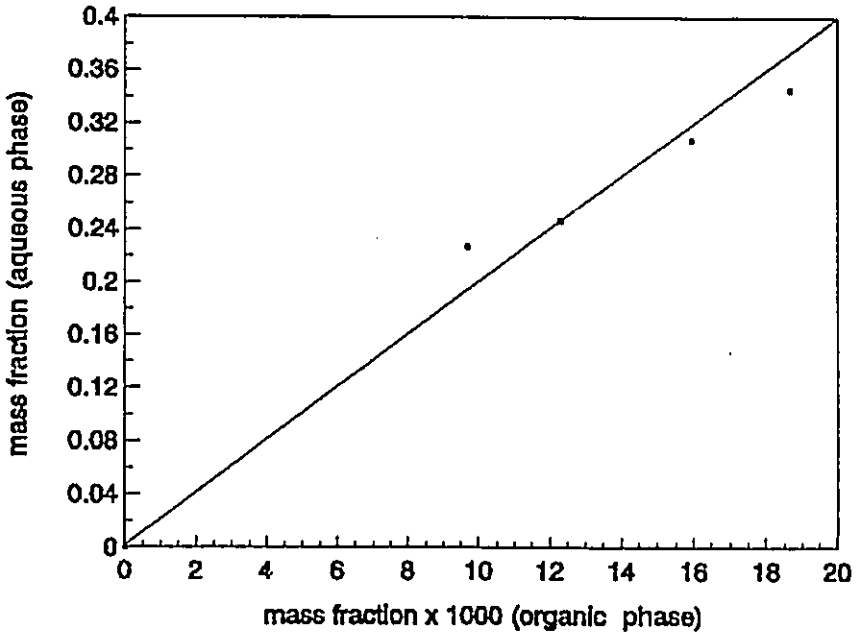

Figure 3.7 Equilibrium line for Isopar M isopropanol-water system at 24°C.

In the second method, a non transferring tracer was steadily injected into the continuous phase during the mass transfer experiments at a very small flow rate so that it did not interfere with the convective flow of the continuous phase. The tracer was a red coloured food dye containing a very dilute mixture of propylene glycol and sodium benzoate. The steady state dye concentration profile was analyzed in terms of the dispersion model without the mass transfer term (section 1.11.1).

3.3.4 Creation of the unstable density gradient

The alcohol concentration of the continuous phase (solvent) increased with increasing distance from the aqueous phase inlet due to the counter-current nature of the process. Alcohol being lighter than water, reduced the density of the continuous phase upon extraction thereby created an unstable density gradient in the continuous phase. It must be noted that unlike the

NaCl solution in the co-current case, the tracer solution (a red coloured dye) was extremely dilute and did not change the density of the continuous phase. When experiments were repeated in the absence of mass transfer, the tracer method still gave the estimate of E_c. The scheme for the co-current and counter-current experiments is summarized in table 3.7.

3.3.5 Experimental set-up and operating procedure

The overall set-up for the counter-current mode of operation is shown in figure 3.8. The continuous phase was distilled water which was fed to the top of the column from tank T4. The organic phase was fed from tank T2 through the distributor D counter-current to the continuous phase. The feed concentration of the i-propanol in the Isopar M was kept below 10 % mass fraction so that dilute conditions are maintained. Both the aqueous and organic flows were metered by the Duplex pump P. Pulsation dampeners (S) were installed downstream of each outlet from the Duplex Pump to maintain uniform flow of the liquids being pumped. The toggle valves were located at the tracer, continuous and dispersed phase inlets and the continuous phase outlet.

These valves were inter-connected such that it was possible to shut them simultaneously. At the start of each run, the column was filled approximately to the continuous phase inlet with distilled water. Then the Duplex pump, tracer pump and the agitation (if applicable) were switched on. The column was operated for 15 minutes to attain steady state. The criterion for steady state was the displacement of 3 times the column volume by the flowing liquids. The interface was maintained at approximately the same level by minor adjustments of the needle valve (NV) located at the aqueous phase outlet.

Needle valves with fine flow control were used to sample the continuous phase. The valves were connected into the pipe threaded holes of the stainless steel collars separating the

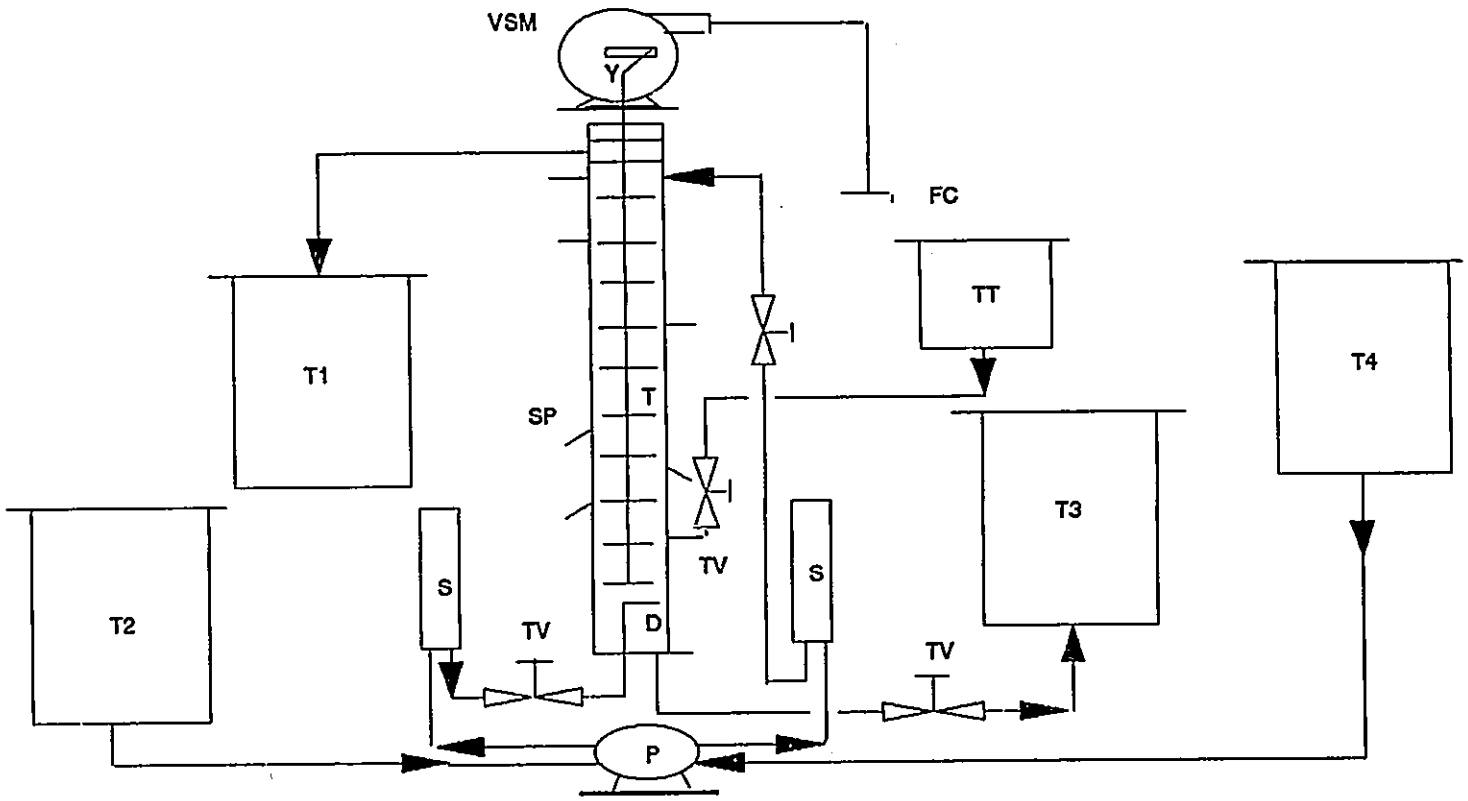

Figure 3.8 Flow diagram for counter-current flow experimental set-up

D-distributor, FC- frequency controller, P-pump, S-surge tank, SP-sample port, T-plate-stack, T1-raffinate tank, T2-feed tank, T3-extract tank, T4-solvent tank, TT-tracer tank, TV-toggle valve, VSM-variable speed motor, Y-yoke

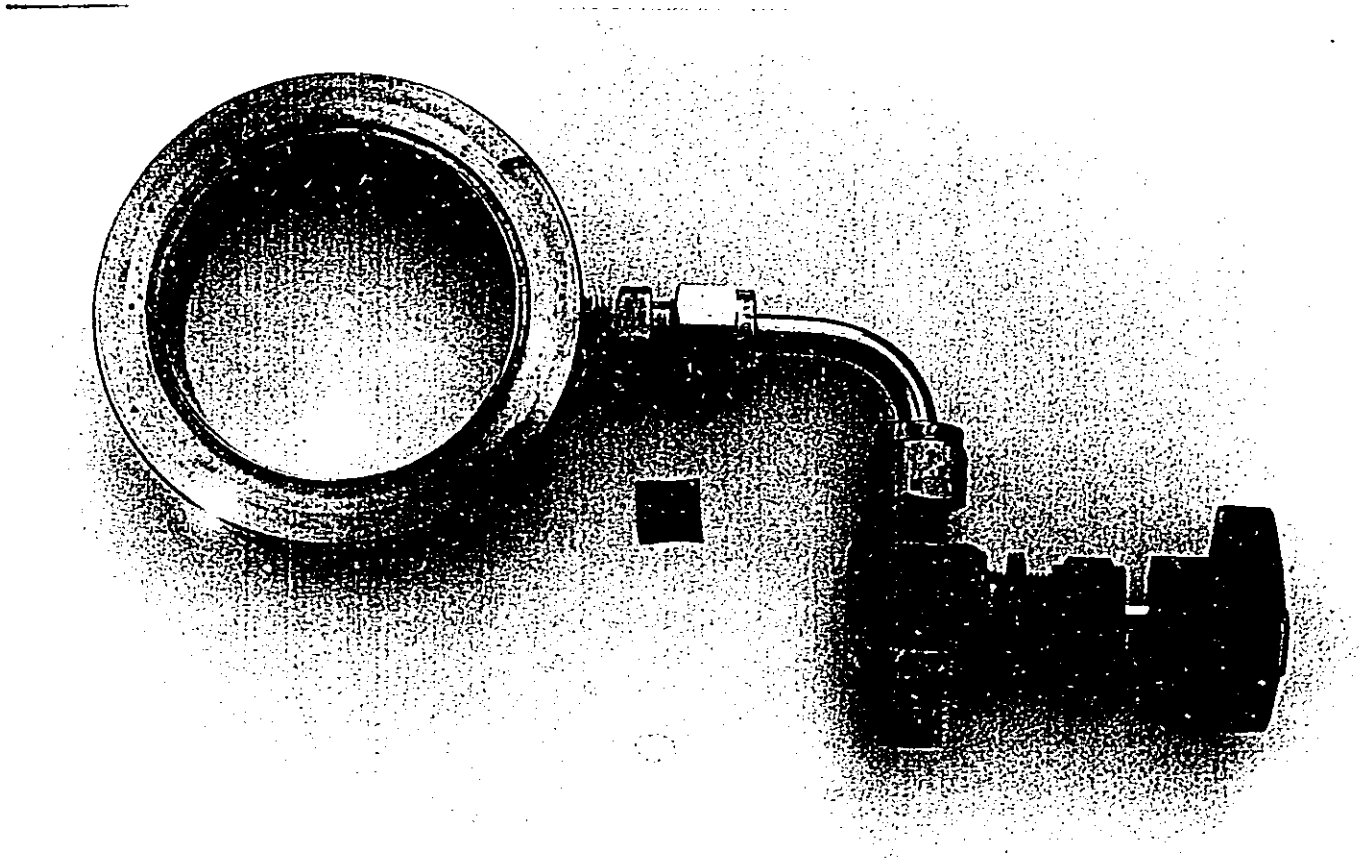

Figure 3.9 Photograph of sampling arrangement with a typical stainless steel mesh

Table 3.7 Summary of experimental schemes and back-mixing estimation techniques

	Co-current non mass transfer	Counter-current flow	
		without mass transfer	with mass transfer
section discussed	3.2	3.3.3	3.3.3
continuous phase	water(↑)	water(↓)	water+i-propyl alcohol (↓)
dispersed phase flow	Isopar M (↑)	Isopar M (↑)	Isopar M +isopropyl alcohol (↑)
tracer in continuous phase	NaCl, NaCl+methanol[4]	red coloured dye	
procedure for estimating back-mixing	S.S. tracer method[5]	S.S. tracer method	simultaneous S.S. method and from mass transfer

flanges by (1/8)" brass or stainless steel tube to pipe swage lock fittings. Several layers of fine stainless steel meshes were inserted into the pipe portion of the fittings. The meshes are preferentially wetted by the continuous phase and thus it is possible to collect pure samples without the entrainment of the dispersed phase. The sampling arrangement including a typical mesh are shown in figure 3.9. Sample tubes were attached to the needle valves by elastic bands. After steady state was attained the sampling was carried out in the following manner to avoid disturbance to the column contents:

i) Sample ports were opened one at a time in a staggered fashion so that a distance of at least 30 cm was maintained between successive sampling points.

ii) The sampling rate was around 5-10 cm^3 per minute so that the organic phase was not entrained in the samples.

---

[4] for the experiments under neutrally buoyant conditions

[5] S.S - steady state

For getting a sufficient number of continuous phase samples a special glass section was used near the tracer inlet. In this glass section inclined cylindrical sample ports were built in. (figure 3.2b) Stainless steel meshes were inserted into these ports as well. The inclination aided in the collection of pure aqueous samples. The location of the sample ports is illustrated in figure 3.10. After sampling from all the ports the toggle valves (TV in figure 3.8) at the column inlets and aqueous phase outlet were shut simultaneously. The displacement of the interface was used to calculate the hold-up.

After each experiment, the column was cleaned several times. The screens used in all the sample ports were removed and fresh screens were cut and inserted. The temperature during the experiments were in the range 23-25°C.

3.3.6. Analysis of samples

(i) Aqueous phase

A portion of the sample collected at each port was analyzed for the alcohol concentration using the PAAR densitometer. It was sufficient to make one repeated measurement to confirm the accuracy of the digital densitometer reading. The accuracy of the densitometer was usually within $\pm$ 1%. The dye tracer concentration in the remaining portion of the sample was analyzed by using the Brinkman PC 800 colorimeter.

(ii) Organic Phase

The feed concentration of *i*-propanol was usually 70 g/L which corresponded to around 9% solution by weight. In-spite of using a Teflon coalescence mesh at the top of the column, some minute quantities of the aqueous phase was entrained in the raffinate sample. A large quantity of the raffinate sample (approx. 500 cc) was collected and analyzed after the aqueous dispersion (approx. 2 cc) had settled down. The raffinate in the receiving tank T1 in figure (3.8)

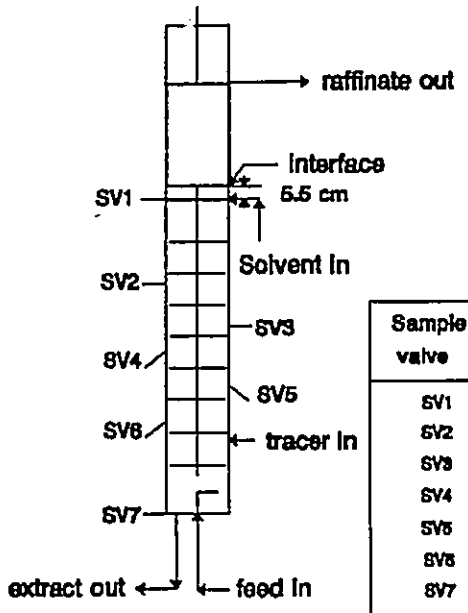

Sample valve	Distance from solvent inlet (cm)
SV1	0
SV2	17.5
SV3	26.55
SV4	34.55
SV5	42.5
SV6	51.5
SV7	68.2

Figure 3.10 Location of sample ports in the column for counter-current mode of operation

was allowed to stand for 3 hours to settle the aqueous phase entrained. Then it was recycled to the feed tank and the solution made up to the original strength by adding more alcohol. The lowest concentrations encountered in the raffinate rarely fell below 10 g/L. Hence the refractometer could be used for all measurements. Usually 2-3 measurements were required, to average out the minor variations of the refractometer which had an analogue scale. The accuracy of the refractometer was around $\pm$ 2%. The material balance check on the alcohol concentration at the inlet and exit usually indicated an agreement within $\pm$ 5%.

The calibration charts for the densitometer, refractometer and the colorimeter are given in figures 3.11, 3.12 and 3.13 respectively. As shown in figure 3.13, the presence of alcohol in the aqueous phase up-to 70 g/L did not have a significant effect on the absorbance. Since the alcohol concentrations in the experiments were within this range, one tracer calibration chart

sufficed.

3.4. Drop size Measurement and Analysis

The drop size measurements were not carried out simultaneously with the mass transfer and non mass transfer counter-current flow experiments. The column length was small (around 70 cm) because the solute had a great affinity for the solvent, thereby making the extraction very efficient. Use of a longer column led very small concentrations in the raffinate and hence more error in estimating these values and hence in the prediction of the number of transfer units N_{ox}. Therefore the column was shortened and consisted of a 1 foot section near the distributor, 1 foot long modified glass section in the middle with glass sample ports forged into its body followed by one more section 6 inches long. The optimum location of the drop size measurement was the middle section. Constructing the view box on this section would have seriously compromised the structural integrity of the glass section and hindered the sampling arrangement. Hence the drop size measurements were conducted separately for all the mass transfer and non mass transfer runs studied.

The rectangular view box made of Perspex (6 cm × 8 cm × 6 cm) was constructed around a regular 12 inches long glass section. The view box filled with the continuous phase (demineralized water) served to eliminate the optical distortion due to the curvature of the tube. The images of the drop sizes were captured in a video camera recorder (SONY CCD-V801).

Through trial and error, it was found the optimum lighting arrangements consisted of powerful tungsten arc lamps located at the back and side of the column. To prevent glare a semi-translucent paper was necessary between the lamp at the back and the column wall. The drop images were analyzed in IBAS image analyzer. This involved manual recording of the major and minor axes of the drops which were assumed to be ellipsoidal in shape. The column shaft acted

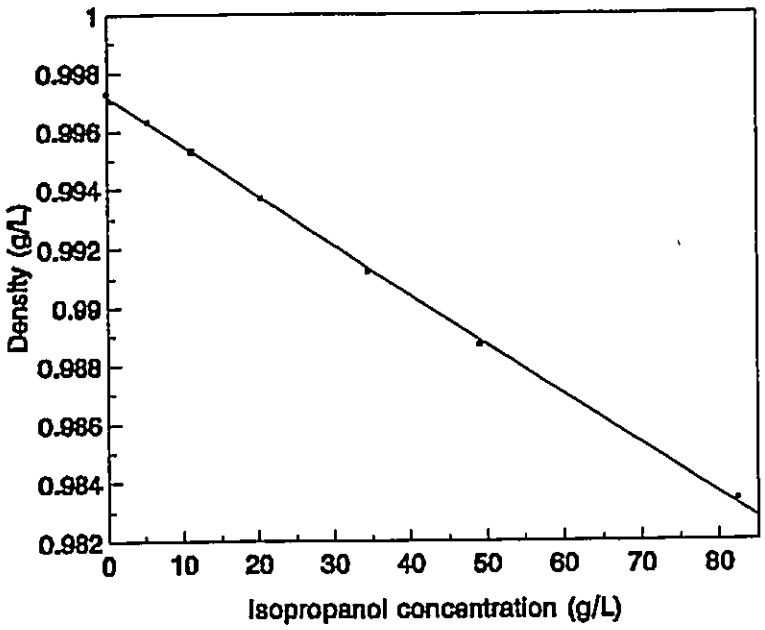

Figure 3.11 Calibration chart for alcohol solution in water (measured by PAAR densitometer at 24°C)

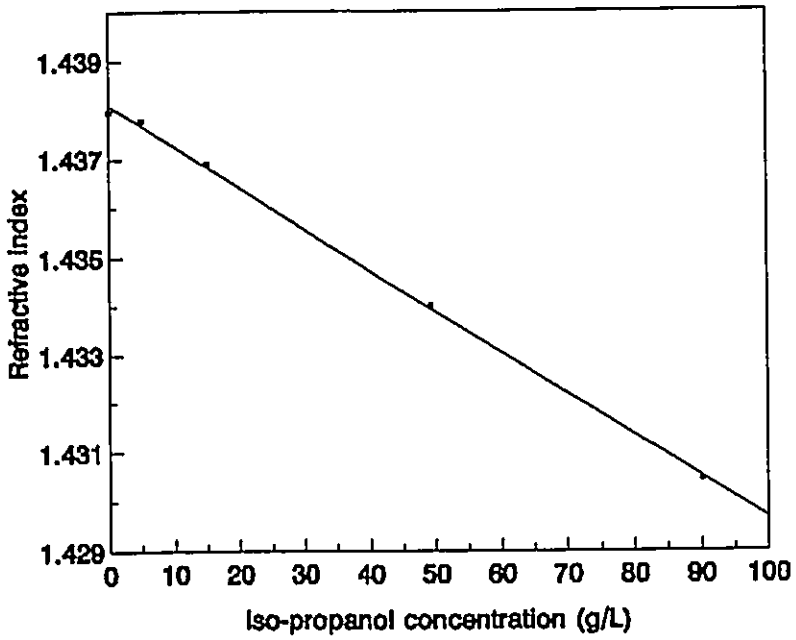

Figure 3.12 Calibration chart for alcohol concentration in Isopar M (measured by ABBE refractometer at 24°C)

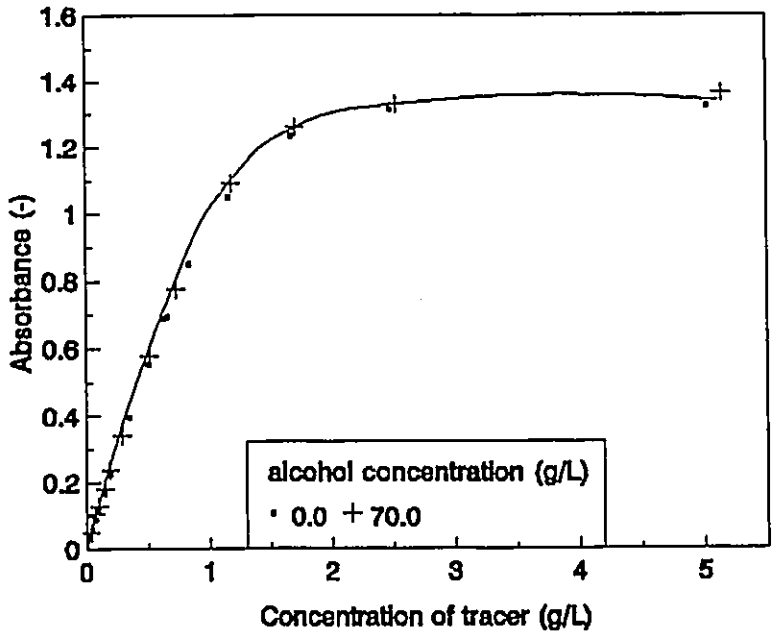

Figure 3.13 Calibration chart for dye solution in the aqueous phase (measured by Brinkman PC 800 colorimeter at 24°C)

as reference for the scale of measurement. Usually 2-3 frames for well agitated conditions and 4-5 frames for zero or low agitation were analyzed for each experiment. The total number of drops counted per experiment ranged from 200-2000. The data was downloaded into a spreadsheet and the Sauter mean diameters were calculated.

CHAPTER 4

Back-Mixing Results : Non Mass Transfer Conditions

4.1 Introduction

In this chapter axial mixing results under non mass transfer conditions are presented. The model based on Kolmogoroff's isotropic turbulence is developed and compared with the experimental data. The implications of the results are analyzed and illustrated through suitable figures.

4.2 Estimation of the back-mixing coefficient

The tracer samples were analyzed for their electrical conductivity. Using the calibration charts (figures 3.5a and b) the conductivity readings were converted into NaCl concentrations and the profiles similar to figure 4.1 were obtained. The following steady state transport equation is valid upstream of the injection plane (z=0) under non mass transfer conditions:

$$E_c \frac{d^2c}{dz^2} - u_c \frac{dc}{dz} = 0 \qquad (1.40)$$

The above equation cannot be integrated in the usual way when the back-mixing coefficient E_c is a function of distance (z) and hence cannot be considered to be a constant. This was found to be the case for experiments performed in the presence of the unstable density gradient. However, E_c can be evaluated from the local slopes of the tracer concentration profiles by re-expressing the above equation as follows

$$E_c = \frac{u_c c}{\frac{dc}{dz}} \qquad (4.1a)$$

It was decided not to evaluate the slopes manually since this procedure proved to be highly subjective and susceptible to error. Hence it was decided to fit the curves by a suitable function and the cubic spline approximation was initially used. However the method had to be discarded as the fit was highly sensitive to the data when it was forced through all the data points, thereby leading to significant error in the slope estimation. In the second method, the smoothed concentration profile was approximated quite effectively by a sixth order polynomial in distance with a correlation coefficient r^2 being better than 0.99 in all the cases. Double precision had to be used to prevent serious round-off error. The resulting expression was easily differentiated to yield the slopes at the distances corresponding to the sample points. For example, the profiles represented in figure 4.1 were fitted as shown in table 4.1.

Table 4.1 Typical polynomial fit and their derivatives (units: c in g/L, z in cm)
H=5.10 cm, u_c=0.40 cm/s, u_d=0.37 cm/s

#	Expt.	Polynomial fit and derivative
1	f=0.0 Hz	$c = 51.533 - 2.4275\, z + 0.00633\, z^2 - 1.1748\times10^{-3}\, z^3 + 1.4344\times10^{-5}\, z^4 - 9.6769\times10^{-8}\, z^5 + 2.6053\times10^{-10}\, z^6$
		$c' = -2.4275 + 0.01266\, z - 3.5244\times10^{-3}\, z^2 + 5.7376\times10^{-5}\, z^3 - 4.83845\times10^{-7}\, z^4 + 1.56318\times10^{-9}\, z^5$
2	f=1.87 Hz	$c = 63.728 - 7.6260\, z + 0.5385\, z^2 - 2.4464\times10^{-2}\, z^3 + 6.5772\times10^{-4}\, z^4 - 9.3713\times10^{-6}\, z^5 + 5.4257\times10^{-8}\, z^6$
		$c' = -7.6260 + 1.0770\, z - 7.3392\times10^{-2}\, z^2 + 2.63088\times10^{-4}\, z^3 - 4.68565\times10^{-5}\, z^4 + 3.25542\times10^{-7}\, z^5$

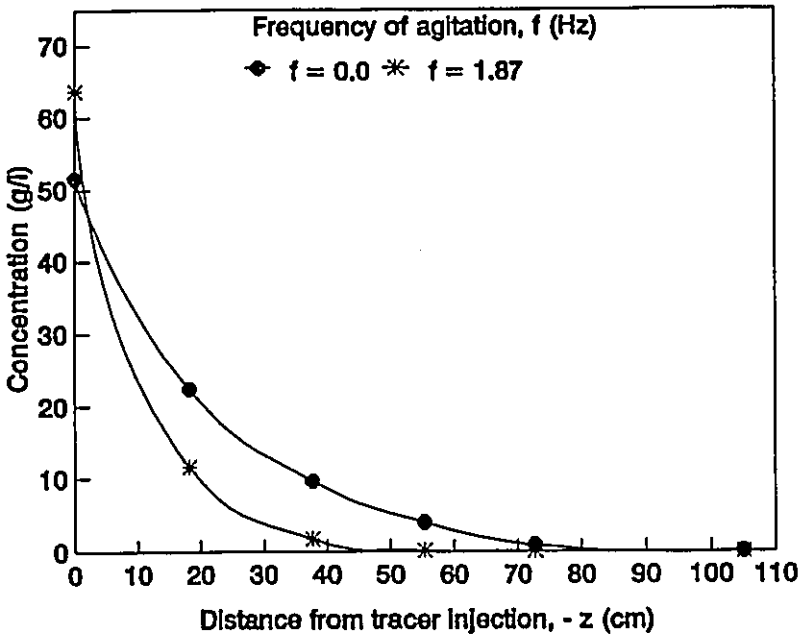

Figure 4.1 Sample tracer concentration profiles

The experimental results for the neutrally buoyant conditions could be modelled in terms of a constant back-mixing coefficient. Integrating equation (4.1) leads to the following well-known expression.

$$\ln c = \frac{u_c}{E_c} z + \ln c_o \qquad \text{(4.1 b)}$$

where c_o is the concentration at the injection plane $z=0$. Hence when concentration is plotted against distance in semi-logarithmic co-ordinates, a linear plot will be obtained. The slope of the line (u_c/E_c) allows the back-mixing coefficient to be calculated. This procedure for measuring E_c from steady state concentration profiles is a standard technique as outlined in section 1.11.1.

4.3 Specific energy dissipation rates

As mentioned earlier, the Kolmogoroff isotropic turbulence theory was used to model the

experimental data. This theory in its simplest form relates the back-mixing coefficient in terms of the mixing length and the total specific energy dissipation rate ($\epsilon = \epsilon_t$) as

$$E_c = l^{\frac{4}{3}} \epsilon_t^{\frac{1}{3}} \tag{2.40}$$

It is required to develop expressions for the energy dissipation terms due to the contributing factors. The factors causing back-mixing in the continuous phase can be classified into

1. Buoyancy effects caused by the unstable density gradient
2. Dispersed phase flow
3. Mechanical agitation

4.3.1 Buoyant energy dissipation

The expression for specific energy dissipation rate due to buoyancy (ϵ_b) was developed by Holmes et al. (1991). Using dimensional analysis the authors related the back-mixing coefficient (E_c) to the density gradient ($d\rho/dz$), gravity (g) and continuous phase density (ρ_c). After assuming that the density gradient and gravity are coupled together the following expression was derived:

$$E_c = l^2 \left(\frac{g}{\rho_c} \frac{d\rho}{dz}\right)^{\frac{1}{2}} \tag{4.2}$$

Assuming a linear variation of continuous phase density with concentration of the tracer given by $\rho_c = \rho_o + kc$, the concentration c can be related to the density difference $\Delta\rho$ ($= \rho_c - \rho_o$) according to equation 4.3. Here ρ_o refers to the density of the pure continuous phase, which in the present case is salt-free water.

Hence using equations (4.1a) and (4.3)

$$c = \frac{\Delta\rho}{k} \tag{4.3}$$

$$\frac{d\rho}{dz} = u_c \frac{\Delta\rho}{E_c} \tag{4.4}$$

Substituting equation (4.4) for the density gradient term in equation (4.2) and solving for E_c,

$$E_c = l^{\frac{4}{3}} \left(\frac{u_c g \Delta\rho}{\rho_c}\right)^{\frac{1}{3}} \tag{4.5}$$

Comparing equation (2.40) with equation (4.5), it can be noted that the term in parenthesis represents the buoyant energy dissipation rate per unit mass (ϵ_b) and has the units cm^2/s^3.

4.3.2 Dispersed phase energy dissipation

Baird and Rice (1975) developed an expression for the energy dissipation rate due to the dispersed phase flow. Using a control volume of unit cross section and length L (fig. 4.2), the authors equated the energy dissipation to the difference between the flow work and the gain in potential energy of the dispersed phase. The flow work term based on unit cross sectional area was given by the following expression.

$$u_d(P_o - P_l) = u_d \rho_m g L \tag{4.6}$$

where ρ_m is the mean density of the dispersion.

The rate of gain in potential energy (PE) of the dispersed phase is given by

$$\frac{d(PE)}{dt} = u_d \rho_d g L \tag{4.7}$$

Hence the net energy dissipation rate expressed as a difference between the rate of gain in potential energy and the flow work rate term is given by

$$u_d g L(\rho_m - \rho_d) = u_d g L(h\ \rho_d + (1-h)\rho_c - \rho_d) \tag{4.8}$$

Simplifying further, equation (4.8) can be expressed as follows

$$u_d g L(\rho_m - \rho_d) = u_d g L(\rho_c - \rho_d)(1-h) \tag{4.9}$$

If it is assumed that all the energy dissipation occurs in the continuous phase of mass $\rho_c L(1-h)$, the energy dissipation rate per unit mass is given by

$$\frac{u_d g L(\rho_c - \rho_d)(1-h)}{\rho_c L(1-h)} = \frac{u_d g \Delta\rho_{cd}}{\rho_c} \tag{4.10}$$

where $\Delta\rho_{cd}$ is the difference in densities between the continuous and dispersed phases.

4.3.3 Mechanical energy dissipation

The expression for the energy dissipation rate per unit mass due to mechanical agitation in a reciprocating plate column has been derived by Hafez and Baird (1978). A momentum balance was made over a control volume of the column (fig. 4.3). If the oscillation of the shaft and the plate stack is considered to be sinusoidal with amplitude a′ and angular frequency ω, the displacement y, velocity dy/dt and acceleration d^2y/dt^2 can be expressed as follows:

$$y = a'\sin\omega t \tag{4.11}$$

$$\frac{dy}{dt} = a'\omega\cos(\omega t) \tag{4.12}$$

$$\frac{d^2y}{dt^2} = -a'\omega^2\sin(\omega t) \tag{4.13}$$

The shaft force F_s from the balance can be expressed as a sum of forces due to (i) fluid friction force, F_f (ii) the accelerating motion of the plate stack and (iii) the net weight of the plate stack.

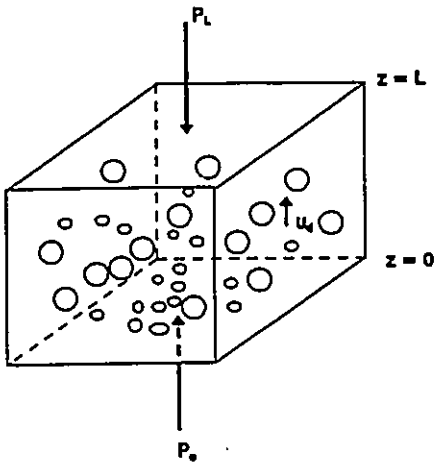

Figure. 4.2 Diagram for deriving energy dissipation in dispersed phase

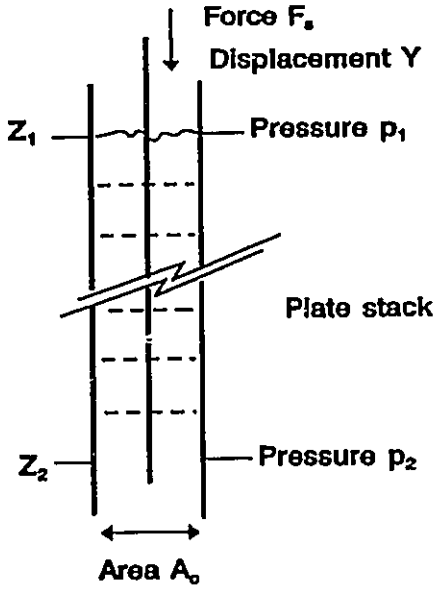

Figure. 4.3 Control Volume for force balace (Hafez and Baird, 1978)

The average power dissipation ($Po_{av.}$) is obtained by integrating, the instantaneous power dissipation (Po) over the time period T. The latter is obtained by multiplying the shaft force F_s with the shaft's rate of displacement viz. the velocity (Hafez and Baird, 1978) as shown in equation (4.14).

$$Po_{av.} = \frac{1}{T}\int_0^T F_s \frac{dy}{dt} dt \tag{4.14}$$

F_s can be expressed as a sum of the inertial and frictional forces according to the following equation (Hafez and Prochazka, 1974 a,b)

$$F_s = A_{cs}\left[\int_{z_1}^{z_2} \rho_c \left(\frac{\partial U}{\partial t}\right) dz + P_f\right] \tag{4.15}$$

The inertial contribution may be expressed, according to the equivalent plate thickness model[1] as follows:

$$A_{cs}\int_{z_1}^{z_2} \rho_c \left(\frac{\partial U}{\partial t}\right) dz = -\rho_c N L^* \left(\frac{1-S}{S}\right) \frac{d^2y}{dt^2} \tag{4.16}$$

The frictional force is obtained by using the approach followed by Jealous and Johnson (1955).

$$P_f A_{cs} = A_{cs} \rho_c N \left(\frac{1-S^2}{2C_o^2 S^2}\right) \frac{dy}{dt} \left|\frac{dy}{dt}\right| \tag{4.17}$$

The modulus term is included in order to have the consistency in signs for the frictional pressure drop with the dy/dt term. Substituting equations (4.16) and (4.17) in equation (4.15) and using

---

[1] In this model it is assumed that the liquid displaced through the perforations moved at an uniform velocity through an equivalent plate thickness or cylindrical column length L^* associated with each perforation.

equations (4.11) - (4.13) the following expression is obtained.

$$Po_{av.q} = \frac{16\pi^2}{3}\rho_c N A_{cs}\left(\frac{1-S^2}{C_o^2 S^2}\right)(a'f)^3 \qquad (4.18)$$

After the integration of equation (4.15), only the fluid friction contribution, F_f survives and the net contribution due to the inertial force terms is zero. The subscript q refers to the assumption of quasi-steady state conditions in the modelling. This equation is often expressed in terms of the energy dissipation per unit mass (ϵ_m) and the stroke A (=2a') so that

$$\epsilon_m = \frac{Po_{av.q}}{\rho_c A_c N H} = \frac{2\pi^2}{3}\frac{(1-S^2)}{C_o^2 S^2}\frac{(Af)^3}{H} \qquad (4.19)$$

For the standard Karr plate this equation was obeyed satisfactorily at high amplitudes and low frequencies. However there was significant deviation at high frequencies and low amplitudes. Use of a constant orifice coefficient is also subject to error. Hence, Hafez and Baird (1978) introduced a correction factor to minimize the discrepancy between the observed and model average power consumption values.

$$\frac{Po_{av.,expt.}}{Po_{av.q}} = 1 + 0.446\left(\frac{f}{2.5}\right)^{1.02}\left(\frac{d_o S}{a'}\right)^{1.26}\left(\frac{4d_o S}{H}\right)^{-0.348}\left(\frac{d_o}{H}\right)^{-0.312} \qquad (4.20)$$

Baird and Rama Rao (1995) recently found that an acoustic model (Baird and Stonestreet, 1995) provided a better fit than the quasi-steady state model in the region of low amplitudes.

4.4 Evaluation of the mixing length (*l*)

The turbulent eddies could be characterized in terms of their velocities and by the distances over which the velocities change significantly. Levich (1962) identified the distances

as the scale of motion. The scales of motion for the largest eddies (l) were comparable with the diameter of the tube. The velocities of these large eddies (ΔU) were comparable to the maximum velocity of the liquid flow. These large scale eddies were broken into intermediate range eddies of decreasing scale and this process continued until viscous effects became important. There is continuous and steady transfer of energy from large scale to small scale eddies until the energy is dissipated by viscous motion. Hence turbulent motion is characterized by considerable dissipation of energy. The specific energy dissipation term is independent of the scales of the smaller eddies but is a characteristic constant for the given flow. This energy is used to create the smaller scale eddies from the largest eddies and the process occurs at high Reynolds numbers and is independent of the viscosity of the liquid. A detailed description of the eddy behaviour has been given in section 2.4.1. In the present work, ϵ_t was expressed as a sum of specific energy dissipation rates due to buoyancy, mechanical agitation and dispersed phase flow. Hence,

$$\epsilon_t = \epsilon_b + \epsilon_m + \epsilon_d \tag{4.21}$$

The experimental mixing length $l_{expt.}$ can be calculated from the experimental back-mixing value and the total energy dissipation using equation (2.40) according to

$$l_{expt.} = \left[\frac{E_{c,expt.}}{\epsilon_t}\right]^{\frac{3}{4}} \tag{4.22}$$

The experiments were performed with all possible combinations of different types of energy dissipation conditions as listed in table 4.2.

4.5. Modelling of the mixing length (l)

The overall mixing length is a measure of the measured back-mixing coefficient. In order to quantitatively evaluate the magnitude and relative importance of each of the three factors viz.

Table 4.2 Organization of experimental results (Co-current flow conditions)

Experimental classification	Contributing factors to ϵ_t	Symbol
ϵ_b	Only buoyancy	○
$\epsilon_b+\epsilon_d$	Buoyancy + dispersed phase flow	⊕
$\epsilon_b+\epsilon_m$	Buoyancy + mechanical agitation	⊗
$\epsilon_b+\epsilon_d+\epsilon_m$	Buoyancy + dispersed phase flow + mechanical agitation	●
ϵ_d	Only Dispersed phase flow	×
ϵ_m	Only Mechanical agitation	□
$\epsilon_d+\epsilon_m$	Dispersed phase flow + mechanical agitation	⊠

buoyancy created by the unstable density gradient in the continuous phase, dispersed phase flow and mechanical agitation, it is necessary to develop a model for the overall mixing length. The preliminary model and its subsequent improvements are briefly listed in this section. A detailed explanation of the ideas behind the model development and improvements is given in section 4.8.

4.5.1 Preliminary model I

The initial modelling of the mixing length under two phase flow conditions was similar to the approach followed for single phase flow conditions by Baird and Rama Rao (1991) as given by equation (1.64). Since the energy dissipation due to the dispersed phase could be expressed

in terms of equation (4.10), it was decided to extend the approach of Baird and Rama Rao (1991) to the two phase flow conditions.

$$l_{model} = l_m+(l_b-l_m)(\frac{\epsilon_b}{\epsilon_t})^{n_1}+(l_d-l_m)(\frac{\epsilon_d}{\epsilon_t})^{n_2} \qquad (4.23)$$

The parameters of this model viz. l_m, l_b, l_d , n_1 and n_2 were determined by minimizing the following objective function (Z_1):

$$Z_1 = \sum_{j=1}^{N_d} (l_{model}-l_{expt.})_j^2 \qquad (4.24)$$

where N_d is the number of experimental data points. The non linear regression was carried out using the software GAMS (General Algebraic Modelling System). The parameters are given in table 4.3.

4.5.2 Improvement of the mixing length model to give model II

The mixing length term l_d was modified to incorporate the interactive effects of the dispersed phase superficial velocity or equivalently the dispersed phase energy dissipation (ϵ_d) and mechanical agitation or equivalently the mechanical energy dissipation rate(ϵ_m). A detailed discussion on this modification is given in section 4.8. Model II can be expressed as follows

$$l = l_m+(l_b-l_m)(\frac{\epsilon_b}{\epsilon_t})^{n_1}+[l_{do}\exp(-\frac{\epsilon_d}{\epsilon_{mo}+\epsilon_m})-l_m](\frac{\epsilon_d}{\epsilon_t})^{n_2} \qquad (4.25)$$

4.5.3 Improvement of the mixing length model to give model III

In order to incorporate the effect of plate spacing (H) in the column, the mixing length term in the original model was re-defined as follows

$$l = l_m+(l_b-l_m)(\frac{\epsilon_b}{\epsilon_t})^{n_1}+[l_{do}^{*}(1+\frac{H}{D})\exp(-\frac{\epsilon_d}{\epsilon_{mo}+\epsilon_m})-l_m](\frac{\epsilon_d}{\epsilon_t})^{n_2} \quad (4.26)$$

Further discussion on the development of this model is given in section 4.8. For the sake of comparison, the model parameters estimated for all the versions are given in table 4.3. As will be shown in a later section (4.7) model III was distinctly superior to models I and II. Hence further analysis and discussion of results will be based on model III.

4.6 Summary of experimental results and model predictions

The range of experimental variables used in this study are given in table 4.4. The experimental mixing length results (from equation 4.22) for the co-current non mass transfer case are presented in tables 4.5-4.8. The mixing lengths were based on equation 4.26. E_c values, experimental and predicted, based on the mixing lengths in tables 4.5-4.8, are given in tables 4.9-4.12. Figure 4.4a and 4.4b represent the comparison of the experimental and predicted mixing

Table 4.3 Comparison of different model parameters obtained by non linear regression

Model	I	II	III
Equation no.	4.23	4.25	4.26
l_m (cm)	0.318	0.339	0.3363
l_b (cm)	3.241	3.206	3.199
dispersed phase mixing length (cm)	l_d = 0.961	l_{do} = 2.092	l_{do}^{*}=1.2306
ϵ_{mo}	-	73.1514	68.5157
n_1	0.486	0.5054	0.4954
n_2	0.614	1.043	1.1300

Table 4.4 Range of variables for co-current flow experiments

u_c (cm/s)	u_d (cm/s)	A (cm)	f(Hz)	H (cm)
0.40	0-0.38	3.10	0-3.5	2.55/5.10

lengths and back-mixing values respectively. In the model for ϵ_m as described in equation (4.19), since the agitation effect was expressed as a combination Af, the stroke (A) was kept at a constant value and frequency which was easier to adjust, was varied.

In the model equation (4.26), the superficial continuous phase flow velocity (u_c) was associated with the density difference $\Delta\rho$ in the continuous phase which varied over a significant range of values. Hence it was decided to fix the continuous phase velocity at 0.4 cm/s.

Table 4.5 Experimental conditions and mixing lengths

u_d cm/s	f Hz	H cm	$\Delta\rho$ g/cc	ϵ_b cm^2/s^3	ϵ_d cm^2/s^3	ϵ_m cm^2/s^3	$l_{expt.}$ cm	$l_{prod.}$ cm	% err. -
ONLY BUOYANCY									
0	0	5.10	0.01579	6.196	0	0	3.309	3.199	3.31
		2.55	0.01655	6.491	0	0	2.989	3.199	-7.04
		2.55	0.00610	2.393	0	0	3.359	3.199	4.75
BUOYANCY + DISPERSED PHASE FLOW									
0.192	0.0	5.10	0.02435	9.552	35.389	0	2.404	2.532	-5.31
0.192	0.0	5.10	0.01084	4.252	35.389	0	2.035	2.282	-12.12
0.365	0.0	5.10	0.01561	6.122	67.155	0	1.759	1.707	2.96
0.365	0.0	5.10	0.00669	2.624	67.155	0	1.709	1.464	14.36
0.365	0.0	5.10	0.00280	1.097	67.155	0	1.513	1.285	15.12
0.365	0.0	5.10	0.00061	0.24	67.155	0	0.647	1.098	-69.70
0.192	0.0	2.55	0.01841	7.223	35.389	0	1.987	2.146	-8.01
0.192	0.0	2.55	0.00867	3.4	35.389	0	1.952	1.884	3.46
0.192	0.0	2.55	0.00173	0.678	35.389	0	1.362	1.486	-9.10
0.370	0.0	2.55	0.01095	4.296	68.056	0	1.363	1.368	-0.343
0.370	0.0	2.55	0.00256	1.002	68.056	0	1.027	1.031	-0.340
0.370	0.0	2.55	0.00022	0.086	68.056	0	0.462	0.789	-70.79

Table 4.6 Experimental conditions and mixing lengths

u_d cm/s	f Hz	H cm	$\Delta\rho$ g/cm^3	ϵ_b cm^2/s^3	ϵ_d cm^2/s^3	ϵ_m cm^2/s^3	$l_{expt.}$ cm	$l_{pred.}$ cm	% err. -
BUOYANCY + MECHANICAL AGITATION									
	1.833	5.10	0.00675	2.65	0	1439.712	0.463	0.463	-0.02
	1.833	5.10	0.00056	0.219	0	1439.712	0.332	0.373	-12.36
	1.050	5.10	0.00735	2.884	0	270.485	0.658	0.637	3.18
	1.050	5.10	0.00018	0.072	0	270.485	0.274	0.385	-40.53
	3.50	5.10	0.01155	4.529	0	10017.95	0.357	0.399	-11.91
	3.50	5.10	0.00278	1.091	0	10017.95	0.334	0.367	-10.00
0	1.05	2.55	0.00748	2.932	0	540.97	0.583	0.552	5.41
	1.05	2.55	0.00064	0.250	0	540.97	0.544	0.400	26.43
	3.317	2.55	0.01855	7.277	0	17054.59	0.432	0.398	7.90
	3.317	2.55	0.00667	2.617	0	17054.59	0.396	0.373	5.64
	1.867	2.55	0.01037	4.067	0	3041.15	0.505	0.444	12.03
	1.867	2.55	0.00215	0.842	0	3041.15	0.392	0.386	1.48
	1.867	2.55	0.00039	0.152	0	3041.15	0.320	0.358	-11.86

Table 4.7 Experimental conditions and mixing lengths

u_d cm/s	f Hz	H cm	$\Delta\rho$ g/cc	ϵ_b cm^2/s^3	ϵ_d cm^2/s^3	ϵ_m cm^2/s^3	$l_{expt.}$ cm	$l_{pred.}$ cm	% err. -
BUOYANCY + DISPERSED PHASE FLOW + MECHANICAL AGITATION									
0.375	1.0	5.10	0.02014	7.902	68.958	233.655	1.402	1.098	21.69
0.375	1.0	5.10	0.00910	3.568	68.958	233.655	1.247	0.954	23.56
0.375	1.0	5.10	0.00347	1.362	68.958	233.655	0.944	0.837	11.37
0.375	1.0	5.10	0.0005	0.194	68.958	233.655	0.387	0.717	-85.08
0.370	1.867	5.10	0.0081	3.179	68.056	1519.769	0.510	0.526	-3.01
0.370	1.867	5.10	0.00118	0.462	68.056	1519.769	0.358	0.445	-24.18
0.192	1.850	5.10	0.00648	2.543	35.389	1479.415	0.442	0.487	-10.17
0.192	1.850	5.10	0.00041	0.161	35.389	1479.415	0.212	0.397	-86.98
0.192	1.017	5.10	0.01511	5.929	35.389	245.534	1.024	0.931	9.13
0.192	1.017	5.10	0.00412	1.614	35.389	245.534	0.850	0.736	13.41
0.192	1.017	5.10	0.00041	0.160	35.389	245.534	0.481	0.587	-21.98
0.192	1.050	2.55	0.00556	2.181	35.389	540.970	0.570	0.577	1.07
0.192	1.050	2.55	0.00044	0.174	35.389	540.970	0.566	0.448	20.85
0.380	1.033	2.55	0.00882	3.458	69.896	515.117	0.577	0.678	-17.67
0.380	1.033	2.55	0.00060	0.237	69.896	515.117	0.382	0.514	-34.76
0.375	3.133	2.55	0.01718	6.741	68.976	14375.10	0.431	0.404	6.27
0.375	3.133	2.55	0.00453	1.778	68.976	14375.10	0.337	0.373	-10.59
0.192	3.333	2.55	0.01819	7.135	35.389	17302.58	0.416	0.398	4.46
0.192	3.333	2.55	0.00600	2.353	35.389	17302.58	0.379	0.372	1.69
0.192	3.333	2.55	0.00255	0.999	35.389	17302.58	0.424	0.360	15.08

Table 4.8 Experimental conditions and mixing lengths

u_d cm/s	f Hz	H cm	$\Delta\rho$ g/cm^3	ϵ_b cm^2/s^3	ϵ_d cm^2/s^3	ϵ_m cm^2/s^3	$l_{expt.}$ cm	$l_{pred.}$ cm	% err. -
ONLY DISPERSED PHASE FLOW									
0.192	0	5.10	0	0	35.389	0	1.828	1.471	19.54
0.370	0	5.10	0	0	68.056	0	1.183	0.913	22.82
ONLY MECHANICAL AGITATION									
0	1.033	5.10	0	0	0	257.808	0.413	0.336	18.55
DISPERSED PHASE FLOW + MECHANICAL AGITATION									
0.37	1.85	5.10	0	0	68.056	1479.415	0.384	0.396	-2.96
0.19	1.85	5.10	0	0	34.948	1479.415	0.318	0.361	-15.05
0.37	1.017	5.10	0	0	68.056	245.533	0.562	0.630	-12.13
0.19	1.017	5.10	0	0	34.948	245.533	0.455	0.514	-12.99

Table 4.9 Experimental conditions and dispersion coefficients
(with reference to table 4.5)

ϵ_b cm^2/s^3	ϵ_d cm^2/s^3	ϵ_m cm^2/s^3	$E_{c,\ expt.}$ cm^2/s	$E_{c,\ prod.}$ cm^2/s	% err. -
ONLY BUOYANCY					
6.196	0	0	9.054	8.657	4.39
6.491	0	0	8.031	8.793	-9.49
2.393	0	0	6.727	6.305	6.28
BUOYANCY + DISPERSED PHASE FLOW					
9.552	35.389	0	11.452	12.269	-7.14
4.252	35.389	0	8.794	10.244	-16.48
6.122	67.155	0	8.886	8.538	3.92
2.624	67.155	0	8.415	6.844	18.67
1.097	67.155	0	7.101	5.707	19.63
0.24	67.155	0	2.279	4.612	-102.40
7.223	35.389	0	8.724	9.668	-10.82
3.4	35.389	0	8.257	7.879	4.58
0.678	35.389	0	4.989	5.603	-12.31
4.296	68.056	0	6.299	6.328	-0.46
1.002	68.056	0	4.251	4.271	-0.45
0.086	68.056	0	1.459	2.978	-104.14

Table 4.10 Experimental conditions and dispersion coefficients

(with reference to table 4.6)

ϵ_b cm^2/s^3	ϵ_d cm^2/s^3	ϵ_m cm^2/s^3	$E_{c,\ expt.}$ cm^2/s	$E_{c,\ prod.}$ cm^2/s	% err. -
BUOYANCY + MECHANICAL AGITATION					
2.65	0	1439.712	4.042	4.043	-0.02
0.219	0	1439.712	2.597	3.033	-16.82
2.884	0	270.485	3.711	3.554	4.21
0.072	0	270.485	1.150	1.811	-57.41
4.529	0	10017.95	5.457	6.341	-16.19
1.091	0	10017.95	4.997	5.674	-13.55
2.932	0	540.97	3.977	3.693	7.15
0.250	0	540.97	3.617	2.402	33.58
7.277	0	17054.59	8.399	7.526	10.38
2.617	0	. 17054.59	7.474	6.917	7.44
4.067	0	3041.15	5.828	4.912	15.71
0.842	0	3041.15	4.150	4.069	1.96
0.152	0	3041.15	3.166	3.676	-16.12

Table 4.11 Experimental conditions and dispersion coefficients

(with reference to table 4.7)

ϵ_b cm^2/s^3	ϵ_d cm^2/s^3	ϵ_m cm^2/s^3	$E_{c,\,expt.}$ cm^2/s	$E_{c,\,pred.}$ cm^2/s	% err. -
BUOYANCY + DISPERSED PHASE FLOW + MECHANICAL AGITATION					
7.902	68.958	233.655	10.625	7.669	27.82
3.568	68.958	233.655	9.051	6.326	30.10
1.362	68.958	233.655	6.231	5.305	14.86
0.194	68.958	233.655	1.896	4.309	-127.24
3.179	68.056	1519.769	4.759	4.951	-4.04
0.462	68.056	1519.769	2.967	3.960	-33.48
2.543	35.389	1479.415	3.867	4.399	-13.78
0.161	35.389	1479.415	1.454	3.349	-130.35
5.929	35.389	245.534	6.809	5.994	11.98
1.614	35.389	245.534	5.287	4.364	17.46
0.160	35.389	245.534	2.468	3.216	-30.33
2.181	35.389	540.97	3.942	3.999	-1.44
0.174	35.389	540.970	3.897	2.853	26.79
3.458	69.896	515.117	4.021	4.995	-24.22
0.237	69.896	515.117	2.315	3.445	-48.85
6.741	68.976	14375.1	7.929	7.273	8.26
1.778	68.976	14375.1	5.718	6.539	-14.36
7.135	35.389	17302.58	8.05	7.575	5.90
2.353	35.389	17302.58	7.094	6.936	2.240
0.999	35.389	17302.58	8.255	6.639	19.58

Table 4.12 Experimental conditions and dispersion coefficients

(with reference to table 4.8)

ϵ_b cm^2/s^3	ϵ_d cm^2/s^3	ϵ_m cm^2/s^3	$E_{c,\,expt.}$ cm^2/S	$E_{c,\,pred.}$ cm^2/S	% err. -
ONLY DISPERSED PHASE FLOW					
0	35.389	0	7.341	5.494	25.16
	68.056	0	5.111	3.618	29.21
ONLY MECHANICAL AGITATION					
0	0	257.808	1.957	1.489	23.93
DISPERSED PHASE FLOW + MECHANICAL AGITATION					
0	68.056	1479.415	3.231	3.359	-3.97
	34.948	1479.415	2.491	3.003	-20.55
	68.056	245.533	3.148	3.667	-16.50
	34.948	245.533	2.290	2.696	-17.69

4.7 Statistical analysis of the models developed

4.7.1 Comparison of model III with previous models

The improvements of the final model III, as given by equation (4.26) over the earlier versions I and II, given by equations (4.23) and (4.25) respectively were estimated in terms of the statistical parameters (a-c) defined below. While the sum of squares criterion was based on mixing length (l) in order to estimate the model parameters, the criterion Z_2 and standard deviation s were based on the back-mixing coefficients. The percentage error was determined for both mixing length and back-mixing coefficient. These criteria are defined below:

a. Sum of squares of the residuals (Z_1)

$$Z_1 = \sum_{i=0}^{N_d} (l_{model} - l_{expt.})^2 \tag{4.24}$$

The minimization of this criterion was used in the optimization program to estimate the model parameters.

b. Average absolute relative deviation or AARD (Z_2)

$$Z_2 = \frac{\sum_{i=0}^{N_p} | E_{c,model} - E_{c,expt.} | / E_{c,expt.}}{N_p} \times 100 \tag{4.27}$$

c. Root mean square deviation (s)

$$s = \sqrt{\frac{\sum_{i=0}^{N_p} (E_{c,model} - E_{c,expt.})^2}{N_d - N_p}} \tag{4.28}$$

d. Percentage error

In order to evaluate the deviation between the experimental data and model relative to experimental data for the mixing length, the percentage error was defined as follows:

$$\% \ error_l = \frac{(l_{expt.} - l_{model})}{l_{expt.}} \times 100 \qquad (4.29\ a)$$

$$\% \ error_{E_c} = \frac{(E_{c,expt.} - E_{c,model})}{E_{c,expt.}} \times 100 \qquad (4.29\ b)$$

The same formula was applied for the back-mixing coefficient (E_c) as well. The three versions of the mixing length model are compared in the following table 4.13.

Table 4.13 Statistical comparison of models developed

Model	I	II	III
Equation no.	4.23	4.25	4.26
Number of parameters	5	6	6
Number of data points	55		
Z_1	2.3853	1.8570	1.3167
Improvement over model I [2]	0 %	22.16 %	44.80 %
Z_2	27.04 %	25.44 %	22.76 %
s (cm^2/s)	0.2184	0.1947	0.1639

It can be seen that based on the above results Model III is distinctly superior to the

[2] $((Z_{1,\text{model I}} - Z_{1,\text{model i}}) / Z_{1,\text{model I}}) \times 100$; i = I, II and III

previous versions. Since the model is highly non-linear and multiple solutions corresponding to local minima are possible, it was decided to check the predictions from GAMS by using another software that uses the standard Levenberg-Marquardt technique. The predictions from POLYMATH were almost identical to that from GAMS. (POLYMATH's capacity was limited to only 5 variables. Hence, by fixing one of the variables, the remaining were verified. The parameter predictions were independent of the variable whose value was fixed from the GAMS estimate). Further the check on 95% confidence intervals (C.I.) from POLYMATH indicated that all the parameters in the model were significant. None of the parameters had C.I. s which overlapped zero.

4.7.2 Analysis of residuals based on E_ϵ

The residuals (e_i) are defined as the difference between the i^{th} data point and the model prediction. In fitting this model it was assumed that the residuals are random, independent, have zero mean, same variance and follow a normal distribution. The following methods were adopted to test the sufficiency of the model as recommended by Draper and Smith (1981).

a. the residuals were represented in a normal plot (figure 4.5) using MINITAB. A linear relationship with a high correlation (0.992) was obtained thereby confirming that the residuals are random and normally distributed.

b. 95% of the unit normal deviates defined as e_i/s (where s is defined from equation 4.29) should fall within approximately ± 2.01 corresponding to the 95% limits of a t distribution with 49 degrees of freedom. In this work, 52 out of the 55 data points corresponding to 94.5% of the unit normal deviates fell in this category. Using a normal distribution, since there are a large number of data points, leads to the criterion that 95% of the unit normal deviates should be within ± 1.96. This criterion, being more stringent than the t test, led

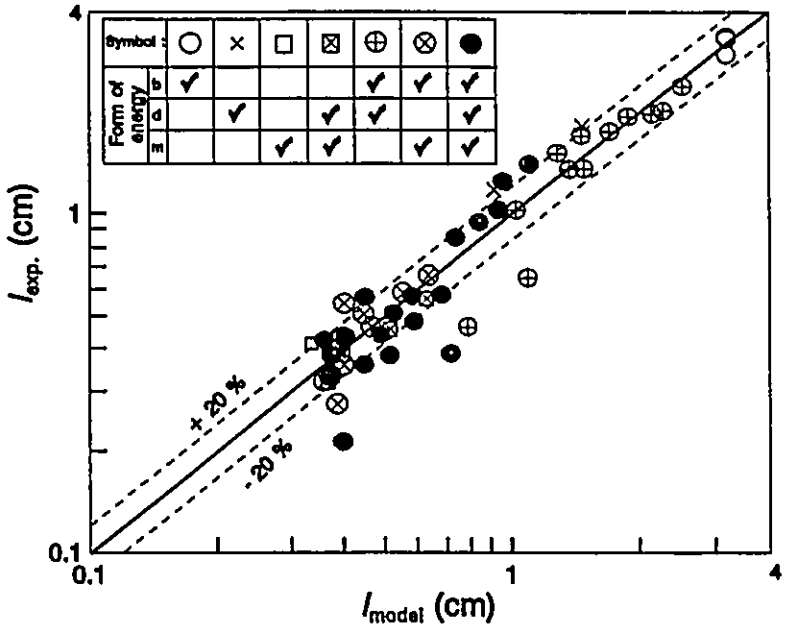

Figure 4.4 a Comparison of experimental and predicted mixing length

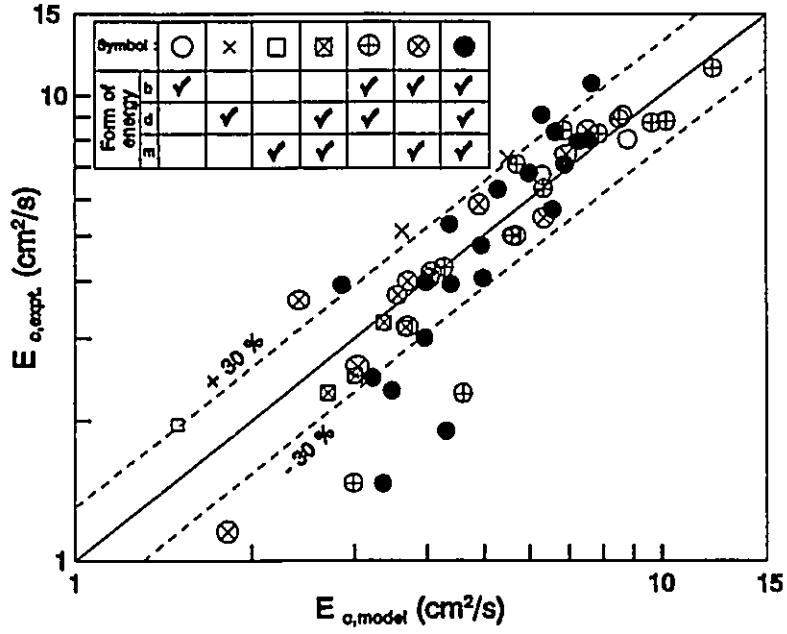

Figure 4.4b Comparison of experimental E_c with predicted E_c

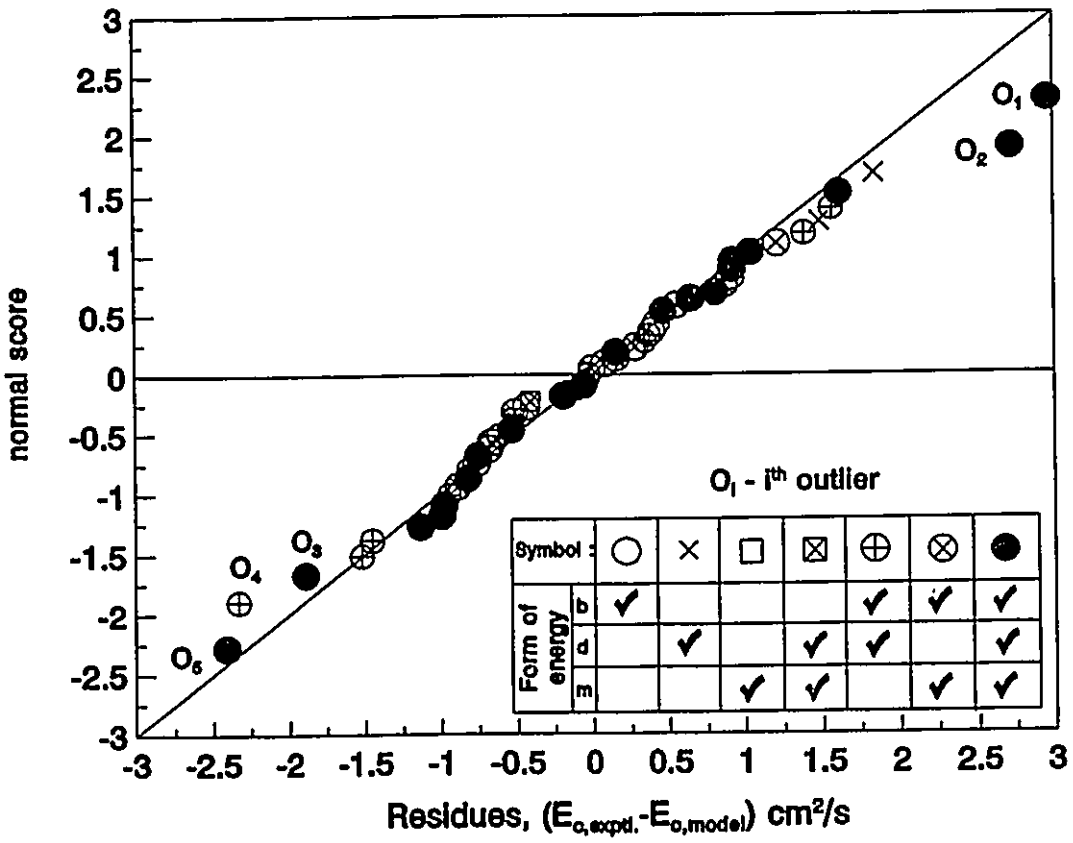

Figure 4.5 Normal plot of residuals (based on E_c) from MINITAB

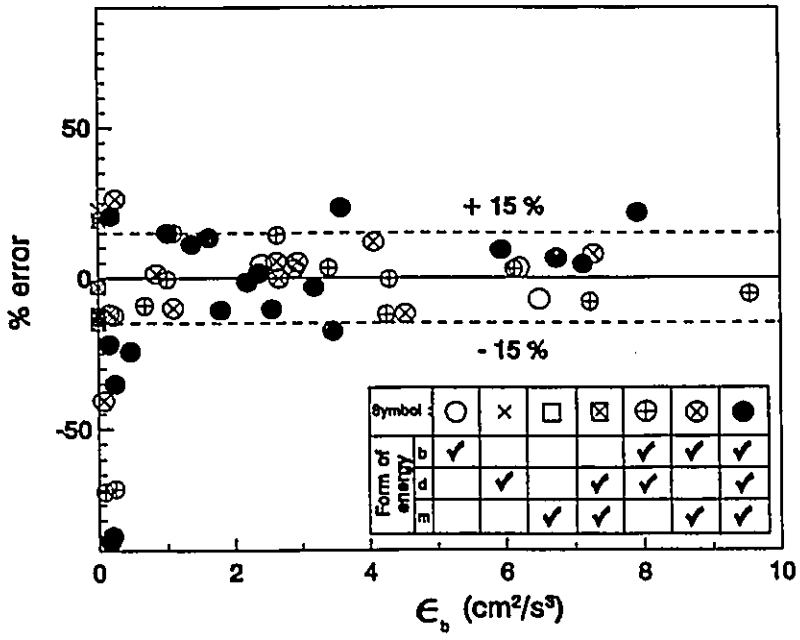

Figure 4.6 a Variation of percentage error (based on I) with ϵ_b

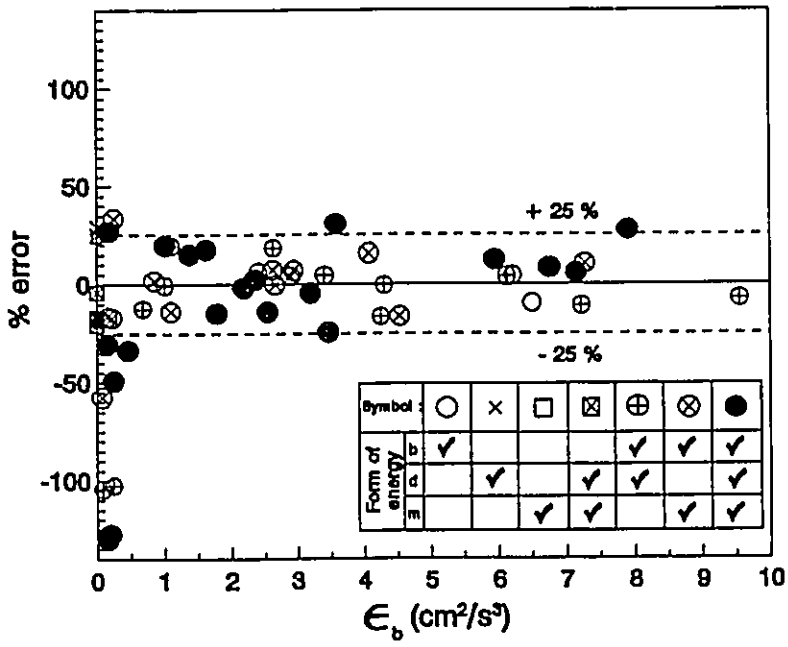

Figure 4.6 b Variation of percentage error (based on E_c) with ϵ_b

to the identification of five outliers which are tagged as O_1 to O_5 in the normal plot (figure 4.5).

From the above results it can be concluded that the errors are random with a normal distribution. The residuals corresponding to the outlier were examined from the data set in tables 4.8-4.11 and discussed below:

1. Outlier 1 and 2 corresponding to ϵ_b of 7.902 cm^2/s^3 and 3.568 cm^2/s^3 (table 4.10) came from the same experiment. In this experiment the agitations were moderate and dispersed phase flow was high. As explained in greater detail in next section, under moderate agitation and high dispersed phase flow, the circulation effects will be negligible, turbulent diffusion will not be high enough (under moderate total energy dissipations) to cause such large values of E_c. Again, as explained later under moderately agitated conditions, the effects of buoyancy though still significant are lower relative to the case with no agitation. The reason for the high values is not quite clear. It is postulated that the increase could have been due a slight misalignment in the column verticality during this run.
2. Outliers 3-5 correspond to measurements of E_c at very low buoyant energy dissipations. These correspond to E_c measurements at the tail of the tracer concentration profile where ϵ_b values were < 1 cm^2/s^3, which corresponded to an extremely small density difference of 0.0025 g/cm^3 in the continuous phase. Further, the concentrations were very low (< 0.001 g/cm^3). In this region, slope estimations were subject to error. All these residuals are negative implying $E_{c,pred.} > E_{c,expt.}$ The polynomial fit tended to flatten the curve at the tail region, so that the slopes were very close to zero leading to higher values of E_c (equation 4.1). Manual slope estimations at the tail ends were even more error prone due to the very low concentrations and lack of sufficient number of points to localize the curve.

The residuals were plotted as a percentage of the experimental values versus ϵ_b in figures 4.6 a

and b to illustrate the above conclusions.

It can be seen that the percentage error range associated with E_c is higher when compared to l. The estimation of E_c from the mixing length according to equation (2.40) , involves the mixing length term to be increased by the exponent of 4/3. Consequently, the error associated with l is magnified when it is used to find E_c. The magnification in percentage error with E_c over l can be represented with reasonable accuracy as

$$M = \frac{\%error_{Ec}}{\%error_{l}} = \frac{86}{81} + \frac{26}{81}\frac{l_{pred.}}{l_{expt.}} - \frac{4}{81}\left(\frac{l_{pred.}}{l_{expt.}}\right)^2 \qquad \text{(B7)}$$

The derivation of this relationship is given in Appendix B. This result suggests that for a ± 20 % error in mixing length, there is a +25.8% and -27.5% error in E_c.

4.8 Analysis and discussion of model and results

In this section, the applicability of the Kolmogoroff's isotropic turbulence theory to the present study is discussed. Since it was beyond the scope of the present work to make a detailed measurement of the turbulent energy spectrum and confirm the existence of the inertial sub-range conditions, indirect evidence based on the results of earlier workers and the present study are presented. This is followed by the extension and further improvement of the original mixing length model developed by Holmes et al. (1991) and Baird and Rama Rao (1991). The implications of the mixing length model are analyzed and its predictions are explained in detail with illustrative tables and figures.

4.8.1 Applicability of the Kolmogoroff's isotropic turbulence

For the successful application of the isotropic turbulence model, there should be sufficient turbulence to ensure the existence of the inertial sub-range. Further the energy dissipation rate and its variation should be properly accounted for in the model. These criteria are discussed

under several operating conditions of the Karr reciprocating plate column.

4.8.1.1 Single phase flow with no buoyancy and mechanical agitation

Under these conditions there is no energy dissipation in the continuous phase to generate turbulence, i.e. ϵ_b, ϵ_d and ϵ_m are all zero. In a carefully aligned vertical column, flow non uniformities like channelling are not serious. Hence, circulation currents cannot develop and back-mixing if any will be negligible. This was confirmed in an experiment performed using a neutrally buoyant salt tracer solution. No tracer concentration could be detected at any of the upstream sample ports.

4.8.1.2 Single phase flow with buoyancy and mechanical agitation

Holmes et al. (1991) working on a 7.62 cm diameter Karr column showed that the isotropic turbulence approach was satisfactory under single phase flow conditions. Baird and Rama Rao (1991) working on the same 5.08 cm diameter Karr column used in this study; successfully accounted for back-mixing under very small density gradients using the same approach. In their work, the mixing length model was improved to account for the effect of the mechanical agitation as described in section 1.14.2.7. Baird et al. (1992) studied axial mixing in both a baffled and open 2.62 cm diameter column having a stationary liquid phase, by adopting the mixing length model to transient state conditions. Flow visualization studies using Rhodamine dye as tracer indicated there was significant eddy turbulence behaviour in the liquid except near the region where the concentrations became extremely small.

In all these studies involving a low viscosity liquid the predicted mixing lengths were a fraction of the column diameter (table 1.8). In the present work also, the predicted mixing length under purely buoyant energy dissipation conditions was 3.199 cm which corresponds to 63% of the column diameter. Only when the column diameters decreased further and the continuous

phase became very viscous, laminar conditions were approached and the mixing lengths exceeded the column diameter. These lengths were identified with the lengths of the laminar striation (Baird et al. 1992). The data due to Baird and Legree (1994) on hot air mixing in columns having diameters greater than 20 cm also indicated *l*/D to exceed unity. Since in this work the unstable density gradient and hence the buoyant energy dissipation were very low and kinematic viscosity of the air was quite high, the authors point out that the isotropic turbulence theory corresponding to the inertial sub-range might have been only approximately valid. In the present work, even the buoyant energy dissipations alone are high and kinematic viscosity is low.

From the above discussion it can be concluded that turbulent conditions prevail under solely buoyant energy dissipation conditions provided (i) the column diameter is not small enough to approach capillary dimensions (ii) the kinematic viscosity is not high. The criterion of the critical density gradient provided by Taylor (1954) at which the unstable density gradients will cease to exist (equation 1.57) is easily exceeded in the present study under all experimental conditions. Assuming the average diffusivity of NaCl in water at room temperature is of the magnitude 10^{-5} cm^2/s (Treybal, 1981), the critical density gradient is:

$$\left(\frac{d\rho}{dz}\right)_{crit.} = \frac{67.94\times10^{-5}\times10^{-2}}{980.665\times1.0\times2.54^4} = 1.66\times10^{-10}\frac{(g/cm^3)}{cm}$$

The smallest density gradient encountered in this study does not go below 10^{-5} to 10^{-6} g/cm^4.

It must be noted that unlike the other two energy dissipation terms viz. ϵ_m and ϵ_d, the buoyant energy dissipation (ϵ_b) varies along the column length. This is due to the changing concentration of the NaCl tracer solution and hence the density of the continuous phase. This caused the variation of the back-mixing coefficient along the column. The slope analysis of the data was therefore used to estimate the local values of E_c as outlined in section 4.2. This

is in contrast to earlier back-mixing studies in literature where only the dispersed phase and the mechanical agitation effects were taken into consideration and a single E_c was used to describe back-mixing in the continuous phase for the entire length of the column for a given operating condition.

The predictions of ϵ_m based on the quasi steady state model have been proven to be satisfactory at high amplitudes (Hafez and Baird 1978; Baird and Rama Rao 1995) as used in the present study. The empirical correction factor proposed by Hafez and Baird (1978), equation (4.20) was incorporated into the expression for ϵ_m on a trial basis and the regression was again carried out for the co-current case. There was a negligible change in the objective function value (Z_1) with no appreciable change in any of the estimated parameters.

The assumption of uniform mechanical energy dissipation has not been verified experimentally for Karr columns. It can be expected that there will be more energy dissipation near the reciprocating plates than in the centre of the stage due to the existence of well mixed zones and diffusion zones (Novotny and Prochazka, 1970).

4.8.1.3 Two phase flow accompanied by mechanical agitation

The introduction of the second phase results in more turbulence and a significant increase in the back-mixing coefficient. When there is no mechanical agitation, the Karr column functions as a baffled spray column. The modification of the mixing length model in an attempt to accommodate the dispersed phase flow is discussed later in section 4.8.2. The flow of the dispersed phase through a low viscosity continuous phase results in increased turbulence due to circulation and wake transport effects. The interaction of the wakes in bubble columns leads to more uniformity in the turbulence in the continuous phase (Kawase and Moo Young, 1990). Baird and Rice (1975) correlated from various sources, the back-mixing data in bubble columns

up to 45.0 cm in diameter using the isotropic turbulence approach. Zakrzewski et al. (1981) obtained data in bubble columns which supported the existence of isotropic turbulence. While the turbulent energy spectrum under single phase flow isotropic conditions varied with wave number (k) as $k^{-5/3}$ (figure 2.6) Zakrzewski et al. (1981) had data which varied as k^{-2}. The authors argued that the 5/3 rd variation was applicable for grid turbulence while in a bubble swarm which was subject to strong fluctuations the k^{-2} variation was acceptable. Finally the authors concluded that in the gas-liquid two phase flow the energy input is mainly dissipated by a mechanism which was identical or very similar to that proposed by Kolmogoroff's theory. However, Kawase and Moo Young (1990) also caution that the mixing lengths and velocities must be recognized as characteristic parameters to be used in engineering design rather than the scales of length and velocity in Kolmogoroff's theory of isotropic turbulence. As mentioned in the previous section the conditions of isotropic turbulence have not been studied through detailed energy spectrum measurements in Karr columns operating under two phase flow conditions. As shown by Nemecek and Prochazka (1974), well mixed zones and calming zones exist under two phase flow mechanically agitated conditions as well. Hence the mixing lengths or equivalently back-mixing coefficients from Kolmogoroff's theory should be considered to be effective values representing the mixing for the entire stage under both single phase and two phase flow.

4.8.2 Extension of the original mixing length model and subsequent improvements

Under single phase flow conditions where energy dissipation occurred due to buoyancy and mechanical agitation only, the mixing length model due to Baird and Rama Rao (1991) has been shown to be applicable.

$$l = l_m+(l_b-l_m)(\frac{\epsilon_b}{\epsilon_t})^{n_1} \quad (1.64)$$

where ϵ_t is the sum of buoyant and mechanical energy dissipation rates.

It can be recalled that l_m term was introduced in order to account for back-mixing due to mechanical agitation alone when ϵ_b term was zero. Extending this approach, the dispersed phase flow term contribution was modelled initially in a similar fashion so that

$$l=l_m+(l_b-l_m)(\frac{\epsilon_b}{\epsilon_t})^{n_1}+(l_d-l_m)(\frac{\epsilon_d}{\epsilon_t})^{n_2} \quad (4.23)$$

where the total energy dissipation (ϵ_t) was now expressed as a sum of buoyancy (ϵ_b), mechanical agitation (ϵ_m) and dispersed phase energy dissipation (ϵ_d). So when both the buoyancy and dispersed phase energy dissipations are zero, mechanical agitation contributes to single phase back-mixing. Under these conditions the overall mixing length becomes l_m.

It can be seen from equation (4.23) that the dispersed phase contribution has also been modelled in terms of a lumped mixing length parameter (l_d). Kawase and Tokunaga (1991) recommend this approach in bubble columns, reasoning that the liquid flows are chaotic and local properties in two phase flow are difficult to measure. Even though the mixing length can be expected to vary radially, an average value of l across the column was felt to be more usable. It was decided to improve upon this approach by resolving the dispersed phase mixing length l_d into factors accounting for the effects of liquid circulation and mechanical agitation.

4.8.2.1 Liquid circulation effects

The introduction of the dispersed phase especially under non agitated conditions produces a remarkable change in the hydrodynamics and consequently back-mixing in the continuous phase. The dispersed phase interacts with the continuous phase in a complex manner which is

yet to be ascertained completely. The rising drops agitate the liquid by the creation of turbulent eddies combined with a steady circulating flow (Walter and Blanch, 1983). The density difference between the continuous phase and the dispersed phase results in buoyancy which forces the dispersed phase to rise along the core of the column. In this process the continuous phase is also translated in the core and it returns along the annulus setting up a recirculating flow. The recirculation currents are especially severe in the absence of plate oscillation and depend strongly on the plate spacing and the dispersed phase flow rate. Hence it was decided to modify the mixing length term in order to incorporate the synergistic effect of these two variables. To facilitate the modelling process especially under zero and low agitation, each stage of the Karr column was visualized to be a bubble (or spray) column.

It is proposed that the length of the circulation cell (β^*) is a measure of circulation inside each compartment. This also represents the extent of back-mixing in the continuous phase. The longer the circulation cell, the more severe is the back-mixing. With increasing plate spacing the length of the circulation cell will increase. It can be seen that this approach visualizes only a pair of circulation cells per stage (fig. 4.6). This is in contrast to earlier works in unbaffled bubble columns where the column was postulated to comprise of multiple circulation cells of height equal to column diameter (Joshi and Sharma, 1979). Devenathan et al. (1990) in a detailed flow mapping study in bubble columns using a radioactive particle tracking technique observed that there was a single pair of circulation cells with liquid ascending along the column centre and descending along the wall. At low gas velocities they observed two such cells. However the second cell was confined to the entry region of the dispersed phase. It is assumed that β^* is proportional to (1+H/D). Incorporating β^* into the overall mixing length leads to

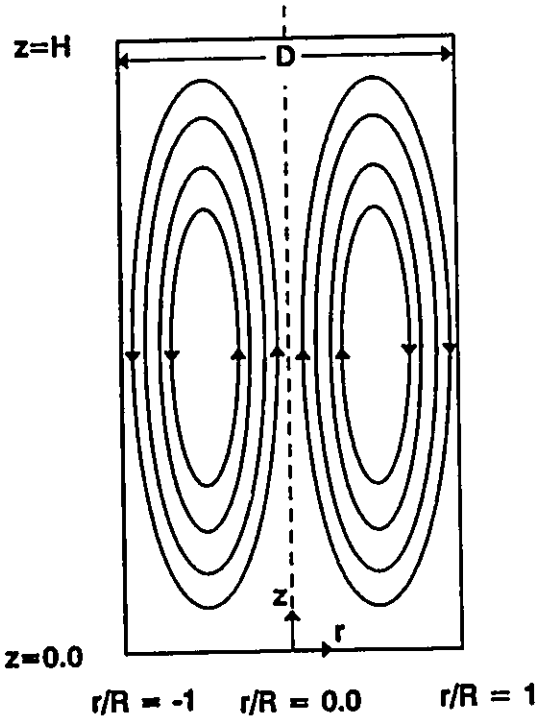

Fig. 4.7 Circulation cell within a stage

$$l_d = l_{do}\beta^* = l_{do}(1+\frac{H}{D}) \tag{4.30}$$

With increasing flow rate, radial distribution of the drops improves and the circulation currents are weakened. Since the drops occupy the entire cross sectional area of the column the return flow of the continuous phase along the column walls is inhibited. Therefore there is a sharp drop in the back-mixing in the continuous phase. Accounting for the dispersed phase flow rate into the model is discussed in the next section.

4.8.2.2 Effect of plate agitation and dispersed phase flow

Introducing plate oscillation drastically alters the mechanism of back-mixing in the continuous phase. Turbulent diffusion effects start becoming more important. Back-mixing is caused mainly due to the presence of turbulent eddies generated by the agitation due to the

oscillating plates and by the dispersed phase drops. The effects of the dispersed phase flow rate, or equivalently the dispersed phase energy dissipation (ϵ_d) and mechanical agitation (or ϵ_m) in determining the mechanism of dispersed phase contribution to continuous phase back-mixing can be summarized as follows:

1. Zero agitation

As described in the previous section, at low dispersed phase flow rates circulation effects are dominant and back-mixing increases relative to the single phase flow conditions. This effect is enhanced at increased plate spacing due to the increase in the height of the circulation cells within the stage. With increasing dispersed phase flow and with increased radial uniformity the circulation effects are very rapidly diminished and back-mixing is reduced. It is assumed that this decrease is exponential with respect to ϵ_d.

2. With plate oscillation

In the presence of plate oscillation there is a change in the mechanism of back-mixing. Eddy (turbulent) diffusion becomes increasingly important with increasing agitation. By the same token, circulation effects are suppressed by increased radial transport of momentum. The intense mechanical agitation results in a denser dispersion of drops within each stage thereby further dampening the circulation effects and greatly improving the radial uniformity. Hence, an expression is needed which takes into account the influence of dispersed phase flow rate (or equivalently ϵ_d) at zero agitation and also the effect of agitation (or equivalently ϵ_m) when applied. Hence the mixing length coefficient l_{do} given by equation (4.30) may be further resolved to incorporate the effects of plate oscillation and dispersed phase flow rate as follows:

$$l_{do} = l_{do}^{*}\exp\left(-\frac{\epsilon_d}{\epsilon_{mo}+\epsilon_m}\right) \tag{4.31}$$

where ϵ_{mo} is a constant parameter. So the final expression for the dispersed phase mixing length l_d becomes

$$l_d = l_{do}^{*}\left(1+\frac{H}{D}\right)\exp\left(-\frac{\epsilon_d}{\epsilon_{mo}+\epsilon_m}\right) \tag{4.32}$$

It can be seen that in the absence of agitation the above model assumes an exponential dampening of the circulation effects with dispersed phase flow rate. For the sake of model illustration if it can be assumed that both buoyant and mechanical energy dissipations are zero, only the dispersed phase is responsible for the back-mixing. The variation of back-mixing coefficient with dispersed phase flow rate is illustrated with the help of table 4.14. From this table it can be seen that the dispersed phase mixing length (l_d) and hence the back-mixing coefficient decreases with increasing dispersed phase flow rate. It is interesting to note that Kawase and Tokunaga (1991) observed a similar qualitative variation of the mixing length in a bubble column with respect to superficial gas velocity. Their correlation and interpretation is discussed in the next section.

The model predictions of the mechanical agitation on the dispersed phase mixing length are illustrated in table 4.15. Even a moderate agitation results in a numerically high value of ϵ_m. For instance the agitation rate Af = 3.26 cm/s corresponds to a mechanical dissipation (ϵ_m) of 270.5 cm^2/s^3 when plate spacing is 5.10 cm. When the plate spacing reduces to 2.55 cm the energy dissipation rate doubles to 541 cm^2/s^3. The dispersed mixing length approaches a constant value with increasing agitation rate as illustrated in table 4.15.

Table 4.14 Model prediction on the effect of increasing dispersed phase flow rate on l_d

(l_{do}^*=1.2306 cm, l_m=0.3363 cm, ϵ_m and ϵ_b absent)

H (cm)	u_d (cm/s)	ϵ_d (cm^2/s^3)	exp ($-\epsilon_d/\epsilon_{mo}$)	l_d (cm)	E_c (cm^2/s)
2.55	0.19	35.389	0.597	1.103	3.740
	0.37	68.056	0.370	0.685	2.463
5.10	0.19	35.389	0.597	1.471	5.494
	0.37	68.056	0.370	0.913	3.618

Table 4.15 Model predictions for effect of plate oscillation on dispersed phase mixing length

(l_{do}^*=1.2306 cm, l_m=0.3363 cm, ϵ_b absent)

H (cm)	Af (cm/s)	ϵ_m (cm^2/s^3)	ϵ_d (cm^2/s^3)	exp ($-\epsilon_d/\epsilon_{mo}+\epsilon_m$)	l_d (cm)	E_c (cm^2/s)
2.55	0.0	0.0	35.389	0.5966	1.103	3.740
			68.056	0.3704	0.684	2.463
	3.2023	515.12	35.389	0.9412	1.739	2.411
			68.056	0.8899	1.645	2.896
	9.7123	14375.1	35.389	0.9976	1.844	5.729
			68.056	0.9953	1.839	5.775
5.10	0	0	35.389	0.5966	1.471	5.494
			68.056	0.3704	0.913	3.618
	3.1	233.655	35.389	0.8895	2.193	2.727
			68.056	0.7983	1.969	3.697
	5.788	1519.77	35.389	0.9779	2.412	3.024
			68.056	0.9580	2.363	3.369

4.8.3 Implications of the mixing length model

4.8.3.1 Significance of the mixing length terms

The back-mixing under various combinations of energy dissipation was modelled in terms of an effective mixing length (l) and total energy dissipation rate (ϵ_t). The effective mixing length has been resolved to account for the buoyancy caused by the unstable density gradient, dispersed phase flow and mechanical energy contributions as shown below by equation (4.26).

$$l = l_m + (l_b - l_m)\left(\frac{\epsilon_b}{\epsilon_t}\right)^{n_1} + \left[l_{do}^{*}\left(1+\frac{H}{D}\right)\exp\left(-\frac{\epsilon_d}{\epsilon_{mo}+\epsilon_m}\right) - l_m\right]\left(\frac{\epsilon_d}{\epsilon_t}\right)^{n_2} \qquad (4.26)$$

Based on the parameter estimates, it can be seen that the effective mixing length l given by equation (4.26) can vary from a minimum value of l_m to a maximum of l_b even though the parameters l_m, l_b and l_d (for a given dispersed phase flow and agitation rate) are constant. This is due to the weights attached to the different mixing length terms. The weight refers to the ratio of a particular mode of energy dissipation rate (ϵ_b or ϵ_d) to the total energy dissipation rate ($\epsilon_b + \epsilon_d + \epsilon_m$). Hence the contribution to the back-mixing due to dispersed phase flow and buoyancy should not be viewed only in terms of the eddy scale associated with these two factors but also in terms of the fraction of their individual energy contribution to the overall energy dissipation. The exponents on the fractional energy dissipation terms viz. n_1 and n_2 relate to the degree of the importance attached to the respective weights.

The smaller is the value of the exponent, the greater is the influence of the weight and hence the mixing length term. Hence as indicated by the estimated parameter n_1 from table 4.3, the buoyant energy dissipation effects caused by the unstable density gradients in the continuous phase are quite important despite their small magnitude. Further the large value associated with

l_b makes it very significant when buoyancy is the only factor contributing to back-mixing. The model leads to three special cases where an individual mixing length becomes the only contributing factor to back-mixing. These special cases are listed below:

1. Only buoyancy effect is present $\epsilon_m \to 0$, $\epsilon_d \to 0$, $\epsilon_b > 0$

$$l = l_m+(l_b-l_m)(1)^{n_1}+(l_d-l_m)(0)^{n_2} = l_b \tag{4.33}$$

2. Only dispersed phase energy dissipation is important $\epsilon_b \to 0$, $\epsilon_m \to 0$, $\epsilon_d > 0$

$$l = l_m+(l_b-l_m)(0)^{n_1}+(l^*_{do}(1+\frac{H}{D})\exp(-\frac{\epsilon_d}{\epsilon_{mo}})-l_m)(1)^{n_2} = l_d \tag{4.34}$$

3. Only mechanical energy dissipation is present $\epsilon_b \to 0$, $\epsilon_d \to 0$, $\epsilon_m > 0$

$$l = l_m+(l_b-l_m)(0)^{n_1}+(l_d-l_m)(0)^{n_2} = l_m \tag{4.35}$$

The three weighted contributions are as follows

$$L_m = l_m = 0.3363 \tag{4.36}$$

$$L_b = (l_b-l_m)(\frac{\epsilon_b}{\epsilon_b+\epsilon_m})^{n_1} = 2.8628(\frac{\epsilon_b}{\epsilon_b+\epsilon_m})^{0.4954} \tag{4.37}$$

$$L_d = [l_{do}(1+\frac{H}{5.08})\exp(-\frac{\epsilon_d}{\epsilon_{mo}+\epsilon_m})-l_m](\frac{\epsilon_d}{\epsilon_d+\epsilon_m})^{n_2}$$

$$=[1.231(1+\frac{H}{5.08})\exp(-\frac{\epsilon_d}{68.52+\epsilon_m})-0.3363](\frac{\epsilon_d}{\epsilon_d+\epsilon_m})^{1.13} \tag{4.38}$$

so that the effective mixing length can now be expressed as

$$l = L_m + L_b + L_d \tag{4.39}$$

Despite its apparent simplicity, this formulation given by equation (4.39), contains important information. The eddies responsible for back-mixing are assumed to belong to the inertial subrange in which viscous effects are negligible and turbulence is only determined by the specific energy dissipation rate. A spectrum of eddy scales is possible in this region due to the exchange of momentum between the eddies generated by different sources of energy dissipation. This spectrum has been divided into three representative classes. L_m represents the scale of the smallest eddies present in the inertial subrange created by the interaction of eddies from different sources of energy dissipation. This is also similar to the scale attained by the eddies under conditions of intense mechanical agitation. L_d and L_b represent the remaining two classes of eddies generated by dispersed phase and buoyant energy dissipations, weighted according to the their respective fractional energy contributions. However, when there is only one source of energy dissipation, it is assumed that the eddies in the inertial subrange are similar in scale and can be represented by l_b, l_d or l_m depending on the source of energy dissipation. The experimental data were used to determine the scales of these eddies.

L_m (=0.3363 cm) constitutes 6.62% of the column diameter and is comparable to the value of 0.34 cm reported by Baird and Rama Rao (1991) for single phase flow conditions. Holmes et al. (1991) did not account for this limiting mixing length in their model.

The buoyant energy mixing length (l_b) constitutes 62.97% of the column diameter and is in the range of values obtained by earlier workers. The value of l_b corresponding to Holmes et al. (1991) work in a 7.6 cm diameter Karr column is 70% of the column diameter while Baird

and Rama Rao (1991) reported values close to 80%. The exponent n_t was 0.34 in their work while n_t is close to 0.5 in the present work. The data of Holmes et al. (1991) and Baird and Rama Rao (1991) focussed only on the single phase situation while the present work had only a limited amount of single phase data and focussed mainly on two phase flow conditions.

The dispersed phase mixing length (l_d) unlike the previous terms is variable and dependent on dispersed and mechanical energy dissipations and plate spacing. In previous studies on bubble columns, the mixing length concept has often been used to describe back-mixing in the continuous phase. But different interpretations have been suggested for these mixing lengths. Kawase and Moo Young (1986) assumed that the mixing length for two phase flow was substantially similar to that for a single phase flow and obtained the average mixing length equal to 10 % of the column diameter.

Rice and Littlefield (1987) in their back-mixing studies in a 14 cm diameter bubble column observed that even a slight tilt in the alignment of the column produced excessive back-mixing. They used a rubber sparger to generate uniform sized bubbles. In a perfectly vertical column under ideal bubbly flow conditions the mixing length scale in the isotropic turbulence model was proportional to the bubble size which was uniform at 0.41 cm. They observed that this scale can become larger tending towards the column diameter as the conditions changed from homogeneous bubbly regime to heterogeneous churn turbulence regime. In the present work, the drop size distribution under non agitated conditions was non-uniform and closer to the churn turbulent regime. Hence the dispersed phase mixing lengths were larger than the drop diameter. As shown in the next chapter, the mean drop size (d_{32}) was only approximately 7% of the column diameter, whereas the lowest dispersed phase mixing length (l_d) corresponding to a plate spacing of 2.55 cm and dispersed phase energy dissipation of 68 cm^2/s^3 corresponded to 13.4%

of the column diameter. Hence it can be concluded that in the present study the dispersed phase mixing length is not proportional to the drop diameter.

Kawase and Tokunaga (1991) used data on bubble columns covering a wide range of column diameters ($0 < D \leq 0.6$ m) and superficial gas velocities ($0.01 \leq u_{sg} \leq 1.45$ m/s). The average mixing length was obtained by integrating the equation governing the radial variation of the velocity in the turbulent core and regressing the available experimental data. The following correlation for the average mixing length was proposed

$$l_{mean} = 4.5\times10^{-2}u_{sg}^{-0.38}D \qquad (4.40)$$

This is qualitatively similar to the results in the present work wherein the decrease in mixing length with dispersed phase flow velocity is accounted for. The authors attributed the inverse dependency of l on the superficial gas velocity (u_{sg}) to the existence of bubbles and their complicated motion. In the present work the model can also be qualitatively interpreted in terms of the ideas proposed by Geary and Rice (1992).

Geary and Rice (1992) discussed the possibility of mixing in the continuous phase due to turbulence generated near the wall propagating to the core of the liquid in addition to the turbulence created by the bubble motion. Near the wall, where essentially only the continuous phase is present, turbulent eddies of scale l_{wall} are created by the boundary layer instabilities. The second concept involves eddies of scale l_{bubble} generated by the movement of the dispersed phase and governed by the bubble size and population density. To resolve this issue the authors recommend to choose the mixing scale which leads to the minimization of the dissipation in the continuous phase. Energy is minimized when the larger of the two mixing scales is chosen. The model developed in this thesis can be interpreted to take into account both terms of the turbulence

generated at the wall (and its corresponding mixing length) and the turbulence generated due to drops. At zero agitation and low dispersed phase flow rates circulation of the continuous phase in the proximity to the wall generates turbulence which propagates to the core of the column. This length contributes mainly to the dispersed phase mixing length l_d. At higher dispersed phase flows this latent turbulence is damped out by the dense dispersion of drops present in the core and the effect of l_{wall} is weakened. At very high dispersed phase flows and intense mechanical agitation, eddy dispersion generated by the drops dominates the disperse phase back-mixing contribution. The same comments apply when the effects of mechanical agitation are considered. As it is increased, the relative effect of the wall turbulence is reduced.

Hence three regimes can be proposed to explain the dispersed phase contribution to the back-mixing in the continuous phase. For the sake of convenience in illustration it is assumed that the buoyant energy dissipation effects are absent i.e. $\epsilon_b = 0$.

1. Circulation Regime I (zero mechanical agitation and low dispersed phase flow rate)

$$E_c = [l_m + (l_{do}^{*}(1+\frac{H}{D})\exp(-\frac{\epsilon_d}{\epsilon_{mo}}) - l_m)(1)^{n_2}]^{\frac{4}{3}}(\epsilon_d)^{\frac{1}{3}}$$

$$=(l_{do}^{*}(1+\frac{H}{D})\exp(-\frac{\epsilon_d}{\epsilon_{mo}}))^{\frac{4}{3}}\epsilon_d^{\frac{1}{3}} \qquad (4.41)$$

In this regime, the total dispersed phase energy dissipation is quite low and turbulent eddy diffusion is less important than the circulation effects. In this regime, l_d is maximum and $\epsilon_t^{1/3}$ is low (see also table 4.14).

2. Intermediate regime II (zero agitation and high dispersed phase flow)

In this regime, the exponential term decays rapidly and l_d decreases as well. The

circulation effects are fast dampened out and the eddy dispersion term starts becoming important due to the increase in ϵ_d and hence in $\epsilon_t^{1/3}$. This corresponds to a region when the back-mixing coefficient passes through a minimum with respect to dispersed phase flow (table 4.14).

3. Eddy diffusion regime III (non zero agitation)

In this regime, the dispersed phase flow rate is no longer the critical factor. In fact, the exponential term tends asymptotically towards unity (table 4.15) with increasing agitation thereby marking a shift in the operating regime of the column. There is a uniform dispersion of the dispersed phase across the column. The circulation effects are absent and the total energy dissipation term $(\epsilon_m + \epsilon_d)^{1/3}$ increases rapidly, leading to eddy dispersion in the core of the column becoming very important. The back-mixing coefficients are higher than those in the intermediate regime if not higher than those corresponding to the regime I. l_d for a given column geometry tends towards a constant value (table 4.15)

NOTE : The model parameters (especially ϵ_{mo}, l_d) are only valid in the range of dispersed flow rates investigated. Extending this model beyond the limits in this work may lead to erroneous results. For example, if ϵ_d is very high the exponential term becomes very small and the term l_d-l_m would become negative, but such conditions have not been reached experimentally.

4.8.3.2 Contribution of wakes to back-mixing

The Kolmogoroff's model described above contains the contributions of unstable density gradient and mechanical agitation (leading to eddy turbulent dispersion) and dispersed phase flow (leading to circulatory flow at low values and eddy dispersion at high flows). However the influence of wakes has not been incorporated in detail. The importance of wakes to the overall back-mixing process seems to be of lesser importance than the circulatory flow (Anderson and Pratt 1978; Steiner and Hartland 1983). To include the contribution of wakes into the back-

mixing model in detail would require additional parameters like wake volume, wake shedding height and droplet volume (Steiner and Hartland, 1983). These parameters are difficult to estimate particularly under agitated conditions. Further, **in co-current flow** both the dispersed and continuous phase are flowing in the same direction. Hence the wakes will comprise of the continuous phase being transported in the same direction as the bulk flow of the continuous phase. **Hence there is no contribution of wake transport to back-mixing in co-current flow situations.** It appears that the magnitude of the mixing length coefficient l_{d_o} incorporates the importance of the wake transport effects. More discussion on this will be given in the next chapter, where counter-current back-mixing results are presented.

4.9 Effect of buoyant energy dissipation (ϵ_b) on back-mixing coefficient

In this section the effect of ϵ_b on E_c is discussed under various operating conditions. Due to the inherent scatter in the data, the model is used as the basis for predicting the trend curves. The trends for the back-mixing coefficient are illustrated in figures 4.8 - 4.10. Experimental data points, when available are also shown. The effect of the different operating variables on the effective mixing lengths are illustrated in figure 4.11 (a-c).

Note: In all these figures, the units of ϵ_m, ϵ_b and ϵ_m are in cm^2/s^3.

4.9.1 Single phase flow conditions:

The effect of ϵ_b is illustrated with the help of figure 4.8 using ϵ_m as the parameter (which includes the effect of plate spacing according to equation 4.19). The effect of plate spacing (H) associated with l_d is not considered since ϵ_d is zero. Three levels of energy dissipation are plotted - zero, moderate ($0 < \epsilon_m < 3500\ cm^2/s^3$) and high ($3500 < \epsilon_m < 17500\ cm^2/s^3$). Since there was a lot of variation in ϵ_m typical ranges had to be considered and the individual data points are labelled in the figure with the applicable values of ϵ_m.

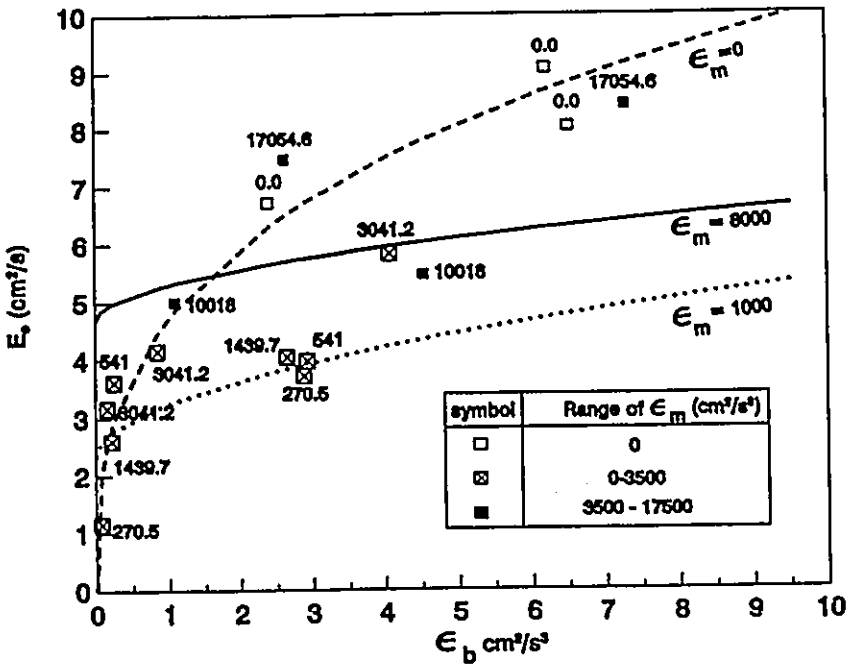

Figure 4.8 Effect of buoyant energy dissipation on E_c under single phase flow conditions

From the trends shown in the figure it can be seen that

1. the buoyant energy dissipations are very small (0-10 cm^2/s^3) when compared to the rates of the mechanical energy dissipation (0-8000 cm^2/s^3).
2. ϵ_b produces a significant enhancement in E_c. Even a very small unstable density gradient in the continuous phase can significantly increase axial mixing.
3. The effect of buoyancy is predominant at zero mechanical agitation. With increasing agitation the rate of enhancement in E_c with ϵ_b is less rapid. Only at intense mechanical agitation, E_c tends towards a more or less constant value almost independent of ϵ_b.

After defining the % enhancement (i) in E_c with ϵ_b according to the following equation, the conclusions are illustrated in table 4.16. The back-mixing coefficients are also shown in table 4.16.

$$i = \frac{E_c - E_{c,\epsilon_b=0}}{E_{c,\epsilon_b=0}} \times 100 \qquad (4.42)$$

Table 4.16 Enhancement of E_c due to buoyant energy dissipation (single phase flow with $\epsilon_d=0$)

ϵ_b (cm^2/s^3)	$\Delta\rho$ (g/cm^3)	ϵ_m=0.0 cm^2/s^3		ϵ_m=1000 cm^2/s^3		ϵ_m= 8000 cm^2/s^3	
		E_c (cm^2/s)	i (%)	E_c (cm^2/s)	i (%)	E_c cm^2/s	i (%)
0	0	0	undef.	2.34	0	4.68	0
5	0.0127	8.06	undef.	4.44	89.84	6.10	30.40
10	0.02548	10.16	undef.	5.39	130.35	6.71	43.42

At zero agitation, the scale of the eddies generated due to buoyant energy dissipation is large and equal to l_b. Hence there is increased back-mixing despite the small energy dissipation. With increasing agitation, the effective mixing length decreases and is in the range $l_m < l < l_b$. Under moderate agitation, ϵ_m and hence ϵ_t is still low and combined with decreased l, E_c decreases relative to the case when $\epsilon_m = 0$. At increasing mechanical agitation, l tends towards the limiting constant value l_m and since total energy dissipation ϵ_t ($=\epsilon_m+\epsilon_b$) is high, E_c defined by equation (2.40) starts to increase again. Hence as shown in figure 4.8, E_c passes through a minimum before starting to increase. The effect of increasing mechanical energy dissipation on the effective mixing length l for an average value of ϵ_b = 5 cm^2/s^3 is illustrated in figure 4.11a.

As can be observed from figure 4.11a, the model predicts that with the presence of mechanical energy dissipation, the effective contribution of the buoyancy term to the effective mixing length is reduced. This situation could arise due to the rapid interchange of energy between eddies of different scales and energy levels (intensities) through momentum transfer so

that the effective mixing length takes an intermediate value. At intense mechanical agitation, the small eddies of high intensity predominate over the larger eddies of much smaller energy intensity generated by the buoyancy effects, and the mixing length tends towards l_m.

4.9.2 Two phase flow conditions:

Under these conditions, there is an additional contributing factor to turbulence viz. the dispersed phase energy dissipation (ϵ_d). First, the situation corresponding to no mechanical agitation (ϵ_m) is discussed. The parameters are ϵ_d and plate spacing H. Two levels of ϵ_d and H are used. Since the variation of the experimental ϵ_d from either of the two levels was very small, the data points are not labelled in the figure (4.9). The situation corresponding to zero dispersed phase flow is also shown for comparison. (As discussed in section 4.9.1, plate spacing has no effect on E_c under single phase flow unagitated conditions. Hence the curves corresponding to H=2.55 cm and H=5.10 cm are coincident).

The results illustrated in figure (4.9) show that

1. the buoyant energy dissipation is still important under two phase flow conditions. The % enhancement in E_c due to buoyancy effects is shown in table 4.17.
2. the trend of increase in E_c with ϵ_b is similar irrespective of the dispersed phase energy dissipation and plate spacing.
3. In addition to the above two effects it can be also noted that the E_c values, are strongly influenced by the dispersed phase energy dissipation and plate spacing as discussed in section 4.8.2.2.

The relative significance of buoyancy and dispersed phase contributions at different plate spacings are illustrated in figure (4.11b). The value of ϵ_b is fixed at a typical 5 cm^2/s^3. The conclusions drawn from this figure are listed below.

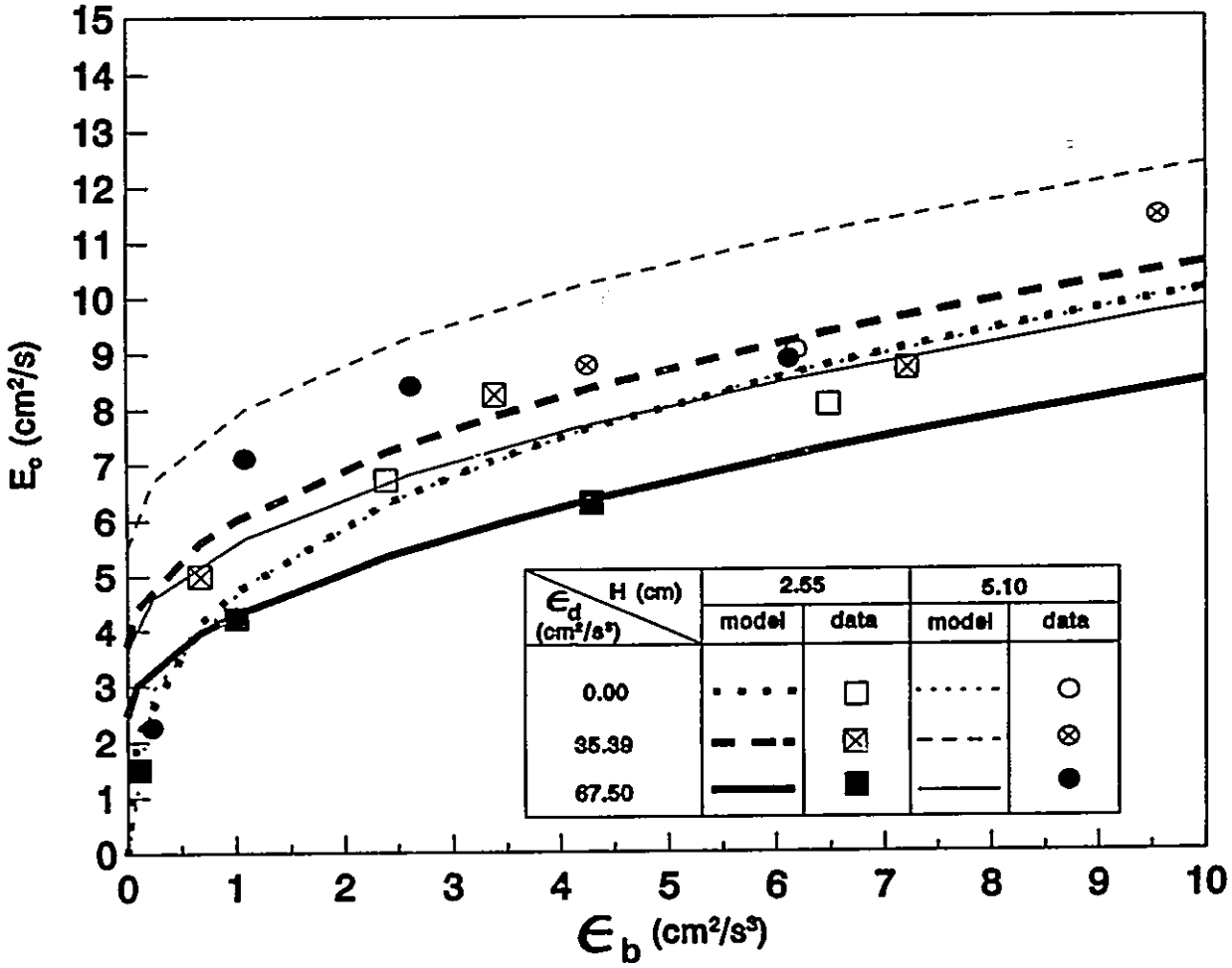

Figure 4.9 Effect of buoyant energy dissipation on two phase flow unagitated conditions

Table 4.17 Enhancement of E_c due to buoyant energy dissipation (two phase flow with $\epsilon_m=0$)

ϵ_b (cm^2/s^3)	$\Delta\rho$ (g/cm^3)	H (cm)	$\epsilon_d=0.0$ cm^2/s^3		$\epsilon_d=35.39$ cm^2/s^3		$\epsilon_d=67.5$ cm^2/s^3	
			E_c (cm^2/s)	i (%)	(E_c) (cm^2/s)	i (%)	E_c (cm^2/s)	i (%)
0	0.0	2.55	0	undef.	3.74	0	2.48	0
		5.10			5.49	0	3.65	0
5	0.0127	2.55	8.06	undef.	8.72	133.2	6.68	169.0
		5.10			10.60	93.1	8.04	120.5
10	0.02548	2.55	10.16	undef.	10.63	184.2	8.50	242.1
		5.10			12.40	125.8	9.85	170.2

1. The effective mixing length decreases with increasing dispersed phase flow at a given plate spacing due to the attenuation in the circulation effects as explained in section 4.8.2.2. Further, the weight ($\epsilon_b/\epsilon_b+\epsilon_d$) is reduced with increasing ϵ_d thereby diluting the contribution of the buoyancy effect.
2. It is interesting to note that L_b and L_d are comparable despite the order of magnitude difference between the two forms of energy dissipations. The model estimates of n_1 (=0.4954) and n_2 (=1.13) attributes a heavier weight to the buoyancy term. Further, the value of the exponent n_2 tends to reduce the weight attached to the dispersed phase mixing length and hence its contribution to the overall mixing length, in spite of the high fraction of ϵ_d/ϵ_t. These factors considered along with a high value of l_b result in a significant enhancement in the back-mixing coefficient due to the buoyancy.
3. Under non agitated conditions, the buoyancy effects are lower under two phase flow when compared to single phase flow, in terms of the contribution to the effective mixing length.

Physically, this could be due to the eddies generated by buoyancy interacting with those created by the droplets and with the droplet themselves thereby leading to a lower effective mixing length.

4.9.3 Effect of buoyancy under two phase flow agitated conditions (ϵ_b, ϵ_m and $\epsilon_d > 0$)

These conditions approximate closely to the actual industrial situation except that mass transfer is not present. Typical model trends are shown in figures 4.10 a and b. Low and moderate mechanical energy dissipations of 530 and 1500 cm^2/s^3 corresponding to plate spacings 2.55 and 5.10 cm respectively are shown in figure 4.10 a and intense mechanical energy dissipation of 15000 cm^2/s^3 corresponding to a plate spacing of 2.55 cm is shown in figure 4.10b. Single phase flow E_c values are also shown in the latter figure for comparison.

Since the experimental ϵ_m varied around the values used in the model trends, they were labelled in the figures. The following conclusions can be drawn based on these results

1. At low and moderate agitations ϵ_b still has an important effect in enhancing E_c as shown in table 4.18. From tables 4.16 and 4.18 it can be seen that under conditions of intense mechanical agitation, the enhancement in E_c due to buoyancy effects is still evident even though it is attenuated and E_c tends towards a constant value as in single phase flow.
2. It can also be observed that the influence of ϵ_d on E_c is stronger at lower levels of mechanical agitation. As ϵ_m increases, the diffeence between E_c values at different dispersed phase flows narrows down as shown in figure 4.10 a. As explained in section 4.8.2.2 the dispersed phase mixing length l_d tends towards a constant value since the exponential term approaches unity. At intense mechanical agitation, E_c attains a constant value insensitive to ϵ_d (figure 4.10b) and approaches single phase values.
3. A column operating with a plate spacing of 5.10 cm accompanied by a mechanical energy

dissipation of 1500 cm^2/s^3 (f=1.87 Hz) experiences nearly equivalent back-mixing to that of a column operating with a plate spacing of 2.55 cm and mechanical energy dissipation of 530 cm^2/s^3 (f=1.0 Hz). This suggests that having a higher plate spacing enables the column to operate at higher agitation levels without a serious deterioration in the back-mixing effects. The effects of H, ϵ_d and ϵ_m (with ϵ_b at an average value of 5 cm^2/s^3) on the mixing length are shown in figure 4.11 c. It can be seen that with increasing total energy dissipation (ϵ_t), the effective mixing length tends towards the limiting value (L_m). Under these conditions, the value of ϵ_t determines the back-mixing coefficient. The dispersed phase contribution to the overall mixing length is low at moderate agitations and nearly zero at high agitations. Hence the two phase dispersion exhibits back-mixing properties resembling single phase conditions.

Table 4.18 Enhancement of E_c due to buoyancy under two phase flow mechanically agitated conditions

ϵ_b (cm^2/s^3)	$\Delta\rho$ (g/cm^3)	ϵ_d (cm^2/s^3)	ϵ_m=530 (cm^2/s^3) H=2.55 cm		ϵ_m=1500 (cm^2/s^3) H=5.1 cm		ϵ_m=15000 (cm^2/s^3) H=2.55 cm	
			E_c (cm^2/s)	i (%)	E_c (cm^2/s)	i (%)	E_c (cm^2/s)	i (%)
0	0	35.0	2.41	0	3.01	0	5.81	0
		69.0	2.91	0	3.37	0	5.85	0
5	0.0127	35.0	4.87	101.68	4.99	65.54	7.08	21.93
		69.0	5.41	85.93	5.38	59.52	7.13	21.79
10	0.02548	35.0	5.98	147.7	5.86	94.58	7.62	31.23
		69.0	6.53	124.34	6.27	85.72	7.67	31.02

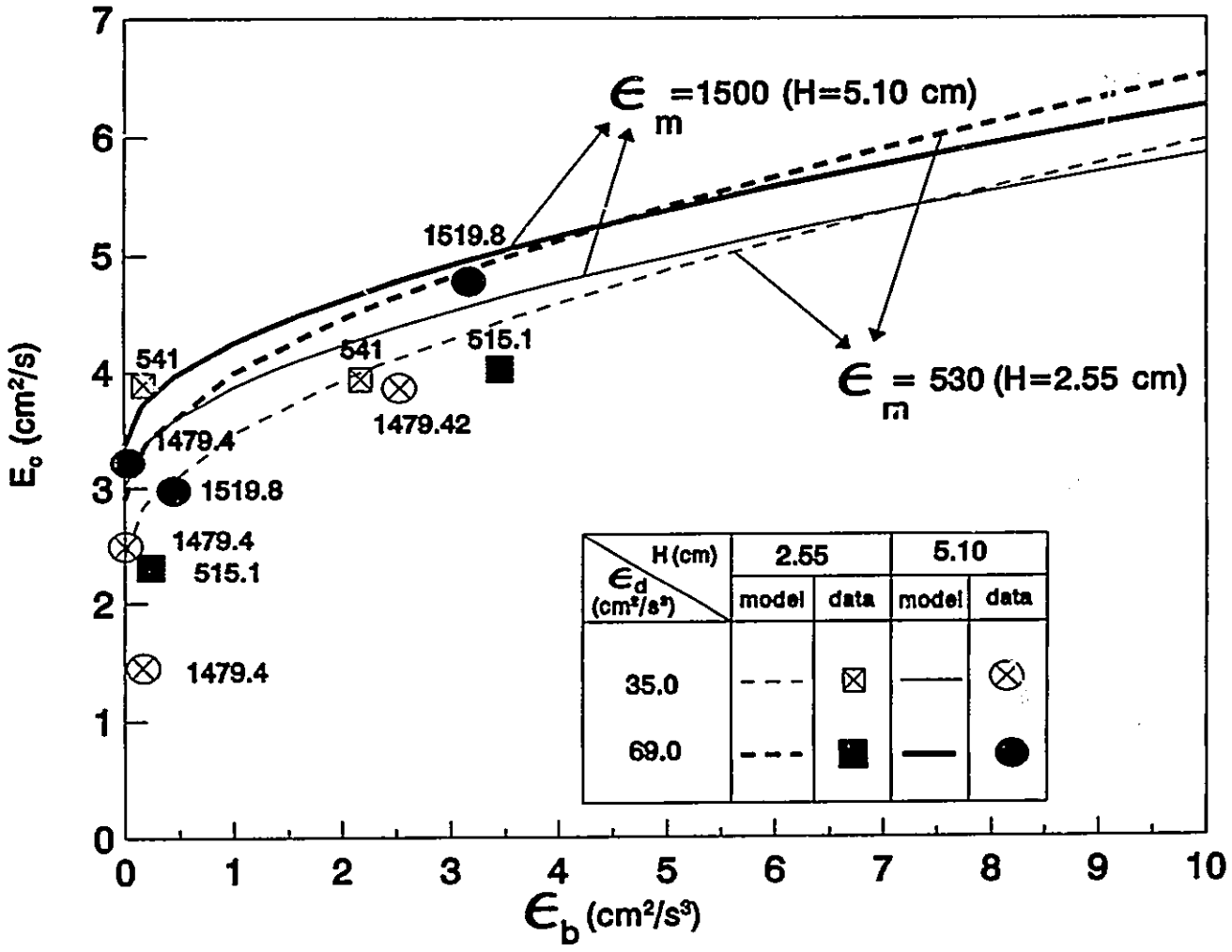

Figure 4.10 a Effect of buoyant energy dissipation under two phase flow moderately agitated conditions

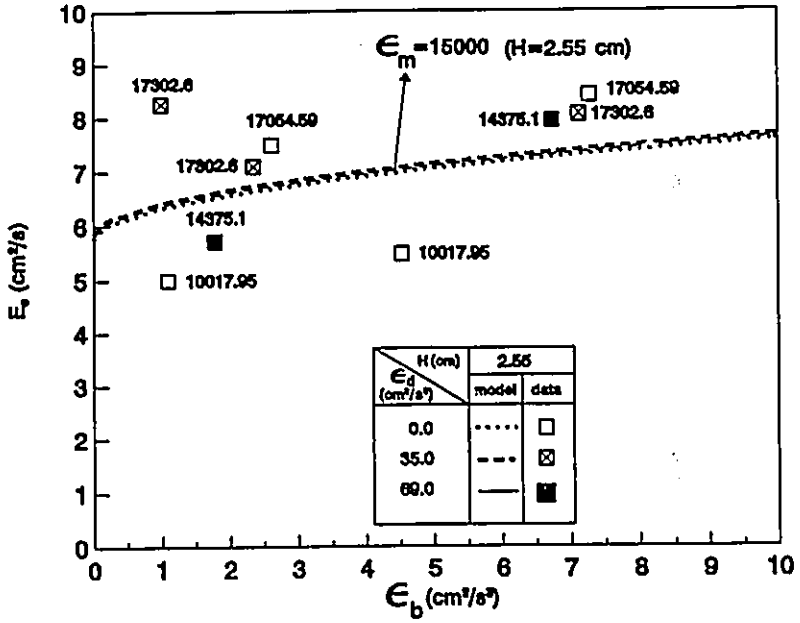

Figure 4.10 b Effect of buoyant energy dissipation at highly agitated two phase flow conditions

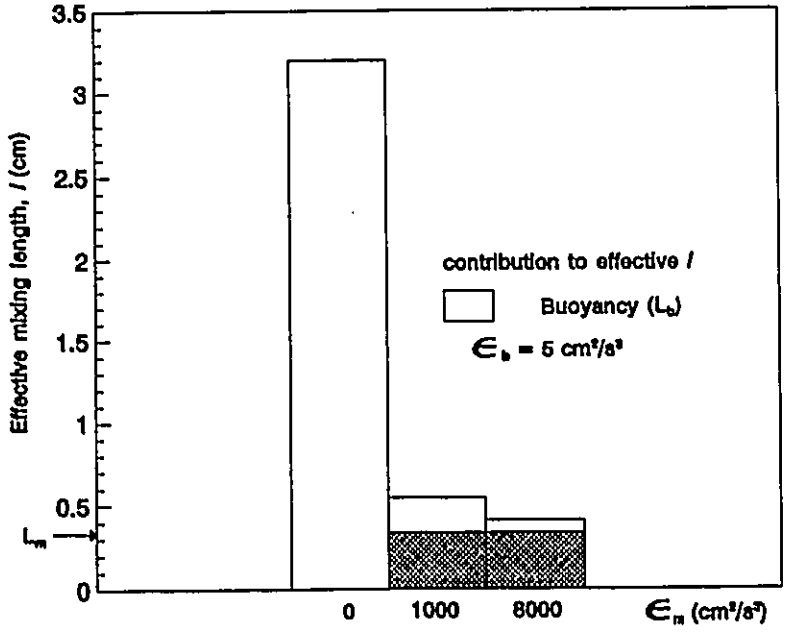

Figure 4.11 a Variation of effective mixing length with agitation under single phase flow conditions

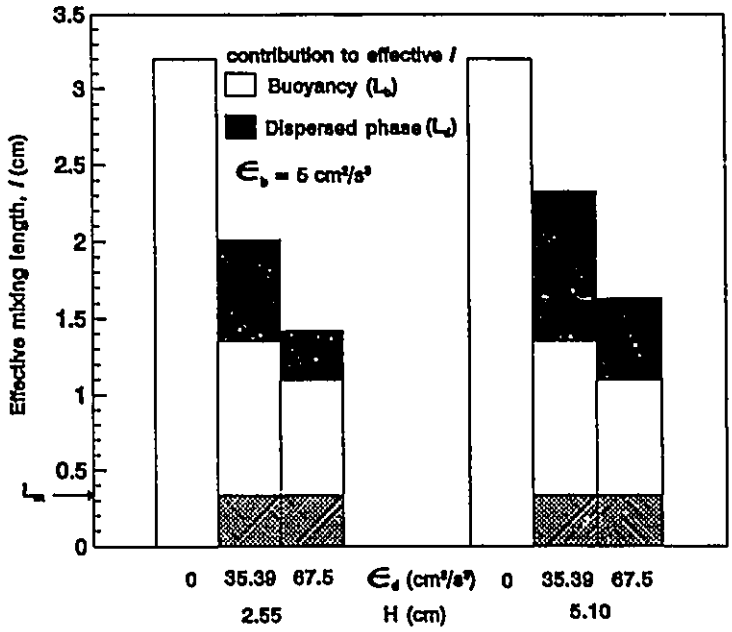

Figure 4.11b Variation of effective mixing length with dispersed phase energy dissipation, $\epsilon_m=0$

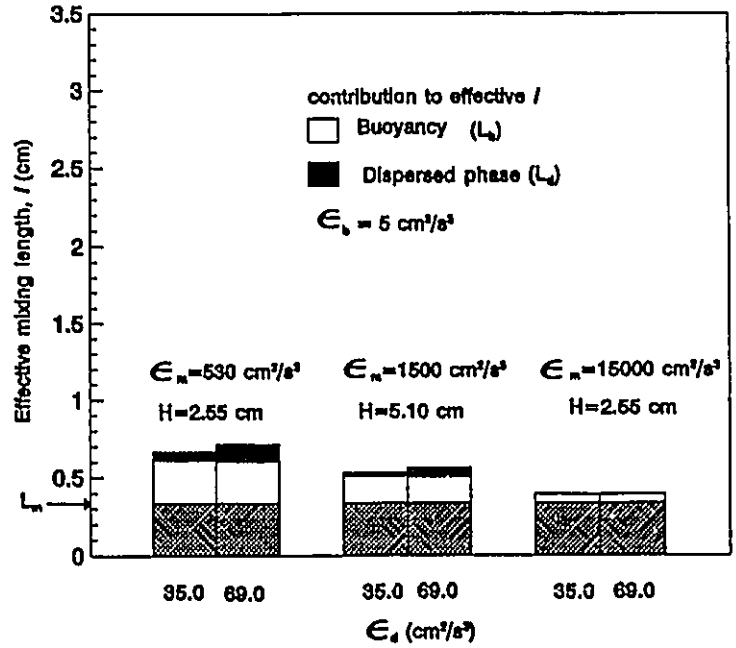

Figure 4.11 c Variation of effective mixing length under two phase flow agitated conditions

4.10 Summary and Conclusions

The effect of three main factors, buoyancy caused by the unstable density gradient, dispersed phase flow and mechanical agitation, on back-mixing were investigated in this study. Kolmogoroff's isotropic turbulence approach was used to model the back-mixing in the continuous phase. According to this approach, the back-mixing was modelled in terms of the effective mixing length and energy dissipation.

$$E_c = l^{\frac{4}{3}}(\epsilon_t)^{\frac{1}{3}} \tag{2.40}$$

The contribution of the different factors viz., buoyancy, dispersed phase flow and mechanical agitation, to the back-mixing must be viewed in terms of the magnitudes of their weighted mixing lengths *and* the magnitude of their energy dissipation terms. First the effect of individual factors are discussed followed by the effect of their interactions.

4.10.1 Individual effect of the main factors on E_c

1. Buoyancy The energy dissipation associated with this factor is small because the density difference in the continuous phase is usually in the range 0-0.03 g/cm^3. However, the mixing length l_b is quite high (3.199 cm corresponding to 63% of column diameter) leading to a large value of the back-mixing coefficient. For example, when ϵ_b is 5 cm^2/s^3 corresponding to a density difference of 0.013 g/cm^3 in the continuous phase, the value of E_c is as high as 8 cm^2/s. If the concept of buoyancy mixing length being 60-70% of column diameter can be extended to commercial spray columns of much larger diameter, i.e. if Kolmogoroff's theory is still applicable, the back-mixing effects due to buoyancy will be very severe.

2. Dispersed phase flow The presence of the second phase leads to a distinct change in the hydrodynamics of the continuous phase especially in the absence of agitation. At low flow rates

of the dispersed phase, the drops are not evenly distributed across the column thereby causing massive circulation within the stage (circulation regime). The dispersed phase mixing length was modelled in terms of the length of the circulation cell which was found to be proportional to the plate spacing. With increasing dispersed phase flow, radial uniformity improved and the circulation currents were dampened leading to the decrease in the back-mixing coefficient. At high dispersed phase flows, it was the energy dissipation rather than the highly reduced mixing length which determined the dispersed phase flow contribution to the back-mixing (eddy diffusion regime).

3. Mechanical agitation When mechanical agitation is the only source of energy dissipation the mixing length is determined by l_m which represents the lowest of the three representative scales of the turbulent eddies.

4.10.2 Effect of interactions between the different factors on back-mixing.

1. Buoyancy and dispersed phase flow effects Under two phase flow conditions there is an order of magnitude difference between the energy dissipation terms ϵ_b and ϵ_d. The two mixing length contributions are comparable and the overall mixing length reduces with increasing dispersed phase flow (figure 4.11b) due to the dampening of the circulation effects. The dispersed phase flow rate determines whether the back-mixing is in the circulation regime or eddy diffusion regime.

2. Buoyancy and mechanical agitation The results indicate that the buoyancy effects are still important under conditions of low and moderate agitation due to its significant contribution to the effective mixing length. At intense agitations the buoyancy effect is attenuated in terms of scale and because of its extremely small energy dissipation relative to ϵ_m leads only to a minor enhancement in the back-mixing of the continuous phase.

3 Dispersed phase flow and mechanical agitation Agitation improves the radial distribution of drops inside the column and dampens the circulation currents. With increasing agitation the contribution of the dispersed phase flow to back-mixing changes from circulation type to turbulent eddy diffusion type. Due to the high value of ϵ_m the exponential term associated with l_d tends towards unity and l_d tends towards a constant value for a given plate spacing. The dispersed phase energy dissipation adds to the total energy dissipation. Since ϵ_d and ϵ_m are an order of magnitude different, the enhancement in $\epsilon_t^{1/3}$ due to ϵ_d for a given ϵ_m is only sluggish. Further, from the data it was inferred that the dispersed phase mixing length contribution has a lower weight. Therefore under two phase flow agitated conditions, the effect of the dispersed phase is less important than the mechanical agitation.

4 All the three factors present An important result with practical implications is the significance of the buoyancy mechanism in increasing the effective mixing length and hence the back-mixing under low and moderate agitations. At low agitations, the dispersed phase contribution to the effective mixing length is lower than that of the buoyancy effects (figure 4.11c). It is possible to conclude that under conditions of moderate mechanical agitation the buoyancy effects, despite their small energy dissipations, can be relatively more important than the dispersed phase flow in affecting the back-mixing.

Magnitude-wise, ϵ_d is an order higher than ϵ_b, but in turn it is at least an order lower than the mechanical energy dissipation. The increase in the total energy dissipation as $\epsilon_t^{1/3}$ due to dispersed phase flow is of lower significance than the increase in the effective mixing length as $l^{4/3}$ due to the contribution of the buoyancy. At high agitations, both dispersed and buoyancy effects make a negligible contribution to the total mixing length and the difference between single phase and two phase back-mixing values is small.

4.10.3 Practical recommendation from this work

Although the present study was conducted under two phase flow non mass transfer conditions, it is still of importance to industrial extraction columns. Due to practical limitations like the difficulty in sampling from actual runs or the toxicity of the chemicals involved in the extraction, it is common for industrial investigations on axial mixing to be restricted to steady state or more usually transient tracer tests conducted on pilot scale or even industrial columns. Tracers involving ionic compounds are often used since they are easy to monitor by on-line instrumentation. However these tracers like NaCl and $CaCl_2$ cause a definite change in the density of the continuous phase. This study has shown that small unstable density change produced in the continuous phase can lead to a significant enhancement in the back-mixing coefficient even under two phase flow agitated conditions.

It is just as important to control the density gradient effects in the tracer measurements of E_c as to take account of density gradient effects on the full commercial scale. Correlations for E_c based on tracer measurements which have been affected by unstable buoyancy will tend to overestimate the axial mixing and therefore may result in column designs which are unnecessarily conservative. However, a failure to account for unstable buoyancy effects at the commercial scale will result in more axial mixing than expected and therefore the column performance may fall short of expectation.

This work has shown that unstable density gradients will enhance axial mixing; it is likely that the converse situation of a stable density gradient in the continuous phase will lead to reduced axial mixing. The effect of stable density gradients on axial mixing does not appear to have been investigated and it is recommended that it should be studied in detail.

The two opposite effects of unstable and stable density gradients lead to a general design

recommendation that extraction columns should be operated with stable density gradients in the continuous phase wherever possible.

CHAPTER 5

HYDRODYNAMIC AND MASS TRANSFER RESULTS UNDER COUNTER-CURRENT FLOW CONDITIONS

5.1 Introduction

In this chapter the results of back-mixing studies, carried out under counter-current conditions are reported. Both mass transfer and non mass transfer conditions were studied. The aim of this preliminary study was to initiate the investigation on the effect of the unstable density gradient induced through solute transfer. Under mass transfer conditions, the transfer of *i*-propanol from the dispersed organic to the aqueous continuous phase created an unstable density gradient. In the absence of solute transfer, the continuous phase was neutrally buoyant. The dispersed phase hold-up and drop sizes were also calculated for all the runs.

5.2 Range of variables studied

The experimental conditions under which the back-mixing tests were conducted are listed in table 5.1. It was decided to restrict the range of variables studied to dispersed phase flow rate, frequency of agitation and plate spacing. For all these combinations both mass transfer and non mass transfer runs were conducted.

Table 5.1 Range of variables studied for counter-current experiments (both mass transfer and non mass transfer cases)

u_c (cm/s)	u_d (cm/s)	A (cm)	f (Hz)	H (cm)
0.4	0.2-0.6	3.10	0-2	5.10 and 7.65

The experimental conditions were chosen for the following reasons:

a. Previous studies in the literature (Holmes et al. 1991; Baird and Rama Rao, 1991) and the present study on co-current flow discussed in chapter 4 indicated that the unstable density gradient effects were very small at high agitations. This was explained by Holmes et al. (1991) as being due to the reduction in the effective eddy size. The present study confirmed that the contribution by the buoyant energy dissipation became small under highly mechanically agitated conditions despite the large mixing length. Hence, to minimize the energy dissipation rate it was decided to set the upper limits on frequency to 2 Hz and the plate spacing to 7.65 cm. Both these decisions led to a decrease in the mechanical energy dissipation rate.

b. Trial experiments indicated that if the agitation rate was increased beyond 2 Hz, the alcohol concentrations in the Isopar M reached extremely small values and entrainment of the continuous phase in the exit organic phase increased thereby making it difficult to get reliable estimates of the raffinate composition.

c. The value of the continuous phase superficial velocity was fixed at an optimum value of 0.4 cm/s as a compromise between controlling the solvent flow rate, tracer solution flow rate and pump capacity.

d. Fixing u_c at 0.4 cm/s enables the comparison of co-current and counter-current non mass transfer back-mixing data. The stroke was also same as that used in the co-current flow experiments, i.e. 3.1 cm.

5.3 Back-mixing results in the absence of mass transfer

The steady state dye tracer injection technique was used to estimate the values of E_c as described in chapter 3. Sample results are illustrated in figure 5.5 along with the corresponding

mass transfer case. The Kolmogoroff isotropic turbulence model was used to explain the back-mixing results. Since there is no solute transfer and the dye solution was neutrally buoyant, the density gradient and the buoyant energy dissipation in the continuous phase are zero. However the dispersed phase and mechanical agitation contribute to the overall mixing. Hence the model equation (4.26) reduces to the following expressions.

$$l = l_m + [l^*_{do}(1+\frac{H}{D})\exp(-\frac{\epsilon_d}{\epsilon_o+\epsilon_m}) - l_m]\,(\frac{\epsilon_d}{\epsilon_t})^{n_2} \qquad (5.1)$$

$$= L_m + L_d$$

where L_m and L_d are respectively the limiting mixing length and the effective contribution of the dispersed phase to the effective mixing length respectively. Further discussion on this model is given in section 5.6. The basis of the model development was explained earlier in chapter 4. The parameters were re-evaluated by using GAMS and the experimental results and model predictions are summarized in table 5.2. The predictions of the model parameters are given in table 5.3. Also given in this table are the parameters estimated under co-current flow non mass transfer conditions for the Isopar M-water system.

5.4 Statistical analysis of the counter-current non mass transfer data

The statistical parameters defined in section 4.7.1 are given in table 5.4. Figure 5.1a gives the comparison of experimental and predicted back-mixing coefficients. In figure 5.1b the residuals are plotted. From figure 5.1a it can be seen that the back-mixing coefficients can be represented satisfactorily within $\pm$ 15%. The normal plot figure 5.1b shows that 11 out of the 12 residuals lying close to the straight line may be attributed to random error while there is an

Table 5.2 Experimental conditions, mixing length and back-mixing values for counter-current flow - experimental and predicted from equation (5.1) in the absence of mass transfer transfer.

u_d cm/s	f Hz	H cm	ϵ_d cm^2/s^3	ϵ_m cm^2/s^3	$l_{expt.}$ cm	$l_{pred.}$ cm	% error -	$E_{c,expt.}$ cm^2/s	$E_{c,pred.}$ cm^2/s	% err. -
ONLY DISPERSED PHASE FLOW										
0.188	0	5.10	39.072	0	2.545	2.550	-0.18	11.789	11.819	-0.24
0.407			84.813		1.398	1.323	5.38	6.870	6.381	7.11
0.402		7.65	83.792		1.642	1.679	-2.21	8.480	8.731	-2.96
0.612			127.491		0.873	0.897	-2.74	4.200	4.354	-3.67
DISPERSED PHASE FLOW + MECHANICAL AGITATION										
0.195	0.983	5.10	40.615	222.093	0.565	0.535	4.49	2.990	2.813	5.93
0.405			84.292		0.572	0.572	0.07	3.200	3.197	0.09
0.402	0.950	7.65	83.792	133.553	0.691	0.667	3.47	3.670	3.501	4.60
0.612			127.491		0.718	0.760	-5.82	4.110	4.432	-7.83
0.612	1.450	7.65	127.491	474.884	0.621	0.555	10.55	4.471	3.853	13.81
0.405	1.467		84.313	491.556	0.621	0.540	13.09	4.410	3.658	17.05
0.190	1.95	5.10	39.573	1732.522	0.410	0.533	-29.81	3.690	5.225	-41.60
0.410			85.334		0.498	0.533	-6.94	4.820	5.271	-9.36

Table 5.3 Counter-current and co-current back-mixing model parameters

Parameter	counter-current flow[1]	Co-current flow[2]
l_m	0.5326	0.3363
l_b	-	3.1990
n_1	-	0.4954
l_d	$l_{do}^* = 2.2281$	$l_{do}^* = 1.2306$
ϵ_{mo}	69.7285	68.5157
n_2	3.3175	1.13

Table 5.4 Statistical parameters based on E_c (equations 4.24, 4.27 and 4.28)

Equation no.	4.1
Number of parameters	4
Number of data points	12
Z_1	0.03761
Z_2	9.52%
s (cm²/s)	0.068

outlier (O_1) corresponding to u_d=0.19 cm/s, f=1.95 Hz, H=5.10 cm. Closer examination of the raw data indicated no abnormality while intense agitation would have ensured good radial mixing despite the low dispersed phase flow. So the outlier may be attributed to experimental error in the value of u_c or u_d (which contributes to the ϵ_d term).

---

[1] Equation (5.1)

[2] Equation (4.24)

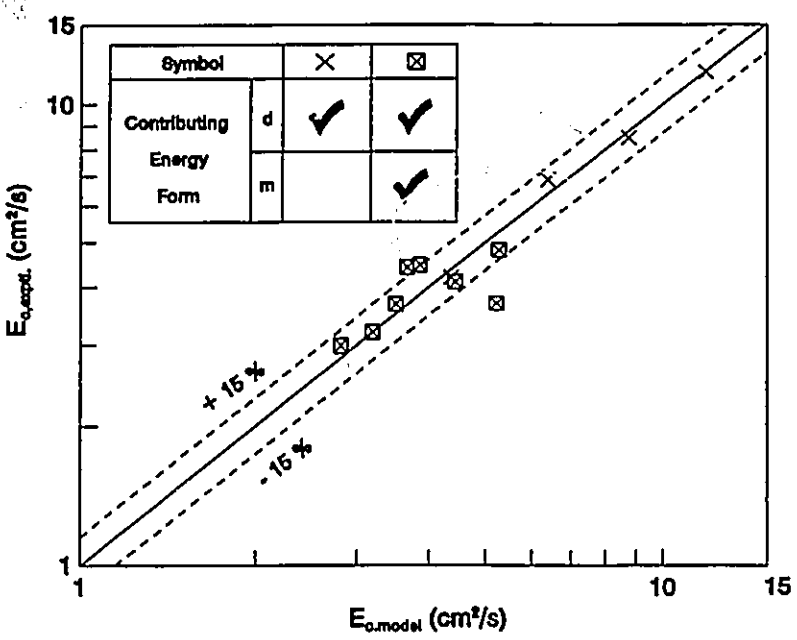

Figure 5.1 a Comparison of experimental with predicted back-mixing coefficient (non mass transfer case)

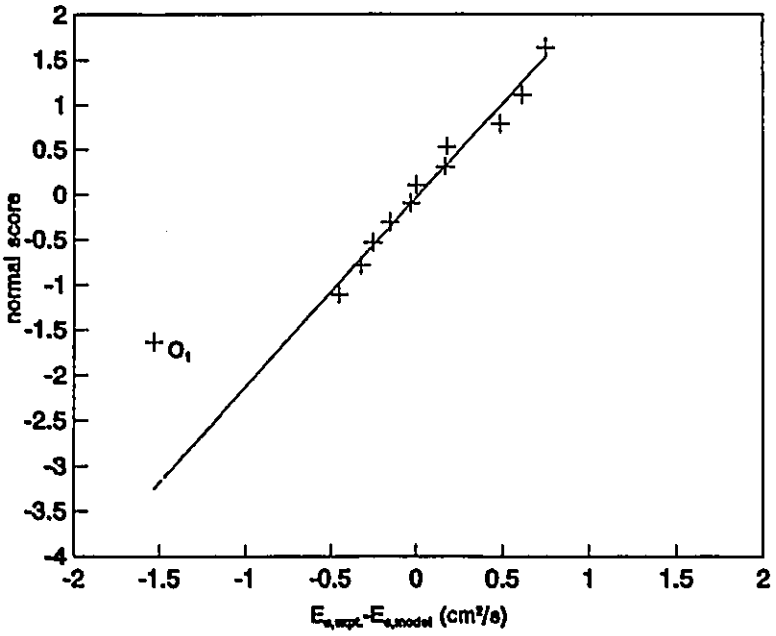

Figure. 5.1 b Normal plot of residuals from MINITAB

5.5 Comparison of co-current and counter-current non mass transfer back-mixing results

In figure 5.2 and table 5.5, the counter-current data is compared with the model in which the parameters were estimated for co-current conditions (table 5.3). The discrepancy between the back-mixing coefficient under counter-current ($E_{c,\uparrow\downarrow}$) and co-current flow ($E_{c,\uparrow\uparrow}$) conditions is very high by a constant factor under unagitated conditions. This is due to the significantly higher value of the counter-current dispersed phase mixing length ($l_{do,\uparrow\downarrow}$). As shown in special case of section 4.8.1, when the dispersed phase is the only source of energy dissipation, the effective mixing length equals l_d. Therefore, under identical operating conditions, the ratio of counter-current to co-current back-mixing coefficients can be expressed as follows:

$$\frac{E_{c,\uparrow\downarrow}}{E_{c,\uparrow\uparrow}} \sim \left(\frac{l_{do,\uparrow\downarrow}}{l_{do,\uparrow\uparrow}}\right)^{\frac{4}{3}} \tag{5.2}$$

The exponential factors in the model equation can also be cancelled out because ϵ_{mo} is almost equal for both cases (table 5.3). From the present model predictions, the ratio of the back-mixing coefficients is 2.207. This is also shown in figure 5.2, where the counter-current experimental back-mixing data at ϵ_m equal to zero, is 2.2 times that of the co-current model predictions. Based on the directions of flow it is possible to offer the following physical explanation.

Irrespective of the flow scheme and in the absence of coalescence effects the drop sizes are largest at zero agitation. If it can be assumed that the amount of the continuous phase transported by the drops is proportional to the drop volume, then the wake transport effect will be highest at zero agitation. In co-current flow, the wake transport effect does not contribute to back-mixing because the entrained continuous phase is transported in the *same* direction as the bulk continuous phase. However in counter-current mode, the wake transport results in transport

Table 5.5 Comparison of counter-current data with model using co-current parameters

H cm	ϵ_d cm²/s³	ϵ_m cm²/s³	$E_{c,expt.}$ cm²/s	$E_{c,pred.,\uparrow\downarrow}$ cm²/s	$E_{c,pred.\uparrow\uparrow}$ cm²/s
ONLY DISPERSED PHASE FLOW					
5.10	39.072	0	11.789	11.819	5.285
	84.813		6.870	6.381	2.810
7.65	83.792		8.480	8.731	3.846
	127.491		4.200	4.354	1.890
DISPERSED PHASE FLOW + MECHANICAL AGITATION					
5.10	40.615	222.093	2.990	2.813	2.925
	84.292		3.200	3.197	4.089
7.65	83.792	133.553	3.670	3.501	5.345
	127.491		4.110	4.432	5.692
7.65	127.491	474.884	4.471	3.853	5.249
	84.313	491.556	4.410	3.658	4.215
5.10	39.573	1732.522	3.690	5.225	3.152
	85.334		4.820	5.271	3.595

of the continuous phase in a direction opposite to the main flow thereby contributing to back-mixing. Hence the dispersed phase mixing length coefficient l_{do} includes the effect of wake transport and has a maximum effect at zero agitation. However it is not possible to incorporate the wake transport effect into the model in detail because of the lack of knowledge of parameters such as wake shedding height. In the presence of mechanical agitation the drop sizes decrease, drop population increases and hence the wake transport effects are curtailed (Nemecek and Prochazka, 1974). Steiner and Hartland (1983) in their review on spray columns also observe that at high dispersed phase hold-ups, the drops are very close to one another so that the wake

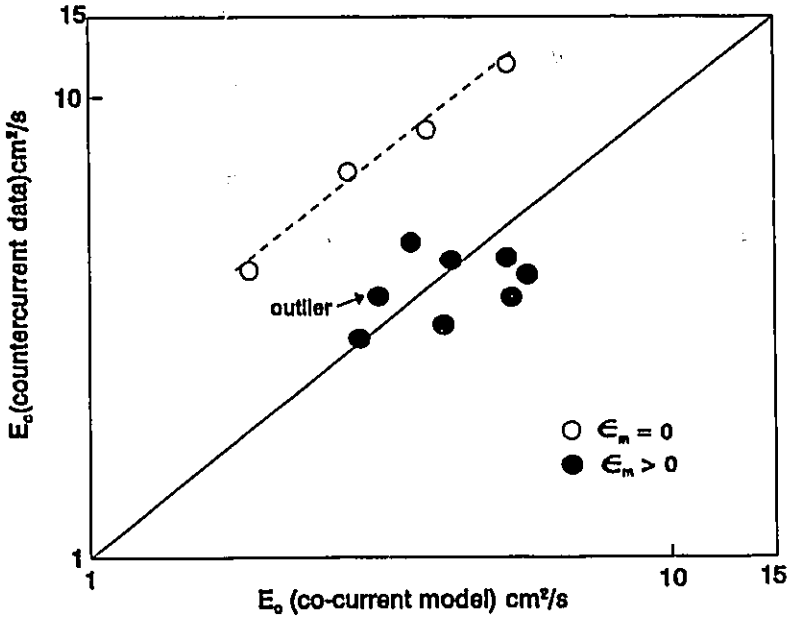

Figure 5.2 Comparison of counter-current data with model using co-current parameters (see table 5.5)

effect is minimized. Figure 5.2 shows that when the mechanical energy dissipation rate is greater than zero, the model with the co-current parameters is better able to predict the counter-current data, though the fit is not as good as the fit of the counter-current model predictions (table 5.5). Table 5.3 indicates that the exponent n_2 in counter-current flow is nearly three times greater than that for co-current flow conditions. This implies that the weight associated with the dispersed phase mixing length $(\epsilon_d/(\epsilon_d+\epsilon_m))^m$ becomes smaller more rapidly than the corresponding situation in co-current flow. This is consistent with the observation (Figure 5.2) that E_c is large when $\epsilon_m=0$ but that it reverts approximately to the co-current behaviour when ϵ_m is greater than 0. Figure 5.3 illustrates that when ϵ_m increases the effective mixing length tends towards the limiting mixing length l_m quite rapidly.

Further, it can be seen from Table 5.3 that the limiting value of the back-mixing

coefficient l_m in counter-current flow is significantly greater than that of co-current flow. The experimental data (table 5.2) also supports this observation. The effect of flow direction in influencing the limiting mixing length is difficult to interpret physically. Tentatively, it can be postulated that the drops clustered near the plate inhibit the transfer of momentum and hence kinetic energy from the large eddies to the smaller ones, thereby resulting in the higher limiting eddy size relative to the co-current flow situation. Figure 5.3 illustrates the variation of the effective mixing length with ϵ_d and ϵ_m under counter-current conditions.

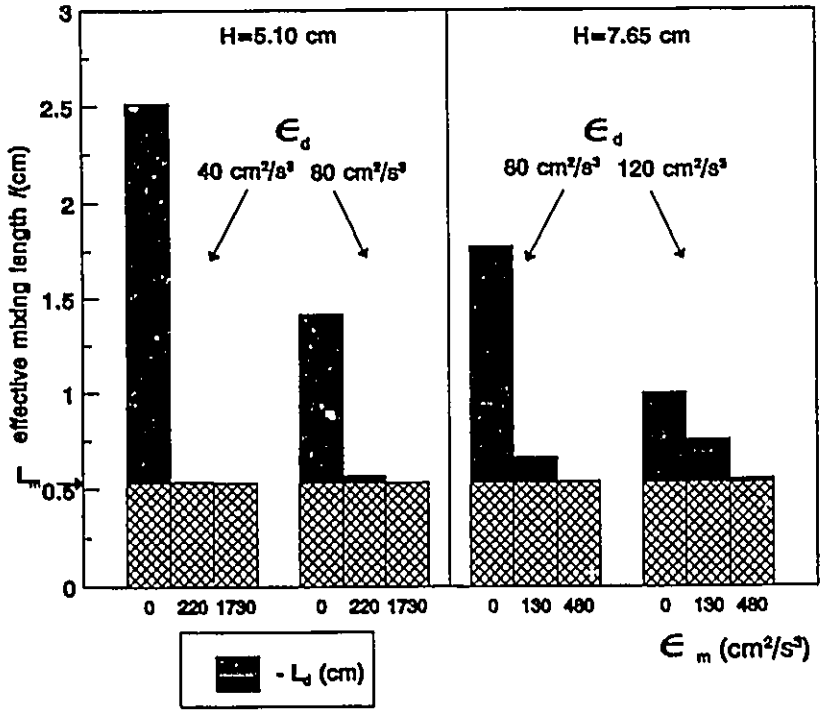

Figure 5.3 Variation of effective mixing length with ϵ_d and ϵ_m

5.6 Back-mixing measurements under mass transfer conditions

As described in chapter 3, the back-mixing coefficient under mass transfer conditions was evaluated by simultaneously using two independent methods. The mass transfer of *i*-propanol from the Isopar M (dispersed phase) to the aqueous (continuous) phase was studied. According to convention shown in figure 1.9, the Isopar M is termed as the X phase and water as the Y phase. The first method involved estimating E_c directly from the mass transfer concentration profile and the second involved the estimation of E_c from the steady state non transferring tracer technique. The tracer was injected at a very small flow rate so that it increased the continuous phase flow rate downstream of the injection point by only a very small amount. Typical results are discussed in detail.

5.6.1 Assumptions made in the dispersion model

In addition to the assumptions made in the development of the dispersion model as mentioned in section 1.18, plug flow was assumed for the dispersed phase for the following reasons:

1. The existence of back-mixing in the dispersed phase is questionable. Compared with that of the continuous phase, the dispersed phase hold-up is small especially under d→c mass transfer conditions. Further the drop sizes are also larger. Hence the entrainment of extremely small drops in the continuous phase, even if it occurs will cause only a very small effect on the mass transfer performance (Mißek, 1994). In addition to these, the measurement of back-mixing in the dispersed phase is unreliable. Pratt and Stevens (1992) observe that the introduction of tracers into the droplet dispersion is impossible. Further results from such tests can be confused with another phenomenon viz. forward mixing (Levenspiel and Fitzgerald, 1983).

2. Due to the variation in drop size so that larger drops ascend faster than the smaller ones, it is the forward mixing of the drops which is important (Rod and Mßek, 1971). However a precise application of this model requires information like drop velocity and mass transfer rate as functions of drop diameter. Knowledge is limited in the literature about these parameters especially for agitated drop swarms in actual columns (Steiner, 1994). The prediction methods incorporating forward mixing are still only in the process of development (Korchinsky, 1994).

5.6.2 Evaluation of number of transfer units :

Since plug flow was assumed for the dispersed phase, its transport equation reduces to the expression given in equation (5.3).

$$u_d \frac{dc_x}{dz} = k_{ox} a (c_x - c_x^*) \tag{5.3}$$

In the range of alcohol concentrations encountered during this study the equilibrium curve could be approximated by the linear relationship $c_x^* = 0.02\ c_y$. This indicates that at the inlet and exit, the equilibrium concentration of solute in the dispersed phase will be very small when compared to the feed and raffinate compositions. Hence, under these conditions the effect of back-mixing in the continuous phase can be neglected when determining the number of transfer units. Hence equation (5.3) can be integrated directly for the overall number of transfer units (N_{ox}) based on plug flow conditions. The analytical expression from Treybal (1981) was used:

$$N_{ox} = \frac{k_{ox} a L}{u_x} \tag{5.4}$$

$$= \frac{(x_1 - x_2)}{(x - x^*)_m} + \frac{1}{2}\ln\frac{(1-x_2)}{(1-x_1)} + \frac{1}{2}\ln\frac{x_2(r-1)+1}{x_1(r-1)+1} \qquad (5.5)$$

where $(x\text{-}x^*)_m$ is the logarithmic mean concentration driving force at the column exits (1 and 2) and r is the ratio of molecular weights of non solute (Isopar M) to solute (*i*-propanol). Following Treybal (1981), x in the above equation refers to the mass fraction of the solute in the dispersed phase. In the present calculations, the molecular weight of solute (*i*-propanol) was taken as 60 and Isopar M as 191 as indicated in section 3.3.2.1.

5.6.3 Presentation of experimental data for counter-current experiments

The experimental results based on concentration profiles of *i*-propanol for the mass transfer experiments are summarized in table 5.6. A few samples had to be discarded due to the entrainment of the dispersed phase in the continuous phase, the former being visible in form of a small film. Density and concentration data from such samples were neither recorded in table 5.6 nor used in the parameter estimation procedure. The E_c values were based on the data obtained from the clean samples. In the calculation of E_c values from the mass transfer profiles, the raffinate compositions (exit Isopar M stream) were estimated from the material balance equation. A detailed explanation is given later.

The dye tracer results obtained under both mass transfer and non mass transfer conditions are presented in tables 5.7 and 5.8. It may be noted that the tracer results obtained under non mass transfer conditions were modelled in terms of the Kolmogoroff isotropic turbulence theory as discussed in section 5.3.

The results of a typical mass transfer run (MTRH2) and non mass transfer run (NMTRH7) are illustrated in figures 5.4 to 5.6. It can be seen from figure 5.6 that the density

variation in the continuous phase due to extraction of i-propanol has been approximated by a linear relationship. This approximation enables the use of a constant E_c value for the entire column. It can also be noted that there is no density variation of the continuous phase in the non mass transfer case. The operating conditions for these runs are given in table 5.9.

Table 5.6 Results of back-mixing studies under mass transfer conditions

phase	distance (cm)	density (g/ml)	concentration (g/l)		model parameters
			experimental	predicted	
aqueous	0.0	0.9905	38.64	38.80	E_c= 11.46 cm²/s
	16.7	0.9913	34.35	35.03	
	25.7	0.9919	30.63	31.65	
	33.7	0.9924	27.77	28.17	
	41.7	0.9929	24.91	24.49	
	50.7	0.9936	20.91	20.28	
	68.2	0.9951	12.33	12.41	
organic	0.0		63.9		N_{ox}= 0.9035
	68.2		25.5		

Mass transfer data for expt. MTR1 (H=5.10 cm, u_d=0.4 cm/s, Af=0.0 cm/s)

phase	distance (cm)	density (g/cc)	concentration (g/l)		model parameters
			experimental	predicted	
aqueous	0.0	0.9921	29.49	29.28	E_c= 4.82 cm²/s
	16.7	-	-	-	
	25.7	0.9936	20.91	18.18	
	33.7	0.9951	12.33	14.12	
	41.7	0.9954	10.61	10.59	
	50.7	0.9960	7.18	7.27	
	68.2	0.9970	1.46	2.59	
organic	0.0		71.5		N_{ox}= 1.9214
	68.2		10.21 (inferred)		

Mass transfer data for expt. MTR2 (H=5.10 cm, u_d=0.19 cm/s, Af= 3.05 cm/s)

phase	distance (cm)	density (g/ml)	concentration (g/l)		model parameters
			experimental	predicted	
aqueous	0.0	0.9920	30.06	30.76	E_c= 3.64 cm²/s
	16.7	0.9927	26.05	22.15	
	25.7	0.9942	17.48	16.27	
	33.7	0.9957	8.90	11.88	
	41.7	0.9960	7.18	8.37	
	50.7	0.9965	4.32	5.33	
	68.2	0.9970	1.46	1.49	
organic	0.0		69.00		N_{ox}= 2.4031
	68.2		6.10 (inferred)		

Mass transfer data for expt. MTR3 (H=5.10 cm, u_d=0.19 cm/s, Af= 5.993 cm/s)

Table 5.6 continued..

phase	distance (cm)	density (g/ml)	concentration (g/l)		model parameters
			experimental	predicted	
aqueous	0.0	0.9924	27.77	27.38	E_c= 17.26 cm²/s
	16.7	0.9924	27.77	25.56	
	25.7	0.9927	26.05	23.55	
	33.7	0.9935	21.48	21.46	
	41.7	0.9937	20.33	19.21	
	50.7	0.9943	16.90	16.62	
	68.2	0.9956	9.47	11.72	
organic	0.0		78.00		N_{ox}= 1.3215
	68.2		20.28 (inferred)		

Mass transfer data for expt. MTR4 (H=5.10 cm, u_d=0.19 cm/s, Af=0.0 cm/s)

phase	distance (cm)	density (g/ml)	concentration (g/l)		model parameters
			experimental	predicted	
aqueous	0.0	0.9886	50.79	50.78	E_c= 4.14 cm²/s
	16.7	0.9892	46.07	40.17	
	25.7	0.9914	33.49	31.99	
	33.7	0.9932	23.19	25.20	
	41.7	0.9940	18.62	19.13	
	50.7	-	-	-	
	68.2	0.9963	5.47	4.07	
organic	0.0		69.0		N_{ox}= 1.3142
	68.2		18.23 (inferred)		

Mass transfer data for expt. MTR5 (H=5.10 cm, u_d=0.40 cm/s, Af= 3.0 cm/s)

phase	distance (cm)	density (g/ml)	concentration (g/l)		model parameters
			experimental	predicted	
aqueous	0.0	0.9874	58.40	57.90	E_c= 2.58 cm²/s
	16.7	-	-	-	
	25.7	0.9916	32.34	31.64	
	33.7	0.9930	24.624	23.79	
	41.7	0.9943	16.90	17.22	
	50.7	-	-	-	
	68.2	0.9967	3.18	2.57	
organic	0.0		68.00		N_{ox}= 1.6899
	68.2		12.38 (inferred)		

Mass transfer data for expt. MTR6 (H=5.10 cm, u_d=0.41 cm/s, Af= 5.993 cm/s)

Table 5.6 continued..

phase	distance (cm)	density (g/ml)	concentration (g/l)		model parameters
			experimental	predicted	
aqueous	0.0	0.9872	59.68	58.53	E_c= 8.71 cm²/s
	16.7	0.9888	48.36	52.59	
	25.7	0.9898	42.64	46.52	
	33.7	0.9904	39.21	40.47	
	41.7	0.9914	33.49	34.24	
	50.7	0.9922	28.91	27.31	
	68.2	0.9941	18.05	14.78	
organic	0.0		65.00		N_{ox}= 0.8853
	68.2		26.50 (inferred)		

Mass transfer data for expt. MTRH1 (H=7.65 cm, u_d=0.61 cm/s, Af=0.0 cm/s)

phase	distance (cm)	density (g/ml)	concentration (g/l)		model parameters
			experimental	predicted	
aqueous	0.0	0.9867	62.87	60.77	E_c= 8.18 cm²/s
	16.7	-	-	-	
	25.7	0.9886	50.79	47.82	
	33.7	0.9902	40.35	41.39	
	41.7	0.9914	33.49	34.80	
	50.7	-	-	-	
	68.2	0.9947	14.62	14.40	
organic	0.0		70.00		N_{ox}= 0.8567
	68.2		29.34 (inferred)		

Mass transfer data for expt. MTRH2 (H=7.65 cm, u_d=0.61 cm/s, Af= 3.05 cm/s)

phase	distance (cm)	density (g/ml)	concentration (g/l)		model parameters
			experimental	predicted	
aqueous	0.0	0.9844	77.71	76.52	E_c= 6.71 cm²/s
	16.7	-	-	-	
	25.7	0.9871	60.31	55.87	
	33.7	0.9894	44.93	46.64	
	41.7	0.9914	33.49	37.71	
	50.7	-	-	-	
	68.2	0.9945	15.76	13.08	
organic	0.0		70.00		N_{ox}= 1.2799
	68.2		19.25 (inferred)		

Mass transfer data for expt. MTRH3 (H=7.65 cm, u_d=0.60 cm/s, Af= 4.702 cm/s)

Table 5.6 continued..

phase	distance (cm)	density (g/ml)	concentration (g/l)		model parameters
			experimental	predicted	
aqueous	0.0	0.9890	47.21	47.11	E_c= 11.50 cm²/s
	16.7	-	-	-	
	25.7	0.9911	35.49	38.92	
	33.7	0.9912	34.63	34.63	
	41.7	0.9922	28.91	30.03	
	50.7	0.9928	25.48	24.84	
	68.2	0.9943	16.90	15.21	
organic	0.0		72.50		N_{ox}= 0.9786
	68.2		26.78 (inferred)		

Mass transfer data for expt. MTRH4 (H = 7.65 cm, u_d=0.41 cm/s, Af=0.0 cm/s)

phase	distance (cm)	density (g/ml)	concentration (g/l)		model parameters
			experimental	predicted	
aqueous	0.0	0.9885	51.42	50.84	E_c= 4.36 cm²/s
	16.7	0.9896	43.78	41.38	
	25.7	0.9914	33.49	33.61	
	33.7	0.9931	23.77	26.91	
	41.7	0.9935	21.48	20.79	
	50.7	-	-	-	
	68.2	0.9961	6.61	5.15	
organic	0.0		67.75		N_{ox}= 1.2715
	68.2		18.70 (inferred)		

Mass transfer data for expt. MTRH5 (H=7.65 cm, u_d=0.41 cm/s, Af= 4.6 cm/s)

phase	distance (cm)	density (g/ml)	concentration (g/l)		model parameters
			experimental	predicted	
aqueous	0.0	0.9877	56.49	55.97	E_c= 6.10 cm²/s
	16.7	-	-	-	
	25.7	0.9908	37.21	40.66	
	33.7	0.9912	34.63	33.88	
	41.7	0.9925	27.20	27.30	
	50.7	-	-		
	68.2	0.9953	11.18	8.98	
organic	0.0		80.00		N_{ox}= 1.1121
	68.2		25.81 (inferred)		

Mass transfer data for expt. MTRH6 (H=7.65 cm, u_d=0.41 cm/s, Af= 3.255 cm/s)

Table 5.7 Steady state back-mixing results with non transferring dye (H=5.10 cm)

Expt. code & operating conditions	distance (cm)	dye concn. (g/l)	Expt.code & operating conditions	distance (cm)	dye concn. (g/l)
MTR1 u_d = 0.40 cm/s Af = 0 cm/s E_c = 10.49 cm^2/s	0	1.7875	NMTR2 u_d = 0.41 cm/s Af = 0 cm/s E_c = 6.87 cm^2/s	0	1.75
	-9	1.455		-9	1.130
	-17	1.17		-17	0.945
	-25	-		-25	0.485
	-34	0.57		-34	0.24
	-51.5	0.263		-51.5	0.052
MTR2 u_d = 0.19 cm/s Af = 3.05 cm/s E_c = 4.02 cm^2/s	0	1.689	NMTR5 u_d = 0.20 cm/s Af = 3.05 cm/s E_c = 2.99 cm^2/s	0	2.315
	-9	0.832		-9	0.685
	-17	0.286		-17	0.18
	-25	0.21		-25	0.08
	-34	0.078		-34	0.029
	-51.5	0.01		-51.5	-
MTR3 u_d = 0.19 cm/s Af = 6.00 cm/s E_c = 3.46 cm^2/s	0	1.658	NMTR3 u_d = 0.19 cm/s Af = 6.05 cm/s E_c = 3.69 cm^2/s	0	1.96
	-9	0.878		-9	0.913
	-17	0.205		-17	0.22
	-25	0.135		-25	0.14
	-34	0.035		-34	0.03
	-51.5	-		-51.5	-
MTR4 u_d = 0.19 cm/s Af = 0.00 cm/s E_c = 11.36 cm^2/s	0	2.048	NMTR4 u_d = 0.19 cm/s Af = 0.0 cm/s E_c = 11.79 cm^2/s	0	2.907
	-9	1.56		-9	1.811
	-17	0.975		-17	-
	-25	0.86		-25	1.099
	-34	0.645		-34	0.895
	-51.5	0.335		-51.5	0.482
MTR5 u_d = 0.40 cm/s Af = 3.05 cm/s E_c = 4.50 cm^2/s	0	1.803	NMTR6 u_d = 0.40 cm/s Af = 3.05 cm/s E_c = 3.20 cm^2/s	0	1.900
	-9	0.845		-9	0.690
	-17	0.396		-17	-
	-25	0.236		-25	0.08
	-34	0.090		-34	0.032
	-51.5	0.020		-51.5	-
MTR6 u_d = 0.41 cm/s Af = 6.00 cm/s E_c = 5.15 cm^2/s	0	1.553	NMTR1 u_d = 0.41 cm/s Af = 6.045 cm/s E_c = 4.82 cm^2/s	0	2.013
	-9	0.825		-9	0.933
	-17	-		-17	0.311
	-25	0.245		-25	0.258
	-34	0.114		-34	0.052
	-51.5	-		-51.5	-

Table 5.8 Steady state back-mixing results with non transferring dye (H=7.65 cm)

Expt. code & operating conditions	distance (cm)	dye concn. (g/l)	Expt.code & operating conditions	distance (cm)	dye concn. (g/l)
MTRH1 u_d = 0.62 cm/s Af = 0.0 cm/s E_c = 9.52 cm^2/s	0	1.125	NMTRH5 u_d = 0.61 cm/s Af = 0.0 cm/s E_c = 4.20 cm^2/s	0	1.325
	-9	0.634		-9	0.603
	-17	0.58		-17	0.365
	-25	0.335		-25	0.165
	-34	0.248		-34	0.070
	-51.5	0.128		-51.5	0.01
MTRH2 u_d = 0.61 cm/s Af = 3.05 cm/s E_c = 7.34 cm^2/s	0	1.764	NMTRH7 u_d = 0.61 cm/s Af = 2.95 cm/s E_c = 4.11 cm^2/s	0	1.341
	-9	1.189		-9	0.648
	-17	0.67		-17	0.367
	-25	0.49		-25	0.125
	-34	0.3		-34	0.062
	-51.5	0.107		-51.5	0.01
MTRH3 u_d = 0.60 cm/s Af = 4.70 cm/s E_c = 7.21 cm^2/s	0	1.777	NMTRH6 u_d = 0.61 cm/s Af = 4.495 cm/s E_c = 4.47 cm^2/s	0	1.895
	-9	1.075		-9	1.035
	-17	0.603		-17	0.377
	-25	0.342		-25	0.196
	-34	0.241		-34	0.069
	-51.5	0.109		-51.5	0.023
MTRH4 u_d = 0.41 cm/s Af = 0.00 cm/s E_c = 11.92 cm^2/s	0	0.879	NMTRH1 u_d = 0.40 cm/s Af = 0.0 cm/s E_c = 8.48 cm^2/s	0	-
	-9	0.589		-9	1.021
	-17	0.536		-17	0.72
	-25	0.354		-25	0.474
	-34	0.276		-34	0.375
	-51.5	0.157		-51.5	0.135
MTRH5 u_d = 0.41 cm/s Af = 4.598 cm/s E_c = 5.13 cm^2/s	0	1.428	NMTRH3 u_d = 0.40 cm/s Af = 4.55 cm/s E_c = 4.41 cm^2/s	0	3.176
	-9	0.820		-9	1.815
	-17	0.335		-17	0.645
	-25	0.280		-25	0.500
	-34	0.114		-34	0.193
	-51.5	0.026		-51.5	0.030
MTRH6 u_d = 0.41 cm/s Af = 3.255 cm/s E_c = 6.49 cm^2/s	0	1.825	NMTRH2 u_d = 0.40 cm/s Af = 2.945 cm/s E_c = 3.67 cm^2/s	0	1.988
	-9	1.135		-9	0.788
	-17	1.025		-17	0.358
	-25	0.634		-25	0.105
	-34	0.368		-34	0.075
	-51.5	0.12		-51.5	-

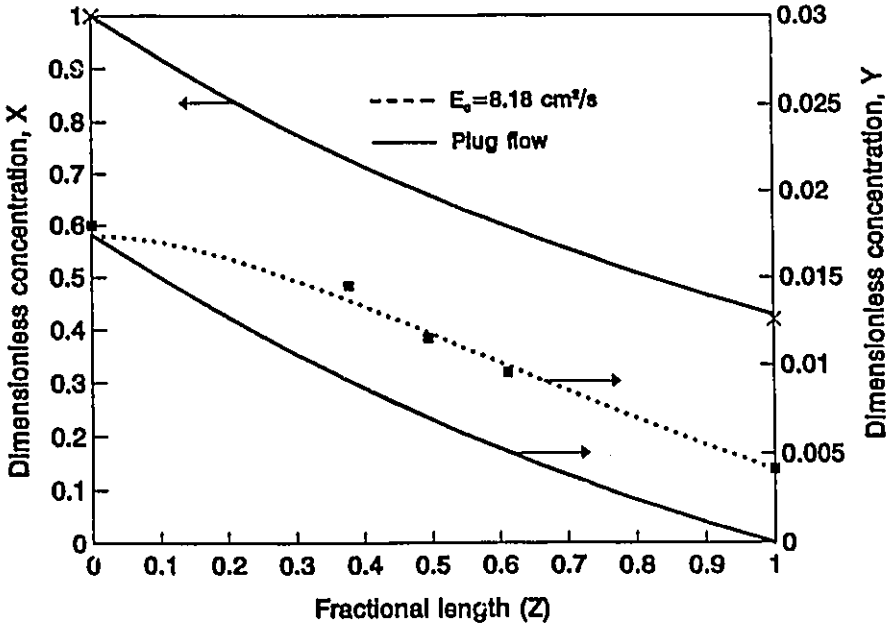

Figure 5.4 *i*-propanol concentration profile for run MTRH2

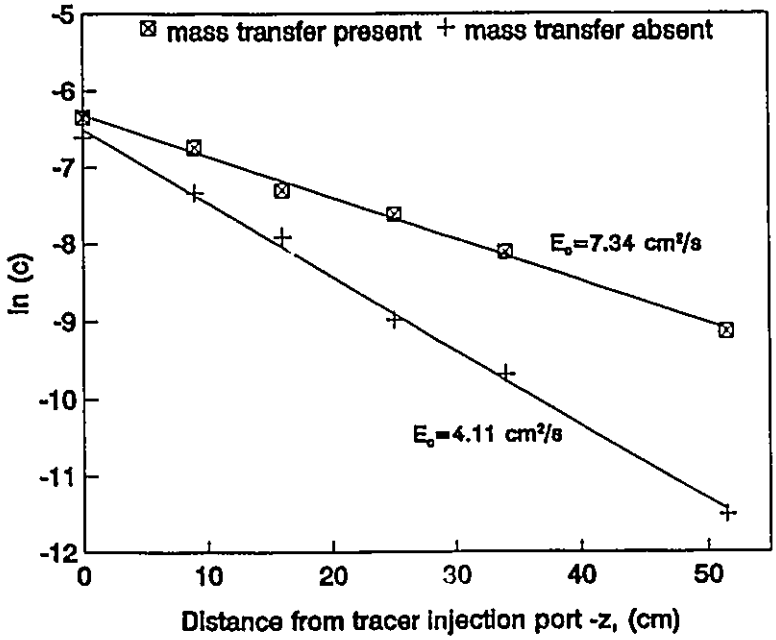

Figure 5.5 E_c from tracer methods for MTRH2 and NMTRH7 (concn. in g/cc)

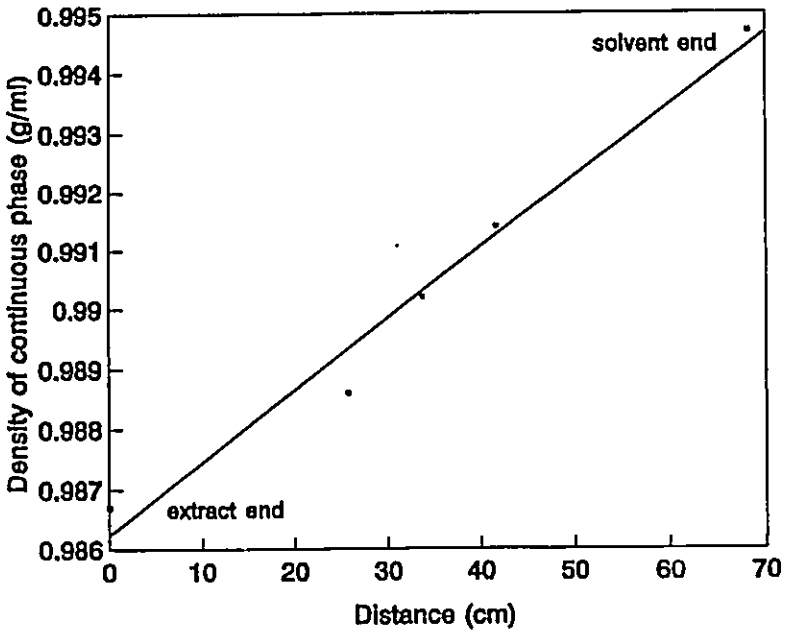

Figure 5.6 Variation of continuous phase density due to solute transfer (run MTRH2)

Table 5.9 Operating conditions and E_c values for typical runs (u_c= 0.40 cm/s, u_d = 0.61 cm/s, H=7.65 cm)

Run	Af (cm/s)	Measurement method	Observed E_c (cm^2/s)
MTRH2	3.05	Fitting solute concentration profile	8.18
		Steady state dye tracer method	7.34
NMTRH7	2.95	Steady state dye tracer method	4.11

5.6.4 Comparison of E_c values obtained from mass transfer profile and tracer methods

The E_c values obtained from two independent techniques implemented in each mass transfer run are given in table 5.10. As mentioned earlier, the first method involves the mass transfer profile and the second method involves the non transferring tracer profile.

It may be noted that two values of E_c from mass transfer profile method are tabulated,

Table 5.10 Summary of continuous phase back-mixing coefficients under mass transfer conditions

Expt.	u_d (cm/s)	Af (cm/s)	H (cm)	N_{ox}		E_c (cm^2/s)			% difference[3] on E_c
						mass transfer profile		tracer	
				measured[4]	material[5] balance	measured	material balance		
MTR1	0.40	0.0	5.1	0.9035	0.9035	11.46	11.46	10.49	9.25
MTR2	0.19	3.05		1.6063	1.9214	4.78	4.82	4.02	19.90
MTR3	0.19	5.99		2.6250	2.4031	3.82	3.64	3.46	5.20
MTR4	0.19	0.0		1.1755	1.3215	19.50	17.26	11.36	51.94
MTR5	0.40	3.0		1.4447	1.3143	3.86	4.14	4.50	-8.00
MTR6	0.41	5.99		1.7640	1.6899	2.58	2.57	5.15	-50.10
MTRH1	0.61	0.0	7.65	0.9924	0.8853	7.40	8.71	9.52	-8.51
MTRH2	0.61	3.05		0.9540	0.8567	7.13	8.18	7.34	11.44
MTRH3	0.60	4.70		1.4657	1.2800	6.16	6.71	7.21	-6.93
MTRH4	0.41	0.0		0.9346	0.9786	12.18	11.50	11.92	-3.52
MTRH5	0.41	4.6		1.4918	1.2715	3.82	4.36	5.13	-15.00
MTRH6	0.41	3.26		1.1638	1.1121	5.82	6.10	6.49	-6.01

[3] % error on E_c :- $(E_{c,mat.bal} - E_{c,tracer}) / E_{c,tracer} \times 100$

[4] measured - based on raffinate composition actually measured

[5] material balance - based on raffinate composition obtained through material balance

and two values of N_{ox} are also shown. The reason for this was due to the uncertainty in measuring the raffinate composition. There was entrainment of some very small droplets of the continuous phase in the dispersed phase layer which overflowed into the collecting tank. Since alcohol has high affinity for the continuous phase, it is believed that some alcohol in the entrained continuous phase droplets would significantly affect the measured dispersed phase raffinate composition. The material balance error in most experiments was due to lower than expected alcohol content in the dispersed phase. The error in the material balance ranged from 1-5%, the higher errors encountered at high agitation rates which led to more entrainment. The error in dispersed phase alcohol concentration will also lead to the error in the estimation of the number of transfer units, N_{ox}, which is a parameter in the expression for the concentration profiles (equations 1.25 to 1.32). Hence the accuracy in the optimization runs for the continuous phase back-mixing coefficient will be affected.

It was not possible to prevent the entrainment completely despite using coalescence meshes near the interface. Therefore it was decided to *infer* the raffinate composition from the alcohol material balance since the remaining concentrations, viz. the continuous phase extract and solvent and the dispersed phase feed concentrations are known with reasonable accuracy. As mentioned in section 3.36, it was possible to estimate the continuous phase (extract) concentration within $\pm 1\%$ accuracy and the dispersed phase feed concentration with approximately $\pm 2\%$ accuracy. Hence the optimization procedure was repeated using N_{ox} values based on the raffinate compositions obtained from material balance. This led to the second columns of N_{ox} values and E_c values from mass transfer profiles.

It can be seen from table 5.10 that in most cases, the E_c values based on concentration profiles with material balance are closer to the tracer values than the E_c values based on actually

measured raffinate compositions. Also the data given in table 5.10 indicate that except for two runs (MTR6 and MTR4), there is a reasonable agreement between the tracer method and the mass transfer profile method. Significant discrepancy occurs at experimental conditions corresponding to zero agitation and low dispersed phase flow (MTR4) and high agitation and high dispersed phase flow (MTR6). Possible explanations for the discrepancies are offered below:

1. MTR4: In this experimental run, large drops formed by mass transfer induced coalescence moved preferentially along one side of the column leading to considerable radial non uniformity which in turn caused radial velocity and concentration gradients. This led to enhanced circulation in the continuous phase and the E_c values from both methods, though different, are rather high.

The deterioration in flow due to radial non uniformities will also contribute to poor mass transfer performance and hence reflected in the corresponding E_c value. It must be also noted that the E_c value (from the tracer method) for the corresponding non mass transfer case (NMTR4) is 11.79 cm^2/s which is close to that predicted by the tracer method under mass transfer conditions as well. This cannot be possible, especially under unagitated conditions when the coalescence effects are the strongest leading to a different drop hydrodynamics in the column. Further under radially non uniform conditions, the tracer method indicates back-flow and not back-mixing. From a conservative view point, the higher value of E_c based on the mass transfer profile seems to be preferable.

2. MTR6 At high agitations and high dispersed phase flow rates the E_c value from the mass transfer profile method was significantly lower than that obtained by the tracer method. This was not a random occurrence for reasons given below.

Preliminary experiments had indicated that the dispersion model predicted very low values of E_c under conditions of (1) high column length (2) high dispersed phase flow rates accompanied

by intense agitation. In the mass transfer tests, the effective column length had to be reduced from 103.0 cm to 68.2 cm. The smaller length proved to be sufficient due to the high affinity of the solute to the solvent. The conditions of high dispersed phase flow rate and high mechanical agitation lead to high dispersed phase hold-up and also axial variations in hold-up. For instance, there will be a local region of large drops near the distributor which are rich in solute and coalescing rapidly. This will be a low hold-up region and due to large drops, the mass transfer coefficient will be high but interfacial area will be low. However the driving force for mass transfer will be high. Proceeding axially up the column the drops are gradually depleted of the solute, and are being increasingly reduced in size by mechanical agitation. k_{ox} is small and interfacial area is high. However the driving force for mass transfer is low due to low dispersed phase concentration in the drops and the increase in interfacial area is not of much consequence. This corresponds to a region where the hold-up will be higher due to the presence of small drops. The N_{ox} value based on the inlet and exit organic phase compositions will not be an accurate reflection of the changing hydrodynamic situation in the column. The steady state non transferring dye tracer technique does not make use of the N_{ox} parameter to estimate the back-mixing coefficient in the column.

Under high agitation and high dispersed phase flow rates, it is therefore concluded that the results based on the tracer methods involving the non transferring dye are more reliable.

5.7 Application of Kolmogoroff's isotropic turbulence model under mass transfer conditions

It was shown in chapter 4 that the back-mixing coefficient E_c, was related to the density gradient from dimensional analysis according to

$$E_c = l_b^2 \left(\frac{g}{\rho_c}\frac{d\rho}{dz}\right)^{\frac{1}{2}} \tag{4.2}$$

The above equation could be modified to a form given by the Kolmogoroff isotropic turbulence model using equation (1.40).

$$E_c = l_b^{\frac{4}{3}} \epsilon_b^{\frac{1}{3}} = l_b^{\frac{4}{3}} \left(\frac{u_c g \Delta\rho}{\rho_c}\right)^{\frac{4}{3}} \tag{4.5}$$

However under mass transfer conditions, equation (1.40) is not applicable due to the presence of the mass transfer flux term. Hence equation (4.5) does not follow directly from equation (4.2) under mass transfer conditions. However it will be very difficult to get a tractable analytical expression for ϵ_b from the mass transfer dispersion model (equation 1.1) which involves a second order differential equation. Even if an expression could be found, it will not be in the form suitable for the application of Kolmogoroff isotropic turbulence approach. Hence as a first approximation it was decided to use the expression given by equation (4.5) for the buoyant energy dissipation ϵ_b. This approximation is based on the assumption that the actual buoyant energy dissipation in the column under mass transfer conditions will be in the same order of magnitude as given by the relation $\epsilon_b \simeq (u_c\ g\ \Delta\rho/\rho_c)$. The continuous phase density profiles, similar to figure 5.6 were fitted by a linear relationship and the density gradient in the contactor was hence determined. The density gradient, energy dissipation terms and the estimated mixing length are given in table 5.11. The dispersed phase and mechanical energy dissipation terms were obtained as usual from equations (4.10) and (4.19) respectively, while the experimental mixing lengths were determined from equation (4.22). The estimates of E_c from the tracer method was used for all cases except for the run MTR4 in which the mass transfer estimate was

used.

These data points were added to the non mass transfer data (neutrally buoyant conditions, table 5.1) and the parameters for the Kolmogoroff model for mixing length (equation 4.26) were determined. The parameter estimation procedure proved to be highly unstable with multiple solutions at different initial guesses. When the results of the best possible fit corresponding to

Table 5.11 Energy dissipation terms and experimental mixing length (mass transfer conditions)

Expt.	$d\rho/dz \times 10^5$ (g/cm^4)	ϵ_b (cm^2/s^3)	ϵ_d (cm^2/s^3)	ϵ_m (cm^2/s^3)	$E_c^{(6)}$ (cm^2/s)	l_{expt} (cm)
MTR1	6.734	1.7911	81.819	0.0	10.49	1.9276
MTR2	7.453	1.9777	39.2291	222.117	4.02	0.7048
MTR3	8.220	2.1810	40.0554	1688.38	3.46	0.3933
MTR4	4.941	1.3129	39.0279	0.0	17.26	3.360
MTR5	12.345	3.2848	81.690	211.153	4.50	0.7448
MTR6	13.786	3.6664	84.872	1688.38	5.15	0.5265
MTRH1	10.092	2.6894	124.322	0.0	9.52	1.6144
MTRH2	12.043	3.2101	122.950	148.078	7.34	1.0958
MTRH3	15.441	4.1198	122.250	543.617	7.21	0.8648
MTRH4	7.695	2.0481	84.602	0.0	11.92	2.1026
MTRH5	11.764	3.1305	84.689	508.338	5.13	0.6898
MTRH6	11.116	2.9595	84.516	180.343	6.49	1.0051

[6] E_c values obtained from tracer method except for run MTR4 when the mass transfer method was used

the lowest objective function estimate (equation 4.24), was analyzed it was observed that the parameter estimates were physically unrealistic. For example, l_b was 12 cm which cannot be identified with the eddy size in the column. Further the exponent on the fractional buoyant energy dissipation term (n_1) was estimated as 10.124.

As will be illustrated in figure 5.9, the drop dynamics under mass transfer conditions were completely different from those under non mass transfer conditions and this effect is not accounted for in the Kolmogoroff model. In co-current flow conditions discussed in chapter 4, the drop dynamics in the presence and absence of the density gradient were similar since both circumstances were in the absence of mass transfer and no surface phenomena were noticeable.

Fitting the counter-current mass transfer data alone again led to similar multiple solutions depending on initial estimates and the limiting eddy size l_m was predicted to be zero. These observations suggest that the Kolmogoroff model cannot be applied when mass transfer induced surface effects are present. In other words, the description of the back-mixing coefficients simply in terms of the mixing length and energy dissipation terms alone is not sufficient when turbulence in the column is affected by coalescence and subsequent influence of large drops on back-mixing. This leads to the conclusion that the approximation of isotropic turbulence when surface active phenomena are present is not correct. It must be emphasized that the above conclusions are only indirect based on the inapplicability of the mixing length model to the mass transfer back-mixing results under coalescence conditions. Direct evidence either under mass transfer or non mass transfer conditions would require a detailed analysis of the turbulence spectrum for the presence of the inertial sub-range.

The results of the counter-current flow experiments under both mass transfer and non mass transfer conditions are illustrated in figures 5.7 and 5.8. The mixing length model based

on the non mass transfer data is also shown as a continuous line on each figure. The data and model parameters for the non mass transfer cases have been given in tables 5.2 and 5.3. As can be seen from the figures 5.7 and 5.8, the back-mixing coefficients are generally higher during mass transfer. The difference is especially evident at zero or moderate agitations, and low dispersed phase flows. This enhancement could be due to both the unstable density gradient and circulation effects caused by the larger drops and wake transport. Both these factors are important at zero and low agitation rates. As can be seen from figures 5.7 and 5.8, at high agitation rates the E_c values under mass transfer conditions are in most cases similar to those obtained under non mass transfer conditions. Again, at high agitations, the circulation effects are dampened by the dense dispersion and the density gradient effects are insignificant relative to the induced turbulence due to agitation as noted in chapter 4 for co-current flow. However, since the Kolmogoroff isotropic turbulence model was found to be inapplicable under the mass transfer conditions accompanied by coalescence effects, it is not possible to distinguish between contributions of unstable density gradient and interfacial phenomena.

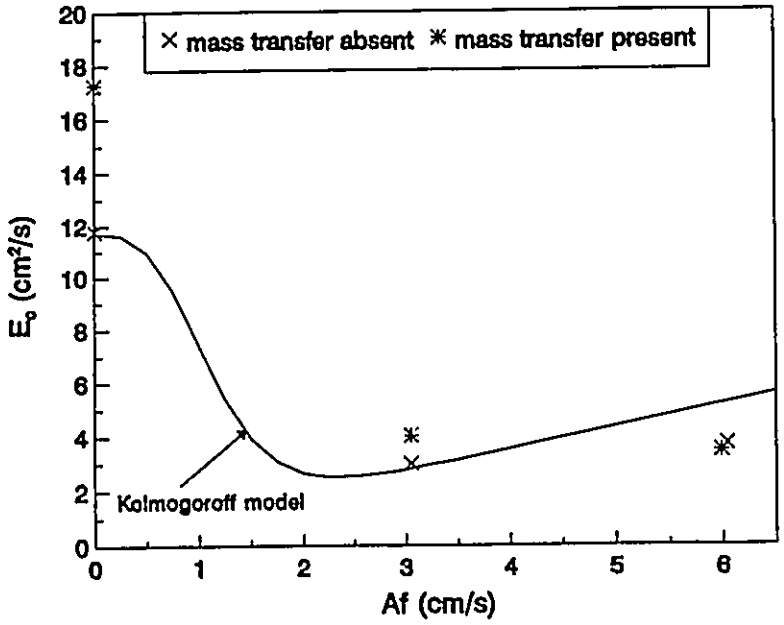

Figure 5.7a Variation of E_c with Af at u_d=0.19 cm/s, H=5.10 cm

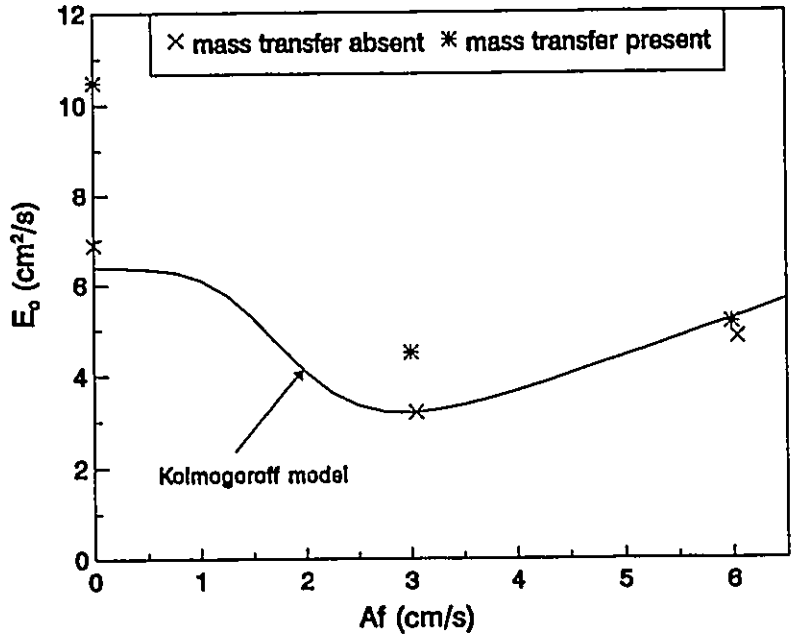

Figure 5.7b Variation of E_c with Af at u_d=0.40 cm/s, H=5.10 cm

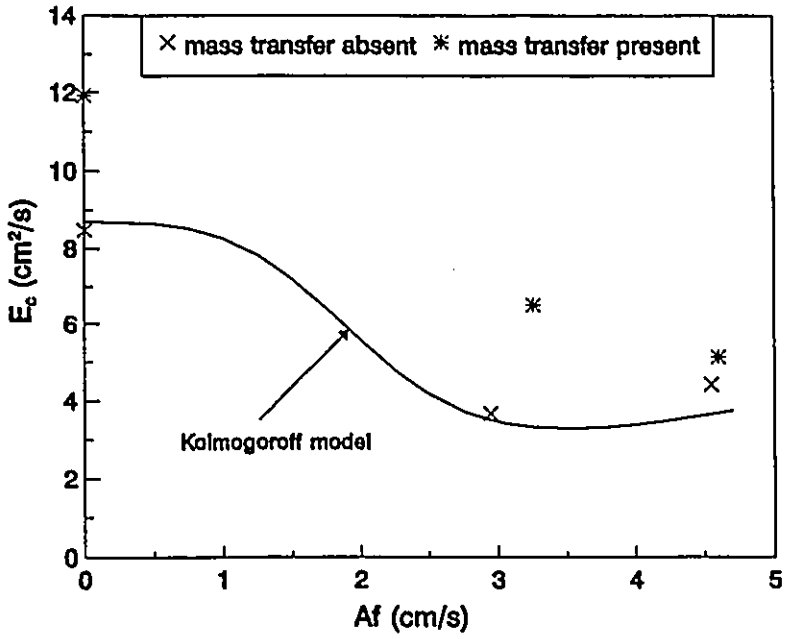

Figure 5.8a Variation of E_c with Af at u_d=0.40 cm/s, H=7.65 cm

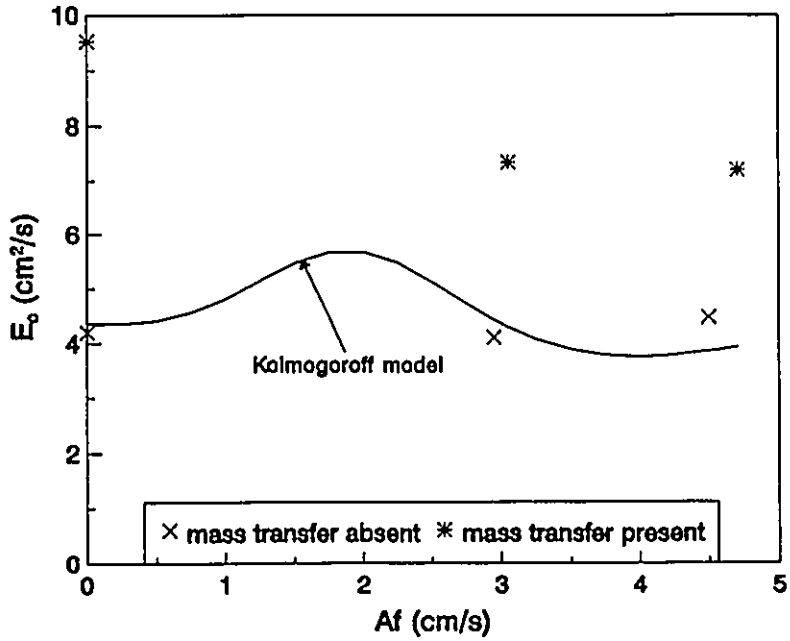

Figure 5.8b Variation of E_c with Af at u_d=0.61 cm/s, H=7.65 cm

5.8 Effect of mass transfer on drop dynamics

5.8.1 Unusual phenomena of the dispersed phase near the plates

A peculiar phenomenon concerning the drop behaviour was noticeable in the presence of mass transfer. The dispersed phase droplet moving past the plate occasionally assumed a 'mushroom' like shape. This effect was however very rare under non mass transfer conditions. This unusual drop formation is illustrated in figure 5.9 which represents the successive video frames at intervals of 1/30 seconds. The following observations could be made regarding the formation and subsequent behaviour of mushroom shaped drops.

1. These drops were observed to originate from the Karr plate under d→c mass transfer conditions. The location and frequency of the appearance of these drops with respect to the plate were random. The frequency increased with increasing dispersed phase flow.
2. These mushroom shaped drops usually penetrated a considerable distance into the continuous phase before rupture occurred at the tip connecting to the head. The disconnected portion eventually broke into two nearly spherical droplets.
3. The neck formation did not appear to have a well defined relation with the size of the drops approaching the plates.
4. Under non mass transfer conditions the mushroom shaped drops were rarely observed at high agitation rates. Moreover the necks were much shorter when compared to the mass transfer case.

A qualitative explanation can be proposed for the stability of the tail of the mushroom shaped drop. It is postulated that the necking effect of the drops is initiated when a fresh drop, rich in solute, coalesces with a drop which has been present under the plate for a relatively long period of time. This particular large drop delayed at the plate eventually moves upwards by

virtue of buoyancy with forces due to interfacial tension opposing the upward motion. These opposing forces coupled with the large diameter of the drop deforms it, leading to the creation of the elongated neck as shown in figure 5.10. As the neck gets elongated, the interface is stretched, increasing the interfacial area thereby promoting more solute transfer into the continuous phase. Thus, the faster depletion of the solute in this portion relative to other regions produces an interfacial tension gradient - locally higher interfacial tension at the narrower part of the neck (region B) and lower interfacial tension in the drop. This gradient results in a force which opposes the stretching force due to buoyancy. Hence the neck is stabilized for a longer duration than it would have been possible if the interfacial gradient had been either non existent or acting in the opposite direction thereby aiding the buoyancy forces. This explanation is similar to that proposed by Bainbridge and Sawistowski (1964) for the stabilization of liquid jets. In this study the authors were studying the factors affecting the plate efficiencies of distillation columns using systems with different surface tension properties. They observed that systems which exhibited a local increase in surface tension at the neck region of the jet caused by faster solute loss had more stable jets while those systems exhibiting decrease in surface tension with solute loss had accelerated jet break-up.

However it must be noted that these tails formed were of different shapes, sizes and durations. As mentioned earlier the location and frequency of the jet formation were random thereby making it difficult to identify definite trends. The drop velocities and sizes (determined by mechanical agitation and coalescence), mass transfer flux and dispersed phase velocity can be expected to have major influence in the drop hydrodynamics. It must also be noted that the necking phenomenon has not been mentioned previously in RPC literature on drop hydrodynamics.

(a)

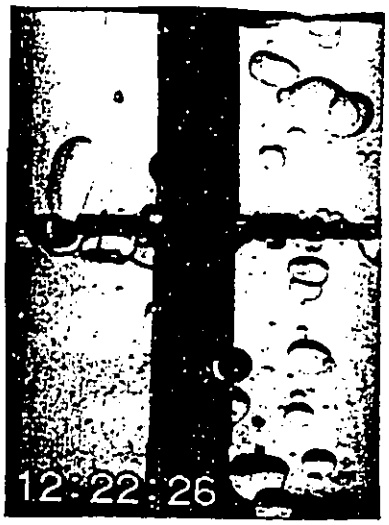

(b)

(c)

(d)

Figure 5.9 Successive video frames showing unusual drop formation under mass transfer conditions (u_d=0.19 cm/s, f=0.0 Hz, H=5.10 cm)

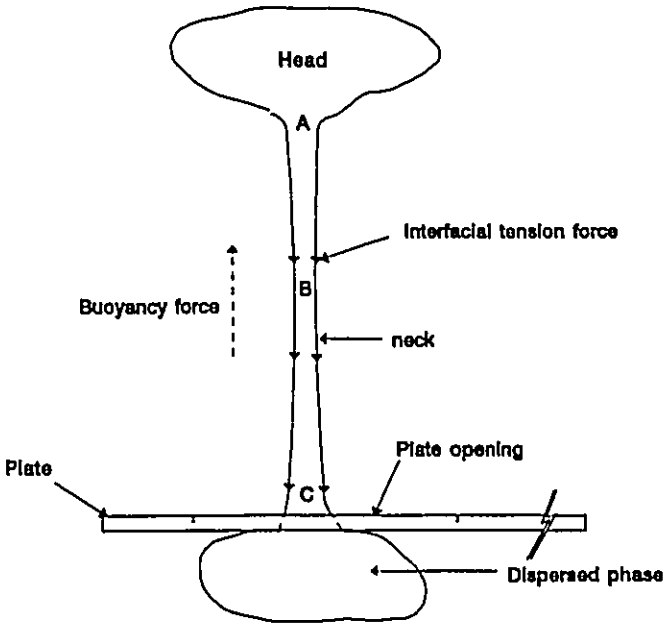

Figure 5.10 Influence of interfacial tension in the stability of mushroom shaped drop

5.8.2 Inter-drop coalescence

The drops under mass transfer conditions were larger than those observed under the same operating conditions but in the absence of solute transfer. This can be explained by the theory proposed by Groothius and Zuiderweig (1960) which was described in section 2.3.1. Essentially the solute transfer into the film between adjacent drops leads to an interfacial tension which is lower than that of the remaining regions surrounding the drops. An interfacial tension gradient is produced leading to a rapid film drainage promoting rapid coalescence.

5.8.3 Effect of mass transfer on drop size distribution

The drop dispersions obtained under mass transfer conditions were significantly different from those obtained under non mass transfer conditions. This is illustrated in figure 5.11 by comparing typical drop size distributions under non mass transfer and mass transfer conditions. The experimental conditions corresponding to these figures are given in table 5.12.

Table 5.12 Operating conditions and d_{32} for figure 5.11

H (cm)	u_d (cm/s)	#	non mass transfer		#	with mass transfer	
			Af (cm/s)	d_{32} (mm)		Af (cm/s)	d_{32} (mm)
5.10	0.4	a	0	3.41	b	0	5.87
		c	3.2	3.27	d	3.10	4.45
		e	6.15	2.07	f	6.20	3.31

Under zero agitation, mass transfer induced coalescence results in a large drop size range. The small drops observed under these conditions can be attributed to the breakage of large coalesced drops primarily by the buoyancy and to some extent by the dispersed phase energy dissipation effects. It is to be noted that coalescence leads to drops even as large as 11 mm.

When agitation is increased to a moderate value, only a small percentage of the drops are broken under non mass transfer conditions leading to a bi-nodal distribution. Under non mass transfer conditions, a large number of small drops tend to cluster under the plates during the upward plate motion with lower drop breakage, while during the downward motion, the drops are pumped upwards with more drop breakage. Under mass transfer conditions, there are relatively fewer larger drops fomed due to coalescence move freely and tend to be broken during both the upward and downward plate motions. Hence there is a sharp drop in the frequency of large drops.

Under intense mechanical agitation, turbulent eddies are primarily responsible for drop breakage, leading to a uni-modal distribution in both cases; but coalescence effects still persist under mass transfer conditions.

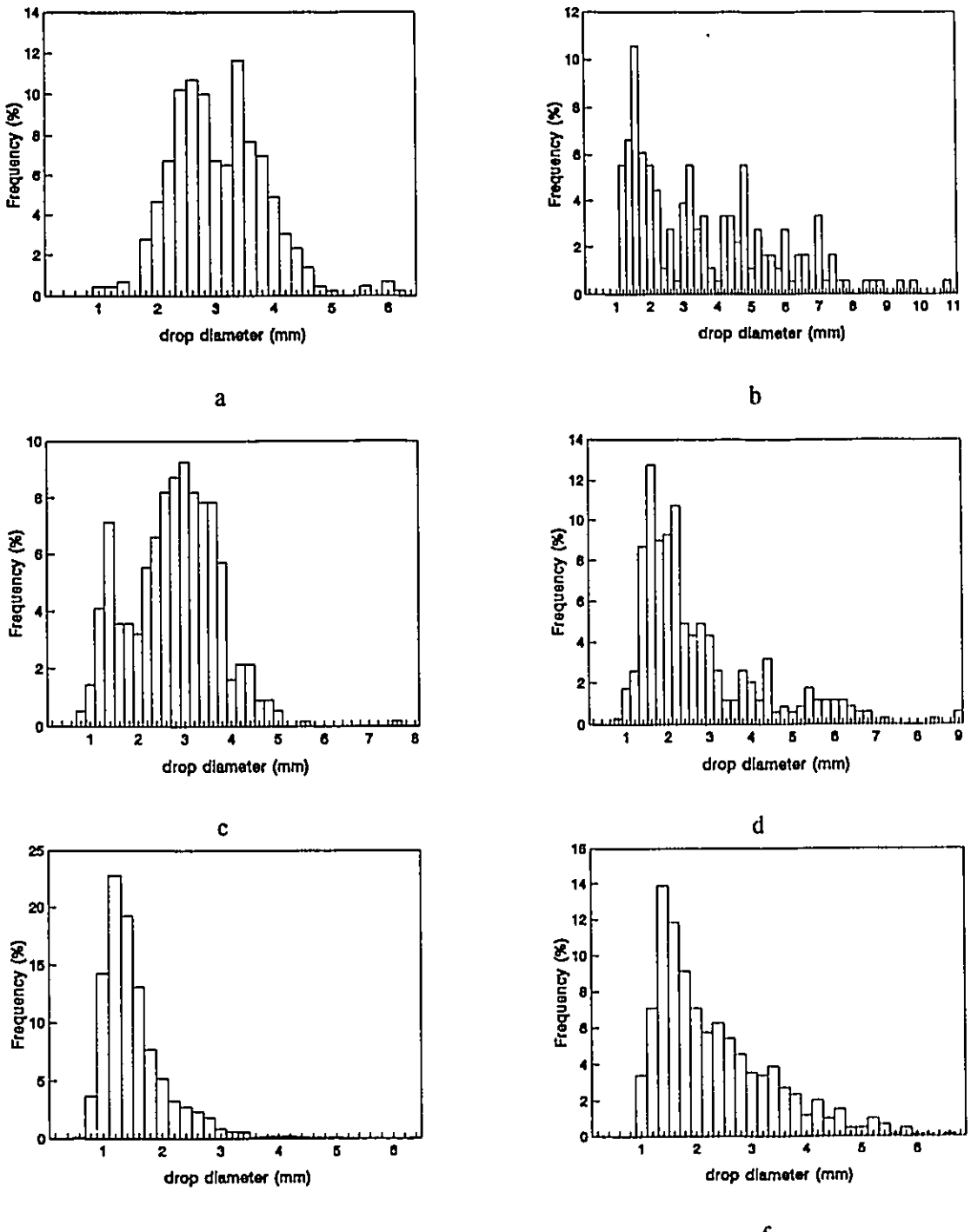

Figure 5.11 Drop size distributions under mass transfer and non mass transfer conditions (operating conditions are given in table 5.12)

5.9 Drop size measurement results and modelling of the Sauter mean diameter

The drop sizes were characterized by the Sauter mean diameter, d_{32} as defined by equation (2.4). The results are given in table 5.15.

The d_{32} values under non mass transfer conditions were modelled in terms of the Kolmogoroff approach (section 2.3.1). The energy dissipation rate due to both dispersed phase flow (ψ_1) and mechanical agitation (ψ_2) were included in the equation following the approach suggested by suggested by Calderbank et al. (1960) and implemented by Baird and Lane (1973).

$$d_{32} = C_f \frac{\gamma^{0.6}}{\rho_c^{0.2}(\psi_1+\psi_2)^{0.4}} \qquad (5.6)$$

The inclusion of both the effects seems more reasonable than just using the mechanical energy dissipation term because the experimental data indicate that the drop sizes are not independent of the dispersed phase flow rate (table 5.15). It can be seen from figure (5.12) that under non mass transfer agitated conditions, the model is reasonably valid. Under mass transfer conditions, the coalescence of drops due to interfacial effects associated with d→c solute transfer as discussed in section 5.8 resulted in drop sizes being larger than predicted by the model. Under mass transfer conditions the presence of *i*-propanol depresses the interfacial tension considerably. Typical equilibrium interfacial tension values in the presence of *i*-propanol are given in table 5.13.

It is not possible to apply these interfacial values to the mass transfer situation since the continuous and dispersed phases are not in mutual equilibrium. However the interfacial tension at any section in the column during mass transfer will be smaller than the value of 50 mN/m estimated for non mass transfer conditions. If the Kolmogoroff model is used to compare the

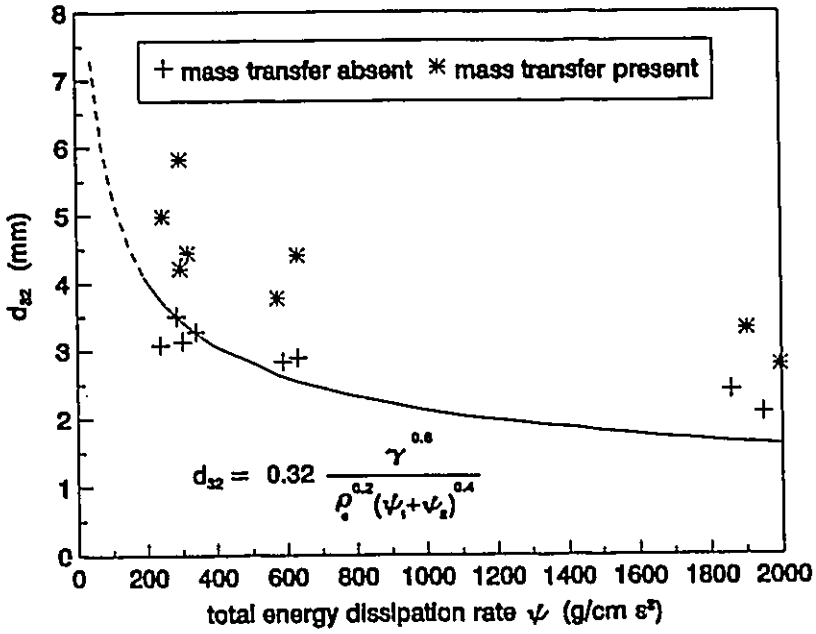

Figure 5.12 Application of Kolmogoroff model to the experimental d_{32} data

Table 5.13 Equilibrium interfacial tension in the presence of *i* propanol

Equilibrium alcohol concentration (g/L)		Interfacial tension (mN/m)
aqueous phase	organic phase[7]	
0	0	50.0
10.75	0.44	35.0
62.0	2.54	24.8

drop sizes under mass transfer and non mass transfer conditions then *smaller* drops would be predicted for the former case. However the experimental results indicate *larger* drop sizes,

[7] Estimated from the partition coefficient value of 0.041 (equation 3.2)

thereby confirming the importance of coalescence under mass transfer conditions.

Further the Kolmogoroff model expressed according to equation (5.6) does not sufficiently account for the drop size at zero agitation where buoyancy forces due to the density difference between the two phases are also important. Models have also been proposed in the literature to correlate the drop sizes over the entire range of agitations (Sovava 1990; Rincon et al. 1994). These models consider the processes determining drop sizes to be additive involving the sum of (i) the ratio of interfacial forces and buoyancy forces and (ii) turbulent breakup. These models also account for coalescence effects on the drop size by assuming it to be determined by the function $(1+C_h h)$ where C_h is an empirical constant. This assumption was based on the observations in agitated tanks and extraction columns (Coulaglou and Talvarides 1976; Haunold et al. 1990). Following a similar approach the model expressed by equation (5.7) was used to correlate the experimental data.

$$d_{32} = \frac{(1+C_h\, h)}{\left[\dfrac{1}{C_{b'}\left(\dfrac{\gamma}{\Delta\rho_{cd} g}\right)^{0.5}} + \dfrac{1}{C_t\left(\dfrac{\gamma}{\rho_c}\right)^{0.6}(\epsilon_d+\epsilon_m)^{-0.4}}\right]} \qquad (5.7)$$

The ratio of the buoyancy to interfacial tension forces are important at zero and moderate agitations while the turbulence created by energy dissipation, due to mechanical agitation and dispersed phase flow becomes important at higher values. The empirical constants obtained after regressing the model with the experimental data are tabulated below.

It can be noted from table 5.14 that the constant representing coalescence (C_h) under mass transfer conditions is much higher than the corresponding value under non mass transfer conditions.

Table 5.14 Model and statistical parameters for equation (5.7)

parameters	Non mass transfer	With mass transfer
C_h	0.2932	16.92
C_{bi}	1.1133	1.4247
C_t	0.7170	0.5015
s (mm)	0.29	0.39
AARD (%)	5.98	5.61

The model predictions are compared with the experimental data in table 5.15.

5.10 Results of hold-up measurements

The dispersed phase hold-up values, measured under both mass transfer and non mass transfer conditions are given in table 5.16 and table 5.17. The variation of hold-up with agitation at plate spacings 5.10 cm and 7.65 cm are given in figures 5.13 a and 5.13 b. It can be seen that under mass transfer conditions the hold-up values are lower than those under non mass transfer conditions. As shown in table 5.15, this can be attributed to the large drops formed by coalescence during mass transfer leading to lower dispersed phase residence time in the extractor.

Under non mass transfer conditions the drops tended to cluster under the plates while moderate agitation inhibited such clustering by pumping the drops through the holes. Hence hold-up decreased with moderate mechanical agitation. A preliminary model for hold-up data is attempted in the following section. The models developed by Baird and Shen (1985), Slater (1986) and Ueyama and Miyauchi (1979) were tried for the current experimental results. The results obtained are discussed in the following section.

Table 5.15 Comparison of model predictions (equation 5.7) with experimental data

condition	u_d (cm/s)	Af(cm/s)	H(cm)	d_{32} (mm)		% error
				exp.	pred.	
Mass transfer absent	0.19	0	5.1	4.34	4.19	+3.60
	0.19	3.15	5.1	3.50	3.25	+7.14
	0.19	6.15	5.1	2.41	2.23	+7.25
	0.40	0	5.1	3.41	3.91	-14.76
	0.40	3.2	5.1	3.27	3.18	+2.69
	0.40	6.2	5.1	2.07	2.24	-8.08
	0.40	0	7.65	3.87	3.91	-1.03
	0.40	3.1	7.65	3.08	3.36	-9.17
	0.40	4.6	7.65	2.83	2.88	-1.66
	0.60	0	7.65	4.24	3.76	11.35
	0.60	3.23	7.65	3.13	3.27	-4.46
	0.60	4.6	7.65	2.89	2.87	+0.54
Mass transfer present	0.19	0	5.1	5	5.44	-8.88
	0.19	3.2	5.1	4.21	3.91	7.18
	0.19	6.3	5.1	2.78	2.62	5.57
	0.40	0	5.1	5.87	5.95	-1.30
	0.40	3.1	5.1	4.45	4.88	-9.63
	0.40	6.15	5.1	3.31	3.31	-0.06
	0.40	0	7.65	6.65	5.87	11.71
	0.40	3.15	7.65	4.99	4.89	1.90
	0.40	4.55	7.65	3.77	4.04	-7.26
	0.6	0	7.65	6.37	6.60	-3.62
	0.6	3.2	7.65	5.83	5.49	5.80
	0.6	4.6	7.65	4.41	4.61	-4.35

5.10.1 Model due to Baird and Shen (1984)

As discussed in section 2.3.2.2, the above authors developed the following correlation for slip velocity (U_s) defined according to equation (2.20).

$$U_s = \frac{(1-h)d_{32}}{K^{*\frac{2}{3}}h^{\frac{1}{3}}}\left[\frac{g^2\Delta\rho_{cd}^2}{\rho_c\mu_c}\right]^{\frac{1}{3}} \qquad (2.29)$$

The single adjustable parameter K^* was recommended to have values of 15 and 30 for circulating and non circulating drops respectively. However the correlation was based mainly on kerosene water systems with interfacial tensions ranging from 22.7-27.7 mN/m. The Isopar water system had interfacial tension of 50 mN/m which is significantly above this range. The authors also observed that the correlation was not applicable to higher interfacial tension systems. This was confirmed by the results obtained in this study when the predicted slip velocities from both K^* values were much higher than those obtained experimentally. Consequently the predicted hold-up values were very low. Hence the above model could not be used in this work.

5.10.2 Model due to Slater (1985)

As discussed in section 2.3.2.2, Slater (1985) suggested the following model for slip velocity

$$U_s = \bar{u}_o(1-h)^m + bh^n \qquad (2.30)$$

with the second term applicable at high hold-ups (> 0.5) and m related to d_{32} as

$$m = 2.4 \times d_{32} \qquad (2.31)$$

with d_{32} in mm. Slater observed that the characteristic velocity u_o was comparable with the terminal velocity of the drops (U_T).

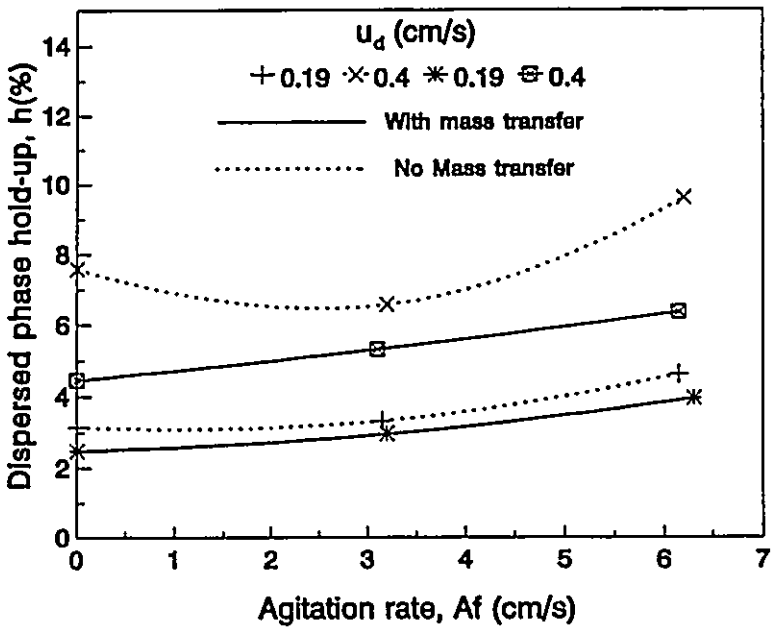

Figure 5.13 a Variation of hold-up with agitation rate at plate spacing (H) = 5.10 cm

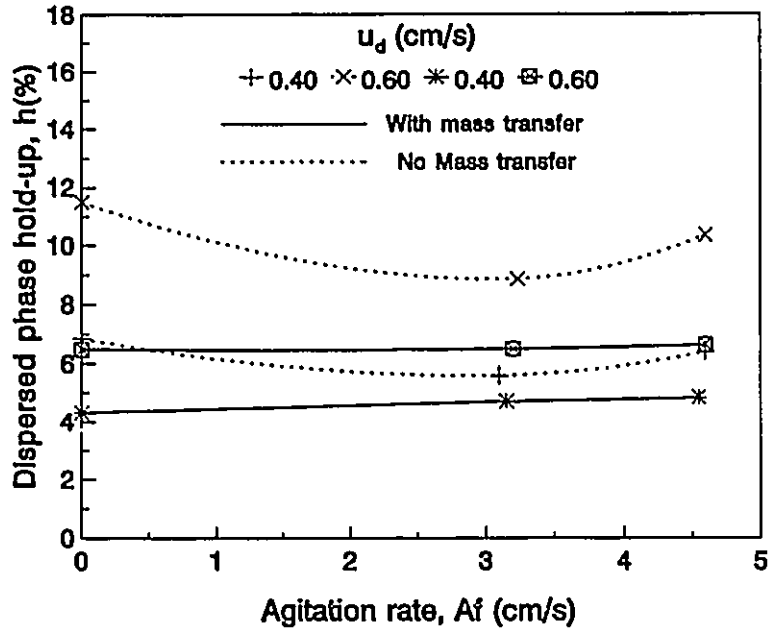

Figure 5.13 b Variation of hold-up with agitation rate at H=7.65 cm

U_T was calculated according to the correlation given by Grace et al. (1976) for contaminated systems as suggested by Kumar and Hartland (1988). These slip velocities predicted from this model were reasonably comparable with the experimentally obtained values. However when it was attempted to predict the hold-up

from the model as

$$\frac{u_c}{1-h}+\frac{u_d}{h} = u_t(1-h)^{2.4d} \tag{5.8}$$

it was found that no solution in the range $0 \leq h \leq 1$ was possible for some of the experimental conditions, especially those involving high dispersed phase flows. Hence it was decided not to use this model for correlating the present experimental data.

5.10.3 Model due to Ueyama and Miyauchi (1979)

Ueyama and Miyauchi (1979) developed an expression for slip velocity in bubble columns operating in the recirculation flow regime. The authors assumed that there was no interaction between the bubbles as they seemed to move independently. The average slip velocity was approximately constant and related to the superficial flows according to

$$\frac{u_d}{h}+\frac{u_c}{1-h}-\frac{1}{1-h}u_i = u_s = constant \tag{5.9}$$

where u_i was defined as the apparent interstitial velocity. Rama Rao et al. (1983) extended this concept to RPCs with gas-liquid and liquid-liquid flow by modifying the above equation to account for plate oscillation and assuming that the interstitial velocity was proportional to hold-up. The modified slip velocity equation had the following form.

$$\frac{u_d}{h}+\frac{(u_c+Af)}{1-h} = \frac{W_1 h}{1-h}+W_2 \qquad (5.10)$$

where W_1 and W_2 are adjustable parameters of the model. This equation could be re-expressed to give an explicit version for h as

$$h = \frac{u_d-u_c+W_2-Af-\sqrt{(u_c-u_d-W_2+Af)^2-4(W_2-W_1)u_d}}{2(W_2-W_1)} \qquad (5.11)$$

Only the second root of this quadratic equation could be used in the parameter estimation procedure. Using the first root led to computational difficulties and unrealistic estimates of W_1 and W_2. The parameters W_1 and W_2 were determined separately for mass transfer and non mass transfer conditions and are given in table 5.16. The model predictions for hold-up are given in table 5.17 and table 5.18.

Table 5.16 Estimated parameters for equation (5.10)

Experimental condition	W_1	W_2	AARD
Mass transfer absent	79.04	3.698	22.5 %
Mass transfer present	118.06	5.550	8.73 %

It can be seen from tables 5.17-5.18 that the model compares more favourably with the data under mass transfer conditions despite the interactions of the drops leading to coalescence. A reason for this is suggested as follows.

Coalescence is a relatively fast phenomenon and it is postulated that due to coalescence the drops are larger and the number of drops in a given volume of the dispersion is significantly lower. This factor accompanied by faster rise velocities of the drops will lead to lower residence time in the extractor and decrease the probability of mutual hindering of the drop velocities under

Table 5.17 Hold-up data and model predictions under non mass transfer conditions

u_d (cm/s)	Af (cm/s)	H (cm)	$h_{exp.} \times 100$	$h_{U\&M}$[8] $\times 100$	% error (U and M)
0.19	0.0	5.10	3.14	3.21	-2.41
0.19	3.15		3.30	4.80	-45.53
0.19	6.15		4.60	7.09	-54.13
0.4	0.0		7.60	5.23	31.13
0.4	3.2		6.55	6.96	-6.31
0.4	6.2		9.60	9.13	4.86
0.4	0.0	7.65	6.84	5.23	23.47
0.4	3.1		5.58	6.90	-23.66
0.4	4.6		6.4	7.91	-23.59
0.6	0.0		11.5	6.70	41.70
0.6	3.23		8.85	8.49	4.05
0.6	4.6		10.35	9.40	9.16

Table 5.18 Hold-up data and model predictions under mass transfer conditions

u_d (cm/s)	Af (cm/s)	H (cm)	$h_{exp.} \times 100$	$h_{U\&M} \times 100$	% error (U and M)
0.19	0.0	5.10	2.48	2.37	4.42
0.19	3.2		2.94	3.27	-11.12
0.19	6.2		3.93	4.56	-15.98
0.4	0.0		4.45	3.99	10.43
0.4	3.2		5.30	4.97	6.18
0.4	6.2		6.35	6.23	1.81
0.4	0.0	7.65	4.32	3.99	7.73
0.4	3.1		4.70	4.99	-6.18
0.4	4.6		4.83	5.53	-14.59
0.6	0.0		6.48	5.18	20.04
0.6	3.2		6.49	6.26	3.60
0.6	4.6		6.63	6.81	-2.70

[8] U&M - Ueyama and Miyauchi equation for mean slip velocity

mass transfer conditions.

Further, larger drops will also lead to more circulation in the column. In a similar vein it can be argued that under non mass transfer conditions, the number of drops in a given volume of the dispersion is higher, and there is increased chance for the drops to interfere with the rise velocities of one another.

5.11 Mass transfer coefficients

The volumetric mass transfer coefficient ($k_{ox}a$) was estimated using equation (5.4). The overall coefficient (k_{ox}) was derived by dividing $k_{ox}a$ by the interfacial area, which was obtained from equation (2.19). Due to the great affinity for the *i*- propanol towards the continuous phase, it is reasonable to assume that all the resistance to mass transfer resides in the organic phase. The estimated coefficient k_x was compared with the dispersed phase mass transfer model predictions in literature. The terminal velocities and drop diameters in the models were based on the Sauter mean diameter (d_{32}), the former being estimated from the correlation of Grace et al. (1976) for contaminated systems. The diffusion coefficient of *i*- propanol in Isopar M (D_{AB}), estimated from Wilke-Chang (1955) equation, was taken to be 0.82×10^{-5} cm^2/s. The models used are briefly discussed below.

5.11.1 Higbie's (1935) penetration model

The exposure time (θ^*) used in this model is deduced as the ratio of the Sauter mean diameter to the terminal velocity (U_T). The model is given as follows.

$$k_x = 2\sqrt{\frac{D_{AB}}{\pi\ \theta^*}}$$

or equivalently

$$Sh = 2\sqrt{\frac{Pe^*}{\pi}} \qquad (5.12)$$

where Sh is the Sherwood number defined here as $k_x d_{32}/D_{AB}$ and the drop Peclet number, Pe^* is defined as $U_T d_{32}/D_{AB}$.

5.11.2 Handlos and Baron (1957) model

This model was developed assuming fully developed toroidal internal circulation patterns inside the drops and has been applied to oscillating drops. A series solution was proposed and assuming that the first term in this series is dominant with zero continuous phase resistance, the solution becomes

$$k_x = 0.00375 \frac{U_t}{(1+\frac{\mu_d}{\mu_c})}$$

or since the drop diameter is taken as the Sauter mean value, the above expression can be equivalently expressed as

$$Sh = \frac{0.00375}{(1+\frac{\mu_d}{\mu_c})} Pe^* \qquad (5.13)$$

It can be noted that this model is independent of the diffusion coefficient, D_{AB}.

5.11.3 Kronig and Brink model (1950)

This model was developed for circulating drops when the continuous phase resistance was zero. The steady state solution for k_x could be approximated as follows

$$k_x = 17.9\frac{D_{AB}}{d_{32}}$$

or

$$Sh = 17.9 \qquad (5.14)$$

5.11.4 Rigid drop model

The models for rigid non circulating drops was expressed by Treybal (1963) as follows

$$k_x = \frac{2\pi^2}{3}\frac{D_{AB}}{d}$$

$$Sh = \frac{2\pi^2}{3} \qquad (5.15)$$

These models were used to compare the experimental data and the results are given in table 5.19. The model trends are compared with the experimental data in figure 5.14. It can be seen from figure 5.14 and table 5.19 that the mass transfer coefficient data are slightly below those indicated by the oscillating drop model of Handlos and Baron (1957) but follow the same trend with respect to Peclet number. Even at high agitations, the drop surface is mobile and rigid drop conditions are not approached. Table 5.20 compares the hold-up, Sauter mean drop size and interfacial areas obtained under mass transfer and non mass transfer conditions.

5.12 Summary and discussion:

In this chapter, the hydrodynamic and mass transfer results under counter-current flow conditions were presented with emphasis on axial mixing. Under mass transfer conditions, the steady state tracer back-mixing results were in reasonable agreement with the results obtained from the mass transfer concentration profiles except at very low dispersed phase flows when the

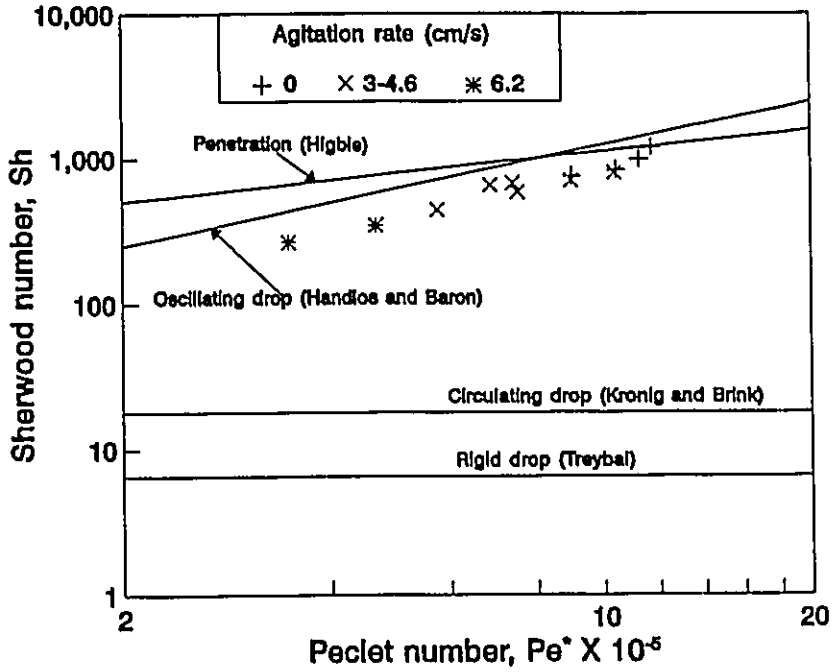

Figure 5.14 Comparison of experimental data with mass transfer coefficient models in literature

latter method is more reliable. Under conditions of high dispersed phase flow and high mechanical agitation, the tracer method is more reliable. The solute transfer from the dispersed phase to the continuous phase resulted in enhanced coalescence of the drops leading to a hydrodynamic situation significantly different from the non mass transfer case. Hence the enhancement in the back-mixing coefficient especially at zero and moderate agitations can be attributed to two different factors occurring in unison, viz. increased circulation created by large drops and the unstable density gradient. The Kolmogoroff model developed based on isotropic condition assumptions involving the mixing lengths and the specific energy dissipation could not be applied to the mass transfer case. Hence it was not possible to distinguish the circulation from the density gradient effects. However the Kolmogoroff model could be successfully applied to

Table 5.19 Experimental mass transfer coefficients and literature model predictions

u_d (cm/s)	Af (cm/s)	H (cm)	h × 100 -	d_{32} (mm)	U_T	k_{ox} (μm/s)		
						exp.	Higbie[9]	H&B[10]
0.19	0	5.1	2.48	5.00	14.80	123.61	175.81	185.03
0.4	0	5.1	4.45	5.87	14.61	116.56	161.14	182.58
0.4	0	7.65	4.32	6.65	14.45	147.34	150.56	180.60
0.6	0	7.65	6.48	6.37	14.50	127.55	154.22	181.30
0.19	3.2	5.1	2.94	4.21	13.40	127.84	182.28	167.60
0.4	3.1	5.1	5.30	4.45	13.89	107.92	180.26	173.19
0.4	3.2	7.65	4.70	4.99	14.81	115.33	176.07	185.06
0.6	3.2	7.65	6.49	5.83	14.62	112.75	161.86	182.7
0.4	4.6	7.65	4.83	3.77	12.53	96.96	186.32	156.61
0.6	4.6	7.65	6.63	4.41	13.78	124.92	180.58	172.29
0.4	6.2	5.1	6.35	3.31	11.55	86.16	190.85	144.43
0.19	6.3	5.1	3.93	2.78	10.29	78.85	196.65	128.58

[9] Higbie's (1935) penetration model

[10] Handlos and Baron (1957) oscillating drop model

the counter-current back-mixing data under non mass transfer conditions. When compared with the co-current flow situation, the back-mixing values for both cases were comparable under agitated conditions. Under unagitated conditions the counter-current back-mixing values were higher due to the additional contribution of the wakes which became significant under these conditions.

The hold-up data were modelled using the approach proposed by Ueyama and Miyauchi (1979) and extended to RPCs by Rama Rao et al. (1983). The Sauter mean diameters were treated using a unified model which incorporated the effects of buoyancy, interfacial tension and mechanical agitation. The model parameter estimates under mass transfer conditions differed from those of non mass transfer conditions for both drop size and hold-up predictions.

The mass transfer coefficients based on the dispersed phase were close to those expected for oscillating drops (Handlos and Baron, 1957). Even under well agitated conditions, the drops did not approach rigid drop behaviour thereby indicating large size and surface mobility.

In this work, all the experimental data were treated in terms of semi-empirical models having general applicability. Due to the limited number of data on a single system purely empirical correlations were avoided.

Table 5.20 Comparison of hold-up, drop size and interfacial area at mass transfer and non mass transfer conditions

u_d (cm/s)	Af (cm/s)	H (cm)	Hold-up		Drop size (mm)		Interfacial area (cm^2/cm^3)	
			no mass transfer	with mass transfer	no mass transfer	with mass transfer	no mass transfer	with mass transfer
0.19	0	5.1	3.14	2.48	4.34	5.00	0.434	0.298
0.19	3.2	5.1	3.30	2.94	3.5	4.21	0.566	0.419
0.19	6.2	5.1	4.6	3.93	2.41	2.78	1.146	0.849
0.4	0	5.1	7.6	4.45	3.41	5.87	1.337	0.455
0.4	3.2	5.1	6.55	5.3	3.27	4.45	1.201	0.714
0.4	6.2	5.1	9.6	6.35	2.07	3.31	2.777	1.150
0.4	0	7.65	6.84	4.32	3.87	6.65	1.062	0.390
0.4	3.1	7.65	5.58	4.70	3.08	4.99	1.086	0.566
0.4	4.6	7.65	6.4	4.83	2.83	3.77	1.357	0.769
0.6	0	7.65	11.5	6.48	4.24	6.37	1.627	0.611
0.6	3.2	7.65	8.85	6.49	3.13	5.83	1.695	0.669
0.6	4.6	7.65	10.35	6.63	2.89	4.41	2.151	0.901

CHAPTER 6

CONTRIBUTIONS AND RECOMMENDATIONS

6.1 Contributions to basic knowledge

In this thesis, back-mixing in the continuous phase was studied in the presence of an unstable density gradient. The main contributions can be listed as follows:

1. Results from this thesis show that the buoyancy effects created due to unstable density gradients in the continuous phase are important under two phase flow conditions as well as single phase conditions. The buoyancy effects lead to a significant enhancement in the back-mixing which persists even under conditions of moderate agitation.
2. Previous work on axial mixing in the RPCs resulted in either complex models which require detailed experimental verification (eg. the two zone model due to Prochazka and co-workers 1970, 1974) or purely empirical correlations which were very specific to the column under study (e.g. Bensalem, 1985). The present thesis, through the assumptions of Kolmogoroff isotropic turbulence theory, presents a compromise. It does not require special experimentation and the model parameters such as the mixing lengths expressed as a fraction of column diameter can be extended to other reciprocating plate columns in the same range of diameters. These mixing lengths, identified with the scale of the eddies generated due to three different sources of turbulence, may be expected to be of similar magnitude for columns in the same diameter range.
3. The complicated effects of the dispersed phase flow behaviour have been incorporated into the framework of Kolmogoroff isotropic turbulence model. This extends and improves the

earlier applications of the mixing length model in the literature (Baird and Rice 1975; Kawase and Tokunaga 1991). Earlier axial mixing models, including those based on the isotropic assumption, were developed for bubble and spray columns in which the operation is not complicated by mechanical agitation. In this work, a new attempt has been made to extend the Kolmogoroff approach to two phase mechanically agitated conditions using reciprocating plates. This model may be adopted to other mechanically agitated extraction columns as well. Table 6.1 summarizes the work done so far in the application of the isotropic turbulence approach to model axial mixing effects in extractors. The mixing length terms can be identified with the eddy sizes generated by different types of energy dissipation (buoyant, dispersed phase and mechanical). The parameters n_1 and n_2 are the exponents of the fractional energy dissipations attached as weights to the buoyancy and dispersed phase mixing length terms, and determining the degree of importance attached to their contributions to the overall mixing process. The strong effect of circulation created due to dispersed phase flow at large plate spacing has been identified. The model also enabled the identification of different regimes in which the relative importance of different effects on back-mixing could be compared. The buoyancy effect was important at zero and moderate agitation; the dispersed phase played an important role at zero agitation. At high agitations, both these effects had only a minor significance. The buoyancy effect, despite its small energy dissipation, led › significant enhancement in back-mixing due to the large eddy scale associated with it.

4. It was possible to compare the back-mixing in co-current and counter-current modes of operation. The back-mixing values for the two modes of operation were found to be considerably different at zero mechanical agitation. Values were higher for the

Table 6.1 Summary of axial mixing models using the isotropic turbulence approach

Investigators	Baird and Rice (1975)	Holmes et al. (1991)	Baird and Rama Rao (1991)	This work
Extraction apparatus	Bubble and spray columns	Karr type RPC	Karr type RPC	Karr type RPC
Forms of energy dissipation	dispersed phase	buoyancy	buoyancy + mechanical agitation	buoyancy + dispersed phase + mechanical agitation
Equation :	2.40	1.61	1.66	4.26
No. of mixing length parameters	1	1	2	3
No. of energy weighting exponents	0	0	1	2
Other parameters	0	0	0	1
Total adjustable parameters	1	1	3	6

counter-current case. This was attributed to the directional influence of wakes contributing to back-mixing in the counter-current the mode. With the onset of mechanical agitation the back-mixing values were comparable for co-current and counter-current modes.

5. When the unstable density gradient was induced in a d→c mass transfer process, its effect was masked by the presence of large drops caused by the coalescence effect. The enhancement in E_c values under mass transfer conditions relative to those obtained from neutrally buoyant non mass transfer conditions could then be due to the unstable density gradient as well as the contribution of large drops to circulation and wake transport, and there is no simple way of separating the contributions. The isotropic turbulence model was found to be inapplicable under these conditions. However, the isotropic turbulence approach is likely to be applicable when the interfacial coalescence effects are not present, as in a c→d mass transfer process.

In the present work, c→d mass transfer could not be applied due to the preference for alcohol to the continuous phase (water) and very small density difference between alcohol and Isopar M. So, even if Isopar M had been used as the continuous phase, its density change would have been extremely small.

6. Two independent methods were used to estimate back-mixing in the continuous phase during mass transfer. Studies of this nature are very scarce in the literature. The two methods gave results in reasonable agreement except under intensely agitated conditions. Under such conditions, since the mass transfer profile method grossly under-predicted the back-mixing coefficient, the steady state dye tracer method is more reliable. However, when radial non uniformity effects were present, the steady state method estimates only the back-flow which may inaccurately predict the deterioration in mass transfer performance. In previous work, the data obtained from tracer tests under non mass transfer conditions have been applied to design RPCs (Hafez et al. 1980; Shen et al. 1985; Karr et al. 1987; Kannan et al. 1991; Harikrishnan et al. 1994). This is acceptable provided mass transfer induced phenomena like coalescence effects and, as discovered recently unstable density gradient effects are absent. If these effects are present and the column to be investigated is of the spray type or uses only moderate agitation (for an easy system) then tracer based correlations from non mass transfer conditions are worthless.

7. The study also indicated that back-mixing is the predominant cause of axial mixing in Karr columns. The steady state tracer method was found to be experimentally convenient, did not require special samplers as the tracer is non transferring and entrainment of the dispersed phase does not affect the readings. On the other hand the mass transfer method is cumbersome, requires slow sampling, special sampling arrangements and the predicted

coefficients are extremely sensitive to measurement errors which are very probable.

8. In this study, the plug flow assumption was made for the dispersed phase. Based on the reasonable agreement between the tracer and concentration profile based values of E_c it may be concluded that dispersed phase back-mixing if present, has very little interaction with the continuous phase back-mixing. However it must be noted that the dispersed phase flow has a considerable impact on continuous phase back-mixing especially at low flow rates and zero or moderate agitation.

6.2 Contributions to extraction technology

1. The role of unstable density gradient under two phase flow conditions has been investigated thoroughly for the first time even though it had been mentioned as an industrial occurrence by Cusack and Karr (1991) and Holmes et al. (1991).
2. If the effects of unstable density gradient are not accounted for, the performance of extractors handling systems in which these effects are present will be lower than expected. On the other hand, data obtained from tracers that inadvertently lead to unstable density gradients in the continuous phase will lead to an overestimate of axial dispersion and an unnecessarily conservative design.
3. As indicated in section 6.1, a 6 parameter model has been developed to predict E_c. In principle this model could be applied to RPCs of different diameters. The parameters will be different, for example, the buoyant and dispersed phase mixing lengths will increase with column diameter. Hence a limited number of experiments under properly chosen conditions could be designed in an industrial column in order to estimate the 6 parameters. This model could then be used in the optimization of the column operating conditions.

6.3 Recommendations based on the observations made in this thesis

1. The Kolmogoroff isotropic turbulence theory has proven to be useful in the quantitative understanding of the back-mixing effects in the RPC. In a future study, it will be extremely useful to make a detailed analysis of the turbulent energy spectrum in the RPC and determine the conditions under which the assumptions of isotropic turbulence theory are valid. Such a study should also analyze the extent of error associated with deviations from the isotropic turbulence assumptions. The model developed in this work was aimed as a compromise between the complex nature of turbulence and the need to account simply for its influence in engineering applications.
2. The first part of this thesis clearly indicated that buoyancy effects enhance the back-mixing even under two phase moderately agitated conditions. Hence it is recommended that future measurements on axial mixing should be performed preferably using a tracer dye that can be detected at the ppm level. Tracers involving ionic compounds or other substances which change the density of the continuous phase are not recommended for study. If used, they should be made neutrally buoyant before being introduced into the column and the measuring instrument must be accordingly re-calibrated.
3. This work has shown that unstable density gradient in the continuous phase will lead to increased axial mixing. Conversely, a stable density gradient, with density decreasing with height may be expected to reduce axial mixing. A general design recommendation would be to avoid the creation of the unstable density gradient in the continuous phase during mass transfer. The stable density gradient appears to have not been studied explicitly as a variable in earlier axial mixing work and such an investigation is recommended.
4. If the extraction column is operated under conditions of low or moderate agitation, special

precautions should be taken to ensure radial uniformity of the dispersion. Otherwise, deleterious circulation effects will lead to high back-mixing.

5. Due to the interfacial effects associated with solute transfer from dispersed to continuous phase, it was not possible to distinguish the effects of buoyancy from those due to large drops. In a future study it is recommended that the system should be so chosen that the c→d direction favours higher mass transfer and leads to a significant unstable density gradient in the continuous phase. This would eliminate the large drop effect. A concentrated solution is recommended to produce a significant effect and it will be necessary to modify the transport equations to accommodate rich systems.
6. The droplet behaviour during mass transfer for the system used in this study exhibited unusual features which have not been reported previously. Further work in this area can shed more light on this interfacial phenomenon.
7. The model developed in this study is not restricted to RPCs. Testing of this model with other types of extraction columns like RDCs, Kühni extraction columns etc is recommended. However this model is not applicable with compartmentalized extractors where the stage-wise back-flow model is more appropriate.
8. On a more general note, there is a great need for axial mixing data in large diameter columns and different systems to facilitate reliable scale-up equations. In any future studies on large diameter columns, full account should be taken of unstable density gradient effects.

LIST OF SYMBOLS

Note: The following symbol definitions were adopted throughout this thesis unless specifically indicated otherwise

A	stroke of oscillation - twice the amplitude, [m]
AARD	Average absolute relative deviation defined by equation (4.27), [-]
A_{cs}	Area of cross section, [m^2]
A_i	coefficients (i= 1 to 4) in equation (1.15), [-]
a	interfacial area, equation (2.19), [m^2/m^3]
a_i	coefficients (i= 1 to 4) in equation (1.16)
a'	amplitude of oscillation, [m]
B	dimensionless distance based on column diameter, [-]
Bo^*	modified bond number given by $(\Delta\rho_{cd}d_d^2g)/\gamma$, [-]
C	dimensionless concentration, defined in equation (1.45)
C_{alc}	concentration of alcohol, [kg/m^3]
C_{bi}	coefficient for buoyancy interfacial tension ratio (equation 5.7), [-]
C_h	coefficient representing coalescence (equation 5.7), [-]
C_o	orifice coefficient, [-]
C_p	specific heat of air at constant pressure, [J/kg.K]
C_t	coefficient used in equations (5.6) and (5.7), [-]
C_1	constant in equation (2.9), [-]
C_2	constant in equation (2.12), [-]
C_3	constant in equation (2.13), [-]
c_j	concentration of the j^{th} phase, j = X, Y [kg/m^3 or $kgmol/m^3$]
$c_{j,n}$	concentration of phase j in stage n, [kg/m^3 or $kgmol/m^3$]
c_o	concentration at plane Z=0, [kg/m^3 or $kgmol/m^3$]
$c_{x,o}$	concentration of the X phase *inside* the column at plane z=0, [kg/m^3 or

	kgmol/m^3]
c_x°	concentration of the X phase *outside* the column at plane z=0, [kg/m^3 or kgmol/m^3]
c_x^*	equilibrium concentration of the X phase, kg/m^3
$c_{x,I}$	concentration of the X phase *inside* the column at plane z=I, [kg/m^3 or kgmol/m^3]
c_x^I	concentration of the X phase *outside* the column at plane z=I, [kg/m^3 or kgmol/m^3]
$c_{y,I}$	concentration of the Y phase *inside* the column at plane z=I, [kg/m^3 or kgmol/m^3]
c_y^I	concentration of the Y phase *outside* the column at plane z=I, [kg/m^3 or kgmol/m^3]
$c_{y,o}$	concentration of the Y phase *inside* the column at plane z=0, [kg/m^3 or kgmol/m^3]
c_y°	concentration of the Y phase *outside* the column at plane z=0, [kg/m^3 or kgmol/m^3]
c→d	continuous to dispersed phase solute transfer
D	diameter of the column, [m]
D_{AB}	diffusion coefficient of solute A in solvent B, [m^2/s]
D_o	true longitudinal dispersion coefficient defined in equation (2.44), [m^2/s]
D_r	radial dispersion coefficient, [m^2/s]
D_{tn}	dispersion coefficient due to transverse non uniformity, [m^2/s]
d	drop diameter, [m]
d_c	characteristic length, e.g. packing size, stage height,etc., [m]
d_d	diameter of disk in Tojo-Miyanami column, [m]
d_h	diameter of hole of partition plate in Tojo-Miyanami column, [m]
d_i	internal diameter of the Tojo-Miyanami column, [m]
d_{max}	maximum drop diameter, [m]
d_o	plate hole or orifice diameter, [m]
d_t	thickness of the plate, [m]

d_{32}	Sauter mean drop diameter, [m]
d→c	dispersed to continuous phase solute transfer
E	energy, [J]
E_c	axial or back-mixing coefficient in the continuous phase, [m^2/s]
E_d	axial or back-mixing coefficient in the dispersed phase, [m^2/s]
E_j	axial or back-mixing coefficient in the j^{th} phase (j = X, Y) [m^2/s]
e	stage efficiency referred in equation (2.56), [-]
e	discrepancy between model prediction and experimental value
F_j	volumetric flow rate of j^{th} phase (j = X, Y) defined in equation (1.53), [m^3/s]
Fr	Froude number defined as $u^2/(gd)$, [-]
f	frequency of oscillation, [Hz]
f′	coefficient defined in equation (2.45), [-]
Ga	Galileo's number, defined by $(d_o^3 g\, \rho_d^2/\mu^2)$ in table 2.6, [-]
g	gravitational acceleration of value 9.80665, [m/s^2]
H	plate spacing or stage height, [m]
H_c	numerical coefficient in equation (2.44), [-]
HETS	height equivalent to a theoretical stage, [m]
H_{ox}	true overall height of transfer units based on the X phase, [m]
HTU	height of transfer unit, [m]
h	fractional hold-up of dispersed phase, [-]
h_f	hold-up at flooding, [-]
h′	void fraction in Ergun's equation, [-]
i	% enhancement, [-]
I	intensity of agitation, [m/s]
j_{actual}	actual number of theoretical stages, [-]
j_{model}	equivalent theoretical number of stages, [-]
K	constant in equation (2.8)
K*	empirical parameter defining degree of circulation in drops defined in equation (2.28), [-]
$K_x a$	overall mass transfer coefficient based on the X phase, [kg/m^2s]

k	density coefficient, $d\rho/dc$, [-]
k	ordinal number of the stage in equation (2.56), [-]
k_x	individual mass transfer coefficient based on the x phase, [m/s]
$k_l a$	individual volumetric mass transfer coefficient for the liquid phase, [s^{-1}]
$k_x a$	individual mass transfer coefficient based on X phase, [s^{-1}]
$k_y a$	individual mass transfer coefficient based on Y phase, [s^{-1}]
$k_{ox} a$	overall mass transfer coefficient based on the x phase, [s^{-1}]
k_1, k_2	empirical parameters in equation (2.32), [-]
L	length of the column, [m]
L_b	weighted contribution of the buoyancy effect defined by equation (4.37), [m]
L_d	weighted contribution of the dispersed effect defined by equation (4.38), [m]
L_f	flooding ratio given by u_d/u_c, [-]
L_m	limiting mixing length as defined by equation (4.36), [m]
L^*	equivalent liquid column length due to inertia at each hole (equation 4.16), [m]
l_b	buoyancy mixing length, [m]
l_d	dispersed phase mixing length, [m]
l_{do}	dispersed phase mixing length defined in equation (4.31), [m]
l_{do}^*	resolved dispersed phase mixing length given in equation (4.31), [m]
l_{lab}	characteristic length dimension based on the lab scale column, [m/s]
l_m	limiting value of the mixing length, [m]
M	Magnification factor, defined in equation (B1), [-]
m	height of the well mixed zone, [m]
m_e	slope of the equilibrium curve, dc_x^*/dc_y [-]
m_t	mass of tracer injected at time t=0, [kg]
N	number of plates/stages, [-]
N_{eq}	number of well mixed stages, [-]
N_{ox}	overall number of true transfer units based on the X phase, equation (1.37), [-]
N_{oxD}	overall number of dispersion transfer units based on the X phase, equation (1.39), [-]
N_{oxp}	overall number of plug flow transfer units based on the X phase, equation (1.38),

[-]

N_D number of data points, [-]

N_P number of parameters, [-]

N_{vi} viscosity group defined as $\mu_d/(\rho_d\gamma d)^{0.5}$

N_{we} Weber number, defined as $\rho_c v^2 d_{max}/\gamma$, [-]

N_z mass or molar flux in the axial direction, [kg/m^{2}s or kgmol/m^{2}s]

n_1 exponent in the fractional power dissipation rate term for buoyancy (equation 4.23), [-]

n_2 exponent in the fractional power dissipation term for dispersed phase flow (equation 4.23), [-]

O_i Outlier corresponding to the i^{th} data point

Pe_j Peclet number of j^{th} phase (j=X,Y), [-]

Pe^* Peclet number based on drops defined as $U_T d_{32}/D_{AB}$, [-]

P ambient pressure, [Pa]

P^* partition coefficient defined by equation (3.2), [-]

P_f stress due to frictional effects, [Pa]

P_L pressure at location z=L, [Pa]

P_o pressure at location z=o, [Pa]

Po power dissipation, [W]

$Po_{av.}$ average power consumption, [W]

Po_{cr} critical power consumption, [W]

Po_{lg} power consumption for the liquid-gas system

Po_{max} maximum power consumption, [W]

Q heat flux, [W/m^2]

q net back-flow coefficient through the stage, [-]

q_c net back-flow coefficient through the stage for the continuous phase, [-]

q_d net back-flow coefficient through the stage for the dispersed phase, [-]

q_e effective back-mixing coefficient through the plate, [-]

q^* intercept of equilibrium line given by equation (1.3), [kg/m^3 or kgmol/m^3]

R gas constant of air used in equation (1.80), J/(kg K)

R^*	variable defined by equation (1.50), [-]
Re	Reynolds number, given by $du\rho/\mu$, [-]
Re_v	Reynolds number based on vibrating speed given by $Af\, d_o\, \Delta\rho/(S\mu)$
r	radius of tube, [m]
r	ratio of molecular weights in chapter 5, [-]
S	fractional free area of plate, [-]
S_c	fractional free area in the downcomer region (equation 2.16), [-]
S_d	also refers to vibrating disk area in Tojo-Miyanami columns, [m^2]
S_d^*	fractional free area in the hole region of the plate (equation 2.16), [-]
S_h	partition plate hole area in Tojo-Miyanami columns, [m^2]
S_i	column internal cross sectional area in Tojo-Miyanami columns, [m^2]
S_p	effective fractional free area of the plate with downcomer (equation 2.16), [-]
S_q	sum of fractional free areas of S_c and S_d, [-]
Sc	Schmidt number defined as $\mu/(\rho D_{AB})$, [-]
Sh	Sherwood number defined as $k_x d_{32}/D_{AB}$, [-]
s	root mean square deviation
T	temperature, [°K]
U_s	slip velocity defined in equation (2.21), [m/s]
U_T	terminal velocity, [m/s]
u	velocity, [m/s]
u_c	superficial velocity of the continuous phase, [m/s]
u_{eff}	effective velocity used in equation (2.44), [m/s]
u_g	superficial gas velocity, [m/s]
u_j	superficial velocity of the j^{th} phase, j = X,Y, [m/s]
u_o	characteristic velocity, [m/s]
u_{sg}	superficial gas velocity, [m/s]
V	volume of the stage, [m^3]
V_i	superficial velocity listed in the caption of figure (2.1), [m/s]
v_s	superficial velocity of the continuous phase relative to the drops (equation 2.24), [m/s]

v'	characteristic vortex velocity, [m/s]
W_i	parameters in Ueyama and Miyiuchi model with i=1,2, equation (5.10), [-]
X	dimensionless concentration of X phase defined by equation (1.4), [-]
X_o	dimensionless concentration of X phase at distance z=0, [-]
Y	dimensionless concentration of Y phase given by equation (1.5), [-]
Y_I	dimensionless concentration of Y phase defined at location z=I, [-]
y	displacement defined by equation (4.11), [m]
Z	dimensionless distance, z/L, [-]
Z_1	objective function defined by equation (4.24), [m^2]
Z_2	absolute average relative deviation defined by equation (4.27), [m^2]
z	axial distance, [m]
z^*	height of agitated zone defined by equation (2.18), [m]

Greek letters

α	constant defined in equation (1.70), [$kg^{1/2}m^4/s$]
α_j	back-flow ratio for the j^{th} phase, j = c,d [-]
α_v	back-flow ratio defined for Tojo-Miyanami column, [-]
β	parameter defined in [table 2.6 sect. 7(22)], $\delta^2/[(1-\delta)(1-\delta^2)]$, [-]
β^*	length of the circulation cell referred in equation (4.30), [m]
γ	interfacial tension, [mN/m]
σ^*	surface tension, [mN/m]
σ^*_w	surface tension of water, [mN/m]
γ_i	weight defined in equation (1.56), [-]
Δ	difference operator between two quantities
$\Delta\rho$	density difference in the continuous phase [kg/m^3]
$\Delta\rho_{cd}$	density difference between continuous phase and dispersed phase, [kg/m^3]
δ	plate voidage, [-]
δ_i	weight defined in equation (1.56), [-]
ϵ	energy dissipation rate, [m^2/s^3]
ϵ_b	buoyant specific energy dissipation rate, [m^2/s^3]

ϵ_d	dispersed phase specific energy dissipation rate, [m^2/s^3]
ϵ_m	mechanical agitation specific energy dissipation rate, [m^2/s^3]
ϵ_t	total agitation specific energy dissipation rate, [m^2/s^3]
η	Kolmogoroff microscale defined in equation (2.36), [m]
η^*	volumetric efficiency, [s^{-1}]
θ	dimensionless time, [-]
θ^*	exposure time, [s]
Λ	extraction factor defined as $m_o\ u_x/u_y$, [-]
μ	first moment from the tracer response curve
μ_c	viscosity of the continuous phase, [Pa.s]
μ_d	viscosity of the dispersed phase, [Pa.s]
ν	kinematic viscosity, μ/ρ, [m^2/s]
ρ_c	density of the continuous phase, [kg/m^3]
ρ_d	density of the dispersed phase, [kg/m^3]
ρ_j	density of the j^{th} phase, [kg/m^3]
σ	square root of the second moment of the tracer response curve
σ^*	surface tension, [mN/m]
τ	shear stress, [Pa]
τ_r	residence time, [s]
Φ	variable defined in table 2.11 sect. 1(5), [kg m^3/s^3]
ψ	energy dissipation rate per unit volume, [$kg/(ms^3)$]
ω	angular frequency, $2\pi f$, [s^{-1}]
ω_i	roots of the characteristic equation, [-]

subscripts

A	solute
aq.	aqueous
av.	average
B	solvent
b	buoyancy

c	characteristic
c	continuous
cd	continuous and dispersed
cr	critical
cs	cross section
d	disk
d	dispersed
e	equilibrium
expt.	experimental
f	frictional
g	gas
h	hole
h	influenced by hold-up
I	X phase exit end within the contactor
i	internal
i,j	representation of a group of collective terms
K-W	kerosene - water
lab	laboratory
l	liquid
lg	liquid-gas
m	mechanical
m	minimum
max	maximum
n	stage n
o	orifice or hole of plate
o	X phase inlet end within the contactor
oc	overall, based on the continuous phase
od	overall, based on the dispersed phase
org.	organic
ox	overall, based on the x phase

ox	overall, based on the x phase
p	plate
p	plug
p	constant pressure
pred.	predicted
q	quasi-steady state
r	radii
r	residence
s	slip
sim.	simulation
T	terminal
t	thickness
tn	transverse non uniformity
v	vibrational
x	represents the X phase
y	represents the Y phase
z	axial distance

superscipts

I	X phase exit end, outside the contactor
o	Y phase exit end, outside the contactor
*	equilibrium; modified;

REFERENCES

Anderson W. J. and H. R. C. Pratt, "Wake formation and circulatory flow in bubble and droplet-type contactors", Chem. Eng. Sci., 33, 995-1002 (1978).

Aravamudan, K., "Advances in the Practical Application of Research on Axial Mixing in Extraction Columns", Internal Project Report, Chem. Eng. Dept., McMaster University (1993).

Aris, R., "Notes on the Diffusion Type Model for Longitudinal Mixing in Flow ", Chem. Eng. Sci., 9, 266-267 (1959).

Bailes, P. J., J. Gledhill, J. C. Godfrey, and M. J. Slater,"Hydrodynamic Performance of a Kühni Column", Chemie Ingenieur Technik (1985).

Bainbridge, G. S., and H. Sawistowski, "Surface Tension Effects in Sieve Plate Distillation Columns", Chem. Eng. Sci., 19, 992-993 (1964).

Baird, M. H. I., "Axial Dispersion in a Pulsed Plate Column", Can. J. Chem. Eng., 52, 750-757 (1974).

Baird, M. H. I., K. Aravamudan, N. V. Rama Rao, J. Chadam, and A. P. Peirce, "Unsteady Axial Mixing by Natural Convection in a Vertical Column", AIChE J., 38, 1825-1834 (1992).

Baird, M. H. I., and B. A. Legree, "Natural Convection Heat Transfer From Open Vertical Tubes", Can. J. Chem. Eng., 72, 755-758 (1994).

Baird, M. H. I., and S. J. Lane, "Drop Size and Hold-up in a Reciprocating Plate Extraction Column", Chem. Eng. Sci., 28, 947-957 (1973).

Baird, M. H. I., R. G. McGinnis, and G. C. Tan, "Flooding Conditions in a Reciprocating Plate Extraction Column", Proc. Intnl. Solvent Extraction Conf. (ISEC 71), The Hague, The

Netherlands, 251-259 (1971).

Baird, M. H. I., and N. V. Rama Rao, "Characteristics of a Countercurrent Reciprocating Plate Bubble Column: II. Axial Mixing and Mass Transfer", Can. J. Chem. Eng., 66, 222-231 (1988).

Ibid, "Axial Mixing in a Reciprocating Plate Column in Presence of Very Small Unstable Density Gradient", AIChE J., 37, 1019-1026 (1991).

Ibid., "An Inverted Cup Reciprocating Plate for Gas Absorption", Can. J. Chem. Eng., 69, 927-932 (1991).

Ibid., "Power Dissipation and Flow Patterns in Reciprocating Baffle Plate Columns", Can. J. Chem. Eng. (submitted for publication, 1995).

Baird, M. H. I., N. V. Rama Rao, J. Prochazka, and H. Sovava, "Reciprocating-Plate Columns", in Godfrey J. C. and Slater M. J. (eds), Liquid-Liquid Extraction Equipment, 307-362, Wiley (1994).

Baird, M. H. I., and P. Stonestreet,"Energy Dissipation in Oscillatory Flow in a Baffled Tube", Chem. Eng. Res. Des. (submitted for publication, 1995).

Baird, M. H. I. and Rice, R. G., "Axial dispersion in large unbaffled columns", Chem. Eng. J., 9, 171-174 (1975).

Baird, M. H. I., and Z. J. Shen, "Holdup and Flooding in Reciprocating Plate Extraction Columns", Can. J. Chem. Eng., 62, 218-227 (1984).

Bensalem, A. K., "Hydraulics and Mass Transfer in a Reciprocating Plate Column", Ph.D. Thesis, Swiss Federal Inst. Tech., Zurich, (1985).

Bischoff, K. B., "Notes on the Diffusion Type Model for Longitudinal Mixing in Flow", Chem. Eng. Sci., 69, 69-70 (1960).

Boyadzhiev, L., and M. Spassov, "On the Size of Drops in Pulsed and Vibrating Plate Extraction Columns", Chem. Eng. Sci., 37, 337-340 (1982).

Brajinskii, L. N., Yu. V. Kokotov, and L. S. Gordeev, "", Teor. Osn. Khim. Tekhnol., 20, 375-(1976).

Breyesse, J., U. Bülmann, and J.C. Godfrey, "Axial Mixing Characteristics of Industrial and Pilot Scale Kühni Columns", AIChE SYMP. SERIES, 80, 94-101 (1984).

Calderbank, P. H., F. Evans, and J. Rennie, Proc. Intl. Symp. on Distillation, Instn. of Chem. Engrs., Brighton, (1960).

Cavers S. D. and Ewanchyna J. E., "Circulation and End Effects in a Liquid Extraction Spray Column", Can. J. Chem. Eng., 10, 113-128 (1957).

Chen, B. H., and C. H. Liu, " Liquid-Liquid Extraction in a Reciprocating Screen Plate Column", Can. J. Chem. Eng., 69, 300-307 (1991).

Coulaloglou, C. A., and L.L. Talvarides, "Drop Size Distributions and Coalescence Frequencies of Liquid-Liquid Dispersions in Flow Vessels", AIChE J, 22, 289-297 (1976).

Cusack R. W. and P. Fremeaux, "A Fresh Look at Liquid-Liquid Extraction", Chem. Eng., 3, 132-138 (1991).

Cusack R. W. and A. Karr, "A Fresh Look at Liquid-Liquid Extraction", Chem. Eng., 4, 112-117 (1991).

Danckwertz, "Continuous Flow Systems-Distribution of Residence Times, 2, Chem. Eng. Sci., 1-13 (1953).

Devanathan, N., D. Moslemian, and M. P. Dudukovic, "Flow Mapping in Bubble Columns Using CARPT", Chem. Eng. Sci., 45, 2285-2291 (1990).

Dongaonkar, K. R., "Mass Transfer and Axial Dispersion in a Kühni Extraction Column", Ph.D. Thesis, Univ. of Melbourne, Melbourne (1989).

Dongaonkar, K. R., H. R. C. Pratt, and G. W. Stevens, "Mass Transfer and Axial Dispersion in a Kühni Extraction Column", AIChE J., 37, 694-704 (1991).

Draper, N. R., and H. Smith, "The Examination of Residuals", Applied Regression Analysis, Second edition, 141-192, Wiley, New York (1981).

Elsässer, K. H., and U. Bühlmann, "Scale-up of Kühni Column Based on the Back-flow Model," Proc. Intl. Solvent Extraction Conf. (ISEC 86), Munich, III-167 to III-174 (1986).

Ergun, S., "Fluid Flow through Packed Columns", Chem. Eng. Progr., 48, 89-94, (1952).

Geary, N. W., and R. G. Rice, "Circulation and Scale-Up in Bubble Columns", AIChE J, 38, 76-82 (1992).

Garner, F. H., and M. Tayeban, "The Importance of the Wake in Mass Transfer From Both Continuous and Dispersed Phase Systems", Anal Real Soc Espan Fis Quim, B56, 479-498 (1960).

Gayler, R., Roberts, N. W., and H. R. C. Pratt, "Liquid-Liquid Extraction: Part IV. A further Study of Hold-Up in Packed Columns", Trans. Inst. Chem. Engrs, 31, 57-68 (1953).

Geankoplis, C. J., and A. N. Hixon, "Mass Transfer Coefficients in an Extraction Spray Tower", Ind. Eng. Chem., 42, 1141-1151 (1950).

Geankoplis, C. J., Wells, P. L., and Hawk, E. L., "Extraction in a Pilot Unit Spray Tower", Ibid., 43, 1848-1856 (1951).

Geankoplis, C. J., "Spray Tower Extraction", Ibid., 44, 2458 (1952).

Gier, T.E., and J. O. Hougen, "Concentration Gradients in Spray and Packed Extraction Columns", Ind. Eng. Chem., 45, 1362-1370 (1953).

Godfrey, J. C., and M. J. Slater, Liquid-Liquid Extraction Equipment, Wiley (1994).

Göebel, J. C., Booij, K., and J. M. H. Fortuin, "Axial Dispersion in Single Phase Flow in Pulsed Columns", Chem. Eng. Sci., 41, 3197-3203 (1986).

Gomma, H. G., J. Landau, and A. M. Al Taweel, "Gas Liquid Contacting in Reciprocating Plate Columns : I. Hydrodynamics", Can. J. Chem. Eng., 69, 228-239 (1991).

Gorodetski, I. J., Vasin A. A., Olevski V. M., Kostanyan A. E., and Lupanov, P. A. Proc. Intl. Solvent Extraction Conf. (ISEC 88), Moscow, paper 4-10 (1988).

Grace, J. R., T. Wairegi, and T. H. Nguyen, "Shapes and Velocities of Single Drops and Bubbles Moving Freely through Immiscible Liquids", Trans. Inst. Chem. Engrs, 54, 167-173 (1976).

Groothuis, H., and F. J. Zuiderweg, "Influence of Mass Transfer of Drops", 12, 288-289 (1960).

Hafez, M. M., and J. Prochazka, "The Dynamic Effects in Vibrating Plate and Pulsed Extractors-I. Theory and Experimental Technique", Chem. Eng. Sci., 29, 1745-1753 (1974a).

Ibid., "The Dynamic Effects in Vibrating Plate and Pulsed Extractors-II. The Forces Under the Steady and Pulsating Single Phase Flow", Chem. Eng. Sci., 29, 1755-1762 (1974b).

Hafez, M. M., and M. H. I. Baird, "Power Consumption in a Reciprocating Plate Extraction Column", Trans. Inst. Chem. Engrs, 56, 229-238 (1978).

Hafez, M. M., M. H. I. Baird, and I. Nirdosh, "Flooding and Axial Dispersion in Reciprocating Plate Extraction Columns," Can. J. Chem. Eng., 57, 150-158 (1979).

Ibid., "A Model for Reciprocating Plate Extraction Columns", Proc. Intl. Solvent Extraction Conf. (ISEC 80), Liege-Belgium, 80-41, 1-10 (1980).

Haunold C., Cabassud, M., Gourdon C., and Casamatta G., "Drop behaviour in a Kühni Column for a Low Interfacial Tension System", Can. J. Chem. Eng., 68, 407-414 (1990).

Heyberger, A., M. Kratky, and J. Prochazka, "Parameter Evaluation of an Extractor with Back-mixing", 38, 1303-1307 (1983).

Handlos, A. E., and T. Baron, "Mass and Heat Transfer from Drops in Liquid-Liquid Extraction", AIChE J., 3, 127-136 (1957).

Harikrishnan, T. L., Prabhavathy, N. K., and Y. B. G. Varma, "Liquid-Liquid Mass Transfer in a Reciprocating Plate Column", Chem. Eng. J., 54, 7-16 (1994).

Higbie, R., "The rate of Absorption of a Pure Gas into a Still Liquid During Short Periods of Exposure", Trans. AIChE, **31**, 365-389 (1935).

Hinze, J. O., "Fundamentals of the Hydrodynamic Mechanism of Splitting in Dispersion Processes", AIChE J., **1**, 289-295 (1955).

Holmes, T. L., A. E. Karr, and M. H. I. Baird, "Effect of Unfavourable Density Gradient on Axial Mixing", AIChE J., **37**, 360-366 (1991).

Hussain, A., N. J. Slater, and A. Marrocchelli, "Aspects of Pulsed Column Behaviour", Proc. Intnl. Solvent Extraction Conf. (ISEC 86), Munich, III-149 to III-156 (1986).

Ionnou, J., M. M. Hafez, and S. Hartland, "Mass Transfer and Power Consumption in Reciprocating Plate Extractors", Ind. Eng. Chem. Proc. Des. Dev., **15**, 469-471 (1976).

Isaac, N., and R. L. DeWitte, "A new type of Countercurrent Column for the Zirconium-hafnium Separation", AIChE J., **4**, 498 (1958).

Janosi, T., and J. Hunek, "An investigation of Axial Mixing in an Extraction Column", Int. Chem. Eng., **28**, 731-738 (1988).

Jares, J. and J. Prochazka, "Break-Up of Droplets in Karr Reciprocating Plate Extraction Column", Chem. Eng. Sci., **2**, 283-292 (1987).

Jealous, A. C., and H. F. Johnson, "Power Requirements for Pulse Generation in Pulse Columns", Ind. Eng. Chem., **47**, 1159-1166 (1955).

Jiricny, V., and J. Prochazka, "Countercurrent Flow of Dispersed and Continuous Phase -III, Measurement of Holdup Profiles and Particle Distribution in a Vibrating Column", Chem. Eng. Sci., **35**, 2237-2245 (1980).

Joshi, J. B., and M. M. Sharma, "A Circulation Models for Bubble Columns", Trans. Inst. Chem. Engrs, **57**, 244-251 (1979).

Kannan, A., T. L. Harikrishnan, and Y. B. G. Varma, "A Numerical Technique for the Estimation of the True Mass Transfer Coefficient in Extraction Columns", Chem. Eng. J.,

45, 133-135 (1990).

Karr, A. E., "Performance of a Reciprocating-Plate Extraction Column", AIChE J., 5, 446-452 (1959).

Karr, A. E., and T. C. Lo, "Performance and Scale-up of a Reciprocating-Plate Extraction Column", Proc. Intnl. Solvent Extraction Conf. (ISEC 71), The Hague, The Netherlands, 299-320 (1971).

Ibid., "Scale-up of Large Diameter Reciprocating-Plate Extraction Columns", Chem. Eng. Progr., 11, 68-70 (1976).

Ibid., "Performance of a 36 in. Diameter Reciprocating Plate Extraction Extraction Column", Proc. Intnl. Solvent Extraction Conf. (ISEC 77), Toronto, 21, 355-361 (1979).

Ibid., "Amplification of Scale-up Procedure for the Reciprocating Plate Extraction Column", AIChE J., 31, 690-692 (1985).

Karr, A. E., S. Ramanujam, T. C. Lo, and M. H. I. Baird, "Axial Mixing and Scale-up of Reciprocating Plate Extraction Column", Can. J. Chem. Eng., 65, 373-381 (1987).

Kawase, Y., and M. Moo-Young, "Liquid Phase Mixing in Bubble Columns with Newtonian and Non-Newtonian Fluids", Chem. Eng. Sci., 41, 1969-1977 (1986).

Kawase, Y. and M. Tokunaga, "Characteristic Mixing Length in Bubble Columns", Can. J. Chem. Eng., 69, 1228-1231 (1991).

Kehat E., and R. Letan, "The Role of Wakes in the Mechanism of Extraction in Spray Columns", AIChE J., 17, 984-990 (1971).

Kertes A. S. and C. J. King, "Extraction Chemistry of Low Molecular Weight Aliphatic Alcohols", Chem. Rev., 87, 687-710 (1987).

Kim, S. D., and M. H. I. Baird, "Axial Dispersion in a Reciprocating Plate Extraction Column", Can. J. Chem. Eng., 54, 81-89 (1976a).

Ibid, "Effect of Hole Size on Hydrodynamics of a Reciprocating Plate Extraction Column", Can. J. Chem. Eng., 54, 235-237 (1976b).

Kawase, Y., and M. Moo-Young, "Mathematical Models for Design of Bioreactors: Applications of Kolmogoroff's Theory of Isotropic Turbulence", Chem. Eng. J., 43, B19-B41 (1990).

King C. J., "Solvent-Extraction in the Process Industries: Quo-Vadis ?", Proc. Intnl. Solvent Extraction Conf. (ISEC 93), York, England, 3-14 (1993).

Kolmogoroff, A. N., Akad. Nauk U.S.S.R. 30, 301 (1941).

Korchinsky, W. J., "Rotating Disk Contactors", in Godfrey J. C. and Slater M. J. (eds), Liquid-Liquid Extraction Equipment, 247-275, Wiley (1994).

Kostanyan, A. E., and Pebalk, V. L., "Longitudinal Mixing in Subdivided Column Extractors with Mixers", Teor. Osn. Khim. Tekhnol., 27, 557-564 (1973).

Kostanyan, A. E., and I. Ya. Gorodetski, "Determination of Back and Longitudinal Mixing in Industrial Extraction Columns", Teor. Osn. Khim. Tekhnol., 11, 724-728 (1977).

Kostanyan, A. E., Pebalk, V. L., and T. K. Pelevina,"Energy Consumption and Dispersion in Extractors with Vibrating Plates", Teor. Osn. Khim. Tekhnol., 13, 624-627, (1979).

Ibid, "Study of the Operational Characteristics of Column Extractors with Vibrating Plates", Teor. Osn. Khim. Tekhnol., 14, 174-177 (1980).

Kostanyan, A. E., Pebalk, V. L., T. K. Pelevina and Kovaleva, G. K., "Study of Column Vibration Extractors with Plates of Different Types ", Khim. Prom-st. (Moscow), (4), 229-231 (1979).

Kosters, W. C. G., "Rotating Disk Contactor", in Lo, T. C., M. H. I. Baird, and C. Hanson (eds), Handbook of Solvent Extraction, 391-405, Wiley-Interscience, New York (1983).

Kronig, R., and J. C. Brink, "On the Theory of Extraction From Falling Droplets", Appl. Sci. Res. A, 2, 142-154 (1950).

Kumar, A. and S. Hartland, "Prediction of Dispersed Phase Holdup and Flooding Velocities in Karr Reciprocating-Plate Extraction Columns", Ind. Eng. Chem. Res., 27, 131-138 (1988).

Ibid., "Prediction of Continuous Phase Axial Mixing Coefficients in Pulsed-Perforated Plate Extraction Columns," Ind. Eng. Chem. Res., 28, 1507-1513 (1989).

Ibid., "Prediction of Axial Mixing Coefficients in Rotating Disc and Asymmetric Rotating Disc Extraction Columns," Can. J. Chem. Eng., 70, 77-87 (1992).

Laddha, G. S., and Degaleesan, T. E., "Dispersion and Coalescence", in Lo, T. C., M. H. I. Baird, and C. Hanson (eds.), Handbook of Solvent Extraction, 125-149, Wiley-Interscience, New York (1983).

Landau, J., J. Prochazka, F. Souhrada, and P. Nekovar, "Studies on Extraction II. Liquid-Liquid Extractor with Vibrating Plates", Collect. Czech. Chem. Commun., 29, 3003-3019 (1964).

Lapidus, L., and J. C. Elgin, "Mechanics of Vertical Moving Fluidized Systems", AICHE J., 3, 63-68 (1957).

Letan R., and E. Kehat, "The Mechanism of Heat Transfer in a Spray Column Heat Exchanger", AICHE J., 14, 398-405 (1968).

Levenspiel, O. and T. J. Fitzgerald, "A Warning on the Misuse of the Dispersion Model", Chem. Eng. Sci., 38, 489-491, (1983).

Levenspiel, O. and W. K. Smith, " Notes on the Diffusion type Model for the Longitudinal Mixing of Fluids in Flow", Chem. Eng. Sci., 6, 227-233 (1957).

Levich, V. G., Physicochemical Hydrodynamics, Prentice-Hall, New Jersey (1962).

Linton, M., and K. L. Sutherland, "Transfer From a Sphere into a Fluid in Laminar Flow", Chem. Eng. Sci., 12, 214-229 (1960).

Lo, T. C., M. H. I. Baird, and C. Hanson, (eds), Handbook of Solvent Extraction, Wiley-Interscience, New York (1983).

Lo, T. C., and M. H. I. Baird, "Extraction (Liquid-Liquid)", Kirk-Othmer Encyclopedia of Chemical Technology, Fourth edition, 125-180, Wiley, New York (1994).

Lo, T. C., and J. Prochazka, "Reciprocating Plate Extraction Columns", in Lo, T. C., M. H. I. Baird, and C. Hanson (eds), Handbook of Solvent Extraction, 373-389, Wiley-Interscience, New York (1983).

Lowell M. E., and Anderson J. L., "Stable Concentration Gradients in a Vertical Tube", Chem. Eng. Commun., 18, 93-96 (1982).

Mathur, N. K., "Newer acylation methods for the determination of organic hydroxyl and amino compounds, " Talanta, 13, 1601-1611 (1966).

Morello V. S. and N. Poffenberger, "Commercial Extraction Equipment", Ind. Eng. Chem., 42, 1021-1035 (1950).

Mecklenburgh, J. C. and S. Hartland, The Theory of Backmixing, Wiley-Interscience, New York (1975).

Mišek, T., "General Hydrodynamic Basis for Columns", in Godfrey J. C. and Slater M. J. (eds), Liquid-Liquid Extraction Equipment, 95-113, Wiley (1994).

Mišek, T., and J. Marek, "Asymmetric Rotating Disk Contactor", in Lo, T. C., M. H. I. Baird, and C. Hanson (eds), Handbook of Solvent Extraction, 407-417, Wiley-Interscience, New York (1983).

Miyanami K., Tojo, K., and T. Yano, "Liquid-Phase Mixing in a Multistage Vibrating Disk Column with Concurrent Gas-Liquid Flow", J. Chem. Eng. Japan, 6, 518-522 (1973).

Miyanami K., K. Tojo, T. Yano, K. Miyaji and I. Minami, "Drop Size Distributions and Holdups in a Multistage Vibrating Disk Column", Chem. Eng. Sci., 30, 1415-1420 (1975).

Miyanami K., K. Tojo, I. Minami, and T. Yano, "Gas-Liquid Mass Transfer in a Vibrating Disk Column", Chem. Eng. Sci., 33, 601-608 (1978).

Miyauchi, T., and T. Vermeulen, "Longitudinal Dispersion in Two Phase Continuous Flow

Operations", Ing. Eng. Chem. Fund., 2, 113-126 (1963a).

Ibid., "Diffusion and Backflow Models for Two Phase Axial Dispersion", Ind. Eng. Chem. Fund., 4, 304-310 (1963b).

Mogli, A. and U. Bühlmann, "The Kühni Extraction Column", in Lo, T. C., M. H. I. Baird, and C. Hanson (eds), Handbook of Solvent Extraction, 441-447, Wiley-Interscience, New York (1983).

Newman A. B., "The Drying of Porous Solids-Diffusion Calculations", Trans. AIChE., 27, 310 (1931).

Newman, M. L., "Spray Tower Extraction", Ind. Eng. Chem., 44, 2457-2458 (1952).

Nemecek, M., and J. Prochazka, "Longitudinal Mixing in a Vibrating Column Two Phase Flow", Can. J. Chem. Eng., 52, 739-749 (1974).

Noh, S. H., and M. H. I. Baird, "Mass Transfer and Pressure Drop in a Cocurrent Reciprocating Plate Extraction Column", AIChE J., 30, 120-127 (1984).

Novotny, P., J. Prochazka, and J. Landau, "Longitudinal Mixing in Reciprocating and Pulsed Sieve Plate Column Single Phase Flow", Can. J. Chem. Eng., 48, 405-410 (1970).

Olevskii, V. M., Kostanyan, A. E., and Gorodetskii, I. J., " Main Lines of Refinement of Extractors Having a Vibrating Packing", J. Appl. Chem. USSR, 59, 1899-1903 (1986).

Othmer, D. F., R. E. White, E. Trueger, "Liquid-Liquid Extraction Data", Ind. Eng. Chem., 33, 1240-1248 (1941).

Parthasarathy, P., G. Sriniketan, N. S. Srinivas and Y. B. G. Varma, "Axial Mixing of Continuous Phase in Reciprocating Plate Columns", Chem. Eng. Sci., 39, 987-995 (1984).

Prabhakar, A., G. Sriniketan, and Y. B. G. Varma, "Dispersed Phase Holdup and Drop Size Distribution in Pulsed Plate Columns", Can. J. Chem. Eng., 66, 232-240 (1988).

Pratt, H. R. C., and G. W. Stevens, "Axial Dispersion", in Thornton, J. D. (ed.), Science and

Practice of Liquid-Liquid Extraction, 416-491, Oxford University Press, Oxford (1992).

Ibid., "Selection, Design, Pilot Testing and Scale-Up of Extraction Equipment", in Thornton, J. D. (ed.), Science and Practice of Liquid-Liquid Extraction, 492-589, Oxford University Press, Oxford (1992).

Pratt, H. R. C., " A Simplified Analytical Method for Differential Extractors with Backmixing. I. Linear Equilibrium Relationship", Ind. Eng. Chem. Proc. Des. Dev., **14**, 74-80, (1975).

Ibid., " A Simplified Analytical Method for Differential Extractors with Backmixing. II. Curved Equilibrium Line", Ind. Eng. Chem. Proc. Des. Dev., **15**, 34-41 (1976).

Prvcic, L. M., H. R. C. Pratt, and G. W. Stevens, "Axial Dispersion in Pulsed-Perforated Plate Extraction Columns", AIChE J, **35**, 1845-1855 (1989).

Prochazka, J., J. Landau, F. Souhrada, and A. Heyberger, "Reciprocating Plate Extraction Column", Br. Chem. Eng., 42-44 (1971).

Quinn, J. A., Lin, C. H., and Anderson, J. L., "Measuring Diffusion Coefficients by Taylor's Method of Hydrodynamic stability", AIChE J., **32**, 2028-2033 (1986).

Rama Rao, N. V., and M. H. I. Baird, "Characteristics of a Countercurrent Reciprocating Plate Bubble Column. I. Holdup, Pressure Drop and Bubble Diameter", Can. J. Chem. Eng., **66**, 211-221 (1988).

Ibid., "Characteristics of a Countercurrent Reciprocating Plate Bubble Column. II. Axial Mixing and Mass Transfer", Can. J. Chem. Eng., 222-231 (1988b).

Rama Rao, N. V., N. S. Srinivas and Y. B. G. Varma, "Dispersed Phase Holdup and Drop Size Distributions in Reciprocating Plate Columns", Can. J. Chem. Eng., **61**, 168-177 (1983).

Rama Rao, N. V., S. Vijayan and M. H. I. Baird, "Hydrodynamics of a Vibrating Plate Extraction Column", Can. J. Chem. Eng., **69**, 212-221 (1991).

Rice, R. G., and M. A. Littlefield, "Dispersion Coefficients for Ideal Bubbly Flow in Truly Vertical Bubble Columns", Chem. Eng. Sci., **42**, 2045-2053 (1987).

Ricker, N. L., Nakashio, F., and King, C. J., "An Efficient, General Method for Computation of Countercurrent Separation Processes with Axial Dispersion", AIChE J., 27, 277-284 (1981).

Rincón-Rubio L. M., A. Kumar and S. Hartland, "Drop Size Distributions and Average Drop Size in a Wirz Extraction Column", Trans IChemE, 72, 493-502 (1994).

Rod, V., "Calculating Mass Transfer with Longitudinal Mixing", Brit. Chem. Eng. 11, 483-487 (1966).

Rod, V., and T. Mišek, "Residence Time Distribution of the Dispersed Phase in Agitated Extraction Columns", Proc. Intnl. Solvent Extraction Conf. (ISEC 71), The Hague, The Netherlands, 738-749 (1971).

Rosen A. M., and V. S. Krylov, "The Scaling Up of Mass Transfer Equipment and Reactors: Use of Hydraulic Model Experiments", Chem. Eng. Sci., 22, 407-416 (1967).

Ibid., "Theory of Scaling Up and Hydrodynamic Modelling of Industrial Mass Transfer Equipment", Chem. Eng. Sci., 7, 85-97 (1974).

Sawinsky, J., and Hunek, J., "Methods for Investigation Backmixing in the Continuous Phase of Multiple-Mixer Extraction Columns", Trans. Inst. Chem. Engrs, 59, 64 (1981).

Sege, G., and F.W. Woodfield, "Pulse-Column Variables", Chem. Eng. Progr. Symp. Ser., 50, 179-190 (1954).

Selig, W., "Semi micro determination of Hydroxy and Amino compounds using Pyromellitic Dianhydride", Microchem. J., 21, 92-97 (1976).

Shen, Z. J., N. V. Rama Rao, and M. H. I. Baird, "Mass Transfer in a Reciprocating Plate Extraction Column - Effects of Mass Transfer Direction and Plate Material", Can. J. Chem. Eng., 63, 29-36 (1985).

Sleicher, C. A., "Axial Mixing and Extraction Efficiency,", AIChE J., 2, 145-149 (1959).

Ibid., "Entrainment and Extraction Efficiency of Mixer Settlers," AIChE J., 3, 529-531 (1960).

Siggia, S., " Hydroxl Groups", Quantitative Organic Analysis via Functional Groups, Fourth edition, 28-31, Wiley, New York (1979).

Simons, A. J. F., "Pulsed Packed Columns", in Lo, T. C., M. H. I. Baird, and C. Hanson (eds),Handbook of Solvent Extraction, 343-353, Wiley-Interscience, New York (1983).

Simons, A. J. F., R. van Sluys, J. C. Goebel, and J. M. H. Fortuin, "Axial Dispersion in Pulsed Packed Columns on Both Laboratory and Industrial Scale", Proc. Intnl. Solvent Extraction Conf. (ISEC 86), Munich, III-31 - III-37 (1986).

Skala, D., and V. Veljkovic, "Mass Transfer Characteristics in a Gas-Liquid Reciprocating Plate Column. I. Liquid Phase Volumetric Mass Transfer Coefficient", Can. J. Chem. Eng., 66, 192-199 (1988).

Ibid., "Mass Transfer Characteristics in a Gas-Liquid Reciprocating Plate Column. II. Interfacial Area", Can. J. Chem. Eng., 66, 200-210 (1988).

Slater, M. J., "Liquid-Liquid Extraction Column Design", Can. J. Chem. Eng., 63, 1004 (1985).

Slater, M. J. and W-Y. Fey, "A New Look at the Hydrodynamic Behaviour of Rotating Disk Contactors", J. Sep. Process Technol., 5 (1984).

Souhrada, F., J. Prochazka, and J. Landau, "Studies on Extraction V. Determination of Backmixing and Efficiency of Stagewise Extractors", Collect. Czech. Chem. Commun., 31, 1695-1711 (1966).

Sovova, H., "A Model of Dispersion Hydrodynamics in a Vibrating Plate Extractor," Chem. Eng. Sci., 38, 1863-1872 (1983).

Ibid., "Counter-current Pulsed and Reciprocating Plate Extractors, Prediction of Sauter Mean Drop Diameter", Collect. Czech. Chem. Commun., 55, 409-425 (1990).

Sriniketan, G., A. Prabhakar, and Y. B. G. Varma, Bioprocess Engineering, 2, 161-168 (1987).

Stevens, G. W., and M. H. I. Baird, "A Model For Axial Mixing in Reciprocating Plate Columns", Chem. Eng. Sci., 45, 457-465 (1990).

Steiner, L., "Computational Procedures for Column Simulation and Design", in Godfrey J. C. and Slater M. J. (eds), Liquid-Liquid Extraction Equipment, 115-136, Wiley (1994).

Steiner, L., and S. Hartland, "Hydrodynamics of Liquid-Liquid Spray Columns", in N. P. Cheremisinoff, and R. Gupta (eds), Handbook of Fluids in Motion, 1049-1092, Ann Arbor Science, Michigan (1983).

Sundaresan, A., and Y. B. G. Varma, "Dispersed Phase Holdup and Bubble Size Distributions in Gas-Liquid Cocurrent Upflow and Countercurrent Flow in Reciprocating Plate Column", Can. J. Chem. Eng., 560-568 (1990).

Taylor, G. I., "Diffusion and Mass Transport in Tubes", Proc. Phys. Soc., Sect. B, 67, 857-869 (1954).

Taylor, P. A., M. H. I. Baird, and I. Kusuma, "Computer Control of Holdup in a Reciprocating Plate Extraction Column", Can. J. Chem. Eng., 60, 556-565 (1982).

Thornton, J. D., "Spray Liquid-Liquid Extraction Columns", Chem. Eng. Sci., 5, 201-208 (1956).

Ibid., Science and Practice of Liquid- Liquid Extraction, Oxford University Press, Oxford (1992).

Tojo, K., Miyanami, K. and Yano, T., "Gas Hold-up and Pressure Drop in a Multistage Vibrating Disk Column with Cocurrent Gas Liquid Flow", J. Chem. Eng. Japan, 7, 123-126 (1974a).

Ibid., "Mass Transfer in a Multistage Vibrating Disk Column with Cocurrent Gas Liquid Flow", 7, 126-130 (1974b).

Ibid., "Liquid-Liquid Extraction in a Multistage Vibrating Disk Column", 8, 122-126 (1975).

Ibid., "The effect of wave form of Disk Vibration on Mass Transfer in a Multistage Vibrating Disk Column with Countercurrent Liquid-Liquid Flow", 8, 165-167 (1975).

Ibid., "Axial Mixing in a Multistage Vibrating Disc Column with Countercurrent Liquid-Liquid Flow", **11**, 101-104 (1976).

Ibid., "Design Method and Performance Characteristics of a Multistage Vibrating Disk Column (MVDC) Extractor", Ind. Eng. Chem. Proc. Des. Dev., 459-465 (1980).

Treybal, R. E., Liquid Extraction, second edition, McGraw Hill, New York (1963).

Treybal, R. E., Mass Transfer Operations, Third edition, McGraw Hill, New York (1980).

Ueyama, K., and T. Miyauchi, "Properties of Recirculating Turbulent Two Phase Flow in Gas Bubble Columns", **25**, AIChE J., 258-266 (1979).

Van Dijk, W. J. D., US Patent 2,011,186 (1935).

Veljkovic, V. B., and D. U. Skala, "On the Possibility of General Prediction of Gas Hold-Up in Reciprocating Plate Columns", Can. J. Chem. Eng.,, **67**, 1015-1018 (1989).

van Suijdam, J. C., and B. Metz, " Influence of Engineering Variables upon the Morphology of Filamentous Molds", Biotechnol. Bioeng., **23**, 111-148 (1981).

Vergnes, F., "A Simple and Practical Method for the Determination of the Peclet Number in the Longitudinal Dispersion Model", Chem. Eng. Sci., **31**, 88-90 (1976).

Walter, J. F., and H. W. Blanch, "Liquid Circulation Patterns and their Effect on Gas Holdup and Axial Mixing in Bubble Columns", Chem. Eng. Commun., **19**, 243-262 (1983).

Wehner, J. F., and R. H. Wilhelm, "Boundary Conditions of Flow Reactor", Chem. Eng. Sci., **6**, 89-93 (1956).

Wellek, R. M., M. U. Ozsoy, J. J. Carr, D. Thompson, and T. V. Konkle, "A Liquid Extraction Column with Reciprocated Wire Mesh Packing", Ind. Eng. Chem. Proc. Des. Dev., 515-527 (1969).

Wilke, C. R., and P. Chang, "Correlation of Diffusion Coefficient in Dilute Solutions", AIChE J, **1**, 264-270 (1955).

Yang, N. S., B. H. Chen, and A. F. McMillan, "Axial Mixing and Mass Transfer in Gas-Liquid Karr Column", Ind. Eng. Chem. Proc. Des. Dev., 25, 776-780 (1986).

Zakrzewski, W., J. Lippert, A. Lübbert, and K. Schügerl, "Investigation of the Structure of Two Phase Flows. Model Media in Bubble Column Bioreactors IV. True Liquid Velocities and Bubble Velocity Distributions", Eur. J. Appl. Microbiol.Biotechnol., 12, 69-75 (1981).

Zehner, P., "Impuls-, Stoff- und Warmetransport in Blasensaulen", Verfahrenstechnik (Mainz), 16, 514-517 (1982).

APPENDIX A

QUANTITATIVE ESTIMATION OF ALCOHOL CONCENTRATION IN ISOPAR M

INTRODUCTION

The quantitative estimation of alcohol through wet tests has been extensively reviewed in the literature (Mathur 1966; Siggia 1967; Selig 1976). The PMDA technique due to Siggia et al. (1967) was chosen on account of its speed of reaction, specificity and non volatility.

Principle of the method

The sample containing the hydroxyl group was made to react with excess PMDA to form the corresponding ester and acid. The remaining PMDA is hydrolysed to acid by adding water. These chemical reactions can be represented as follows:

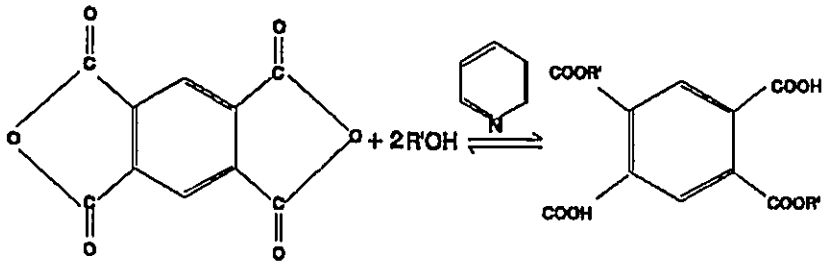

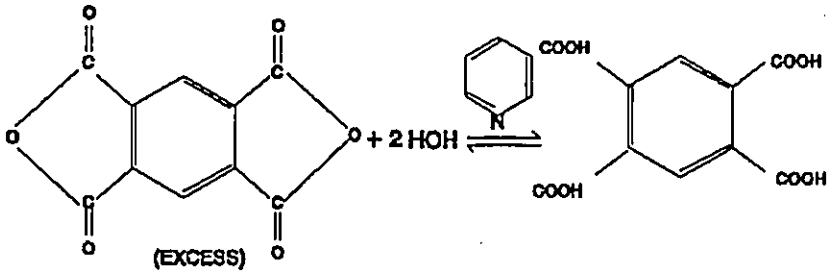

A blank test (without the alcohol sample) is performed under identical conditions. In this test

all the PMDA is hydrolysed to acid. More acid is formed in the blank test when compared to the actual sample test because in the latter some PMDA is converted to the ester. The amount of acid formed in both cases can be determined by titrating with standard sodium hydroxide. The difference in the volume of base consumed in the two cases can be related to the hydroxyl content of the sample.

Procedure

A solution containing 0.5 M of PMDA was prepared by dissolving 109 g of the solid in 575 cc of Dimethyl sulfoxide (DMSO) and making up the solution to 1 litre by adding pyridine. Pyridine accelerates the reaction by tying up the carboxylic acids formed. DMSO is required as a second solvent because PMDA is only sparingly soluble in Pyridine (Siggia 1967).

25 cc of 0.5 M PMDA was pipetted into a 250 cc Erlenmeyer flask. A sample containing 5-7.5 meq was transferred into the flask and a stopper wetted with Pyridine was seated loosely in it. The flask was heated at approximately 100°C for 30 minutes to carry out the esterification reaction. For samples containing 10-15 meq of alcohol, 50 cc of 0.5 M PMDA was used.

10 cc of distilled water was added to hydrolyse the excess PMDA and the heating was continued for an additional 5 minutes. The flask was allowed to cool to room temperature before titrating with standard sodium hydroxide. Since the solution at higher concentrations of PMDA assumed a yellow colour during titration, visual determination of the end point using phenolphthalein indicator was ambiguous. Therefore the titrations were carried out potentiometrically using a pH meter. The equivalence point of the titration was determined by finding the maximum slope of the pH with respect to the volume of the titrant. The above procedure was repeated for the blank test.

The above procedure was scaled down by a factor of 10 for dilute samples, i.e. 25 cc of

0.1 M PMDA was used for hydroxyl contents of 1-1.5 meq. The heating time was doubled.

Testing the method

The method described above was tested on standard solutions of *i*-propanol in Isopar in the concentration range of 5-300 g/l. In order to make the Isopar samples correspond to those taken from the experimental column, the Isopar was saturated with water before preparing the standards. However the mutual solubility of water and Isopar is very small. The measured concentrations of alcohol in Isopar M were lower than expected from the amount of *i*-propanol originally taken in the standards. This trend persisted in spite of varying the reaction time and PMDA / OH ratio. Therefore it was decided to prepare a calibration of the titration procedure in terms of the correction factor required vs. concentration. Two titrations (excluding the blank) were performed for each standard concentration tested. From the results, it was decided to use a constant correction factor (+1.105) for the entire concentration range.

APPENDIX B

DERIVATION OF ERROR MAGNIFICATION FACTOR (M)

The % error terms based on l and E_c are given by

$$\%error_l = \frac{l_{exptl.} - l_{pred.}}{l_{exptl.}} \times 100 \qquad (4.29\ a)$$

$$\%error_{E_c} = \frac{E_{c,exptl.} - E_{c,pred.}}{E_{c,exptl.}} \times 100 \qquad (4.29\ b)$$

Defining M as

$$M = \frac{\%error_{E_c}}{\%error_l} = \frac{1 - \frac{E_{c,pred.}}{E_{c,exptl.}}}{1 - \frac{l_{pred.}}{l_{exptl.}}} \qquad (B1)$$

provided $l_{pred.} \neq l_{exptl.}$

which may be further expressed as

$$= \frac{1 - (\frac{l_{pred.}}{l_{exptl.}})^{\frac{4}{3}}}{1 - (\frac{l_{pred.}}{l_{exptl.}})} \qquad (B2)$$

Expressing the discrepancy in mixing length between the model prediction and the experimental data value (Δe) as

$$l_{exptl.} = l_{pred.} + \Delta e \qquad \textbf{(B3)}$$

or, equivalently

$$l_{pred.} = l_{exptl.} - \Delta e \qquad \textbf{(B4)}$$

hence, equation B2 becomes after some simplification,

$$M = \frac{1-(1-\frac{\Delta e}{l_{exptl.}})^{\frac{4}{3}}}{1-(1-\frac{\Delta e}{l_{exptl.}})} = \frac{1-(1-\frac{\Delta e}{l_{exptl.}})^{\frac{4}{3}}}{\frac{\Delta e}{l_{exptl.}}} \qquad \textbf{(B5)}$$

for all cases when $| \Delta e/l_{exptl.} | < 1$, expanding the numerator of equation B5 as a binomial series, and dividing by the denominator , the following expression is obtained after omitting the higher order terms.

$$M = \frac{4}{3} - \frac{2}{9}(\frac{\Delta e}{l_{exp.}}) - \frac{4}{81}(\frac{\Delta e}{l_{exp.}})^2 \qquad \textbf{(B6)}$$

Expressing Δe from equation B3 and expanding B6, the following expression for M is obtained,

$$M = \frac{86}{81} + \frac{26}{81}\frac{l_{pred.}}{l_{exptl.}} - \frac{4}{81}(\frac{l_{pred.}}{l_{exptl.}})^2 \qquad \textbf{(B7)}$$

(for all $l_{pred.} \neq l_{exptl.}$)